



Contents lists available at ScienceDirect

Progress in Nuclear Magnetic Resonance Spectroscopy

journal homepage: www.elsevier.com/locate/pnmrs

Mechanistic analysis by NMR spectroscopy: A users guide

Yael Ben-Tal^{a,1}, Patrick J. Boaler^{a,1}, Harvey J.A. Dale^{a,1}, Ruth E. Dooley^{a,b,1}, Nicole A. Fohn^{a,1}, Yuan Gao^{a,1}, Andrés García-Domínguez^{a,1}, Katie M. Grant^{a,1}, Andrew M.R. Hall^{a,1}, Hannah L.D. Hayes^{a,1}, Maciej M. Kucharski^{a,1}, Ran Wei^{a,1}, Guy C. Lloyd-Jones^{a,1,*}

^aSchool of Chemistry, Joseph Black Building, David Brewster Road, Edinburgh, EH9 3FJ, United Kingdom

^bEvotec (UK) Ltd, 114 Innovation Drive, Milton Park, Abingdon, Oxfordshire OX14 4RZ, United Kingdom

Edited by Gareth Morris and David Neuhaus



ARTICLE INFO

Article history:

Received 18 December 2020

Accepted 6 January 2022

Available online 19 January 2022

Keywords:

NMR
Mechanism
Kinetics
Isotopes
In situ analysis
Titrations
Flow
Reaction monitoring
DOSY
Catalysis
Data processing
Equilibrium

ABSTRACT

A 'principles and practice' tutorial-style review of the application of solution-phase NMR in the analysis of the mechanisms of homogeneous organic and organometallic reactions and processes. This review of 345 references summarises why solution-phase NMR spectroscopy is uniquely effective in such studies, allowing non-destructive, quantitative analysis of a wide range of nuclei common to organic and organometallic reactions, providing exquisite structural detail, and using instrumentation that is routinely available in most chemistry research facilities. The review is in two parts. The first comprises an introduction to general techniques and equipment, and guidelines for their selection and application. Topics include practical aspects of the reaction itself, reaction monitoring techniques, NMR data acquisition and processing, analysis of temporal concentration data, NMR titrations, DOSY, and the use of isotopes. The second part comprises a series of 15 Case Studies, each selected to illustrate specific techniques and approaches discussed in the first part, including *in situ* NMR (¹H, ¹⁰/¹¹B, ¹³C, ¹⁵N, ¹⁹F, ²⁹Si, ³¹P), kinetic and equilibrium isotope effects, isotope entrainment, isotope shifts, isotopes at natural abundance, scalar coupling, kinetic analysis (VTNA, RPKA, simulation, steady-state), stopped-flow NMR, flow NMR, rapid injection NMR, pure shift NMR, dynamic nuclear polarisation, ¹H/¹⁹F DOSY NMR, and *in situ* illumination NMR.

© 2022 Elsevier B.V. All rights reserved.

Contents

1. Introduction	30
2. Practicalities and the reaction environment	31
2.1. General considerations	31
2.1.1. Spectrometers and probes	31
2.1.2. Internal and external standards	32
2.1.3. NMR tubes	33
2.2. Sampling methodologies	33
2.2.1. <i>In situ</i> and <i>ex situ</i> sampling methods	34
2.2.2. Choosing a sampling method	36
2.3. NMR monitoring methods	36
2.3.1. Selection of components and conditions	36
2.3.2. Other instrumental considerations	39
2.3.3. Strategies for monitoring	39
2.4. Specialised techniques	39
2.4.1. <i>Ex situ</i> monitoring by rapid quenched-flow	39
2.4.2. <i>In situ</i> monitoring of reactions requiring external stimuli	40

* Corresponding author.

E-mail address: guy.lloyd-jones@ed.ac.uk (G.C. Lloyd-Jones).

¹ All authors contributed equally in the preparation of this review.

<https://doi.org/10.1016/j.pnmrs.2022.01.001>

0079-6565/© 2022 Elsevier B.V. All rights reserved.

2.4.3.	Real-time monitoring by flowing the sample into the spectrometer	41
2.4.4.	<i>In situ</i> assembly of reaction mixture within the spectrometer	42
2.4.5.	Hyperpolarisation	42
3.	Measurement, Processing, and quantification	43
3.1.	Temporal resolution	43
3.2.	Longitudinal relaxation, T_1	43
3.3.	Spatially-selective acquisition	44
3.4.	Integration and automation	44
3.4.1.	Signal-to-Noise ratio (S/N)	44
3.4.2.	Acquisition parameters	45
3.4.3.	Post-acquisition parameters (processing)	46
3.4.4.	Spectral deconstruction	47
3.5.	Pure shift NMR	47
3.6.	2D acquisition	48
3.6.1.	Quantitative 2D NMR	48
3.6.2.	Non-uniform sampling	49
3.6.3.	Polarisation sharing	49
3.6.4.	Ultrafast 2D	49
3.6.5.	Multiple acquisition	50
4.	Kinetics and speciation	50
4.1.	Non-equilibrium vs equilibrium systems	50
4.2.	NMR analysis of non-equilibrium systems	51
4.2.1.	'Chemical relaxation' methods	51
4.2.2.	Processing spectra for data extraction	52
4.3.	Kinetics of non-equilibrium systems	52
4.3.1.	Rate equations	52
4.3.2.	Power laws and rate order	52
4.3.3.	Rate laws for linear reaction systems	52
4.3.4.	Rate laws for catalytic reaction systems	52
4.3.5.	More advanced model building – Numerical integration of systems of differential equations	54
4.3.6.	Fitting data to a kinetic model	54
4.3.7.	Graphical and visual kinetic analysis	54
4.4.	NMR analysis of systems at dynamic equilibrium	56
4.4.1.	Disturbing the magnetic equilibrium of the system	56
4.4.2.	Line shape analysis	58
4.5.	Titrations	59
4.5.1.	Single equilibrium	59
4.5.2.	Competitive equilibria	59
4.5.3.	Cooperative equilibria	60
4.5.4.	Preparing the sample for analysis	60
4.5.5.	Model selection	60
4.6.	Analysis of intermediates using DOSY	61
4.6.1.	The DOSY experiment	61
4.6.2.	Interpreting DOSY in mechanistic studies	62
5.	Use of isotopes	63
5.1.	Introduction	63
5.2.	Atom accountancy and tracking	64
5.2.1.	Isotope shifts	65
5.3.	Kinetic isotope effects	65
5.3.1.	Background	65
5.3.2.	Theory	66
5.3.3.	Measuring KIEs: Isotopically enriched substrates	66
5.3.4.	Measuring ^{13}C KIEs: Natural abundance substrates	70
5.4.	Isotopic entrainment	72
5.5.	Signal elimination and spectral simplification	72
5.6.	Using natural abundance satellites	73
5.7.	Enhanced sensitivity, S/N	74
6.	Case studies	74
6.1.	Case study 1: Base-catalyzed Aryl-B(OH) ₂ protodeboronation revisited: From concerted proton-transfer to liberation of a transient Arylanion [24]	75
6.2.	Case study 2: A dinuclear mechanism implicated in controlled carbene polymerization [337]	77
6.3.	Case study 3: Anion-initiated trifluoromethylation by TMSCF ₃ : Deconvolution of the siliconate–carbanion dichotomy by stopped-flow NMR/IR [25]; and difluorocarbene generation from TMSCF ₃ : Kinetics and mechanism of NaI-mediated, and Si-induced, anionic chain reactions [26]	78
6.4.	Case study 4: Insight into catalyst speciation and hydrogen co-evolution during enantioselective formic acid-driven transfer hydrogenation with bifunctional ruthenium complexes from multi-technique operando reaction monitoring [158]	81
6.5.	Case study 5: Practical aspects of real-time reaction monitoring using multi-nuclear high-resolution flow NMR spectroscopy flow NMR spectroscopy [39]	82
6.6.	Case study 6: Still shimming or already measuring? – Quantitative reaction monitoring for small molecules on the sub-minute timescale by NMR [340]	83
6.7.	Case study 7: Mono-oxidation of bidentate bis-phosphines in catalyst activation: Kinetic and mechanistic studies of a Pd/Xantphos-catalyzed C–H functionalization [341]	84

6.8. Case study 8: SHARPER reaction monitoring: Generation of a narrow linewidth NMR singlet, without X pulses, in an inhomogeneous magnetic field [190].....	85
6.9. Case study 9: Base-free enantioselective C(1)-ammonium enolate catalysis exploiting aryloxides: A synthetic and mechanistic study [342].....	85
6.10. Case study 10: Aryl trifluoroborates in Suzuki–Miyaura coupling: The roles of endogenous aryl boronic acid and fluoride [25].....	86
6.11. Case study 11: Sub-minute kinetics of human red cell fumarase: ¹ H spin-echo NMR spectroscopy and ¹³ C rapid-dissolution dynamic nuclear polarization [343].....	88
6.12. Case study 12: Glycosylation intermediates studied using low temperature ¹ H- and ¹⁹ F-DOSY NMR: New insight into the activation of trichloroacetimidates [344].....	89
6.13. Case study 13: Kinetics and mechanism of the Arase-Hoshi R ₂ BH-catalyzed alkyne hydroboration: Alkenylboronate generation via B–H/C–B metathesis [28].....	90
6.14. Case study 14: Analysis of auto-induction, inhibition and auto-inhibition in a Rh-catalyzed C–C cleavage: Mechanism of decyanative arylsilylation [49].....	91
6.15. Case study 15: Discovery of a photoinduced dark catalytic cycle using <i>in situ</i> illumination NMR spectroscopy [102].....	93
7. Summary and outlook.....	94
Declaration of Competing Interest.....	95
Acknowledgements.....	95
References.....	95

1. Introduction

This review discusses the application of NMR in the investigation of the mechanism of homogeneous organic and organometallic reactions, and is based on the hands-on research experience of the authors [1]. The stimulus for the review stems from a meeting when a newly joined member of the team asked some practical questions about how best to go about analysing a specific aspect of a reaction that they were investigating by *in situ* NMR. Many of the group members felt that the answers that they provided were ones they had heard many times before, but that the questions were also ones that at some point in their career they too had asked. We concluded that an assembly of the collective experience of the group in the interrogation of reaction mechanisms using NMR, in a practical guide or ‘compendium’, would be useful, for the group and perhaps also for others. This guide covers the basic principles, both physical and chemical, behind the various approaches to the elucidation of reaction mechanism using NMR, as well as practical advice and hard-won experience: the ‘tips, tricks, and traps’ that are more customarily conveyed by the mentor–mentee relationship in the research laboratory. It aims to present these topics at a level accessible to a first-year graduate student, and to be comprehensive enough to provide them with everything they will require to begin to engage competently, productively, and confidently in the NMR investigation of reaction mechanisms. A series of 15 ‘Case Studies’, drawn from work in the authors’ group and from the general literature, is used to illustrate the principles and practical aspects of each of the specific techniques presented, together with 345 references to the primary literature, reviews, textbooks, and websites. An extended Glossary is also provided.

Before going into the details of how to approach mechanism using NMR, it is not unreasonable to question the motivations for doing this, for example, why study reaction mechanism at all, and why, in many cases, is NMR so well suited to this. The motivations for the mechanistic study of a chemical reaction or process are diverse. From the perspective of pedagogy, mechanisms provide a means of classification, simplification and correlation; for example, a general understanding of the mechanistic factors that govern the feasibility of an S_N1 reaction means that one does not need to memorise every known example. From the perspective of research, both academic and industrial, mechanisms provide a framework by which the outcomes of reactions can be predicted, explained, compared, and evaluated, and new reactions, reagents, and catalysts developed in a logical manner. Mechanism also allows the design and tuning of molecular function, an essential

component in the development of modern materials, agrochemicals and pharmaceuticals. From the perspective of industrial production, knowledge of mechanism allows an informed refinement of a process – an apparently marginal improvement of yield from 99% to 99.5% represents a doubling in efficiency, when considered in terms of loss of the substrate. At the multi-tonne scale this has major implications in terms of the economic costs, energy input, and environmental impact in the generation and disposal of waste streams from purification steps. Mechanism is also essential in the defence of intellectual property, and in its challenge, and bypass. And finally, there is the role of curiosity: there is deep intellectual challenge and reward in the elucidation of the mechanism(s) by which a chemical reaction proceeds, and in the development of overarching and widely-applicable mechanistic concepts.

The detailed investigation of mechanism is not a trivial undertaking but should not be viewed as impenetrable. One of the key factors governing success is a preparedness to devote the time and effort required for the acquisition, curation, and interrogation of large sets of data. This takes patience, and perhaps more demandingly, an intellectual plasticity in which creation and testing of an evolving series of hypotheses must be conducted simultaneously with critical evaluation of the growing collection of data. Ignoring dogma, thinking ‘outside of the box’, and a willingness to drop the current hypothesis for a new one, rather than the natural inclination to continue to defend it by ignoring inconsistent results, can make the crucial difference between success and an ultimately frustrating and expensive journey of self-delusion. A key aspect, often overlooked, is that chemical intuition, or the influence of prior studies of others, can lead to chemical or physicochemical phenomena being *assumed* to occur, without justification. As emphasised by the late Joseph F. Bunnett: “Don’t make verifiable assumptions!” [2] – many assumptions, usually relating to ‘simple’ steps or processes, prove to be not entirely valid when rigorously tested, and some prove to be completely invalid. Their careful scrutiny can lead to valuable new directions in a study.

Chemical reaction mechanisms are primarily a description of the molecular, and sometimes physicochemical, choreography of a reaction – in terms of energy, structure and timescales. Fundamental to this is the correct identification of the products, and side products, of the reaction, and if not too transient, any intermediates, or ‘off pathway’ equilibria. The stoichiometry involved in the decay of the substrates, and growth of intermediates and products, must be identified, and the fluxes of these species as a function of time analysed. Side reactions provide mechanistically

valuable information. Thus, unless absolutely necessary, for example due to spectral congestion, the reaction conditions should not be adjusted to severely attenuate or eliminate them. The selectivity of the reaction must also be accounted for, as well as any changes in this as a function of temperature, concentration, medium, and additives etc. The mechanisms of reactions should ideally be studied under the conditions in which they are applied (concentrations, solvent, temperature, etc.), and any catalysts or inhibitors, if present, identified.

Solution-phase NMR spectroscopy most often proves ideal for many or all of the above requirements. It is non-destructive, is quantitative (with appropriate experimental set-up) thus allowing determination of concentrations, is applicable to a wide range of nuclei common in organic and organometallic reactions, provides exquisite structural detail, is reasonably sensitive – particularly at the concentrations used in synthesis – and the instrumentation is routinely available, most often as a shared facility, in nearly every chemistry research department worldwide.

Whilst alternative techniques offer other advantages, e.g. rapid data acquisition by UV or IR, the extremely high sensitivity of mass-spectrometry, and the (static) atomic resolution of X-ray diffraction, and should always be employed when beneficial, none of these techniques have the flexibility and amenability to application under 'normal' reaction conditions that makes NMR, in the authors' opinion, by far the most powerful general tool for the interrogation of reactions. As a research group that has focussed for the last twenty five years almost exclusively on the investigation of organic reaction mechanisms, we have embraced NMR whole-heartedly. In doing so, we have explored a very wide range of reaction classes, each with their own challenges in terms of approach of analysis, reaction conditions, temperature, velocity, symmetry, resolution, complexity of kinetics, etc. We have also developed new techniques to aid us in these studies, as well as considerable expertise in the synthesis and application of isotopically-labelled species. Along the way we have made mistakes, then identified, rectified and learned from them; and in many cases these events have proved crucial in the outcome of later studies. Indeed, one should seek to find satisfaction in proving the current hypothesis wrong, and using this as the impetus for generation of the next.

2. Practicalities and the reaction environment

A number of practicalities need to be taken into account in order to effectively monitor reactions and analyse their mechanism by NMR, and we start by briefly discussing some key points. These include general principles for NMR spectroscopy and choice of instrument, *ex situ* versus *in situ* analysis, choice of internal standard, solvent, nucleus, and instrument parameters, and the identification of conditions when specialised techniques are required.

2.1. General considerations

2.1.1. Spectrometers and probes

When conducting mechanistic work, one should bear in mind the general principles of the NMR experiment [3–7], the equipment available, and the scope and limitations of the information that can be elicited. Most experimentalists have limited access to a small range of NMR instruments. Prior to conducting a detailed mechanistic study relying heavily on NMR it is therefore useful to understand the key parameters that affect what it will be possible to achieve with the facilities available. Standard NMR spectrometers for solution phase chemistry come in two classes: high field and low field. They both operate on the same principles, and almost all of the reaction monitoring techniques discussed in

this review can, in principle, be performed on either type. High field spectrometers, typically in the range 200 to 600 MHz (^1H), employ cryogenically-cooled superconducting electromagnets, usually stand taller than a human, require dedicated laboratory space, and are expensive to purchase and maintain. Nonetheless, the quality of the spectra obtained makes them ubiquitous in chemistry research. In contrast, low field spectrometers, typically 40–80 MHz (^1H), use permanent magnets, are smaller, portable, much cheaper to buy and to operate, and are often referred to as 'benchtop spectrometers'. Developments over the past two decades have led to benchtop instruments with sufficient sensitivity and resolution for some reaction monitoring applications [8–10].

The greatest functional variation between different NMR solution-state probes is in the number and position of the coils, which generally can be used to transmit and to receive. A single-resonance probe contains a single radiofrequency (RF) coil and only allows observation of one nuclear species at a time, limiting the type of NMR experiments that can be performed. Most modern probes contain two, but these are often tuned to have more than one resonance (or "channel"), each optimised to monitor a different nucleus. The nuclei monitored using the inner coil can be detected with enhanced sensitivity compared to the nuclei monitored using the outer coil. Although each channel can only be tuned to one class of nucleus (^1H , ^{13}C , ^{19}F etc.) at a time, on some spectrometers it is, in principle, possible to conduct time-shared heteronuclear double resonance on the same coil [7].

The detection sensitivity of a given experiment will also vary between spectrometers. Higher field magnets afford a greater signal intensity and resolution for the same volume of sample. The signal-to-noise ratio (S/N) can also be increased by reducing thermal noise through the use of cryogenically-cooled (He, or N_2) RF coils and preamplifiers. Specialised probes for use with smaller diameter NMR tubes than the standard 5 mm probe are available, and these lead to higher sensitivity per unit mass of sample [11]. The use of *para*-hydrogen (*p*- H_2) techniques, though beyond the capacities of most routine NMR facilities, can be a very effective tool to increase NMR sensitivity in some cases, see Section 2.4.5 below, including selective enhancement of selected peaks [12–14].

2.1.1.1. Pre-acquisition and thermal equilibration. Several steps must be taken between sample insertion into the probe and spectrum acquisition. Magnetic field stability can be ensured by locking to a relevant signal frequency, most commonly to deuterium. The probe must be tuned to the frequency of the measured nucleus, matching the transmitter and preamplifier impedances with that of the probe, and the magnetic field homogenised across the sample ('shimming') [3,5,7].

A general workflow is: prepare sample, insert into spectrometer, allow sample to equilibrate at temperature, set acquisition parameters, tune probe, lock, shim, collect data. Many or all of these steps can be performed automatically. The sample temperature is usually controlled by changing the temperature of gas ('VT gas' – usually dry air or nitrogen) passing through the probe and past the sample, and on many spectrometers this can be adjusted across a wide range of temperatures. The temperature control of reactions conducted in NMR tubes within the probe is usually sufficiently stable (within ± 0.5 °C) unless rapid exothermic or endothermic processes are being investigated [15]. Five main parameters govern the rate and thus time taken for thermal equilibration after insertion of the sample into the probe: (i) the initial temperature difference (ΔT_0) between the sample and the probe; (ii) the flow-rate of the VT gas passing through the probe; (iii) the heat capacity of the sample, primarily dependent on the identity and volume of the solvent; (iv) the NMR tube material and dimensions, and heat flux attainable through the tube walls; and (v) the specific design and thermostatic efficiency of the probe.

For example, with the NMR cryoprobe employed in the work of the authors, it takes less than about two minutes for stabilisation ($\Delta T < 0.5\text{ }^{\circ}\text{C}$) of a typical 0.6 mL organic solvent sample in a standard 5 mm borosilicate NMR tube (see red line in Fig. 1).

When rapid thermal equilibration prior to acquisition is required, it is advisable to estimate the thermostatic efficiency of the probe employed, using the solvent for the reaction to be analysed, Fig. 1. It is also advantageous to pre-heat or cool the sample prior to insertion, and to pre-shim using a dummy sample (Section 2.2.1.2.1) at the required temperature. For experiments where complete temperature stabilisation is required, for example to minimise convection in DOSY measurements, samples should be left to equilibrate for tens of minutes.

2.1.2. Internal and external standards

When performed with appropriate delays, standard pulse-acquire NMR sequences can be inherently quantitative, with the area of each peak directly proportional to the concentration and number of nuclei. Thus, for a series of spectra generated by *in situ* monitoring of a chemical reaction, if the concentration of one species in one spectrum is known (typically the initial concentration, in the first spectrum), it is possible to calculate the concentration of all species in the dataset. Whilst the quantitative nature of NMR is one of the key benefits of the technique, it remains common practice to use an internal standard to eliminate any instrumental variability when accurate concentrations are required [3,16–18]. The internal standard nullifies the effects of any differences in absolute integral between the individual spectra that will make up the kinetic dataset; it can also be used to normalise the chemical shift axis. Thus, in contrast to routine internal reference compounds expressly used for normalising chemical shift, e.g. tetramethylsilane (b.p. $26\text{ }^{\circ}\text{C}$), an internal standard for quantification must be (i) relatively non-volatile (to avoid loss during the reaction), (ii) have a similar longitudinal relaxation rate (see Section 3.2) to the species being monitored (to avoid the need to increase relaxation delays) [16,18,19], (iii) have a well-resolved

peak, or peaks, and (iv) be fully soluble in the reaction medium throughout the reaction evolution.

Most importantly, the internal standard must be inert under the reaction conditions – not just towards the species present in the NMR tube (or the surface of the tube itself), but also to any conditions applied externally such as heat or light. In addition to being of constant concentration, the internal standard is ideally also of known concentration, in order to allow calculations of absolute, rather than merely relative, concentrations. For the concentration of the standard to be known, it must also be of known purity. The corresponding concentration of any species in solution can then be accurately calculated (see Section 3.4). To minimise errors in establishing the concentration of the internal standard, it is preferable to prepare it as a solution in the reaction solvent. This stock solution can also be used to dissolve all components, over multiple reactions. Alternatively, a stock solution containing the internal standard and one or more of the reaction components can be prepared. The standard should be present in the reaction at a concentration that gives an NMR signal intensity at least comparable to one of the limiting reagents, in order to minimize errors when analysing relative integrations. Selecting a suitable internal standard is not always a trivial matter. Table 1 provides a small selection of internal standards that we have recently employed.

If a suitable internal standard cannot be found, there are two alternative approaches. One is to use an external standard [16], within the NMR tube but physically separated from the reaction solution, by use of a sealed capillary tube or coaxial insert. While many of the requirements for an internal standard still apply, that of inertness to the reaction conditions is circumvented by physical separation. This separation may also cause different instrument responses between the standard and the compounds to be measured, making the external standard a less common method for quantification in reaction monitoring. The second approach is to use an electronic reference which relies on a digital reference peak [16,19]. After calibration, the digital reference signal can be added to the experimentally acquired spectrum and used analogously to a physical standard. The advantage of this method is that nothing

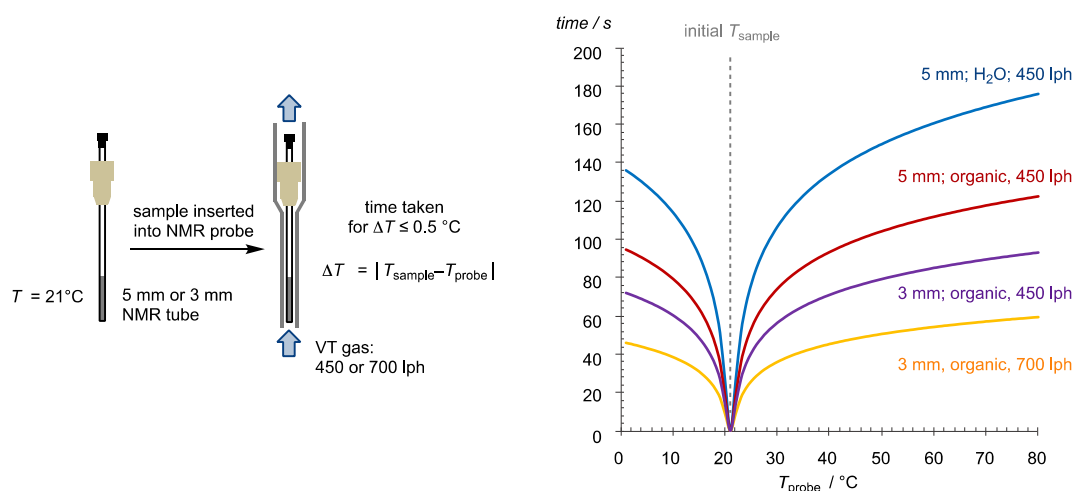


Fig. 1. Approximate time taken (y-axis, seconds) for the solution in an NMR tube initially at $21\text{ }^{\circ}\text{C}$ to equilibrate to within $\pm 0.5\text{ }^{\circ}\text{C}$ of the probe temperature (T_{probe} , x-axis) after insertion into a Bruker Avance 400 Prodigy probe, equipped with a Bruker BCU 1 temperature control unit; A.M.R. Hall, G.C. Lloyd-Jones, unpublished results, 2021. The lines are calculated using the empirical relationship: $T_{\text{sample}} \approx T_{\text{probe}} - \Delta T_0 e^{-kt}$, where t is the time after insertion, ΔT_0 is the initial temperature difference between the sample ($21\text{ }^{\circ}\text{C}$) and the probe (x-axis, T_{probe}), and k is a heat-transfer rate constant, specific to the solvent, sample volume, NMR tube, VT gas flow rate, and probe. The k values were estimated from a series of heating and cooling curves, in which T_{sample} was measured at 5 s intervals using a Pt-100 sensor immersed in the specified solvent in the NMR tube (0.60 mL in 5 mm tube, 0.4 mm wall thickness; 0.22 mL in 3 mm tube, 0.3 mm wall thickness) prior to insertion. Blue curve, H_2O , $k = 0.027\text{ s}^{-1}$; red curve, average value from THF (0.038 s^{-1}), toluene (0.039 s^{-1}), hexane (0.037 s^{-1}), chloroform (0.041 s^{-1}), and benzene (0.041 s^{-1}); purple curve, $k = 0.051\text{ s}^{-1}$; yellow curve, $k = 0.080\text{ s}^{-1}$. Comparison of the blue and red curves shows the impact of the high heat capacity of water ($4.18\text{ J g}^{-1}\text{ K}^{-1}$) compared to the organic solvents ($1.48 \pm 0.04\text{ J g}^{-1}\text{ K}^{-1}$). The purple and yellow curves show the impact of sample volume and gas flow rate.

Table 1
Selected examples of internal standards recently employed by the authors in reaction monitoring.

Reference compound	Nucleus	δ /ppm	Reaction being monitored
Trifluoroacetic acid	^{19}F	-75.33	Kinetics of aryl-B(OH) ₂ protodeboronation in 1/1 (v/v) H ₂ O:1,4-dioxane, low pH [24]
Trifluoroacetate	^{19}F	-75.14	Kinetics of aryl-B(OH) ₂ protodeboronation in 1/1 (v/v) H ₂ O:1,4-dioxane, high pH [24]
(<i>p</i> -Tolyl) ₃ P = O	^{31}P	29.20	Quantification of $^{16}\text{O}/^{18}\text{O}$ Ph ₃ P=O from Pd(II) reduction in 9/1 (v/v) THF/H ₂ ¹⁸ O [25]
Dibromomethane	^1H	4.95	Kinetics of Au-catalysed arylation in 50/1 (v/v) CDCl ₃ /CD ₃ OD [26]
1,3,5-Trimethoxybenzene	^1H	6.09, 3.77	Kinetics of the alkylation of triazoles in CDCl ₃ [27]
1-Fluoronaphthalene	^{19}F	-123.95	Kinetics of alkyne hydroboration in 100/1 (v/v) dioxane/CHCl ₃ [28]
Fluorobenzene	^{19}F	-113.15	Kinetics of CF ₃ and CF ₂ transfer from TMSCF ₃ in THF [29,30]
Mesitylene	^1H	6.93, 2.41	Kinetics of Cu/Fe-catalysed oxidation of benzylic compounds in CDCl ₃ [31]
α,α,α -Trifluorotoluene	^{19}F	-62.90	Kinetics of [2,3]-rearrangement of ylides in CDCl ₃ [32]
Dimethyl sulfoxide	^1H	2.50	Kinetics of a photocatalytic reaction in CD ₃ CN [33]

needs to be added to the NMR sample, and whilst care must be taken to obtain an accurate signal [19], both the intensity and position (chemical shift) of the reference peak can be adjusted, making this a useful but underutilised technique in reaction monitoring.

2.1.3. NMR tubes

Almost all NMR experiments are conducted within NMR tubes. Routine NMR tubes are thin-walled, made of borosilicate glass, and are available in a range of different sizes and outer diameters (1–10 mm). The selection of the diameter depends primarily on the NMR probe, Section 2.1.1. NMR tubes with an outer diameter (O. D.) of 5 mm (Fig. 2) are the most common, although 3 mm tubes can also be used in 5 mm NMR probes.

When only small volumes of sample are available (tens of microliters), microcells that fit within standard 5 mm NMR tubes can be used; in these cases it is advisable to also fill the outside volume with solvent to ensure simpler shimming. NMR tubes are also available amberised (for light sensitive samples) and in other materials such as quartz, sapphire or zirconia (for boron and silicon NMR, as well as for the containment of highly-reactive samples)



Fig. 2. A selection of 5 mm O.D. NMR tubes. (a) plain borosilicate, polyethylene cap; (b) amberised borosilicate; (c) J Young valve capped borosilicate; (d) titration tube with screw cap; (e) Shigemii tube with insert – sample held between two ‘matched’ solid glass plugs; (f) Shigemii insert.

although the cost of these specialised tubes is higher than that of the standard transparent borosilicate.

For addition of solids to NMR tubes we normally employ a short disposable Pasteur pipette. This can be placed horizontally on a simple V-shaped support, e.g. the mouth of a small empty beaker, placed on a microbalance. Using a micro-spatula, the solid is then carefully added into the wider bore of the pipette until the desired weight is measured. Then, after inserting the narrow bore end of the pipette into the tip of the open NMR tube, simply raising the pipette vertically usually transfers the solid into the tube. If need be, a sharp tap on the side of the pipette, or rinsing through with solvent, can be employed to ensure complete transfer. NMR tubes are generally capped with Kel-F caps, however silicone or rubber septum caps can be employed for air-sensitive reactions as they allow for the injection of sample through a self-sealing lid (see Section 2.2.1.2.1) [20,21]. It should also be noted that sample contamination can arise from inadvertent extraction of the plasticiser present in some NMR tube caps by common organic solvents.

Some variation in the configuration of the tubes exists for different purposes. For example, J Young valve NMR tubes have a screw fitting in the glass designed to accommodate a PTFE compression-seal plunger (Fig. 2c). With this system, samples highly sensitive to oxygen and moisture can be prepared, and tubes can be kept connected to a Schlenk line if needed. Shigemii tubes minimise the amount of sample required: the bottom section is made of solid glass, and an insert (Fig. 2f), again of solid glass, is then placed above the sample. This ensures that most of the sample is in the detection region of the radiofrequency coil. The solid glass sections are designed to match the magnetic susceptibility of the particular solvent being used. This allows improved shimming of the magnetic field and thus improved spectral resolution [20,21]. When running chemical reactions in NMR tubes one has to take into account that the glass surface may react with the components of the sample. As an example, borosilicate and quartz glass react with high concentrations of fluoride or hydroxide anions [22]. These features may not only affect the reaction, but also permanently damage the NMR tube; in such cases, inserts made of perfluorinated polymers can be used to avoid direct contact between the glass and the solution [23].

Several reaction monitoring techniques also require the use of more specialised equipment such as inserts, capillary tubes, flow cells, connectors and so on (for more details see Section 2.4). Aside from the glassware, materials used in these types of equipment include polymers such as PTFE and PEEK. However, these materials are not always inert to the reaction conditions. For example, PEEK absorbs DMSO and MeOH and is incompatible with strongly acidic or corrosive oxidants such as bromine [34]. As reaction kinetics can change unpredictably through unplanned reactivity with the reaction vessel and other components used to assemble the reaction mixture (syringes, needles, septa, gasses, etc.), care must be taken to ensure the compatibility of all materials in the experimental set up.

2.2. Sampling methodologies

Two crucial initial considerations when designing a mechanistic study using NMR are the sampling method, and access to the NMR spectrometer. There are a broad range of techniques available for sampling, allowing the majority of chemical reactions to be monitored, but although many studies have been reported which make use of these techniques, very few go into sufficient detail to allow the uninitiated to apply them [35–40]. One aim of this review is to provide a more detailed practical account of how these various techniques are used.

2.2.1. *In situ* and *ex situ* sampling methods

There are two distinct categories of methods available to monitor and sample reactions: [39] *ex situ*, where the reaction is conducted outside the NMR tube, and *in situ*, where the reaction is conducted entirely within one NMR tube. In all cases, there is a time gap between reaction initiation (“ t_0 ”) and the acquisition of the first spectrum after the reaction has started. This gap is often referred to as the ‘dead time’. The velocity of the reaction relative to the dead time is a key consideration in deciding what technique to apply.

2.2.1.1. *Ex situ* monitoring. In *ex situ* monitoring, the reaction is conducted exactly as it would be under standard laboratory conditions, with the exceptions that an internal standard is (usually) also added to the reaction, and that prior to reaction initiation an aliquot of the solution is taken out and set aside [36,39,41]. Once the reaction is initiated, small aliquots are taken from the bulk solution at various recorded time increments. Each aliquot is immediately quenched and set aside. The quenching technique used is very dependent on the specific reaction under investigation, but common methods include addition of acid, base, ligand, or water, etc., filtration of heterogeneous components, simple exposure to air, heat/cooling or UV light. Each aliquot can be then placed in its own NMR tube and diluted (if necessary), and NMR spectra can then be measured essentially at leisure (Fig. 3). It is worth noting that this technique is very reliant on the ability to completely stop the reaction upon exposure to the quenching agent. It is therefore advisable to test that such quenching is complete, for example by measuring samples again after a short time delay. If the samples are found to evolve slightly after quenching, the data can sometimes be corrected, after careful calibration, based on the time interval between adding the quenching agent and the NMR analysis.

A variant of this technique involves a series of two or more parallel reactions, each of which is quenched at a different time point. Although this adds a degree of uncertainty to the data (each reaction vessel must be kept under identical conditions over the course of the reaction), it can be useful in the case of slow reactions. For example, by setting up a pair of identical reactions, one started

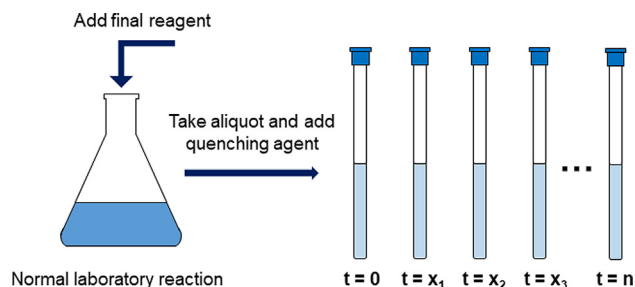


Fig. 3. Schematic of the process of *ex situ* sampling for reaction monitoring.

about 10 h after the other, one can ‘interleave’ data-sets to avoid gaps in the *ex situ* sampling data while the operator sleeps (Fig. 4).

Ex situ sampling has several advantages: (i) it is compatible with almost any laboratory reaction, provided a suitable quenching agent can be found; (ii) it requires only minimal time access to the NMR spectrometer; (iii) it allows for detailed NMR experiments on the ‘frozen’ reaction aliquots; (iv) these ‘frozen’ aliquots can be further investigated using other analytical techniques; and (v) after gaining some experience, it is possible to conduct multiple kinetic experiments in parallel. However, the *ex situ* method is highly labour-intensive, increasingly so as the number of parallel reactions increases. The method also requires a sufficiently large reaction volume that repeated sampling does not perturb the reaction conditions. As each time point is individually quenched and measured in a separate vessel, *ex situ* monitoring is more prone to random measurement error than *in situ* techniques that employ a single tube, see for example the study of Carbery and Hintermair and co-workers [33]. Furthermore, the nature of reaction quenching means that transient intermediates are usually lost. Despite the limitations, *ex situ* monitoring remains a very powerful, but somewhat underutilised tool – possibly due to the amount of work required to generate a single kinetic profile.

2.2.1.2. *In situ* monitoring. If sufficient access to an NMR spectrometer can be secured, reaction monitoring can be conducted by *in situ* techniques, where the reaction takes place entirely within the volume of the NMR tube or flow cell. There are some important differences in the implementation of chemical reactions within NMR tubes compared to ordinary laboratory ‘benchtop’ procedures. The most important distinction is mixing: without specialist techniques, reactions in NMR tubes cannot be stirred [40,42]. As much as is practically feasible, solutions and components should be pre-mixed prior to addition to the NMR tube. When additional components do need to be added individually direct to the tube, the tube should then be sealed with a cap, septum, or PTFE valve (Fig. 2), and the solution thoroughly mixed through a combination of inversion and vigorous horizontal shaking of the NMR tube along its length; we emphasise *vigorous*, as solutions in NMR tubes tend to move as a plug when only moderately agitated. Vortex mixers can also be useful in this regard, but should be used with care with fragile NMR tubes.

In the case of oxygen- or water-sensitive reactions and reagents, special care needs to be taken. Several excellent guides are available on this topic [43–47]. For NMR reaction monitoring, the reaction must be conducted using solvents (and liquid reagents) that

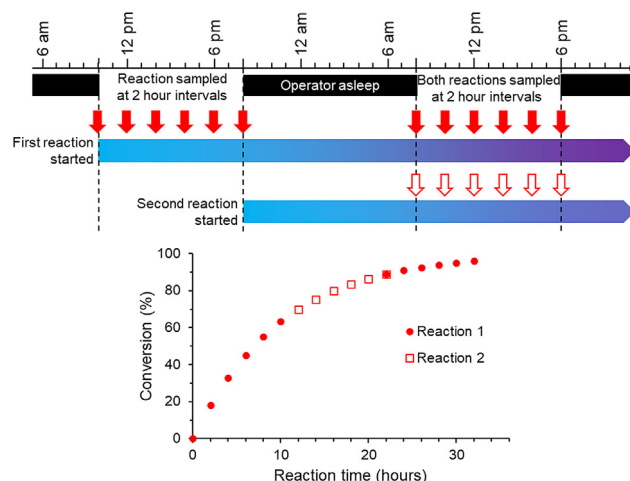


Fig. 4. The staged-initiation strategy for reactions taking >12 h in which two (or more) datasets are ‘interleaved’.

have been rigorously dried and degassed, and it is advisable to conduct the monitoring in a J Young valve NMR tube [28]. If it proves necessary to add reagent to the tube, several options are available depending on the degree of sensitivity of the reaction. The atmosphere within an NMR tube remains relatively static, so for many reactions the process will not be noticeably altered if the cap is briefly removed to add a reagent and then rapidly replaced. For more sensitive reactions, reagents can be injected directly through a septum cap, or added via the J Young valve which is then immediately purged with inert gas. In the case of especially air-sensitive reactions, the tube should be opened within a glove box, additional reagents added, resealed, and taken out for mixing and monitoring. This operation can consume a considerable amount of time, and if required the solution in the sealed NMR tube can be frozen prior to transport back to the spectrometer and then rapidly thawed for analysis.

2.2.1.2.1. Continuous *in situ* monitoring. In the continuous *in situ* procedure, the reaction takes place entirely within the NMR tube in the spectrometer probe, allowing for the monitoring of reactions over a period of minutes to hours, with very good control over the reaction temperature. Unless one has exclusive access to a spectrometer, the technique is not suited to the monitoring of reactions that take hours to days. The first stage in the process is to assemble as many of the reaction components as it is possible to combine in solution without initiating the reaction, or side reactions, (in most cases all but one reagent) in an NMR tube. The solution volume should ideally be as close to the final volume as possible; and the volume should be such that there is a sufficient portion above the active volume of the probe to avoid the need to change shim settings later. For standard 5 mm O.D. NMR tubes, the required total volume is usually about 600 μL . The tube is then inserted into the probe of the spectrometer, the pre-acquisition operations (Section 2.1.1.1) are performed, and a spectrum is acquired. This initial spectrum provides the ' $t = 0$ ' datapoint. The NMR tube is then removed from the spectrometer and the final reagent added. The tube is sealed, the contents rapidly mixed (see above) and the tube reinserted into the spectrometer (Fig. 5a) [26,28,48].

As the spectrometer has just been tuned, matched and shimmed on the $t = 0$ sample, and provided there is not a significant change in the contents, the first spectrum can usually be acquired without delay; i.e. avoiding many of the pre-acquisition operations such as matching, tuning, and shimming (Section 2.1.1.1). The tube remains in the NMR probe until the reaction proceeds to the desired extent of completion. Most spectrometers can be programmed to automatically acquire a series of spectra at defined intervals. In cases where addition of the final component(s) results in a significant change in the sample (e.g. volume, density, ionic strength, or homogeneity), a 'dummy sample' can be used for the pre-acquisition operations (Section 2.1.1.1). The dummy sample is prepared using an identical NMR tube, containing an identical volume of solution to the reaction to be studied, with as similar as possible a composition to the reaction mixture, but chemically inert. It is often possible to use an identical reaction that has been initiated earlier as the dummy sample [28].

2.2.1.2.2. Interrupted *in situ* monitoring. This process is similar to continuous *in situ* monitoring, but employs the typical automation set up found in most research NMR facilities; that is, the spectrometer automatically loads, locks, tunes, matches and shims the sample, before measuring a spectrum and then returning the tube to the auto-sampler system. The first step of this protocol, Fig. 5b, is identical to continuous *in situ* monitoring, up to the point that the final components are mixed into the tube and returned to the spectrometer. The final components are added to the tube, the time recorded, and the tube returned to the auto-sampler. This time, rather than programming the spectrometer to take a series of spectra without re-shimming the sample each time, the spectrom-

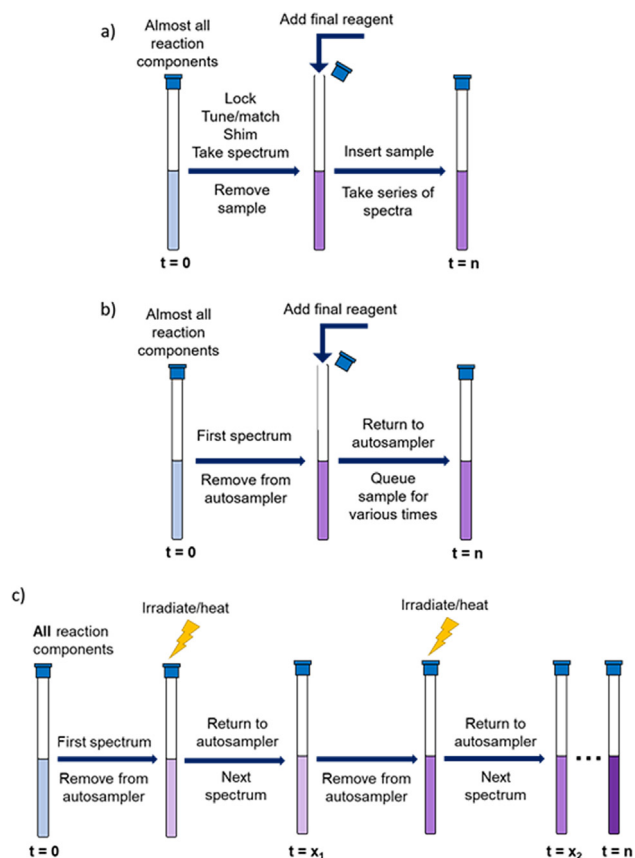


Fig. 5. Schematic representations of (a) the continuous *in situ* reaction monitoring process; (b) the interrupted *in situ* reaction monitoring process; (c) the periodic activation *in situ* reaction monitoring process.

eter is commanded to automatically insert the sample, conduct all the necessary preliminaries, take a spectrum, and then eject the sample, repeating this cycle a set number of times at pre-set intervals; most standard NMR control software has easy-to-use pre-existing options for this. This has the major advantage that it allows for other samples to be run on the same spectrometer between kinetics time points; however, this means that the time points by necessity must be much further apart than those that can be achieved with continuous *in situ* monitoring [26]. Additionally, as the sample is continuously changing position from within to outside of the probe and vice versa, the temperature of the reaction cannot be accurately controlled, although this can be partially overcome by manually removing the sample and storing in a thermostat bath between time points [24].

2.2.1.2.3. In situ monitoring by periodic activation. The final, and least common, methodology we term 'periodic activation *in situ* monitoring'. This is a technique that is only applicable in the case of reactions where the rate of reaction can be controlled through external stimuli [49]. Examples of such stimuli are light, heat and microwave irradiation. It is important to note that, despite the use of an external stimulus, this is not an *ex situ* technique as the entire reaction is conducted within a single NMR tube. If the reaction only proceeds at a significant rate in the presence of the stimulus, it is possible to interrupt the reaction at any point by removing the stimulus, measure a spectrum, and then to restart the reaction by reapplication of the stimulus. This is notably distinct from quenching, which irreversibly stops the reaction. Thus, after acquiring an initial NMR spectrum of the solution, it is removed from the spectrometer and then subjected to the external stimulus for a set amount of time (Fig. 5c).

After this time the stimulus is removed (for example the tube is rapidly cooled to room temperature, or placed in the dark) and an NMR spectrum can be taken at leisure. The sample is then ejected from the spectrometer, and subjected to the external stimulus, and the cycle repeated until the reaction reaches the desired extent of completion. Care must be taken that there is no reaction, or other undesired process, in the absence of the stimulus, and control experiments should be conducted to establish this. Periodic *in situ* reaction monitoring can be a powerful tool, since the NMR spectroscopy can be conducted at leisure – allowing high S/N and more complex NMR experiments to be conducted. Another important consideration is that the NMR spectrum is being measured in the absence of the reaction stimulus, and the sample is thus under different conditions to those that apply when the reaction is proceeding. As such, it can sometimes be possible to analyse and characterise intermediates that would be short-lived under the reaction conditions; see Case Study 14 for an example of this.

2.2.2. Choosing a sampling method

There is a wide choice of standard techniques that can be employed for reaction monitoring by NMR, as well as some more advanced and specialised methods that are discussed in Section 2.4. Each method has its own advantages and disadvantages, and a number of considerations must be taken into account when choosing a suitable sampling method to be used, as summarised in the flowchart in Fig. 6.

The first factor to consider is 'NMR tube compatibility'. Not every reaction can be conducted within an NMR tube. The presence of a heterogeneous component in the reaction medium causes two problems. Firstly the volume within a static (or spinning) NMR tube undergoes very poor vertical (z-axis) mixing, leading to stagnancy and chemical gradients. Secondly, if the heterogeneous component is a solid or suspension, this can reduce, sometimes severely, the line shape and spectral resolution [3,7]. Similarly, reactions that require the presence of an aerobic oxidant are often unable to proceed efficiently due to the limited headspace above the reaction volume, and the poor vertical (z-axis) gaseous mixing in the headspace. Reactions that require the addition of gaseous reagents are technically challenging, with gas bubbles causing S/N reductions due to inhomogeneity and decreased amount of sample in the active volume. Reactions that generate gas can also be unsuitable due to pressure build-up in a sealed NMR tube and potential for damage to the probe. If such reactions can be quenched, then they can still be monitored by *ex situ* sampling; otherwise, a more specialised technique, such as continuous flow NMR (discussed in Section 2.4.3), or the use of high-pressure NMR tubes, is required. If the reaction can be conducted *in situ*, the next factor to consider is whether the reaction can be controlled by external stimuli.

In many cases a reaction that can be monitored by periodic activation can also be monitored with other specialised or non-specialised techniques. For example, photochemical reactions can be monitored either by periodic activation or by continuous *in situ* illumination NMR spectroscopy (see Section 2.4.2.2), or both. Another major factor to consider is temperature. In the case of reactions conducted *ex situ* the usual considerations for any laboratory reaction apply. However, several more are present in the case of reactions conducted within NMR tubes. In addition to factors such as solvent freezing and boiling points, the possible temperature ranges the specific spectrometer used can operate in must be considered. In the case of reactions conducted at extreme temperatures the practicality of NMR tube assembly must also be considered. Thus, even if the spectrometer probe is capable of measuring samples at cryogenic temperatures, without the use of specialised equipment it is challenging to keep a sample in an

NMR tube cold whilst adding it to and removing it from the probe, or whilst adding additional reagents.

For interrupted monitoring employing automatic sample changers, the temperature of the sample when it is outside of the probe will depend on the ambient temperature in the NMR instrument room or sample changer thermostat. For manual interrupted monitoring, samples can be placed in thermostatic heating or cooling baths when outside the probe. Within the probe, however, the temperature can often be very well controlled in comparison to a benchtop laboratory reaction, and spectroscopic methods such as the NMR methanol thermometer can be used to measure sample temperature with a reasonable degree of accuracy [50].

The final, and arguably most critical, consideration when choosing a sampling technique is timescale. While technically either continuous or interrupted *in situ* monitoring is possible for long reactions, in the interests of conserving valuable instrument time, interrupted *in situ* monitoring is often preferred if possible. However, for reactions shorter than a few hours, continuous monitoring is required to achieve useful data density. As reactions become faster, the limit of what can be easily achieved even by continuous *in situ* monitoring by conventional means is reached. By changing factors such as catalyst loading, concentration, and temperature, the timescale of a reaction can sometimes be adjusted to facilitate NMR analysis by simple conventional sampling methods. However, for very fast reactions (lifetimes shorter than a few minutes) specialised techniques such as rapid-injection or stopped-flow NMR (Section 2.4.4) must be used.

2.3. NMR monitoring methods

After selecting the sampling method, a number of other factors must be considered prior to embarking upon kinetic measurement. There is usually little choice of which reagents can be employed, as these are specific to the process being studied, but if there are options, low reactivity and ease of handling should be considered: the NMR laboratory is usually far less well equipped for chemical manipulation than the standard wet chemical research laboratory. Most importantly however, one must select which nucleus/nuclei will be used to monitor the reaction, and what specific NMR parameters will be employed, e.g. pulse sequence, number of scans, acquisition time, or relaxation delay.

2.3.1. Selection of components and conditions

2.3.1.1. Choice of substrate. Mechanistic studies do not usually apply to just a single transformation, but rather to a class of transformations, often with a large range of viable substrates. However, to constrain an NMR-based investigation to a reasonable timescale, and to more directly isolate the process from other variables, it is normal practise to select just one or a few examples for detailed study. This selection must occur at a very early step in the mechanistic study, and should thus be made carefully to avoid having to revise the selection later and repeat a large number of measurements. The examples should be representative of a typical reaction of the class being studied. The chemicals employed will ideally be safe, stable, non-volatile, soluble in the desired solvent system (Section 2.3.1.3) and readily available in reasonable quantities. It is also pertinent to choose substrates containing functional groups which contain nuclei favourable for NMR monitoring. While it is good to study a system that primarily undergoes the desired reaction (i.e. proceeds to high conversion with reasonable yield), the presence and behaviour of side reactions can often also provide much insight into the system, and one or more substrates displaying such behaviour should be included [29].

2.3.1.2. Choice of nucleus. In principle, all nuclei with non-zero spin quantum number are NMR active. It is common that the studied

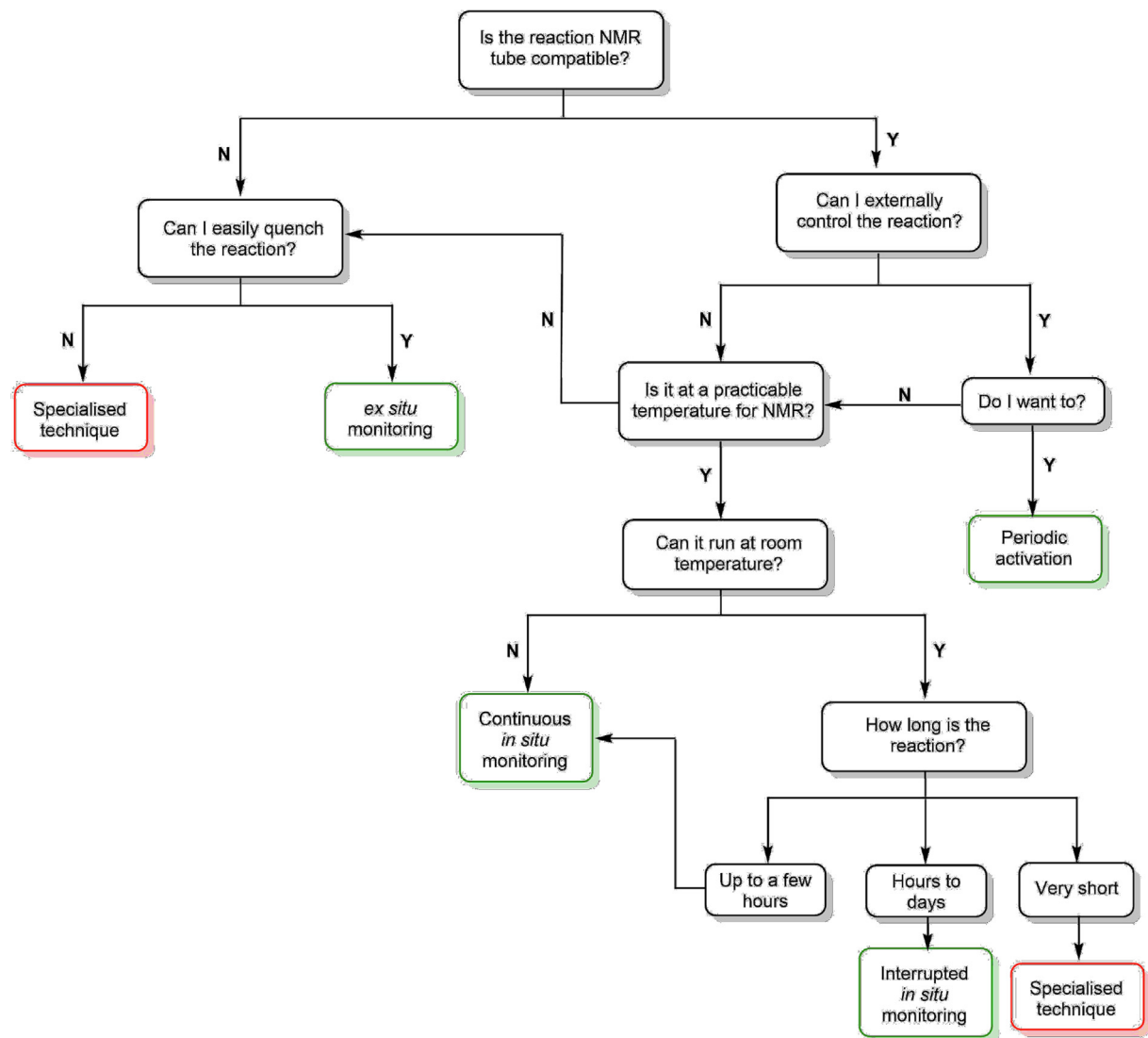


Fig. 6. Flowchart for method selection in the analysis of organic/organometallic reactions and their kinetics by NMR spectroscopy.

system contains more than one NMR-active nucleus which could be used to monitor the reaction. However, not all of these nuclei will be suitable for the timescale of the studied reaction. There are at least four factors which need to be considered: sensitivity, relaxation time, chemical shift range, and the complexity of the spectrum. As one limitation of NMR spectroscopy can be its intrinsically low sensitivity, the first thing to be considered is the sensitivity of the nuclei available to be studied. Nuclei with low sensitivity result in lower signal-to-noise ratios, and at the limit of sensitivity the signal becomes hidden in the noise [51]. In order to achieve suitable S/N, nuclei with high natural abundance and gyromagnetic ratio are preferable. The properties of selected nuclei are shown in Table 2; ^1H has the highest sensitivity, closely followed by ^{19}F .

Although lowering the temperature of the probe or increasing the magnetic field can improve the S/N, a more practical way is to increase the number of scans or to use a more concentrated sample. The former can only be used when monitoring a slow reaction, because of the longer time required to acquire a spectrum. Ideally, there should be as little as possible change in the chemical state of the sample between the start and end of the measurement of a single time point. Similarly, it is often impractical to increase sample concentration, particularly if one wants to investigate a

reaction at a series of concentrations. In the cases of nuclei with low natural abundance (e.g. in the cases of ^2H or ^{13}C) isotopic enrichment (see Section 5) can be employed to improve the sensitivity [52,53].

The second factor that needs to be considered is the relaxation time. There are two types of relaxation: spin–lattice relaxation (T_1) and spin–spin relaxation (T_2), see Section 3. The practical implications of T_1 relate to signal intensity and hence effective quantitation, and as a general rule a shorter T_1 is desirable. In contrast, the effect of T_2 is to determine the linewidth of the signal – a longer T_2 corresponds to a sharper line, and so typically a longer T_2 is preferred. There are many relaxation mechanisms [4], and the relaxation rates of the same type of nucleus in different compounds can be substantially different. For example, the T_1 values for PPh_3 and OPPh_3 (both 0.1 M in 9:1 THF/ H_2O , at 27 °C) are 16.0 s and 3.6 s respectively [54]. In addition, as a general rule nuclei with spin = 1/2 have signals with a narrower line than those from quadrupolar nuclei (spin > 1/2; some common examples include ^{11}B , ^{14}N and ^{17}O), which tend to have broad signals, due to fast quadrupolar relaxation.

Quadrupolar nuclei can also cause line broadening of the signals of other nuclei coupled to them. Broader signals are typically both harder to integrate than narrow signals, and much more prone to

peak overlap, making them less suitable for reaction monitoring, although with care they can be used. Hydrogen and carbon are ubiquitous in organic chemistry, and $^1\text{H}/^{13}\text{C}$ NMR spectroscopy can provide a large amount of structural information about the system being studied. However, as the number of species present in one solution (the starting materials, product, side products and any observed intermediates) increases, the ^1H and ^{13}C spectra of the monitored system become increasingly complex. In such cases, peak overlap can be so severe that discriminating between peaks, and hence reaction monitoring, becomes unfeasible.

Often the observation of X-nuclei (i.e. nuclei other than ^1H) can greatly simplify the spectrum and provide some extra insights into the reaction. Additionally, the use of nuclei other than ^1H can eliminate the need for solvent peak suppression techniques or use of deuterated solvent (see also Section 2.3.1.3). Among the X-nuclei, ^{19}F is a particularly good candidate: it has spin = 1/2, 100% natural abundance, a sensitivity close to ^1H , and a large chemical shift range [55]. Many reactions result in only subtle changes in the structures of the reactants, intermediates and products. Nuclei with larger chemical shift ranges are thus more suited to reaction monitoring because their chemical shifts, δ , are more sensitive to changes in the chemical environment, making ^{19}F labelling (see Section 2.3.3.1) a useful strategy for reaction monitoring. In general, ^{19}F has a T_1 similar to ^1H , meaning that with suitable parameters quantitative NMR spectra of ^{19}F can be obtained in a comparable time. ^{31}P also has spin = 1/2, a 100% natural abundance, and a large chemical shift range, but it has lower sensitivity than e.g. ^1H or ^{19}F . Hence a ^{31}P NMR experiment usually requires a longer time, with a longer delay between scans, and more scans are required for acceptable S/N. Nonetheless, it remains a powerful technique, for example in kinetic studies of reactions catalysed by metal-phosphine complexes [56,57].

Finally, extra precautions are required for ^{10}B , ^{11}B , ^{27}Al or ^{29}Si NMR spectroscopy. Ordinary NMR tubes are made of borosilicate glass, and most NMR probes also contains glass. The glass gives rise to broad background peaks that can affect the measurement. The signals from the tube can be eliminated by using special tubes made of other materials, as discussed in Section 2.1.1. Alternatively, one can take a reference blank spectrum prior to experiment, and subtract it during processing. However, this procedure is time-consuming, and the resultant spectrum may not be accurate enough for quantitative analysis.

2.3.1.3. Choice of solvent. Many of the factors to be considered when choosing a suitable solvent for a particular experiment are the same as those for the equivalent laboratory reaction. It is essential that all reactants, intermediates and products are soluble, so that there is no precipitation during the course of experiment which will affect kinetics, quantitation and the resolution of the spectra. It is also important to consider the chemical properties of the solvent. Chloroform is rarely used in laboratory chemistry, but frequently employed as a solvent for NMR. On exposure to

air and light, or heat, chloroform slowly degrades to HCl and toxic phosgene [58]. The presence of stabilisers that decompose the phosgene leads to further accumulation of HCl, and potentially the decomposition of acid-sensitive analytes. Furthermore, etheral solvents, such as THF, undergo autoxidation to form peroxides, which in addition to being a safety hazard can also affect the mechanism and kinetics of the reaction being monitored [25,59].

Solvent viscosity also affects the quality of spectra: samples prepared in a less viscous solvent, for example acetone, tend to have a longer T_1 and T_2 , which leads to better S/N and narrower lines [60]. Viscosity also affects mass transfer and diffusion rates which can also affect spectral quality, as well as the reaction kinetics [61].

Cost might be another factor to consider, especially if the experiment requires large amounts of solvent, such as in the case of a flow system. The price of some deuterated solvents is very high, and many common laboratory solvents are not available in deuterated form. Although deuterated solvents are routinely used for preparation of NMR samples, their use is not essential for NMR experiments, and with appropriate solvent suppression, non-deuterated solvents can also be used for ^1H NMR spectroscopy [62,63]. There are many solvent suppression methods, each of which has different advantages and disadvantages [64]. Reactions where the solvent plays a role may also be subject to solvent isotope effects, usually by exchange of protons with the analyte, a kinetic aspect that can be valuably probed using defined mixtures of the deuterated and non-deuterated solvent.

One advantage of using deuterated solvent is that it provides a convenient lock reference. It is crucial that NMR spectrometers maintain a stable magnetic field strength during an experiment, because fluctuations in magnetic field strength will cause shifts in signals and a loss in resolution. The lock system regulates the field strength by monitoring the dispersive-mode signal of the solvent deuterium resonance [51]. In principle, other nuclei can also be used (e.g. ^1H , ^{19}F) [65], but deuterium is the most convenient one, and most spectrometers are set up to use it by default. For samples which contain no lock nuclei, a co-axial insert or capillary insert containing deuterated solvent can be used to provide an external lock (Fig. 7) [19].

Spectra can also be recorded in unlocked mode. For experiments with short single spectrum acquisition time (e.g. up to several minutes), using the unlocked mode is completely harmless as the change in magnetic field strength over this period is tiny, and will have a negligible effect on the resultant spectrum; the exact time limit depends on the drift rate of the magnet. The effect of drift is more problematic for spectra with longer acquisition times. For NMR experiments which take a long time due to sensitivity considerations, the acquisition can be subdivided into shorter blocks where the field drift is negligible. After Fourier transforming and manual frequency referencing, the frequency domain spectra may then be added to produce the final spectrum corrected for drift [51]. The deuterium signal is often used for field homogeneity

Table 2

Properties of selected NMR-active nuclei. Sensitivities are relative to ^1H assuming an equal number of nuclei at constant magnetic field and temperature. Chemical shift ranges are for routine spectra. Relative sensitivity values are compared at 100% abundance.

Nucleus	Spin quantum number	Natural abundance (%)	Relative sensitivity (%)	Chemical shift range (ppm)	Resonance frequency at 9.4 T (MHz)
^1H	1/2	99.99	100	13	400.13
^2H	1	0.01	0.965	13	61.42
^{11}B	3/2	80.10	16.5	110	128.38
^{13}C	1/2	1.07	1.59	200	100.61
^{19}F	1/2	100.00	83.4	700	376.50
^{29}Si	1/2	4.69	0.786	540	79.50
^{31}P	1/2	100.00	6.65	430	161.98

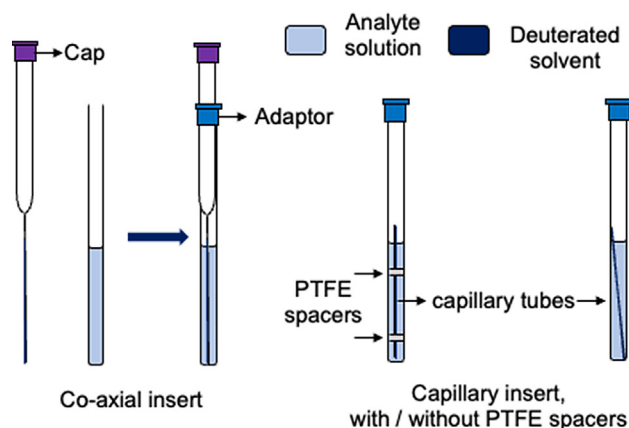


Fig. 7. Experimental assembly for co-axial and capillary inserts. The use of PTFE spacers ensures the capillary tube is held co-axial. Use of a capillary tube without spacers allows for addition of reagents and mixing, etc., albeit with an impact on shimming.

(shimming), so alternative approaches are required to shim a non-deuterated sample; Hoyer et al. provide a practical and detailed guide [62].

For ^1H NMR spectroscopy, another advantage of using a deuterated solvent is that it strongly attenuates the solvent signal. An NMR sample typically contains hundreds to thousands of times more solvent than analyte. The presence of a large solvent peak can mask the peak of interest, and lead to distortion of spectra if the concentration difference between solvent and analyte is too large [64]. For a dilute sample, even with a 99%-deuterated solvent the residual solvent peak can still be large. Thus, it is advisable to consider the chemical shift of the solvent to avoid peak overlap; a guide to the ^1H and ^{13}C NMR chemical shifts for common solvents is available [66]. Deuterated solvents, especially D_2O and CD_3OD , can cause loss of signal of labile protons due to H/D exchange.

Chemical shifts can vary significantly between different solvents. The extent to which the chemical shifts change and the direction of change, can vary substantially between different compounds. Changes can also occur in other components in a mixture. For example the chemical shift of water ranges from 0.40 ppm in C_6D_6 to 4.87 ppm in CD_3OD . [66,67] In cases where reaction monitoring is affected by signal overlap, it can sometimes be beneficial to change the solvent, or add a co-solvent; however the potential for this to change the mechanism should be borne in mind.

2.3.2. Other instrumental considerations

Prior to acquiring a series of individual NMR spectra at varying time points as the reaction progresses for kinetic analysis, several acquisition parameters such as number of scans, acquisition time, and relaxation delay must also be considered. Spectral sensitivity is proportional to the square root of the number of scans: increasing number of scans will increase sensitivity, but at the expense of increasing the time taken to acquire a single spectrum. This in turn reduces the data density in the final temporal concentration dataset, i.e. the number of specified time-points during the reaction for which the concentrations of various species are determined. This is especially problematic for fast reactions. The acquisition time and relaxation delay are both related to the T_1 relaxation times of the species being studied. Thus, if one or more of the species has a long T_1 , it will not fully recover magnetisation prior to application of the next RF pulse, leading to unreliable quantitation. Details of how to ensure quantitative NMR analyses can be found in reviews by Roy and Bharti [19], and by Larive and co-workers [53].

2.3.3. Strategies for monitoring

2.3.3.1. ^{19}F labelling. For kinetic studies, one should aim to determine the concentration of as many of the reaction components as feasible or convenient for each time point. A useful strategy for this is ^{19}F labelling [55], and we have developed this extensively over the last decade using $p\text{-F-C}_6\text{H}_4$. ^{19}F labelling is usually effected by using a reagent or reactant containing a $-\text{F}$, $-\text{CF}_2$ - or $-\text{CF}_3$ group (commercially available or synthesised in-house) and monitoring the reaction by ^{19}F NMR spectroscopy. By strategic placement of the ^{19}F label, the process of interest can often be monitored with very little influence of the label on the kinetics or selectivity, although control reactions should be made to confirm that this is the case. The use of ^{19}F labelling is advantageous for a number of reasons [68]. As discussed previously, ^{19}F has an intrinsically high sensitivity, and as such can be used for monitoring fast reactions, even with just single-scan spectra. Additionally, as the chemical shift of fluorine is very sensitive to its environment, the ^{19}F label does not need to be very close to the reactive centre. This prevents a significant influence of the label on the reaction of interest, while often still allowing for the ready distinction between different reaction components, without peak overlap. However, full assignment of signals can be difficult because the changes in chemical shift can be small or negligible for structurally-similar compounds. Moreover, as small changes in chemical shift can be caused by differences in sample temperature, concentration or composition, the use of literature chemical shift values is often not sufficient for reliable assignments. If feasible, 'spike-in' experiments using independently prepared reference materials are recommended.

2.3.3.2. Reaction monitoring by proxy. In cases where the direct determination of the concentration of the compound of interest is impossible (for example, due to serious peak overlap, or the lack of an NMR-active nucleus), an indirect approach can be used. With some insights into the mechanism and/or stoichiometry of the reaction, the concentration of the compound of interest can be indirectly determined based on the concentrations of other compounds with determinable concentrations. For example, in the hydrolytic decomposition of an arylboronic acid (Ar-B(OH)_2), to generate the corresponding arene (Ar-H) plus B(OH)_3 (see Case Study 1), the arene concentration can be determined indirectly from the growth of the B(OH)_3 signal in the ^{11}B NMR spectrum. However, great care must be taken to ensure that the assumed correspondence is correct. In the latter example, B(OH)_3 can also be extracted from the borosilicate glass wall of the NMR tube and thus corrupt the analysis.

2.4. Specialised techniques

The following section summarises the type of instrumentation and most common specialised techniques used in the monitoring of reactions. The representative set-ups discussed here have been chosen both due to their acceptance within the community, and the fact that they can be used within different spectrometers without the need for probe modification. For each method, there will be a brief description of its design, as well as a short discussion of the main factors to take into account when applying it. This is not intended to be an exhaustive detailed list. For further information on additional designs, probes or alternative special methods for reaction monitoring [69–73] we encourage the reader to consult the publications cited in this section and references therein.

2.4.1. Ex situ monitoring by rapid quenched-flow

Quenched-flow is an *ex situ* sampling method that uses flow chemistry to both initiate and then quench the reaction. Although a series of experiments are needed to build up the temporal profile,

the technique benefits from the ability to make NMR measurements over any time period on the quenched, and thus ‘time-stable’ sample. Using this method high S/N can be gained with low concentration samples, and multidimensional NMR methods can be applied, for reactions that occur in the millisecond to second time range [74–76]. In addition, it possesses the advantages of any other *ex situ* technique, e.g. the sample can additionally be analysed by other methods, e.g. IR, UV, HPLC [77,78].

The set-up generally consists of three syringes – two containing reactant solutions, one containing the quencher – and two efficient mixers (Fig. 8) [79]. The three syringes are simultaneously moved at a known velocity by the action of a drive plate, and the reaction is initiated by combination of the reactant solutions in the first mixing chamber. The solution containing the nascent reaction is then flowed through an ‘ageing loop’ into a second mixer where it reacts with the quencher, prior to removal of the sample from the ‘collection loop’ for analysis. Introduction of the quencher generates a stable solution, in which partial conversion of reactant(s) to product(s) has occurred. The quencher must quantitatively terminate the reaction being studied, on a time scale *much faster* than the reaction. It must also generate a solution containing at least one component that quantitatively reflects the evolution of the reaction at the time-point of quench (substrate, or derivative thereof, or product).

There are three mechanisms by which the timing of the quench can be accurately controlled. The first is by changing the flow rate between runs, whilst ensuring that it is above the flow threshold for turbulent flow in the mixing chamber. The second is by varying the ageing loop volume: most equipment is provided with a series of aging loops. The third is by interrupting the flow; in other words temporarily leaving the reaction static in the ageing loop before beginning flow again to transport the ‘aged’ reaction to the quench point. All modes require large volumes of reactant solutions to generate a series of quenched samples with sufficient temporal data density. This aspect must therefore be considered when using expensive, hazardous, or precious chemicals.

2.4.2. *In situ* monitoring of reactions requiring external stimuli

2.4.2.1. High-pressure NMR. Several metal-catalysed reactions require the use of gas reagents such as hydrogen [80,81], carbon monoxide [82,83] or ethylene under high pressures to proceed. In addition, some chemical processes can also exhibit pressure-dependent kinetics, and the study of this can provide further mechanistic insight [84–86]. The use of high pressures (>2 bar) is not compatible with standard NMR glass tubes. In these cases, monitoring the reactions within the spectrometer requires the use of specialised NMR tubes, pressure control systems, and efficient ways to effect proper mixing between the gas and the liquid phase [87–92].

The most common designs used to carry out chemical reactions involving gaseous reagents under high pressure involve thick-walled NMR tubes attached to an engineered gas inlet. These set-

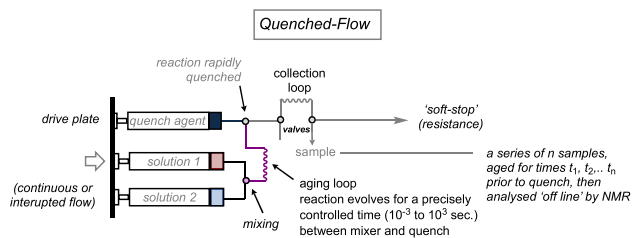


Fig. 8. Schematic representation of a quenched-flow system, operated in ‘continuous flow’, or in ‘interrupted flow’ modes, for shorter and longer ageing times respectively.

ups can be transported, and do not require modification of the NMR probe. As such, they have the advantage that they can be used in any spectrometer, with all the benefits of its associated properties (sensitivity, temperature control, and customisations). The tubes are commonly made of sapphire due to its robustness, chemical stability and non-magnetic properties, although quartz and zirconia tubes are also used. However, despite the resistance of sapphire to high pressures, the tubes are sensitive to vibration and should not be used with sonicators.

A particular design called the Wisconsin-High Pressure NMR Reactor (Wi-HP-NMRR) has attracted attention in the community since its appearance in 2015 [91]. This system has recently allowed the *in operando* NMR study of organometallic processes at pressures up to 70 bar [93–96]. The system has a titanium holder that couples to the tube, and delivers liquid, gas, and washing solvent. The reaction can therefore be fed with gas during the delays in the pulse sequences prior to excitation and acquisition, allowing efficient gas–liquid mixing and preventing the ‘starvation’ of the reaction. Additionally, the use of the liquid delivery system and wash unit makes it possible to conduct a series of batch reactions, washing the reactor between runs without taking it out from the spectrometer.

2.4.2.2. *In situ* illumination NMR. The use of *in situ* illumination devices is important both to study various photochemical processes (such as photocatalytic reactions and photoswitches), and for more NMR-focused applications such as photo-CIDNP (Chemically Induced Dynamic Nuclear Polarisation) and sensitivity amplification by use of *para*-H₂ (briefly discussed in Section 2.4.5) [97]. The properties of the light source (wavelength, intensity, efficiency and width of emission band) must be known, as these will influence the reaction being monitored. In addition, during *in situ* illumination NMR the sample must be irradiated in a uniform manner, particularly in optically dense samples, to maximise the sensitivity of the experiment and minimise concentration gradients. In this context, several devices involving irradiation from the bottom, the side or the top have been explored and reviewed in the literature [98,99].

In general, systems that involve illumination from above or inside the sample have been widely adopted due both to their simplicity and to their versatility and lack of spectrometer customisation required. The *in situ* illumination-NMR set-up in Fig. 9, first reported in 2013 [100] has been the most extensively used to date, with a number of applications in the study of organic and organometallic reactions [101]. The set-up is based on the use of a co-axial insert containing a sand-blasted fibre-optic cable, connected to a light-emitting diode, inside an amber 5 mm NMR tube. This allows uniform irradiation of the solution while preventing external interference. The use of the light-emitting diode (LED) as illumination source allows for narrow emission bands, high emission efficiencies, and the coverage of a wide range of wavelengths (265–1100 nm). In addition, the device is controllable directly from the NMR console, which is useful for investigating the behaviour of the reaction under both continuous and pulsed irradiation, important for testing for the presence of ‘dark’ processes [102].

Taking advantage of the simplicity of the *in situ* illumination-NMR system, the same group has developed a combined UV–VIS/NMR device that not only illuminates the reaction, but also allows simultaneous monitoring by NMR and UV–VIS spectroscopy [103]. Despite the wide applicability of both of these devices, they still present some limitations: they are not compatible with high-pressure tubes, they cannot be used to study reactions that need a constant supply of gases, and the *in situ* addition of liquids while illuminating is not yet possible. Moreover, although the individual

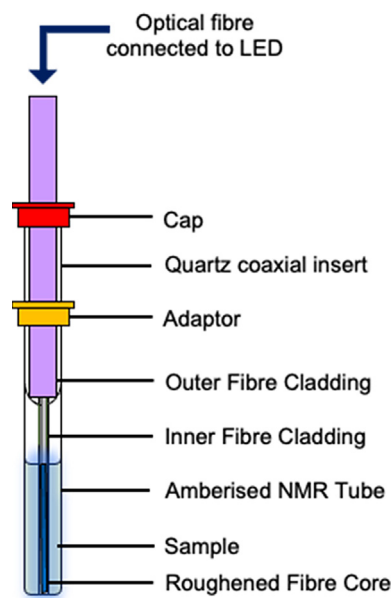


Fig. 9. Schematic representation of an *in situ* illumination NMR system [100,103]. For an example application of *in situ* illumination NMR see Case Study 15.

components can be purchased from commercial suppliers, the overall system is not, and currently has to be built in-house.

2.4.2.3. *In situ* Electrochemistry-NMR. The study of electrochemical reactions *in situ* may lead to the identification of important intermediates and the assessment of their structure, which is difficult by other sampling methods [104–106]. In addition to the advantages linked to monitoring the reaction by NMR, the use of electrochemistry means that it is also possible to measure the temporal evolution of the current, and electrochemical potential, and even simultaneously record a voltammogram [107]. However, precautions must be taken as the effect of a magnetic field in an electrochemical process is not innocent: the current density generated interacts with the magnetic field of the spectrometer to generate the so-called Lorentz force. As a result, the sample is stirred, which affects both the transport of electrolytes and the difference in potential between the solution and the electrode [108–110]. These are parameters of the utmost importance in reactions controlled by mass transport and charge transfer, respectively. To avoid drawing incorrect conclusions, it is highly advisable to assess whether this type of monitoring affects the kinetics and mechanism of the process, by comparison with a reaction outside the magnet.

Similarly to the *in situ* illumination devices, electrochemical cells also involve the use of NMR tubes and inserts containing electrodes, and have also not been commercialised to date, and must therefore be built in-house [106,108,111,112]. As with all in-house systems, they should be calibrated before use. For this purpose, the reduction of parabenzoquinone can be used as a test reaction. Contrary to the *in situ* illumination set-ups, *in situ* electrochemistry-NMR devices require radio-frequency filters (chokes) at the tops of the electrodes to attenuate the noise in both the NMR and electrochemical data caused by interference between the two components. In addition, the presence of the electrodes inside the NMR tube negatively influences the quality of the NMR spectra, leading to broadening of the signals and poorer signal to noise ratio. For this reason, the applicability of this technique has been restricted to simple reactions producing NMR signals with little or no overlap [113–115]. Different systems with different electrode configurations (wires, metal-coated thin-films, car-

bon fibres) have been reported in the literature, and their properties, ease of fabrication and influence in the NMR spectra reviewed [112]. However, no particular device has yet been widely adopted, and a more accessible and practical set-up is yet to be developed.

2.4.3. Real-time monitoring by flowing the sample into the spectrometer

A technique that is compatible with the real-time monitoring of reactions requiring a high degree of manipulation or control is on-line NMR. In this case the appropriate flow instrumentation is utilised to continuously pump a small proportion of the reactor contents through the spectrometer (Fig. 10).

This has been made possible by the development of different flow cells and NMR probes compatible with both high-field and low-field spectrometers [116–121]. For smaller reaction volumes, microfluidic flow probes have been developed, and are ideal for monitoring biological reactions with limited sample availability [122–125]. The general advantages of on-line monitoring are better control of the reaction parameters (temperature, pressure and stirring), compatibility with different types of reactors and reaction mixtures, and the possibility of adding chemical agents without the need to stop data acquisition [8,126,127]. In addition, reactions can be simultaneously analysed by other methods [128–130] and the use of a flow system can facilitate the concatenation of NMR with other analytical tools such as UV–VIS, IR or HPLC [131,132].

One of the parameters that influences the time-scale of the experiments to be monitored is the flow rate. Most systems do not employ a pre-polarisation reservoir, and thus the maximum flow rate will be limited by the nuclei with the longest T_1 present in the sample [133–135], although faster rates can be used if the effect of a flowing sample on the intensity of the signals is properly taken into account [39]. Thus, it is highly advisable to measure the T_1 relaxation times of all the nuclei to be monitored under static conditions, prior to carrying out monitoring under continuous flow conditions. Also, it is beneficial to check that appropriate NMR pulse flip angles and delays are being used while monitoring, as they may affect the signal intensity as well [39].

Undesired results arising from flowing a sample through the spectrometer can include insufficient pre-magnetisation (i.e. the unequal spin population required for the RF-pulse-induced FID, see Section 2.1.1) and incomplete purging (flushing out) of the active volume [134]. Efficient pre-magnetisation requires slower flow, efficient purging requires faster flow. Insufficient pre-magnetisation arises when the sample does not interact long enough with the magnetic field prior to application of the RF pulse, and leads to reduced signal intensities. In addition, the different T_1 values of the species being measured will translate into incorrect measured relative signal intensities. Pre-magnetisation can be improved by extending the residence time of the sample in the magnetic field prior to the RF pulse, either by reducing the flow rate or by lengthening the system within the high field region of the magnet using pre-magnetisation loops/coils. Alternatively, if measurements are carried out at a constant flow rate and the identities of the components are known, a mathematical correction of the signals can be made using known T_1 values [39]. In contrast to routine (static) NMR samples, the volume to which the RF-pulse has been applied and which is emitting the FID, is being 'purged' from the cell in the probe head in the continuous flow method. This flow-induced attenuation of the signal leads to a faster FID decay and thus broadening of the signals. Although the effects of flow in NMR monitoring have been extensively documented [134], their magnitude is dependent on the set-up being used (tubing, flow rate, spectrometer and NMR probe). Therefore, it is highly recommended that, when assembling a new flow-NMR set-up, the influence of the flow rate on the various effects

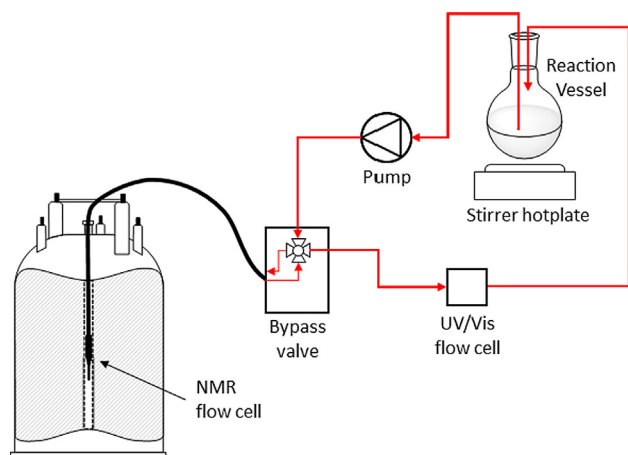


Fig. 10. Graphical representation of a closed-loop recirculating flow system for reaction monitoring, based on the work of Hintermair et al. [39]. For an example of flow NMR see Case Study 5.

discussed above be measured prior to the use of the system to acquire data. The major contributor to the broadening of the peaks can often be field inhomogeneity rather than the flow rate itself.

2.4.4. *In situ* assembly of reaction mixture within the spectrometer

The effective *in situ* monitoring of rapid non-equilibrium reactions (half-lives less than half a minute) requires either initiation by an external stimulus, e.g. a pulse of light, or assembly of the reaction from the different reactants inside the spectrometer. The main reason why these types of systems are only rarely used in reaction monitoring is that most such systems require bespoke probes, and spectrometer modifications. In all cases, the monitoring timeframe of these methods will be limited by their 'phenomenological dead time': the earliest time after initiating the reaction at which a pulse can be applied to acquire a satisfactory NMR spectrum. A number of processes contribute to this, including mixing, transport to the active volume, and cessation of any oscillations and pressure waves in the sample. The two techniques in this family that have been extensively used are rapid-injection (RI-NMR) and stopped-flow (SF-NMR).

2.4.4.1. Rapid-injection NMR (RI-NMR). In RI-NMR the reaction is set up and analysed in a batch mode: one of the reactants is injected into an NMR tube that is already located in the bore of the magnet and contains the rest of the reaction components (Fig. 11) [136]. The injection is achieved either by using a mechanical stirrer, with an impeller that is subsequently retracted from the active volume, or by the impact of a fast-moving solution jet. With the former the dead times are 1–2 s, whereas in the latter they can be as short as 0.03 s [137–139]. Because the reagents added are already located in the tube and therefore in the full magnetic field, all of the nuclei are fully 'pre-magnetised' (see Section 2.4.3). A major advantage to RI-NMR is the ability to use a very wide range of reaction temperatures, and to be able to add further samples of reagent to an evolving reaction mixture. However, in contrast to SF-NMR techniques, see below, the whole RI-NMR system (sample, stirrer and injector assembly) has to be removed from the probe and a new tube of reactants prepared for each experiment. Moreover, only a single reactant solution can be injected into the tube [140]. In addition, the dead volume (defined as the volume from the external reservoir to the injector tip) can be large, imposing limitations when using precious samples [137].

2.4.4.2. Stopped-Flow NMR (SF-NMR). Using this technique the reaction is initiated under flow conditions within the probe but the subsequent analysis is carried out under static conditions. In a classical stopped-flow set-up the plungers on two syringes containing the reagents are simultaneously pushed to deliver the solutions at a high flow rate into a highly-efficient mixer located inside the magnet, thus initiating the reaction (Fig. 11a) [141,142]. Due to the high flow rate, the pre-magnetisation of the samples is mainly achieved by storing the reagent solutions in small reservoirs located immediately before the mixer and in close proximity to the magnet centre [143,144]. The solution obtained after mixing is delivered into the NMR flow tube, and significantly greater volume (e.g. $\times 3$) is delivered than that required to fill the flow cell, in order to ensure complete 'push-out' of the previous contents by the fresh reaction mixture. The rapid flow continues until the waste-stream causes the plunger of the 'stop syringe' to hit a physical barrier, a so-called 'hard stop', and in doing so activates a micro-switch, which sends a trigger voltage to the spectrometer console. Prior to the hard stop, the reaction flow-cell contains a rapidly flowing, freshly-assembled reaction mixture, with reactant concentrations corresponding to a pseudo steady-state that has evolved during the short period of time between the reactants mixing and the reaction mixture leaving the reaction flow-cell. On rapid cessation of the flow, data acquisition can take place to monitor the decay from the initial pseudo steady-state condition.

In SF-NMR the phenomenological dead time strongly depends on the specific instrument design, but in general the technique is limited to reactions with half-lives greater than about 0.05 s, typically considerably greater [15,142–145]. For relatively fast reactions (lifetimes of a few tens of seconds or lower), the number of FIDs that can be acquired during a single run of the reaction can be insufficient for satisfactory kinetic analysis. In such cases, a series of reactions can be conducted, with a precisely incremented delay between the trigger signal and the first FID in each reaction. The combined ('interleaved') dataset then affords substantially enhanced temporal resolution of the reaction kinetics [15]. For irreversible chemical evolution of a reaction during FID acquisition to significantly affect the spectral linewidths, intensities, and phase, the half-life of the reaction must usually be ≤ 0.01 s [145]. Such processes are faster than the dead times of current SF-NMR systems, and these phenomena do not (yet) need to be taken into consideration [145].

The classical stopped-flow set-up (Fig. 11a) has some practical limitations: the total reaction volume is limited by the volume of the stop syringe, and the reagent solutions can only be mixed in a fixed volumetric ratio, usually 1:1, due to the use of a single pushing plate. These limitations have been recently addressed by the development of a hardware-controlled three-syringe driver system (Fig. 11b) [15,29]. In this system the volumetric ratios between syringes can be programmed and the acquisition triggered after delivering the desired volume, using a 'soft-stop' system based on the resistance to flow in the overall circuit. This new design allows a systematic and precise evaluation of concentration-dependent reaction parameters, without the need to replace the syringes or take out the sample tube. Limitations of stopped-flow NMR techniques include restriction to homogeneous reactions, and in contrast to Rapid Injection NMR, the inability to add reagents partway through the monitoring process. Moreover, none of the set-ups highlighted above is yet suitable for monitoring processes occurring at high pressure or involving/generating gases.

2.4.5. Hyperpolarisation

The sensitivity of NMR experiments is inherently limited by the small thermal equilibrium difference in populations between different nuclear energy levels. While not a specialised sampling or

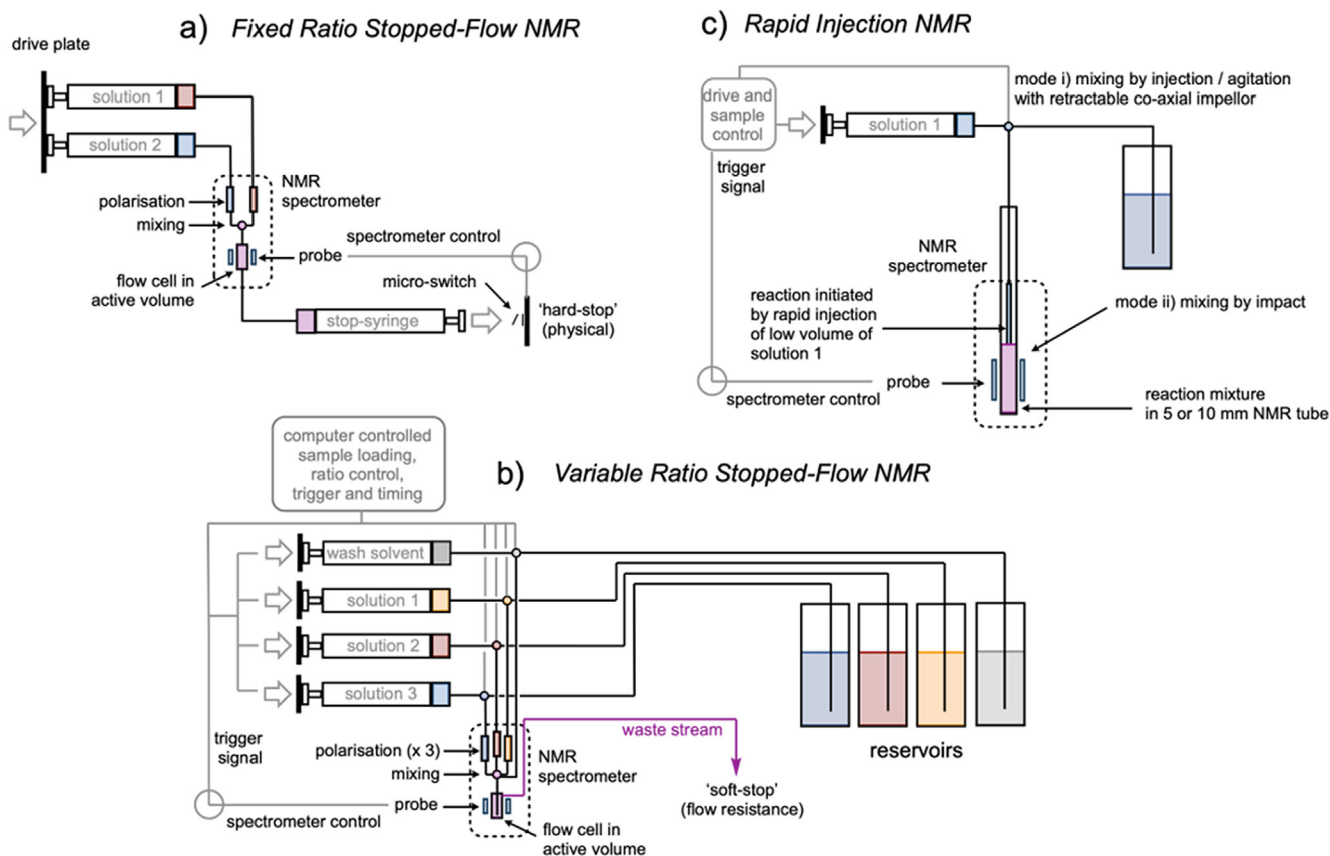


Fig. 11. Schematic representations of (a) the classic SF-NMR technique (b) variable volumetric ratio SF-NMR technique [15], and (c) Rapid-Injection NMR technique. For examples of the application of variable ratio SF-NMR see Case Study 3, and for RI-NMR see Case Studies 2 and 6.

monitoring technique as such, the hyperpolarisation technique boosts the NMR signal by artificially altering these populations. *Para*-Hydrogen Induced Polarisation (PHIP) uses *para*-hydrogen generated at low temperature to generate hyperpolarisation when the hydrogen is reacted with a metal centre [146]. PHIP and associated polarisation transfer experiments such as SABRE (Signal Amplification By Reversible Exchange) can be used in reaction monitoring to increase sensitivity, and are particularly useful for measurements at low field [13,14,147]. Dynamic Nuclear Polarisation (DNP) uses microwave irradiation at low temperature to transfer polarisation from unpaired electrons, with potential signal enhancements of several thousand times [148]. DNP has not yet found widespread use in reaction monitoring due to the cost and complexity of the apparatus required, however a few examples have been reported in the literature [149,150].

3. Measurement, Processing, and quantification

3.1. Temporal resolution

High temporal resolution is essential for monitoring fast reactions. However, the conventional preparation steps (Section 2.1.1) before the execution of the pulse sequences delay the collection of data, and important information may have been lost before the measurement begins. In the extreme, specialised techniques (Section 2.4), such as rapid injection methods [137–139,151], and stopped-flow devices [15,29,142,152,153] are essential.

A limiting factor on temporal resolution is the repetition rate of successive scans, determined by the longitudinal relaxation times (T_1 , Section 3.2) of the spins being detected. To avoid saturation,

the magnetisation should be allowed to recover to thermal equilibrium before the next pulse. For a multiple-spin system, and a 90° pulse, the delay normally needs to be 5 times the longest T_1 value, so that all spins approach $\geq 99.3\%$ equilibrium before the next pulse. If this condition is not met, the differential relaxation of spins can lead to significant integration errors, and we strongly advise estimation of T_1 values *before* kinetics experiments are conducted. Shorter interscan delays can be allowed by using smaller pulse flip angles, at the cost of reduced sensitivity, or by adding paramagnetic relaxation agents [154–156], at the cost of reduced peak resolution (and potential perturbation of the chemistry under study).

An alternative strategy to allow more data acquisition in a given timescale relies on the interleaving process, which is practically a pseudo real-time approach [157]. Interleaving requires accurate and precise control of the timing, as each datapoint, or subset of datapoints, in the final dataset is collected by an individual measurement. For fast reactions interleaving is conducted using rapid injection or stopped-flow methodologies (see Section 2.4.4). For slow reactions where kinetic data density is easily attained, interleaving of different NMR experiments (different nuclei, selective excitation etc.) can make use of the time between data points to acquire complementary data at no additional cost in time [158].

3.2. Longitudinal relaxation, T_1

Longitudinal relaxation time, T_1 , determines the interscan delay required between acquisition cycles for accurate quantification. There are a variety of well-established methods for T_1 determination including 'inversion recovery' [159,160], 'progressive

saturation' [161], 'saturation recovery' [162], and the 'null approximation'. Inversion recovery (Fig. 12a) is by far the most widely used. A series of spectra are acquired (Fig. 12b) in which τ , the delay time between the 180° and 90° pulses, is varied. The T_1 value is determined by fitting to Eq. (1), in which I_t is the measured signal intensity and I_0 the intensity at thermal equilibrium (Fig. 12c). A minimum of 10 variations in τ is recommended, with the relaxation delay (RD) and the largest τ value both set to $\geq 5 T_1$. If RD is too short T_1 could be underestimated.

$$I_t = I_0 \cdot (1 - 2 \cdot e^{-\tau/T_1}) \quad (1)$$

The inversion recovery method can be time-consuming, and most work in the authors' group now routinely employs a saturation sequence ('FLIPS', Fig. 13a) [163]. FLIPS allows rapid estimation of T_1 values with sufficient accuracy for parameterising pulse sequences for kinetics determination. FLIPS uses a train of pulses to establish a steady-state where relaxation and excitation reach a dynamic balance. The T_1 value is estimated using Eq. (2), where I_0 and I_{SS} are the thermal equilibrium and the steady-state signal intensities (Fig. 13b).

$$T_1 = \frac{t_R}{\ln \left[\frac{I_0 \sin \theta - I_{SS} \cos \theta}{I_0 \sin \theta - I_{SS}} \right]}; \quad \text{when } \theta = 90^\circ, \text{ then } T_1 = \frac{t_R}{\ln \left[\frac{I_0}{I_0 - I_{SS}} \right]} \quad (2)$$

3.3. Spatially-selective acquisition

One method to overcome the limitations imposed by relaxation on acquisition rate is to use different volumes ('slices') within the sample for each data point, in a similar way to an MRI experiment. Electrical current is supplied to a coil around the sample, creating a linear gradient in the magnetic field strength along the sample length (Fig. 15) and causing the Larmor frequency of the nuclei to vary as a function of position. A selective pulse is applied to excite each slice individually and the spectrum recorded [5,164]. Providing that sample motion (diffusion, convection, etc.) between slices is slow, the magnetisation in each slice can be sampled independently of its neighbours. The latter aspects means that the technique cannot be applied with flow-NMR (Section 2.4.3).

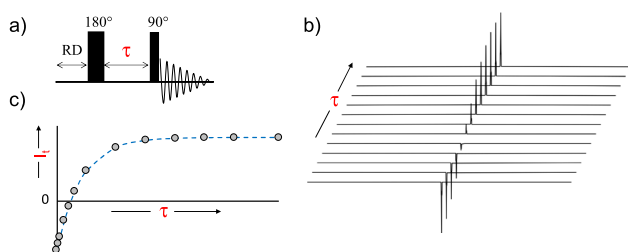


Fig. 12. (a) The inversion recovery method for determination of T_1 . The experiment (b) is repeated with variable delay time τ ; and data fitted (c) to Eq. (1) to give T_1 .

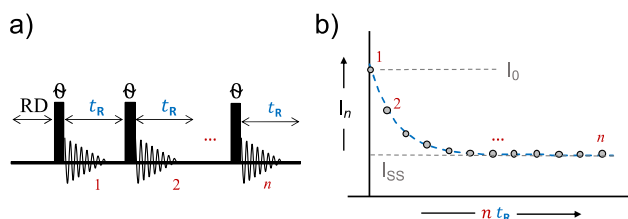


Fig. 13. The 'FLIPS' method for rapid estimation of T_1 . Identical pulses are spaced by repetition time, t_R . The method requires that $5 T_1 > t_R \gg 2 T_2$, to ensure complete loss of transverse components, without allowing complete relaxation to thermal equilibrium between the pulses [163].

Sampling slices in parallel with different pulses/delays applied to each slice allows 2D spectra to be constructed in a single scan (Section 3.6). Alternatively, sampling each slice separately allows reaction kinetics to be monitored, without having to wait for relaxation of the whole sample between each measurement [165]. However, as each slice is a small volume of the total reaction, the signal-to-noise decreases as a function of the slice size (volume). This means that spatially-selective experiments require more concentrated samples than conventional NMR experiments. To minimise cross-talk, slices should be sampled in a non-adjacent manner. Care should also be taken to account for B_1 inhomogeneity which will affect the absolute signal intensities in the various slices (Fig. 14).

3.4. Integration and automation

The quantitative capability of NMR undoubtedly empowers the technique for versatile application in the investigation of reaction mechanisms. It provides a platform to determine kinetic and thermodynamic data, including reaction rate, chemical equilibrium, identification of side products, selectivity, etc. In an NMR spectrum, chemically distinct spins give rise to signals whose area, under the correct measurement conditions, is proportional to the number of nuclei. This species-independent direct proportionality is one key advantage of NMR over other techniques such as mass spectrometry, infra-red and UV-Vis spectroscopy, and chromatographic methods, all of which require calibration curves for quantitative reference. Quantitative NMR can be divided into relative and absolute methods [19,166]. Relative quantitation compares the integrals of signals with one another and determines the ratio of different compounds by employing Eq. (3), where M , I , and N are molar ratio, integral and number of nuclei respectively.

$$\frac{M_x}{M_y} = \frac{I_x}{I_y} \cdot \frac{N_y}{N_x} \quad (3)$$

For absolute quantitation, a known concentration standard compound, or digital reference signal [18] is needed (see Section 2.1.2) in addition to the relative quantitation method. With the known standard compound concentration and number of nuclei contributing to each signal, the absolute values of concentration of the analytes can be obtained by employing Eq. (4), or the purity of analytes by using Eq. (5) where P , I , N , M , and W are compound purity, signal integral, number of nuclei, molar mass and gravimetric weight respectively.

$$C_x = \frac{I_x}{I_{std}} \cdot \frac{N_{std}}{N_x} \cdot C_{std} \quad (4)$$

$$P_x = \frac{I_x}{I_{std}} \cdot \frac{N_{std}}{N_x} \cdot \frac{M_x}{M_{std}} \cdot \frac{W_{std}}{W_x} \cdot P_{std} \quad (5)$$

3.4.1. Signal-to-Noise ratio (S/N)

Good S/N is essential to ensure accurate NMR quantification [19,166]. Eq. (6), where N is the population of spins in the system, γ_{exc} and γ_{det} are gyromagnetic ratio of the excited nucleus and the detected nucleus respectively, T_2 is the transverse relaxation time, B_0 is the external magnetic field, NS is the number of scans, T is the sample temperature, and T_c is the probe coil temperature, indicates parameters that affect the S/N. [19]

$$S/N \propto \frac{N \gamma_{exc} T_2 (\gamma_{det} B_0)^{\frac{3}{2}} \sqrt{NS}}{T \sqrt{T_c}} \quad (6)$$

It can be seen from the equation that spectrometers with higher magnetic field strength (B_0) provide higher sensitivity. The type of probe [167] will also have a large effect; cryoprobes cool down the

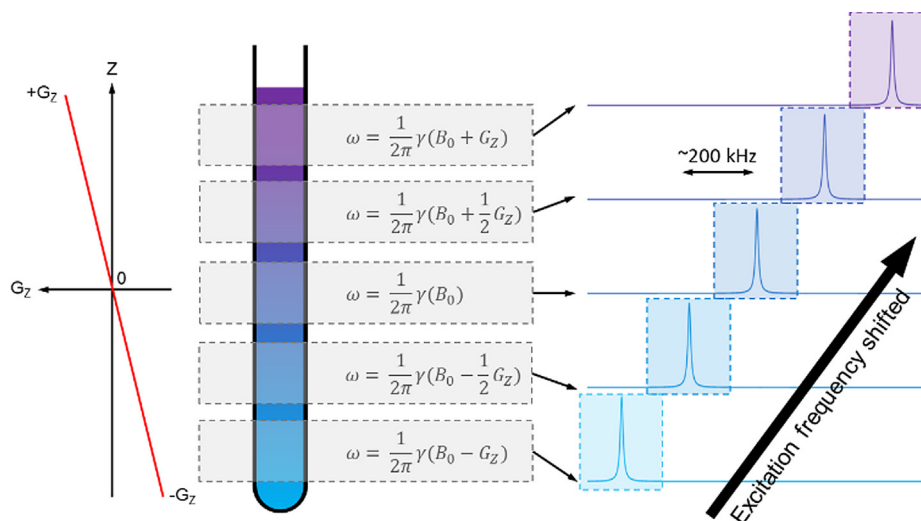


Fig. 14. General principle of spatially-selective NMR. A magnetic field gradient is applied causing the Larmor frequency to vary as a function of position. Selective excitation at the Larmor frequency allows spatially resolved slices to be detected, with the frequency of each slice offset due to the gradient. For an example of the application spatially selective acquisition see Case Study 6.

RF coil and resonant circuit to about 77 K (N_2) or 20 K (He) to reduce the noise from the electronics. Helium cryoprobes routinely provide an approximately 3.5-fold increase in S/N over an ambient temperature probe. Usually one is limited to the spectrometer that is available, so in practice, the S/N can be adjusted by changing the acquisition and processing parameters, see Sections 3.4.2 and 3.4.3. The simplest changes, increasing the number of scans (NS), or the sample concentration, which directly determines the population of nuclei (N) contributing to the signal, or changing the type of NMR tube (i.e. the volume of sample in the active coil region) all have an immediate and predictable effect.

For a given repetition time t_R and known T_1 value of spins detected, an optimal pulse angle θ , referred to as the Ernst angle [168] can be determined, to give the highest S/N; Eq. (7). However, care must be taken with regard to quantitation, and careful selection of an internal standard that has a similar T_1 value to the species being monitored is one strategy to minimise errors (see Section 2.1.2).

$$\theta = \arccos(e^{-t_R/T_1}) \quad (7)$$

3.4.2. Acquisition parameters

To obtain quantitative NMR spectra, an essential feature for analysis of kinetic isotope effects, especially those arising from heavy atoms (Section 5.3) a range of factors need to be considered carefully before the acquisition.

3.4.2.1. Shimming. Well-resolved peaks are a pre-requisite for accurate quantitation, and signal overlap hinders spectral interpretation. In order to generate sharp signals where the linewidth at half-height $\Delta_{1/2} = 1/(\pi T_2)$ is only limited by the inherent transverse relaxation, the static magnetic field across the whole sample volume needs to be homogenous. Good shimming is a process to minimise the field inhomogeneity by adjusting the currents in a set of 'shim coils' around the probe. These coils create small magnetic fields that correct small inhomogeneities in the field of the main magnet, such that the sample experiences a near-homogenous field overall. Shims are designed to produce fields with different geometries and detailed examples of 'imperfect' FIDs caused by particular types of poor shimming and their corresponding Fourier transformed peaks have been reviewed [169]. Nowadays the shimming process is generally conducted automatically,

however, if one suspects distorted peaks are arising from poor shimming, one can manually optimise the relevant shimming parameters [169].

3.4.2.2. Acquisition time and repetition time. Acquisition time plays an essential role in sensitivity and quantification. If the acquisition time is too short, the FID truncation will result in 'wiggles' alongside the peaks in the final NMR spectrum. Conversely if the acquisition time is too long, then the tail of the FID is simply recording noise, rather than signal, thus reducing the S/N. An appropriate relaxation delay between pulses in acquisition of sequential spectra is vital for quantitative measurements. For a multi-spin system, the repetition time needs to be long enough for the slowest relaxing spin to fully recover. Therefore, a knowledge or estimation of the T_1 values (Section 3.2) for all of the species that will be monitored is valuable prior to experiments; with judicious choice of signals in the species present, a sub-set of signals can be monitored if required.

3.4.2.3. Receiver gain. To allow processing and storage on a computer, the analogue signal detected by the probe must be converted to a digital signal. To ensure that the signal fills the full range of the analogue-to-digital converter the analogue signal is amplified by a receiver gain (RG) factor before digitisation. If the RG is too low, the NMR signal will occupy only part of the digital range, leading to a reduction in vertical (voltage) resolution in the FID. Conversely, if the RG is too high the receiver will become saturated and broad 'sinc' wiggles may be observed in the baseline of the FT spectrum [170]. For quantitative analysis of signals, it is sufficient to select an RG value that allows the time domain signal (FID) to fit comfortably within the dynamic range of the analogue-to-digital converter. A calibrated receiver gain function method [171] can be implemented to allow quantitative comparison between separate experiments recorded with different RG.

3.4.2.4. Excitation bandwidth. For quantitative assessment, all resonances must be excited equally across the whole chemical shift range. Setting the transmitter frequency offset at the midpoint of anticipated or known range of resonances, for the entire set of reaction components, is a reasonable first approach. For more uniform excitation, the CHORUS pulse sequence [172,173] can be employed to increase the quantitative bandwidth, particularly for

spectra with wide chemical shift range (e.g. ^{13}C , ^{19}F , and ^{31}P). However, it is noteworthy that a rectangular excitation pulse of duration t_p gives >95% excitation over an effective spectral width (in Hz) of approximately $\text{SW} = 1/(4 \times t_p)$, where t_p is generally in the order of tens of microseconds. Tuning, matching and pulse calibration help ensure optimal pulse amplitudes. Pulse calibration is advisable before performing experiments that are particularly sensitive to pulse angle, such as those with large numbers of refocusing or inversion pulses where small variations in pulse amplitude may accumulate, reducing the signal, however for most experiments the default pulse calibration usually suffices. In practice, using smaller pulse angles for higher temporal resolution also comes with the benefit of broader excitation coverage. Therefore, it is not a problem for nuclei such as ^1H with a typical chemical shift range of $\sim 10\text{--}15$ ppm, but for nuclei that cover a much larger frequency range, for example ^{19}F nuclei – often used for reaction monitoring – achieving uniform excitation can be more challenging. Indeed for reactions where a wide range of ^{19}F chemical shifts are present, the quantitation can be compromised for nuclei at the ‘edge’ of the spectrum if conventional 90° pulse excitation is used. If this is not taken into account, later analysis of the reaction kinetics may be significantly impacted by under-estimation of the concentration of the signals close to the edges of the spectrum.

3.4.2.5. Spectral width. It is important to make sure that the spectral width (SW) is sufficient that all signals from species present in the reaction mixture are captured, or, if some are to be omitted, that they are well away from the edge of the spectral window. Signals that are within the spectral window but too close to its edge may be affected by receiver filters, leading to phase and amplitude distortion. In general, it is recommended to extend the spectral window approximately 10% beyond the signals at both edges. Signals that are insufficiently outside of the spectral window can cause signal folding or alias peaks, that is, a peak at a frequency ($f_{\text{max}} + F$) greater than the Nyquist frequency (f_{max}) would appear at the incorrect frequency at $(-f_{\text{max}} + F)$ [4], where $f_{\text{max}} = 1/(2\text{DW})$, DW is the dwell time. Such folded signals are usually harder or impossible to phase, and can be recognised by the way their frequencies change on changing the transmitter offset.

3.4.2.6. Broadband decoupling. Heteronuclear decoupled experiments are sometimes necessary to achieve a simplified spectrum with better-resolved signals. This can allow species to be more accurately quantified, and can be especially useful in cases where satellites, e.g. due to $^1J_{\text{CH}}$ for strong ^1H NMR signals of carbon bound hydrogens, overshadow neighbouring weak signals arising from intermediates or side products. Composite pulse sequences such as WALTZ and GARP are still commonly used for effective heteronuclear decoupling. However, adiabatic methods such as CHIRP pulses are now recommended, as they offer wider decoupling bandwidths, in addition to reducing sample heating. If applied, different decoupling modes should be evaluated carefully. For example, ^{13}C spectra recorded with continuous ^1H decoupling are rarely straightforwardly quantitative, due to the Nuclear Overhauser effect (NOE) build-up during the relaxation delay [174,175]. To improve quantitation, decoupling should be applied only during the acquisition time and turned off during the relaxation delay time, with a long relaxation delay (or if chemically feasible, the addition of paramagnetic relaxation agents) for full magnetisation recovery and dissipation of the NOEs. This inverse-gated decoupling is also commonly utilized in ^{15}N or ^{29}Si acquisition to suppress NOE build-up as these negative gyromagnetic ratio nuclei exhibit negative NOE enhancements, which can lead to reduced or even negative signals for the observed nucleus. It is not infrequent to find that quantitation has been assumed (but not tested) in an NMR investigation, e.g. using $^{31}\text{P}\{^1\text{H}\}$ NMR signals from phos-

phine ligands in an organometallic process, resulting in large errors propagating unnoticed into the kinetic analysis and reporting of rate and equilibrium constants etc.

3.4.3. Post-acquisition parameters (processing)

3.4.3.1. Window functions (apodization). There are different types of weighting functions available in most processing software and these functions have different effects on sensitivity and resolution. For example, multiplying the FID by a decaying function can improve the sensitivity (or more strictly, the signal-to-noise ratio, S/N), but at the penalty of signal broadening. For well-resolved signals in a reaction time series, such a function can be of benefit. In contrast, multiplying the FID by a function that first rises and then falls can enhance resolution but at the cost of sensitivity. A reasonable compromise of weighting function is usually used, with a half-Gaussian function being a popular choice. It is important to note that not all weighting functions are appropriate for quantitation, as functions where the first point is zero result in zero integral in the normal phase-sensitive spectrum and are therefore of very limited value for quantitative NMR.

A distorted baseline obstructs the accurate quantification of signals, and significant baseline rolls can even disguise extremely broad, weak signals in a spectrum. Methods for flattening the baseline can be generally categorised into time-domain baseline correction and frequency-domain baseline correction. Time-domain methods correct data points in the FID. For example, a major source of baseline artefacts lies in corruption of the first points of the FID caused by strong, rapidly decaying background signals from materials used in the construction of the probe or NMR tube (commonly observed for ^{10}B , ^{29}Si and ^{19}F). Acoustic ringing caused by RF pulses inducing mechanical resonance of metallic components in the probe also causes strong, rapidly decaying signals to appear in the FID, particularly for nuclei with low Larmor frequencies. A third source of baseline artefacts is ‘ring-down’ caused by the dissipation of pulse energy in the probe electronics and is commonly observed with cryoprobes. In most cases the corrupted points can be deleted and the missing information replaced by backward linear prediction [176], while proper setup of the pre-acquisition delay can reduce the effects of ring-down. Frequency-domain correction methods reconstruct the baseline in Fourier transformed spectra by applying algorithms that distinguish between signal and baseline regions, and then subtract a function that is fitted to the baseline [177–179]. Modern spectrometers and software today offer both automated and manual baseline correction approaches to this process. However, such techniques must be applied with great caution. Signals from reaction intermediates that are involved in dynamic processes, and as a result have broad lines, can experience apparent intensity distortions as a result of inappropriate baseline correction, leading to highly misleading integrals and erroneous reaction kinetics. Comparison of relative integrals of various species in the reaction mixture before and after baseline correction is advisable.

3.4.3.2. Phase correction. Phase correction is routinely applied during processing of a spectrum. It aims to adjust the signals to pure absorption mode lineshape, or to maximise peak symmetry. Although auto-phasing is available in most software and is fast to carry out, it is recommended that spectra should be manually phased for a more accurate result. This is particularly important for low-intensity signals, which can be of great relevance, for example, in the analysis of kinetic isotope effects (Section 5.3). Phase correction includes both a zero-order correction, applied equally across the whole spectrum regardless of offset, and a first-order correction, which corrects phase errors that vary linearly with the offset. Excessive first-order phase correction, caused

by an incorrect pre-acquisition delay, can cause baseline distortion and affect quantitation.

3.4.3.3. Zero-filling. Before the FID undergoes Fourier transformation into the frequency domain, it is composed of time-domain data points which define the signals. Zero-filling is a post-acquisition manipulation that adds a set of data points (zeroes) to the end of the original FID, where the signal has normally already decayed close to zero, so that the signals in the Fourier transformed spectrum are better represented by more data points. Adding the same number of zeroes as there are experimental points to the end of the FID before transformation both doubles the amount of information in the resultant spectrum and improves digital resolution. Further zero-filling just interpolates between data points, but may still aid interpretation.

3.4.3.4. Integration region. A reliable method for determining the strength of an NMR signal is essential for quantitative analysis of reaction kinetics, titrations, equilibria, etc. The most common way of determining peak area is by integration, however peak fitting can also be used. It is imperative that integral regions are consistent throughout a series of spectra. Thus, for instance, one must consistently include or exclude satellites for all peaks measured. If the satellites severely overlap with neighbouring signals, then appropriate decoupling or filtration [180] is recommended (Section 3.4.2.6). The integral regions should cover the same proportion of each peak; for example, integrating a single Lorentzian over a range of at least 20 times the line width in either direction should cover 99% of the peak area, however smaller integration regions may be more appropriate if peaks are close together.

3.4.4. Spectral deconstruction

In complex reaction mixtures it is common to encounter overlapping peaks, particularly when spectral dispersion is limited or peaks are broad, but for which relative quantitation is required. 2D NMR can help separate overlapping peaks (Section 3.6), however 2D NMR is not always a practical or desirable solution, and in such cases deconvolution of spectra by mathematical fitting of peaks is the best method to separate overlapping resonances.

In principle, NMR peaks are purely Lorentzian in shape, however in practice distortions caused by magnetic field inhomogeneity, relaxation and chemical kinetics mean that hybrid functions with more degrees of freedom (for example a Voigt function comprising a mixture of Lorentzian and Gaussian functions) can provide a better fit [4]. Fitting a single NMR spectrum using multiple Voigt functions is straightforward, however automatic fitting of large numbers of spectra from reaction monitoring can be problematic as there are often several ways in which a given peak can be fitted (Fig. 15). Generally, minimising the number of degrees of freedom by using fewer peaks and restricting large changes in linewidth and position between adjacent spectra tends to provide

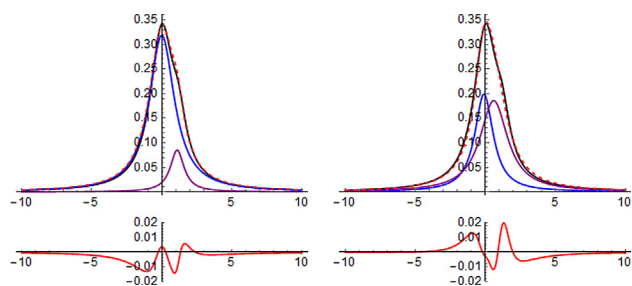


Fig. 15. Two possible pairs of fitting functions (blue and purple) to fit the same data (black). Both sets of functions result in a comparable residual (red) but with very different component weightings.

the best results when fitting large datasets. Once a dataset has been deconvoluted, and the data is analysed, e.g. in a kinetics simulation, it is important to remember that the deconvolution may not be correct for some or all data points. Chemical common sense should prevail, and the deconvolution returned to for reprocessing if required.

3.4.4.1. Principal component analysis. The number of variables used in peak fitting (frequency, linewidth, peak shape, amplitude) usually exceeds the number of variables that are changing due to the reaction. Principal Component Analysis (PCA) offers a more intelligent way of processing data, by identifying the variables (principal components) which contribute the most to changes between spectra, ignoring any variables which are not statistically significant [181]. In this way the dimensionality is reduced to include only those variables which are important to the reaction kinetics.

3.4.4.2. Spectral hard modelling. Whilst PCA makes no prior assumptions about the data, an alternative method is to construct a model based on known information about the reaction species. A model is constructed for each species, either directly from a pure component spectrum or indirectly from spectra containing different mixtures [182,183]. Since the relative integrals of the peaks in each molecule remain constant, this adds 'stiffness' to the model, reducing the number of degrees of freedom and hence reducing fitting uncertainties. The reaction spectra are then modelled as a linear combination of the pure components.

3.4.4.3. Reference deconvolution methods. Reference deconvolution methods can be used to remove systematic imperfections that affect all peaks in the spectrum equally [184]. The lineshape of an internal reference singlet peak is compared to the idealised shape to produce a correction waveform which is applied to the experimental FID. The Fourier transform of the corrected FID produces a frequency domain spectrum where all peaks have an ideal lineshape.

3.5. Pure shift NMR

Pure shift NMR, also known as broadband homonuclear decoupled NMR, aids in the interpretation of overcrowded or poorly resolved spectra, and can be particularly useful for complex reaction mixtures with numerous intermediates or side products. Pure shift techniques address this problem by eliminating the effect of homonuclear scalar couplings while retaining the chemical shift information. As a result, multiplets are collapsed into singlets, where one singlet represents one distinctive chemical site, hence offering much 'cleaner' spectra. Despite the sensitivity reduction and generally long experimental time, the unique characteristic of significant enhancement in spectral resolution of pure shift NMR still empowers this technique with the capability to resolve signals that are difficult to assign in conventional NMR.

Comprehensive reviews on this relatively recent area can be found in publications; [185,186] the main pure shift approaches [187–191] are introduced here chronologically, based on their date of publication. BIRD [187] (Bilinear Rotational Decoupling) utilizes the low isotopic abundance of ^{13}C (1.1%), by decoupling a ^{13}C -bound proton from its neighbouring ^{12}C -bound protons. Scalar couplings between geminal protons are thus excluded from BIRD decoupling as they are bound to the same ^{13}C nucleus. Although providing high-quality quantitative spectral data, BIRD decoupling comes at the cost of sensitivity –1.1% of a normal spectrum. The idea of a spatially- and frequency-selective decoupling method, introduced by Zangger and Sterk [188], employs a weak pulsed field gradient along with a selective refocusing pulse. Different

locations in the NMR sample tube experience different magnetic fields, allowing signals at different chemical shifts to be spatially-selectively decoupled. One limitation of this method is its low sensitivity: the more selective the slice-selective excitation pulse, the lower the sensitivity. The band-selective approach [189] is particularly efficient when only a targeted region of the spectrum requires analysis. The difference between the band-selective and Zangger-Sterk pulse sequences is the absence of the weak pulsed field gradient. Band-selective decoupling only suppresses the effects of coupling to spins outside the selected band of frequencies, but has excellent sensitivity because all spins in the selected region contribute to the measured signal.

SHARPER [190] (Sensitive, Homogenous, And Resolved PEaks in Real time) presents a pure shift method that is particularly suitable for the analysis of chemical reactions and the monitoring of reaction kinetics. This method focuses on a single selected signal and removes its heteronuclear couplings (and homonuclear couplings in the case of *sel*-SHARPER), generating an extremely narrow singlet with significant improvement in the *S/N*. PSYCHE [191] (Pure Shift Yielded by CHirp Excitation) uses two low pulse angle (approximately 15°) chirp pulses that sweep frequency in opposite directions. This pair of frequency-swept pulses separates the nuclear spins into two populations, where the separation is purely statistical. *J* refocusing is achieved by the combination of the CHIRP pulses and a hard 180° pulse; the magnetic field gradient during the CHIRP pulses serves to suppress signal pathways that do not refocus the effects of *J*. PSYCHE is relatively sensitive, and particularly robust in strongly coupled systems.

The main benefits of the SHARPER experiment lie in its line narrowing effect and significant *S/N* enhancement (~20-fold gains for the reported ¹⁹F measurement) in heteronuclear and homonuclear decoupling while the quantitative capability is still retained. It is particularly tolerant of pulse imperfections and of magnetic field inhomogeneity, both static (e.g. shims) and dynamic (e.g. gas generation), allowing analysis of chemical reactions and equilibria in challenging environments. However, the technique is limited to analysis of one selected resonance at a time. The basic SHARPER experiment adopts the pulse sequence of Fig. 16 and removes broadband heteronuclear couplings by pulsing on the detected nucleus only. Without the necessity of pulsing on the decoupled nucleus channel as in traditional heteronuclear decoupling methods, this feature tackles spectrometer hardware limitations where the delivery of dual radio frequencies, for example ¹H and ¹⁹F pulses, is problematic. This ‘single channel heteronuclear decoupling’ executes the simultaneous removal of all splittings caused by *X* nuclei for the signal of interest.

Minor modifications of the SHARPER experiment lead to the *sel*-SHARPER pulse sequence (Fig. 17), where both heteronuclear and homonuclear decoupling is achieved. This pure shift experiment

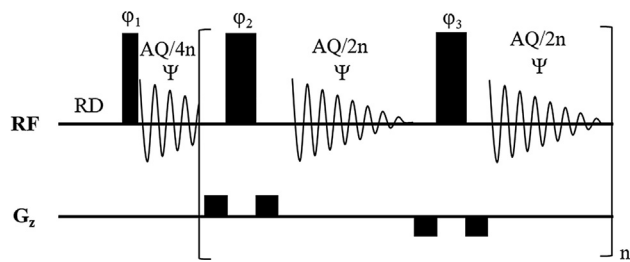


Fig. 16. Pulse sequence of SHARPER experiment. Narrow and wide filled rectangles represent 90° and 180° pulses respectively. Phase cycle: $\phi_1 = 2x, 2(-x), 2y, 2(-y)$; $\phi_2 = 2(y, -y), 2(x, -x)$; $\phi_3 = 2(-y, y), 2(-x, x)$; receiver phase: $\Psi = 2x, 2(-x), 2y, 2(-y)$. Low-level field gradient pulses (PFGs) are applied surrounding the inverting pulses, loop parameter *n* denotes the number of loops for the double 180° pulses. See Case Study 8.

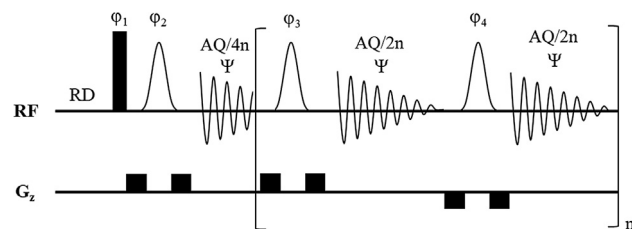


Fig. 17. Pulse sequence of *sel*-SHARPER experiment. Filled rectangles represent 90° pulses, un-filled shapes represent 180° selective pulses. Phase cycle: $\phi_1 = 4x, 4(-x), 4y, 4(-y)$; $\phi_2 = 2y, 2x, 2(-y), 4(-x), 2y, 2x, 2(-y)$; $\phi_3 = 4(y, -y), 4(x, -x), \phi_4 = 4(-y, y), 4(-x, x)$; receiver phase: $\Psi = 2x, 4(-x), 2x, 2y, 4(-y), 2y$. Low-level field gradient pulses (PFGs) are applied surrounding the inverting pulses, loop parameter *n* denotes the number of loops for the double 180° pulses. See Case Study 8.

utilises the same real-time acquisition method as SHARPER, with the acquisition time divided into chunks separated by two selective 180° pulses that invert the subset of passive spins while leaving the active spins unperturbed. The acquisition sequence is looped, with each successive chunk appended to the end of the FID to construct the time domain spectrum. The phases of the pulses and receiver are rotated by 90° between chunks to compensate for pulse imperfections and static magnetic field inhomogeneity. This results in substantial sensitivity improvement by collapsing the multiplets in the normal ¹H-coupled spectrum to a narrow singlet (typically < 0.5 Hz linewidth) in the *sel*-SHARPER spectrum. Chemical equilibrium kinetics can also be studied by analysing the excess line broadening of signals, arising from the relaxation caused by fast chemical exchange. [190]

In general pure shift spectra can be used for quantitative measurements, providing appropriate precautions are taken. Spin manipulations including the selective pulses used in Zangger-Sterk, band-selective and *sel*-SHARPER experiments mean that integrals from different parts of the spectrum cannot be directly compared, in part because different signals will experience different relaxation losses, however integrals from a single peak can be compared across successive spectra acquired with the same parameters. The distinct benefits of pure shift NMR methods have mostly been applied in the analysis of ¹H-detected species. However, we expect applications of this technique in reaction monitoring, and in the interrogation of exchange processes and equilibria via analysis of other nuclei, to grow.

3.6. 2D acquisition

Two-dimensional NMR techniques [192,193] provide valuable information about the couplings between nuclei which may be used to help determine the structures of intermediates and products in reaction monitoring.

3.6.1. Quantitative 2D NMR

2D NMR is usually considered to be a non-quantitative technique, since peak volumes are dependent not only on the *T*₁ and *T*₂ relaxation times (cf. quantitative 1D-NMR, q1D), but also coupling constants, evolution delays, pulse imperfections and other pulse sequence variables [194]. The large number of parameters involved in 2D acquisition makes generating quantitative 2D spectra (q2D) much more complicated than q1D. For most purposes, including use for determining the structures of reaction intermediates and products, it is not necessary to acquire fully quantitative 2D spectra. Useful information can still be obtained by comparing the integrals of a single peak in successive spectra acquired with the same parameters, even when the relative integrals of different peaks in the same spectrum are not quantitative. The exception is when 2D NMR is being used to determine concentrations of species

with overlapping peaks that cannot be quantified by other means. The simplest approach to obtaining quantitative concentration data from 2D spectra is to build a calibration curve using known concentrations of reagents and internal standard (Section 2.1.2) that can be used to convert peak volumes to concentration [195]. This approach is common across other analytical techniques such as mass spectrometry and infrared spectroscopy, but is time consuming and requires reaction and calibration data to be acquired under identical conditions. Additionally, many reactive intermediates that are of interest for reaction monitoring are too short-lived to allow calibration using this method. If relaxation rates, coupling constants and other pulse sequence parameters are known, the calibration factor for each peak may be calculated [196], however this presents many of the same challenges as acquiring a full calibration curve.

An alternative approach is to design the NMR experiment to eliminate or otherwise minimise sources of quantitation errors. The number of parameters involved in 2D acquisition makes this challenging, however pulse programs can be modified to compensate for delays and evolution of *J*-coupling [197–200]. A more general approach is the extrapolated time-zero HSQC₀ experiment [201,202].

Instead of compensating for pulses and delays individually the HSQC₀ experiment treats the HSQC pulse sequence as a process that attenuates the signal for each peak. Repeating the part of the HSQC sequence following the initial 90° pulse twice would therefore mean that the signal is attenuated twice. The HSQC₀ experiment acquires several spectra with different number of repetitions ($i \geq 2$). Linear fitting of the logarithms of peak volumes (V_n^i for peak n , where f_n^A is the attenuation factor for peak n) for the different spectra allows the ‘time-zero’ peak volume (V_n^0) to be extrapolated Eq. (8).

$$\ln V_n^i = \ln V_n^0 + i \times \ln f_n^A \quad (8)$$

This effectively corrects any errors that have a linear dependence on time, such as those associated with evolution delays, pulse imperfections and relaxation during the pulse sequence, resulting in more quantitative data [203]. The usual requirement for quantitative NMR of ensuring an adequate relaxation delay remains necessary for HSQC₀ experiments. Good signal-to-noise ratio is also necessary to ensure that the peak volumes can be accurately fitted. Due to the requirement for repeated acquisition and long relaxation delays, q2D NMR experiments are considerably slower to acquire than conventional 2D NMR experiments and may not be suitable for monitoring all reactions.

3.6.2. Non-uniform sampling

Conventional 2D NMR requires a new FID to be acquired for each point in the indirect dimension (Fig. 18). As a result, digital resolution in the indirect dimension is usually much lower, typically with 10 – 200 times fewer points compared to the direct dimension. Increasing the number of indirect points acquired improves digital resolution, but at a time penalty *pro rata*. This can be a major impediment, even for relatively slow reactions.

Non-Uniform Sampling (NUS) techniques allow significant time savings to be made by sampling a random or semi-random subset of all the indirect points (typically 25–50% of the total number of points) [204–207]. As the sampled points are representative of the full range of indirect dimension frequencies, a 2D FID can be reconstructed during processing and then Fourier transformed to produce the two-dimensional spectrum (Fig. 18). As fewer points are required to construct the spectrum when using this approach, NUS can be used to decrease the total acquisition time without degrading spectral resolution. Alternatively, the time saved can be used to acquire extra points to increase the digital resolution.

Good *S/N* is required for NUS, since noisy data will corrupt reconstruction of the missing points leading to artefacts in the spectrum. Equally, if too few points are sampled there is not enough information for the computer to reconstruct the missing data points, resulting in a loss of resolution, poorer quantitation, and missing peaks (Fig. 19).

Although significantly faster than conventional 2D NMR, performing sequential NUS experiments is still too slow to achieve an acceptable kinetic data density for many reactions. To increase data density, time-resolved NUS techniques continuously acquire 1D spectra with random evolution time delays throughout the course of the reaction. The 1D slices are processed as a moving block to produce a series of 2D spectra, each representing a different time point in the reaction [208,209].

3.6.3. Polarisation sharing

Like their 1D counterparts, the time taken for acquisition of 2D NMR spectra is dominated by the relaxation delay, τ_R , that is required to allow the return to equilibrium magnetisation (Section 3.2). The relaxation delay can be reduced by using smaller pulse angles or by adding paramagnetic relaxation agents. However this comes at a cost of decreased signal to noise, and loss of resolution respectively; moreover addition of a relaxation agent can chemically interfere with the process of interest.

An additional pathway to accelerate return to equilibrium magnetisation is available in both 1D and 2D heteronuclear NMR experiments. Since the natural isotopic abundance of NMR-active heteronuclei such as ¹³C or ¹⁵N is low, the NMR signal measured e.g. in an HSQC experiment arises initially only from the small number of protons that are directly coupled to these nuclei. The remaining protons in the sample are either left untouched or have their magnetization dephased by the pulse sequence and can represent a reservoir of magnetisation that can be tapped to accelerate the return to equilibrium.

Many different methods have been developed to enhance relaxation via polarisation sharing [210–212], however the most relevant to small molecule reaction monitoring is Acceleration by Sharing Adjacent Polarization (ASAP) [213–217]. ASAP experiments use a TOCSY mixing pulse of around 40 ms to transfer magnetisation from donor protons (H_d) in the reservoir to the acceptor proton (H_a) that is detected in the NMR experiment (Fig. 20b, c). Polarisation sharing returns the acceptor proton to close to equilibrium magnetisation much faster than if it were relaxing freely, allowing a shorter relaxation delay (τ_R) to be used.

An advantageous side effect of the ASAP pulse sequence is that the mixing pulse can help to suppress t_1 -noise, caused by instabilities in magnetic field, temperature, lock signal etc. during the acquisition, that appears around large peaks in the indirect (F_1) domain [213]. ASAP polarisation sharing is compatible with other fast 2D techniques such as NUS, however care must be taken that the faster acquisition rate does not exceed the recommended transmitter duty cycle, leading to excessive heating of the sample or the probe electronics [217].

3.6.4. Ultrafast 2D

Ultrafast 2D experiments are an example of how slice selection (Section 3.3) can be used to greatly increase the rate of data acquisition. Rather than using the whole sample volume for each scan, the magnetisation of the sample is divided into slices, with each slice used to measure one point in the indirect dimension with a unique evolution delay [218–220]. The signal from all volumes is acquired simultaneously and processed using NUS to give the complete 2D spectrum.

Ultrafast techniques allow a complete 2D spectrum to be acquired in the same time as a 1D experiment, making them particularly relevant for reaction monitoring [221–225]. Since each

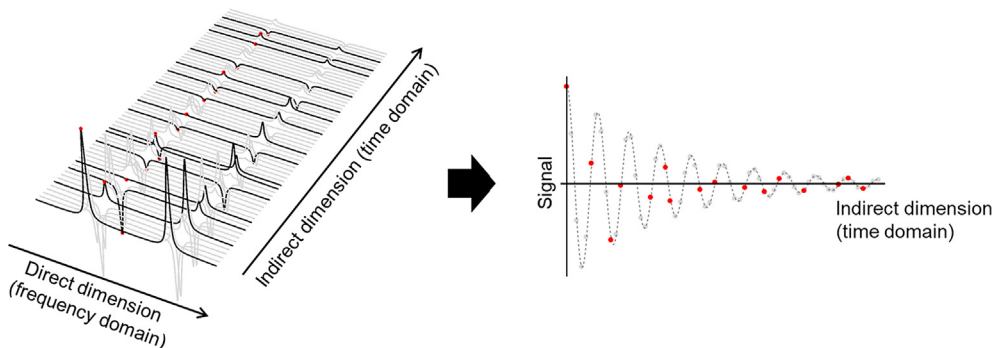


Fig. 18. Simulated 2D COSY spectra using 25% NUS, after Fourier transform of the direct dimension. Missing data points in the indirect dimension are reconstructed by fitting a model to the data.

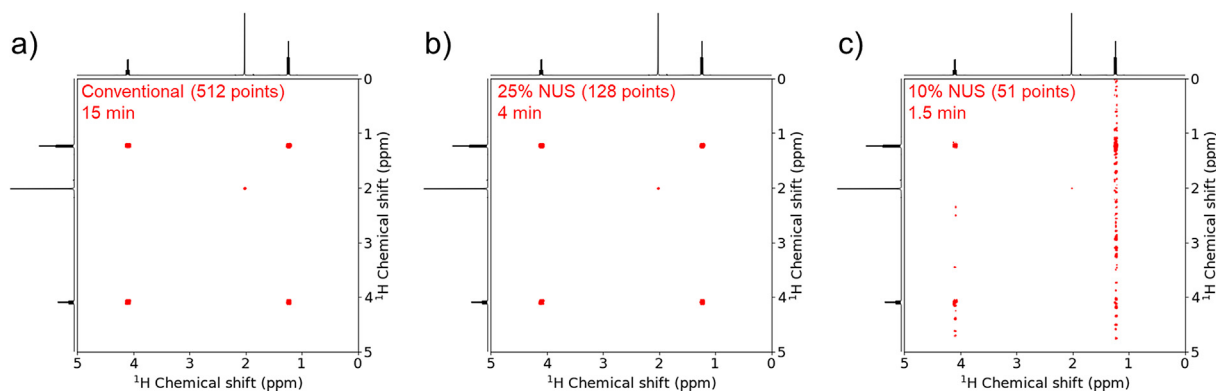


Fig. 19. COSY magnitude spectrum of ethyl acetate acquired using (b) a conventional pulse sequence (512 points), (c) 25% Non-uniform sampling (128 points) and (d) 10% Non-uniform sampling (51 points).

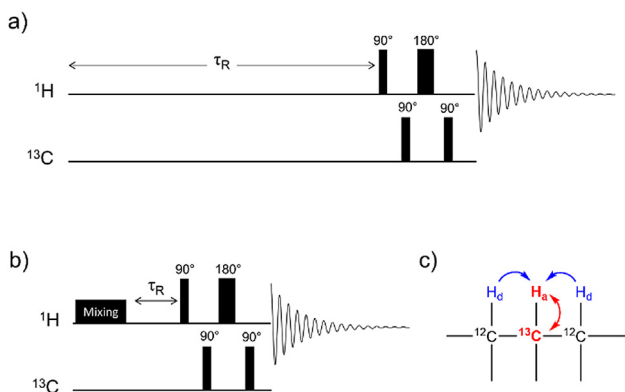


Fig. 20. Pulse sequence for (a) basic HMQC acquisition, (b) ASAP-HMQC pulse sequence, with TOCSY spinlock pulse used to enhance relaxation by polarisation sharing. τ_R = relaxation delay. (c) Polarisation sharing (blue arrows) from donor protons (H_d) to an acceptor proton (H_a) coupled to a ^{13}C nucleus (red arrow).

slice represents only a small portion of the sample volume, signal-to-noise for ultrafast experiments is very low. As with other NMR experiments, repeat measurements may be made to increase signal-to-noise. In many cases, particularly where the spectra contain substantial t_1 noise, acquiring multiple scans for an ultrafast experiment may prove more effective than a conventional acquisition of the same duration [226].

3.6.5. Multiple acquisition

The approaches discussed above have mainly considered methods to mitigate the long recovery time required for quantitative NMR. An alternative approach is to make use of the recovery time

to gain additional information. In a typical NMR experiment, regardless of whether it is 1D, 2D etc., the signal is recorded on just one channel. Any magnetisation remaining on other NMR active nuclei is unobserved and 'wasted'. Simply adding an extra receiver to detect this magnetisation increases the amount of information that can be acquired in a single experiment, and can even allow parallel acquisition of two different experiments [227–229].

Whilst some newer spectrometers are equipped with multiple receiver channels as standard, most spectrometers have a single receiver which is shared between all channels, and so are incompatible with multiple receiver experiments. A special suite of experiments has been developed that allow multiple acquisition on a single receiver spectrometer, using the residual magnetisation after acquisition of the first FID. 'Time-share' experiments use this residual magnetisation to record several spectra with correlations to different heteronuclei or different evolution delays by acquiring multiple FIDs within a single pulse sequence [230–232]. Alternatively, a group of different NMR experiments can be chained together to produce a 'supersequence' with up to five separate spectra recorded with only one relaxation delay [233,234].

Multiple acquisition techniques have yet to be widely exploited in the determination of kinetics, the analysis of complex reaction pathways, and the identification of transient intermediates; nonetheless we consider it an area likely to see future development.

4. Kinetics and speciation

4.1. Non-equilibrium vs equilibrium systems

In organic and organometallic chemistry, the most common method to obtain data for kinetic analysis is to measure the

changes in concentrations of species as a system approaches equilibrium (Scheme 1a); in many cases the reverse reaction is undetectable. Depending on the reaction, the experiment can be conducted in two distinct ways. In the more conventional approach, the reaction is initiated, by adding for example a reagent or catalyst, or an external trigger (e.g. light) is used, and the ensuing approach to equilibrium is analysed. Alternatively, a rapid change in conditions is applied to a system already at equilibrium, and the ensuing changes in concentrations are followed as the system 'relaxes' to establish a new equilibrium state (Scheme 2, Section 4.2.1).

There are several limitations to the above method (Scheme 1a), the most important being the timescale of the chemical reaction of interest. Firstly the overall process, or some elements of it, must be slow with respect to the differences in Larmor frequencies between peaks, so that distinct signals are detected for substrates, products, and if they significantly accumulate, intermediates. Secondly, the reaction must not be so fast that it proceeds to completion before measurements can be made, although specialised *in situ* methods (Section 2.4.4) can help. However, if the process is at dynamic equilibrium (Scheme 1b), it can still be possible to obtain kinetic information by NMR. Depending on the rate, this can be achieved by probing changes in spin populations after the system has been disturbed by an appropriate pulse sequence, or more generally by line shape (bandshape) analysis (see Case Studies 3 and 8). These approaches are discussed in Section 4.4.

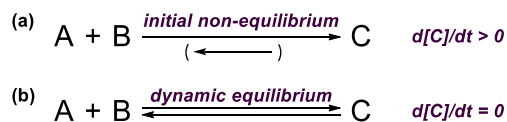
The two methods (Scheme 1) are thus complementary in terms of the timescales of the processes for which they are effective. This Section describes some of the most common ways to study equilibrium and non-equilibrium systems, the choice of an appropriate method for a given reaction, and the analysis of the resulting data.

4.2. NMR analysis of non-equilibrium systems

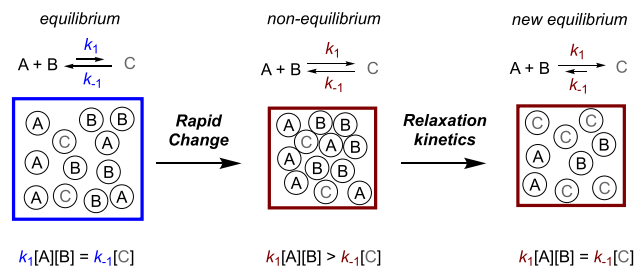
Acquiring kinetic data for non-equilibrium systems usually comprises three stages: i. optional measurement of an initial (t_0 ; time zero) NMR spectrum, ii. initiation of the reaction or perturbation of the conditions; iii. periodic acquisition of spectra comprising single or multiple FIDs. With an appropriate standard (see Section 2.1.2) the initial concentrations to be used in kinetic modelling can usually be determined from the initial spectrum; one exception to this is in the case of fast reaction initiated by stopped flow, where a genuine t_0 spectrum is not measured. The rate of acquisition of spectra is dependent on the nature of the experiment, and is sometimes the most challenging aspect for the experimentalist. The reliability of the primary data must be borne in mind when extracting kinetic information from it. For a process that is relatively rapid, steps must be taken to reduce the time needed to acquire a spectrum (e.g. reducing the pulse angle and decreasing the number of scans) to increase kinetic data density. These adjustments can lead to loss of S/N and make quantitative study of low concentration species unreliable.

4.2.1. 'Chemical relaxation' methods

The general principle of the relaxation-based kinetics experiment is illustrated in Scheme 2. Examples of chemical relaxation



Scheme 1. Two approaches to reaction monitoring. (a) Concentrations of reagents change over time for a system initially at non-equilibrium, and (b) the concentrations of reagents are independent of time for a system at dynamic equilibrium.



Scheme 2. A schematic representation of the response of a system to change of conditions in a chemical relaxation experiment. After the rapid change of conditions, the system is no longer at equilibrium, and its attainment of the new dynamic equilibrium is analysed.

experiments include a rapid change ('jump') in temperature, pH, pressure, or concentration (e.g. via dilution). A useful feature of the temperature jump [235–240], and of the pressure jump [241], experiment is that they can be repeated numerous times on the same sample, provided that the system is chemically stable. Moreover, as the reactants are already pre-mixed in the solution, there are no mass transfer considerations, provided that the system is thermally homogeneous.

Temperature jump is the most common method for chemical relaxation NMR experiments, and has been widely utilised in studying protein folding dynamics. NMR spectrometers can operate over a range of temperatures, and the temperature of the probe can routinely be changed, within instrument-specific limits (Section 2.1.1.1). However, the rates of heat transfer from the VT gas to the solution are too slow (see Fig. 1) for rapid temperature jump experiments *in situ*. Thus, the first temperature jump experiment in NMR spectroscopy, the refolding of Ribonuclease A, was performed by *external* temperature jump. The NMR tube containing the sample was maintained at 45 °C in a heating block, then rapidly cooled to 10 °C by partial immersion in a water–ice bath. The 10 °C sample was then rapidly inserted into the probe, pre-cooled to 10 °C. Data acquisition began about 30 s after the (external) 35 °C temperature drop, and the refolding was monitored at 10 °C for about 25 min inside the probe [235]. In order to improve the method, various techniques have been developed to perform rapid *in situ* temperature jumps, some of which enable temperature changes of up to 25 K in <20 ms [236–240]. Achieving solution phase pressure jumps in the sample in the NMR probe is technically much more demanding, and has mostly been used to study protein folding [241]. The technique has not yet been adopted for mechanistic NMR analysis of organic and organometallic processes, but offers great potential.

The data obtained in an NMR chemical relaxation experiment is intensity (and thus concentration) vs time. Both the forward and reverse processes must be accounted for, and in a first order $A \rightleftharpoons B$ system, Fig. 21, a simple differential equation (Eq. (9)) can be applied. Here k_1 and k_{-1} are the rate constants of the forward and reverse reaction under the new conditions (after the 'jump'), with x being the difference between the temporal and final (equilibrium) concentrations, i.e. $[A]_t = [A]_\infty + x$. Integration of Eq. (9) gives the concentration dependence as a function of time (Eq. (10)) where x_0 is the shift from the new equilibrium immediately after the jump, and x the shift after time t . The equation can then be fitted to the experimental data, Fig. 21, using standard non-linear regression.

$$\frac{dx}{dt} = k_{-1}([B]_\infty - x) - k_1([A]_\infty + x) \quad (9)$$

$$x = x_0 e^{-(k_1 + k_{-1})t} \quad (10)$$

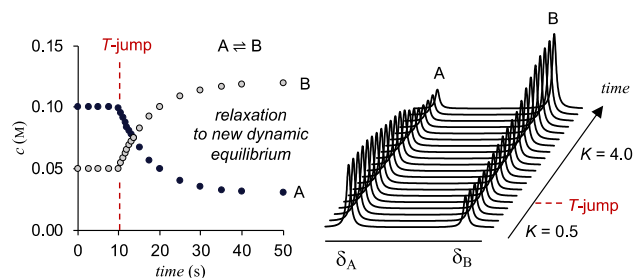


Fig. 21. A simulation of a temperature-jump relaxation experiment. Under the initial conditions, the equilibrium constant of the $A \rightleftharpoons B$ reaction is 0.5. Upon rapid change of temperature, the system relaxes to reach a new dynamic equilibrium with an equilibrium constant of 4.0. Each data point in the plot corresponds to a separate NMR spectrum acquired during the experiment.

4.2.2. Processing spectra for data extraction

For both the classical irreversible initiation, and chemical relaxation methods, appropriate steps should be taken when processing the acquired data to ensure that it reflects the evolution of the reaction, and not progressive errors or irregularities resulting from spectral acquisition or processing. Thus the spectra must all be processed under identical conditions to minimise any differences between the spectra that might corrupt the relative integrals between or within the series. For convenience, the NMR spectra can be opened in parallel in a “stacked” format, available in all common NMR spectral processing software packages. Phase and baseline corrections should be applied (in that order) before integration, ensuring that peaks have the correct line-shape (using reference deconvolution methods, Section 3.4.4.3, if needed) and that the spectral baseline is flat. The integrated areas of broad peaks can be substantially attenuated by some baseline correction methods. Chemical shift correction (referencing) is also recommended in order for spectra to be externally comparable.

Finally, before integration of the signals relevant to the reaction evolution, the integral of the internal standard should be normalised to eliminate any external changes in absolute intensity such as receiver gain re-optimisation. This is often not an issue, especially when spectra are all acquired using the same acquisition parameters, but it should be noted that any re-optimisation of these parameters will likely result in variation of the absolute intensity of the signal. This underscores the importance of choosing the right internal standard. Without such a standard, kinetic data acquired by integrating spectra where the acquisition parameters are continually re-optimised, for example in reactions run in interrupted *in situ* mode (see Section 2.2.1) can become unreliable.

4.3. Kinetics of non-equilibrium systems

4.3.1. Rate equations

The kinetics of chemical reactions are described mathematically using differential equations, often referred to as rate equations. Such equations are derived directly from the law of mass action and the chemical equations used to define the elementary step(s) in a reaction mechanism. This in turn means that the characteristics of an empirical rate equation, i.e. one determined by experimentation, can be used to interrogate a reaction mechanism. It should always be borne in mind, however, that numerous mechanistic scenarios can all lead to similar or identical empirical kinetics. In other words, rigorous mechanistic analysis should not be based on kinetics alone.

It is much more common for temporal concentration data, rather than rate data, to be extracted directly from a series of NMR spectra, and there are a number of different approaches for

the treatment of differential equations that allow mechanistic hypotheses to be tested using this temporal concentration data.

4.3.2. Power laws and rate order

Rate equations for simple reactions are often written in the form of a power law.

$$\frac{d[P]}{dt} = k[A]^x[B]^y \quad (11)$$

$$x[A] + y[B] \xrightarrow{k} [P] \quad (\text{for a single step reaction}) \quad (12)$$

In the example in Eq. (11), $[A]$ and $[B]$ are the concentrations of the reactants, x and y are the partial orders of the reaction with respect to each reactant, and k is the rate constant. The sum of these powers is known as the order of the reaction. For elementary reactions (those which occur in a single step) the partial orders are equal to the stoichiometric coefficients of each species, as defined in the chemical equation, Eq. (12). However, most reactions of interest contain multiple steps, with the rates of later reaction steps depending on the concentrations of reaction intermediates generated in earlier steps. Thus the overall rate equation for a multistep reaction of any complexity usually applies the assumption that the intermediate species exist in a steady state.

4.3.3. Rate laws for linear reaction systems

Using the steady-state approximation, where the rate of change of the concentration of a reaction intermediate is assumed to be negligible, allows simplifications to be made. In the example shown in Eq. (13), substrate A converts to product P , via equilibrium with reactive intermediate B , and a steady-state approximation rate equation can be simply derived. This is easily extended to an analogous reaction involving an additional reagent C which captures intermediate B (Eq. (14)). In the first case (Eq. (13)), where all steps are unimolecular, the resulting steady state rate equation takes the form of a power law, where all of the individual rate constants are collapsed into a single constant denoted k_{obs} (the observed rate constant). This is often not strictly applicable, as in the common case (Eq. (14)) where step 2 (k_2) is bimolecular. This leads to an equation whose structure requires a split denominator, containing concentration terms as well as constants. Here it can be seen that the concentrations cannot be separated into the form of a power law, which means that the reaction order is (at least technically) undefined unless limiting conditions are applied. As the complexity of a reaction increases, and more intermediates are added, the complexity and number of terms in the steady state rate equation also increase, often disproportionately. Fortunately, matrix and graphical methods are available for assembling steady state equations for extended linear systems [242].

4.3.4. Rate laws for catalytic reaction systems

Similar steady-state methods have been developed to allow rapid generation of rate equations for reactions involving cyclic (catalytic) arrangements of species. The best known of these are the method of King and Altman and related approaches [243–245]. These methods have found significant application in enzymology, biochemistry, synthetic and physical-organic chemistry.

$$\text{for } \left\{ \begin{array}{l} k_1 \\ [A] \rightleftharpoons [B] \xrightarrow{k_2} [P] \\ k_{-1} \end{array} \right\}, \quad \text{where } \left\{ \frac{d[P]}{dt} = k_2[B] \right\} \text{ and } \left\{ \frac{d[B]}{dt} \approx 0 \right\};$$

$$\text{then } \frac{d[P]}{dt} = \frac{k_1 k_2 [A]}{k_{-1} + k_2} = k_{\text{obs}} [A] \quad (13)$$

$$\text{for } \left\{ \begin{array}{l} k_1 \\ [A] \rightleftharpoons [B] \xrightarrow{k_2[C]} [P] \\ k_{-1} \end{array} \right\}, \quad \text{where } \left\{ \frac{d[P]}{dt} = k_2[B][C] \right\} \text{ and } \left\{ \frac{d[B]}{dt} \approx 0 \right\};$$

$$\text{then } \frac{d[P]}{dt} = \frac{k_1 k_2 [A][C]}{k_{-1} + k_2 [C]} \neq k_{\text{obs}} [A]^x [C]^y \quad (14)$$

4.3.4.1. The pre-equilibrium approximation. The Michaelis-Menten rate expression rests on the assumption that all catalyst species are connected in a rapidly attained (non-rate limiting) equilibrium state [246]. The other key assumption made by this (and other) steady state analyses of catalytic systems is that the substrate (or substrates) is in large excess over the catalyst. A general rule is that the catalyst loading should not exceed 10% of the concentration of the limiting substrate. This is because this model is unable to account for the amount of substrate that is used to populate substrate- or product-containing intermediates in the catalytic cycle. As the catalyst loading increases, so does the proportion of substrate that is required to maintain the catalytic intermediates; when this amount is a large proportion of the total substrate concentration (at high catalyst loadings), this offset starts to noticeably affect the quality of the analysis. In rate equations of this type, the numerator corresponds to the product of the equilibrium and rate constants (with substrates as required) representing a complete productive cycle round the catalytic system. The denominator represents a normalised sum of all of the possible catalyst states; the number 1 corresponds to an initial state, and subsequent states are defined as the products of the equilibrium constants and substrates, Fig. 22.

4.3.4.2. Briggs-Haldane rate equations. The Briggs-Haldane rate expression [247], Fig. 22, is the second most common form used for catalytic cycles, and again assumes that all of the catalyst species are in a steady state; it is distinguished from the Michaelis-Menten expression in that it breaks all equilibrium terms (K_n) down into their microscopic rate constants (k_n and k_{-n}). This approach leads to superficially more complex rate equations, but

is much more generally applicable than the Michaelis-Menten approach. In the Briggs-Haldane rate expression, any of the steps can be rate determining; this is true even of a forward rate constant for a reversible step, which would be assumed to be very rapid in a Michaelis-Menten rate equation. The numerator of these equations is very similar to that of the Michaelis-Menten equations, but the denominator is derived differently; the collection of terms represents all possible ways in which a given catalytic state can be generated from each of the other catalytic states.

4.3.4.3. Catalyst speciation. The speciation of a catalyst refers to the temporal populations of the different catalyst states during the progress of the reaction; the populations of these states relate to their rate(s) of formation and decay in the same way as the linear systems described earlier. A common term when discussing catalytic reactions is the catalyst “resting state”. This is the most populated state (where the catalyst “rests”) and is sometimes the state that undergoes the turnover rate limiting step in the cycle, or an intermediate in equilibrium with this. It is also not uncommon for the resting state to be ‘off cycle’, thus connected by equilibrium to only one ‘on cycle’ intermediate.

When using NMR to monitor and study reactions, the direct detection of catalyst speciation states is dependent on two conditions being met. Firstly, there must be sufficient concentration of catalyst present (compared to substrate and product) for detection to be feasible, and thus low catalyst concentrations can result in species being undetectable above the noise. Secondly, the resonances corresponding to different catalyst states must be in a slow-exchange regime. Fast exchange of catalyst species results in a single set of resonances, whose integral corresponds to the sum of the concentrations of all states and whose chemical shift represents a weighted average of the shifts of all species involved in the rapid exchange process.

If both of these conditions are met, it is useful to compare this speciation as a function of time to the speciation predicted using a rate equation (or a full model, see Section 4.3.5). It is the capacity of these models to describe catalyst speciation that enables them to describe the rate of the reaction as a whole, and an accurate



Michaelis-Menten:	$\frac{d[P]}{dt} = \frac{K_1 k_2 [A][Cat]_0}{1 + K_1 [A]}$	$\frac{d[P]}{dt} = \frac{K_1 K_2 k_3 [A][B][Cat]_0}{1 + K_1 [A] + K_1 K_2 [A][B]}$
Briggs-Haldane:	$\frac{d[P]}{dt} = \frac{k_1 k_2 [A][Cat]_0}{k_1 [A] + k_{-1} + k_2}$	$\frac{d[P]}{dt} = \frac{k_1 k_2 k_3 [A][B][Cat]_0}{k_2 k_3 [B] + k_{-1} k_3 + k_{-1} k_{-2} + k_1 k_{-2} [A] + k_1 k_3 [A] + k_1 k_2 [A][B]}$
Catalyst Speciation:	$\frac{[Cat]}{[Cat]_0} = \frac{k_{-1} + k_2}{k_1 [A] + k_{-1} + k_2}$	$\frac{[Cat]}{[Cat]_0} = \frac{k_2 k_3 [B] + k_{-1} k_3 + k_{-1} k_{-2}}{k_2 k_3 [B] + k_{-1} k_3 + k_{-1} k_{-2} + k_1 k_{-2} [A] + k_1 k_3 [A] + k_1 k_2 [A][B]}$
	$\frac{[Int1]}{[Cat]_0} = \frac{k_1 [A]}{k_1 [A] + k_{-1} + k_2}$	$\frac{[Int1]}{[Cat]_0} = \frac{k_1 k_{-2} [A] + k_1 k_3 [A]}{k_2 k_3 [B] + k_{-1} k_3 + k_{-1} k_{-2} + k_1 k_{-2} [A] + k_1 k_3 [A] + k_1 k_2 [A][B]}$
		$\frac{[Int2]}{[Cat]_0} = \frac{k_1 k_2 [A][B]}{k_2 k_3 [B] + k_{-1} k_3 + k_{-1} k_{-2} + k_1 k_{-2} [A] + k_1 k_3 [A] + k_1 k_2 [A][B]}$

Fig. 22. Michaelis-Menten and Briggs-Haldane rate equations describing turnover and speciation in two examples of simple catalytic reactions. $[Cat]_0$ is the total amount of catalyst present in the system, i.e. $[Cat]_0 = [Cat] + \sum[Int_n]$.

depiction of temporal catalyst speciation strongly enhances any kinetic model used to support a mechanistic hypothesis.

If the catalyst resting state can be identified, or conversely, catalyst species shown to be in negligible concentration relative to others, rate equations of Michaelis–Menten or Briggs–Haldane form can be greatly simplified. In short, if a rate constant in a proposed cycle is much smaller than the others, then terms containing it can often be omitted, or subsumed into a single collection of terms, for instance in the denominator of a rate equation. Such eliminations are commonplace in both linear and catalytic rate equations and result in simplified forms. In very pronounced cases this can result in further cancellations from the rate equation and lead to more dramatic simplifications. More broadly, this can be considered one of the reasons why superficially complex reaction systems involving multiple reagents can, under limiting conditions, display behaviour consistent with very simple rate equations.

4.3.5. More advanced model building – Numerical integration of systems of differential equations

While closed-form expressions for rate equations are very useful when considering order and reaction mechanism, the nature of the approximations that lead to them means that they are not exact solutions to the set of differential equations describing a reaction system. A more accurate approach is to use software that implements numerical integration techniques to approximate the full system of differential equations. While the computational cost of such procedures scales with the complexity of the system of equations, most mechanistic proposals for chemical reactions studied in the laboratory can be computed rapidly using a variety of freely available or commercial software packages on a single CPU [248–250]. Once a mechanism has been proposed and preliminary datasets acquired for a reaction, the system of differential equations describing this mechanism should be entered into the fitting programme of choice: this is the kinetic model. The goal of any fitting algorithm is to minimise the discrepancy (normally the sum-square error) between the numerical integration outputs from the model and the concentration vs time data extracted from integrating the NMR spectra.

Finding and evaluating such a model, or more usually a series of models, can range from a very simple to an extremely laborious task. The greater the diversity and number of sets of experimental temporal concentration data that are available, the more constrained the fit, and thus the more likely the model reliably reflects the mechanism being investigated. Ideally the initial concentrations of all components should be varied over as wide a range as amenable to the NMR analysis method being employed, and reactions conducted to high levels of conversion.

4.3.6. Fitting data to a kinetic model

When fitting experimental data to a kinetic model (be it a steady state model or a full system of equations model) it is crucial that enough data is provided for meaningful conclusions to be drawn. How much, and what type of, data depends on the complexity of the model and how many components can be monitored. A key advantage of NMR in this regard is that multiple species can be monitored simultaneously. Because of this capacity for multi-species quantification, multiple parameters can often be fitted using a single experimental dataset. To test the robustness of any fit, reactions must be conducted and monitored using different initial conditions (e.g. different concentrations of reagents) and fitted simultaneously with the other data.

4.3.6.1. Underfitting and overfitting. Two limiting regimes should be borne in mind when fitting kinetic models to experimental data. The first is underfitting, and usually arises when a model is incomplete because intermediates, side products, or catalyst

species present in significant concentration have not been detected experimentally, or have not been included in the model (Fig. 23a). This can occur when rapid chemical exchange between intermediates results in a single set of time averaged resonances. It is important to consider that the integral of any resonance in this set will reflect the *sum* of the concentrations of all species in rapid exchange with it, while the chemical shift of this resonance will reflect a weighted average of the shifts of these same species.

The second is overfitting, and occurs when more species are invoked in a model than can be monitored experimentally. Indeed, when multiple species are present in a model and are “untethered” to temporal concentration data, many different sets of rate constants and arrangements of species can be used to achieve an apparently good fit with experiment, making mechanistic interpretation unreliable. In Fig. 23b two intermediates have been added to the model used in Fig. 23a: one is experimentally detected (purple), the other is proposed but undetected (black). The model in Fig. 23b now fits very well to the data, but only does so when the rate constants are adjusted to make the concentration of the undetected intermediate *in the model*, vanishingly low (see inset to graph). In Fig. 23c, removal of the undetected intermediate still allows for a good (in fact slightly better) fit to the experimental data, and this is the model that should be retained, with the caveat that there may be further undetected intermediates. In other words, if more information becomes available at a later date, for example to support the proposal that the NMR-undetected intermediate (black) in Fig. 23b is present, then the complexity of the model can be increased to accommodate it.

4.3.7. Graphical and visual kinetic analysis

Analysis of plots based on integrated rate equations for simple kinetic systems has long been an invaluable tool for determining the empirical rate constants, and kinetic orders with respect to reagents and catalysts. In the majority of cases, fitting to linearised expressions distorts the statistical weights of the experimental data points, and non-linear regression is recommended. For example, a first order temporal decay in the concentration of reactant, ‘A’, is better analysed by non-linear regression of $[A]_t = [A]_0 e^{-kt}$, than linear regression of a $\ln([A]_0/[A]_t) = kt$. It is also important to note that these simple graphical analyses do not account for various phenomena in complex multistep reactions, including for example, changes in rate determining step, catalyst deactivation, induction periods, autocatalysis, and product inhibition. Analogously, monitoring initial rates, and hence discarding most of the reaction course from studies, also results in loss of valuable information on such process, that may only be evident on careful examination of the whole reaction profile.

An increasingly popular tool for analysing the kinetic profiles of non-equilibrium systems is visual kinetic analysis (VKA) [251–253]. This was first used by Michaelis and Davidsohn, but substantially developed and popularised by Blackmond, and by Burés. VKA is based on monitoring the reaction throughout its whole course, and plotting original or modified data, to visually assess the reaction kinetics. In a recent minireview [251], Burés explained two main approaches: reaction profile kinetic analysis (RPKA [253], first described by Blackmond in 2005) and variable time normalised analysis (VTNA). The main advantages of VKA include that the reaction is monitored throughout its whole course rather than solely in its initial stage, and that only a simple analysis, and often only a few experiments, are required. Reaction profiles of complicated catalytic systems can be qualitatively assessed by performing simple experiments and visual comparison of a series of plots based on various functions. However, the lower precision and usually qualitative nature of the approach should be borne in mind when interpreting data using the VKA techniques.

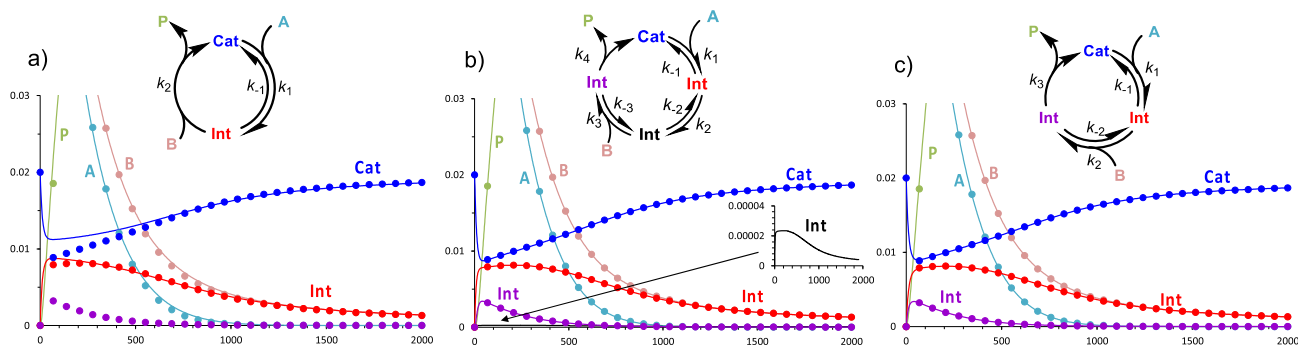


Fig. 23. Three models used to fit a simple catalytic reaction ($A + B \rightarrow P$). Model (a) does not include an observed intermediate (purple) leading to under-fitting; model (b) is over-fitted; the inset shows how the model fits the data by minimising the concentration of an experimentally undetected (and wholly unevicenced) intermediate; see text for full discussion. Model (c) is the simplest solution that provides an acceptable fit. For real examples see Case Studies 3, 10, and 13.

4.3.7.1. Reaction progress kinetic analysis (RPKA) [253]. In RPKA, the reaction is analysed by data from a measurable parameter (e.g. concentration, or rate) as a function of time [253]. This primary data is then processed to transform it into variables convenient for visual analysis. In NMR spectroscopy, signal intensities, which are directly proportional to concentrations of species, are the primary data. With sufficient data density, these can be differentiated as a function of time, e.g. by taking the derivative of a best-fit high-order polynomial, to obtain reaction rates, which are plotted against concentrations of the substrate or product.

In RPKA, three main types of experiments are performed, namely *same excess*, *different catalyst loading* and *different excess*, and the appropriate plots of reaction rates against concentrations compared to account for reaction orders, as well as various other phenomena such as product inhibition, catalyst decomposition, etc.

In the *same excess* experiment (Fig. 24a), the reaction is studied under two sets of conditions, both containing an initial imbalance in the concentrations of two species. The absolute concentrations of these species differ between the two sets of conditions, e.g. $[A]_0 = 0.1 \text{ M}$ and $[B]_0 = 0.05 \text{ M}$ in the first, and $[A]_0 = 0.2 \text{ M}$ and $[B]_0 = 0.15 \text{ M}$ in the second, but the 'excess' of one component over the other is identical: in this case $[A]_0 - [B]_0 = 0.05 \text{ M}$. If the reaction is catalysed, then the same catalyst concentration is employed in both experiments. As the reaction under the second set of conditions ($[A]_0 = 0.2 \text{ M}$, $[B]_0 = 0.15 \text{ M}$) proceeds, and A and B are consumed, their concentrations will eventually fall to be identical to the initial conditions in the first system ($[A]_0 = 0.1 \text{ M}$, $[B]_0 = 0.05 \text{ M}$). The difference between the two systems is that products (and side products) are present in one but not (yet) in the other. Hence, plotting the rate of reaction against concentration of the substrate will only give coincident (often termed 'overlying') [253] curves if there is no product or side-product inhibition, or progressive catalyst deactivation. If the plots do not overlay, then addition of exogenous product, and re-running one of the reactions, enables differentiation between product inhibition and catalyst deactivation.

In order to determine the kinetic order (Section 4.3.2) with respect to a catalyst, a series of (at least two) reactions must be studied with the same initial concentrations of all substrates and different catalyst concentrations (Fig. 24b). Simply transforming the y-axis into rate divided by the concentration of the catalyst to a certain power, x , and finding the value of x for which the data overlay, will indicate the order with respect to the catalyst.

In order to determine the kinetic order in substrate, a *different excess* experiment (Fig. 24c) is conducted. Here only the initial concentration of one of the substrates is varied between two or more reactions, with all other conditions kept the same. Then by plotting

$\text{rate}/[\text{substrate}]^y$ on the y-axis, and finding the value of y for which the data overlay, will indicate the order with respect to that substrate.

4.3.7.2. Variable time normalisation analysis (VTNA) [252]. The main principles of VTNA are similar to those of RPKA, in that a reaction is monitored throughout its whole course [252]. However, the key difference in VTNA is that the data is analysed as concentration (y-axis) vs f -time (x -axis), where f is a function applied to the time data to 'normalise' a series of plots. In the context of NMR spectroscopy, there is a major advantage to directly using temporal concentration data rather than having to convert this first to rate (see RPKA). In VTNA, f is varied until two (or more) plots of the same reaction system started under different initial conditions, overlay. As detailed below, the normalising function, f , depends on the specific type of VTNA experiment. These are referred to, in an analogous manner to RPKA, as *same excess*, *different catalyst loading*, and *different excess*. The experiments are performed to account for catalyst deactivation and/or product inhibition and to determine the reaction orders with respect to the catalyst and all substrates.

In the *same excess* experiment (Fig. 25a), the two plots obtained for two systems at different starting points must be shifted along the x -axis (time), so that the concentrations of substrates (and catalyst) are equal for each point; thus $f\text{-time} = \text{time} + \text{constant}$. Coincidence of the plots indicates no catalyst deactivation and no product inhibition. Plots that do not coincide indicate significant impact of one or both of these phenomena. In these circumstances a further reaction with exogenous product from the start must be studied to distinguish deactivation versus product inhibition.

In the *different catalyst loading* experiment (Fig. 25b), the original plots of concentration of product (or starting material) against time are modified by transforming the x -axis (originally time) into $f\text{-time} = \sum [\text{cat}]^x \Delta t$ (Eq. (15)), and then iteratively finding the value of x (the empirical order in catalyst) for which the plots best match.

$$\sum [\text{cat}]^x \Delta t = \sum_{i=1}^n \left(\frac{[\text{cat}]_i + [\text{cat}]_{i-1}}{2} \right)^x (t_i - t_{i-1}) \quad (15)$$

$$\sum [\text{cat}]^x \Delta t = [\text{cat}]_0^x t \quad (\text{when no catalyst deactivation})$$

Hence, the concentration of the active catalyst must be known to apply the time normalisation in Eq. (15). This variable-time normalisation can be simplified to $[\text{cat}]_0^x t$, assuming constant concentration of the catalyst throughout the course the reaction. Similarly, performing the *different excess* experiment (Fig. 25c), and normalising the time variable according to Eq. (15), where

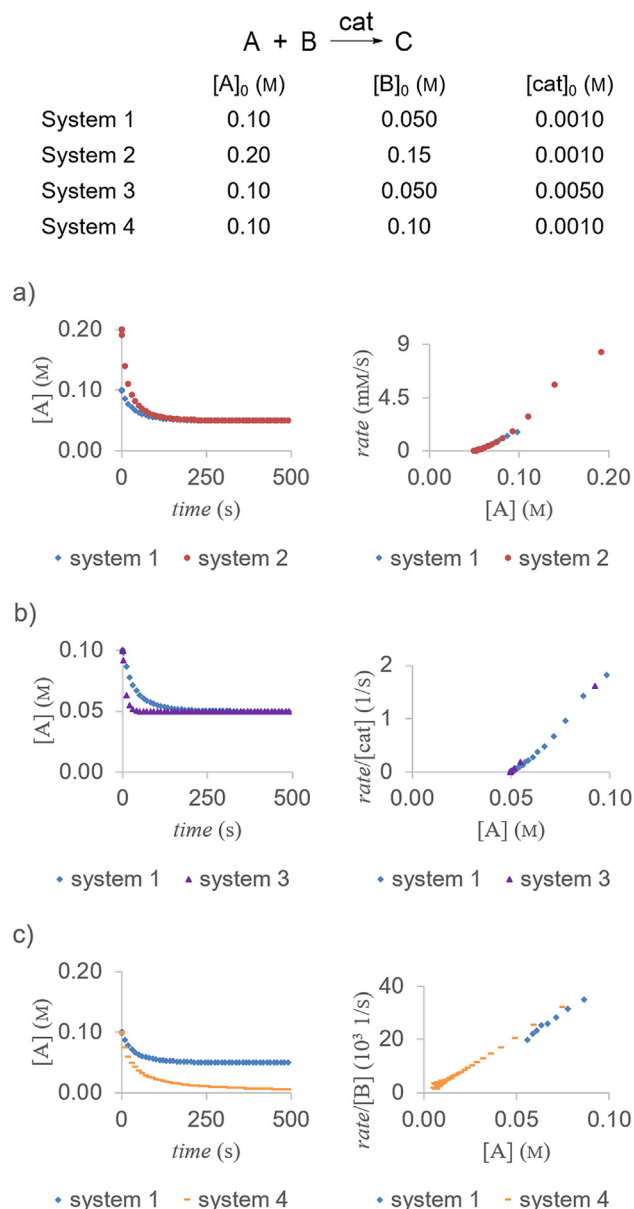


Fig. 24. RPKA: (a) same excess experiment, (b) different catalyst loading, and (c) different excess experiment for a simulated reaction as in scheme at top. For an example of the application of RPKA see Case Studies 7 and 15.

the catalyst concentration is now substituted with the concentration of the reagent of interest, are used to determine the order with respect to that substrate, y .

4.4. NMR analysis of systems at dynamic equilibrium

There are two main advantages to the analysis of the kinetics of systems at chemical equilibrium. Firstly, the durations of experiments conducted on the system are not limited by the reaction rate and thus lifetime, only by the instrument time available and the chemical stability of the sample. Secondly, since the system is already pre-mixed and pre-equilibrated, the mass transfer issues that attend initiation of non-equilibrium systems can be avoided. However, as the net concentrations of all species are independent of time, systems at chemical equilibrium pose a unique challenge for standard chemical kinetic measurements. Here, NMR offers great opportunities for mechanistic analysis, and several tech-

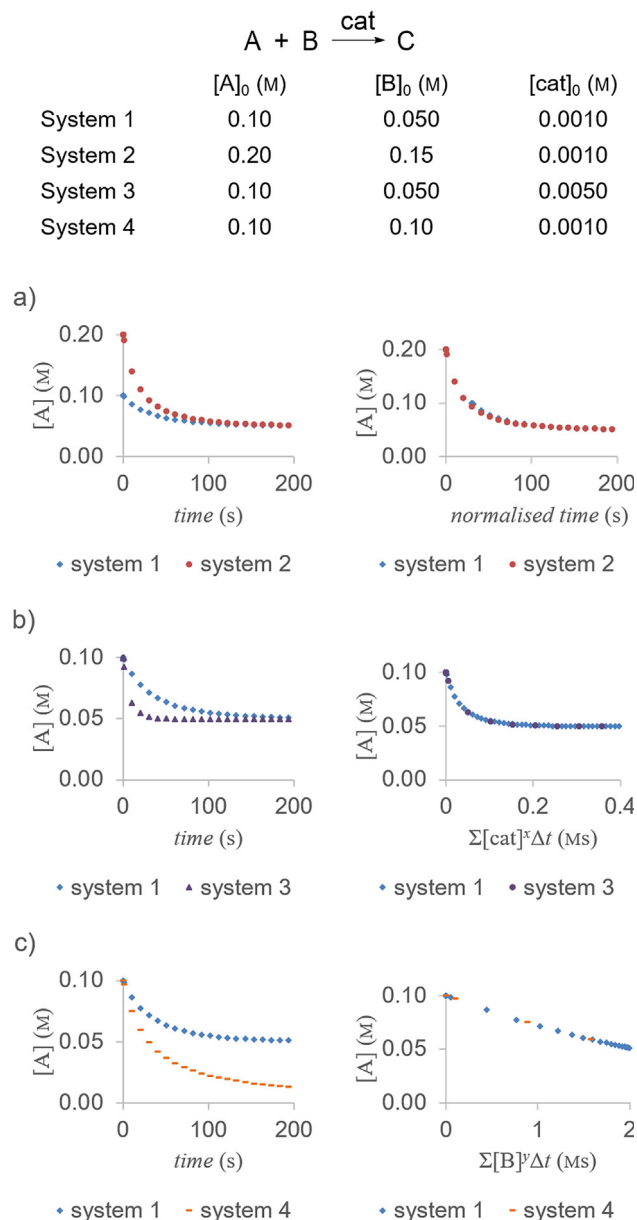


Fig. 25. VTNA: (a) same excess experiment, (b) different catalyst loading, and (c) different excess experiment for a simulated reaction as in scheme at top. For an example of the application of VTNA see Case Study 9.

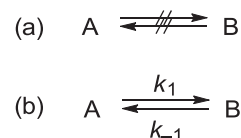
niques have been developed that enable the interrogation of such systems, provided they occur at a sufficiently fast rate [254].

4.4.1. Disturbing the magnetic equilibrium of the system

One approach to monitoring a dynamic equilibrium system is to disturb its magnetic equilibrium, while leaving the chemical equilibrium intact. The return of the magnetisation to its equilibrium state is affected by the dynamics of the chemical equilibrium and can thus be used to interrogate the latter. The most commonly-used techniques to achieve this are magnetisation transfer experiments (also known as Hoffman-Forsén or selective inversion recovery experiments) and EXchange Spectroscopy (EXSY; this uses the same pulse sequence as NOESY) [254–257]. In these experiments, appropriate pulse sequences allow for monitoring the return of the system to its magnetic equilibrium, as the net magnetisation of the appropriate nuclei can be followed as a function of time.

4.4.1.1. Magnetisation transfer. The pulse sequence for a selective inversion recovery experiment is shown in Fig. 26a [254]. At the beginning of the experiment, all nuclei are at magnetic equilibrium, with the net magnetization along the +z-axis. An initial 180° soft (and thus selective) pulse inverts one of the signals (at a chosen frequency) to the -z-axis. Then, after a variable delay, τ , a 90° pulse is applied, with immediate acquisition of the FID. In a single experiment, this pulse sequence is repeated for a number of variable delays, and the intensities of the signals (both the selectively inverted and the initially non-inverted) are recorded as a function of the variable delay, τ . The shapes of the plots of intensity against time for the inverted and non-inverted signals depend on whether chemical exchange occurs between some or all nuclei within the system. Here we discuss the concept by way of a simple two-spin model (non-coupled spins A and B; no cross-relaxation), where spin A is inverted by the soft pulse, and the spins either undergo no chemical exchange (Scheme 3a) or undergo exchange via a single-step unimolecular mechanism (Scheme 3b).

In the case of no chemical exchange (Scheme 3a; Fig. 26b), the initial 180° pulse inverts one of the signals (spin A) to the -z-axis. During the variable delay, the nuclei relax longitudinally, approaching the initial +z-magnetisation. The extent to which the relaxation takes place depends on the variable delay with the limits of negative maximum intensity ($-I_\infty$) for $\tau = 0$, and maximum intensity (I_∞) as $\tau \rightarrow \infty$ (i.e. the intensity of the signal at magnetic equilibrium). The rest of the pulse sequence is a standard NMR experiment, which creates transverse magnetisation and allows for acquisition of the FID. Hence, the plot of intensity against time



Scheme 3. Generic system involving two non-coupled spins, A and B, which (a) do not undergo chemical exchange, and (b) undergo chemical exchange via a single-step unimolecular mechanism.

(Fig. 26b) shows a first order relaxation process from $-I_\infty$ ($\tau = 0$), approaching I_∞ at $\tau > 5T_1$. Since there is no exchange in the system ($k = 0$), it is the same as a plot for an inversion-recovery experiment used to determine T_1 (described in Section 3.2). The soft pulse does not affect any other signals in the system (spin B in the model; Fig. 26a), and hence they show a constant value of their maximum intensity, independent of time (Fig. 26b).

When chemical exchange occurs, Scheme 3b, the selective inversion recovery experiment can provide information about the kinetic behaviour of the system. As above, the initial 180° pulse selectively inverts the magnetisation vector of the appropriate nuclei to the -z-axis, while leaving all other signals unaffected (see boxed species in the kinetic model in Fig. 26a). When $\tau = 0$ and when $\tau \geq 5T_1$, the situation for both the initially inverted and non-inverted signals is the same as for non-exchanging systems. However, at τ values between these two extremes, two interdependent processes take place. The recovery of the initially inverted signal is accelerated by the chemical exchange (A becoming B, and B* becoming A*; Fig. 26a). The faster the exchange, the greater the deviation from first-order kinetics in the recovery of spin A (see e.g. I_A versus τ in Fig. 26d when $kT_1 = 50$). The combined relaxation and chemical exchange effects also cause the signal for B to develop a characteristic asymmetrically stretched 'V-shape' (Fig. 26c). The faster the chemical exchange, the more asymmetric the V-shape (Fig. 26d). Hence, it is straightforward to qualitatively observe chemical exchange between species via the selective inversion recovery experiment. Moreover, the I_A and I_B versus τ data can be analysed to quantitatively interrogate the proposed mechanism, and to determine the rate constants of exchange [256–258].

For selective inversion recovery experiments where the longitudinal relaxation of the isolated spins is inequivalent (e.g. $T_1^A \neq T_1^B$), provided that the rate of chemical exchange is sufficiently fast (e.g. $kT_1 = 50$ in Fig. 26d), the system can be approximated by a single (K_1 -weighted) T_1 value for both nuclei undergoing exchange. However, for systems that undergo exchange at slower rates, the T_1 relaxation times of the individual nuclei should ideally be determined independently (see Section 3.2). This can be challenging when species A and B cannot be isolated or selectively prepared. Under such circumstances, kinetic simulation (Fig. 26a, Section 4.3.6) allows the I_A and I_B versus τ data to be modelled using k_1 , k_{-1} , T_1^A and T_1^B as fitting parameters, albeit with greater uncertainty. If possible one can also determine (k_1/k_{-1}) , T_1^A and T_1^B at a series of temperatures below which there is no significant chemical exchange relative to relaxation. Correlations then allow temperature-extrapolated values to be compared with the fitting parameters in the kinetic model of the I_A and I_B versus τ data at the temperatures required for significant chemical exchange [258].

The length of the 180° pulse depends on the bandwidth chosen for inversion. Short pulse lengths, especially important for rapid exchange processes, mean larger bandwidths, and so large signal separation is essential for reliable quantitative data. Lastly, the above description holds true for non-coupled spin systems. Any scalar coupling between exchanging spins must be taken into consideration, which renders the design of the experiment, as well as analysis and modelling of the data, more complex [259].

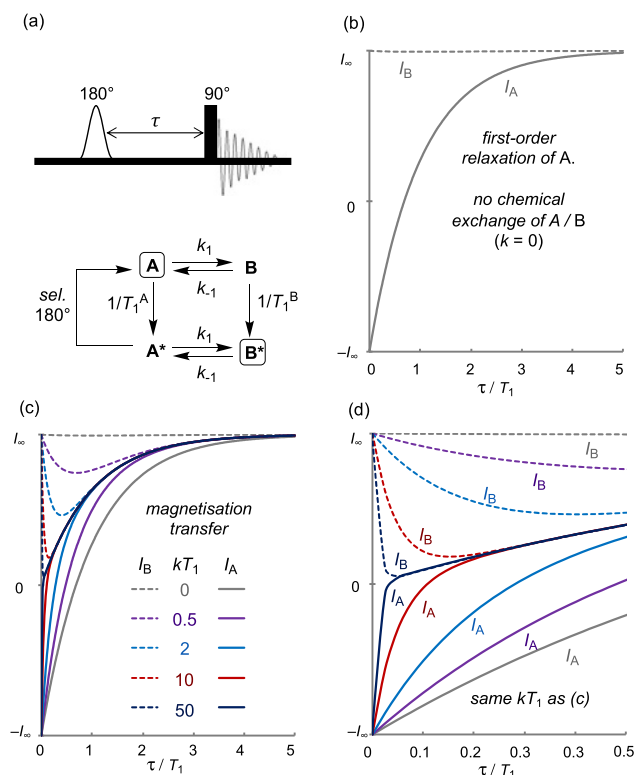


Fig. 26. A selective inversion-recovery experiment in which A is inverted and magnetisation transfer into B is used to determine rates of exchange between A and B. (a) Pulse sequence and kinetic model (boxed species are present at $\tau = 0$). (b) Plot of intensity (I) against delay time (τ) for both the inverted signal (spin A) and the non-inverted signal (spin B) where no chemical exchange occurs between the spins ($kT_1 = 0$). (c) The effect of the rate of chemical exchange ($kT_1 = 0-50$) on I versus τ . In all cases $T_1^A = T_1^B$ and $K_1 = 1$. (d) Expansion of the $\tau/T_1 = 0-0.5$ region of plot (c) showing how chemical exchange is complete in less than one tenth of T_1 when $kT_1 = 50$.

A variation of inversion transfer is saturation transfer, where the initial selective pulse saturates the signal of choice, rather than inverting it. The main principles of the analysis are therefore similar [260], and any form of differential perturbation can be used.

4.4.1.2. EXSY. Two-dimensional EXchange Spectroscopy (2D EXSY) as a technique for monitoring reaction kinetics was first proposed in 1979 [248]. The pulse sequence of a 2D EXSY experiment is identical to that of 2D NOESY, and is presented in Fig. 27a. Three 90° pulses are applied, followed by immediate acquisition of the FID. The acquisition time in EXSY is conventionally labelled as t_2 and corresponds to acquisition time in a standard 1D NMR experiment. The two periods that separate the second pulse from the first one, and the third from the second, are called evolution time (t_1) and mixing time (τ_m), respectively.

In a single EXSY experiment, the pulse sequence is repeated a large number of times, with t_1 as an equally spaced variable. The mixing time, τ_m , is fixed. Because the chemical exchange leading to transfer of magnetisation occurs within this period it must be carefully adjusted to the studied system. The net magnetisation is therefore a function of t_1 and t_2 , which upon double Fourier transformation, is converted into a two-dimensional spectrum.

An example spectrum is shown Fig. 27b [261]. Both axes show frequency, and the diagonal peaks represent the nuclei resonating at their Larmor frequencies. Cross-peaks appear in the spectrum for nuclei which undergo detectable chemical exchange within the mixing time. In this example, nuclei A, $S(\omega_A, \omega_A)$, and B, $S(\omega_B, \omega_B)$, undergo chemical exchange, and the cross peaks have the frequencies of $S(\omega_A, \omega_B)$ and $S(\omega_B, \omega_A)$. It is noteworthy that while the 2D EXSY spectrum is symmetrical about the diagonal, if A and B have different T_1 values, then their cross-peak volumes will only be identical for long recovery times.

It is straightforward to observe chemical exchange qualitatively, simply by looking at the spectrum. However, the utility of EXSY extends to obtaining quantitative data. Before acquiring and analysing an EXSY spectrum, one must appropriately choose a suitable mixing time. If mixing times are too short, cross-peaks will not be observed (due to the system not being allowed to exchange sufficiently during the period). If mixing times are too long, the experiment will not give reliable kinetic data due to the impact of T_1 relaxation of the species involved in the equilibrium. According to Perrin and Dwyer [262], an optimal mixing time for a two-spin exchanging system is as shown in Eq. (16), where T_1 is the relaxation time of the nuclei (assuming these are identical for both spins), and $k = k_{AB} + k_{BA}$ (k_{AB} and k_{BA} are the rate constants of the forward and reverse reactions). These are usually then estimated prior to the EXSY experiment, with further optimisation of τ_m , if needed, as a matter of trial and error.

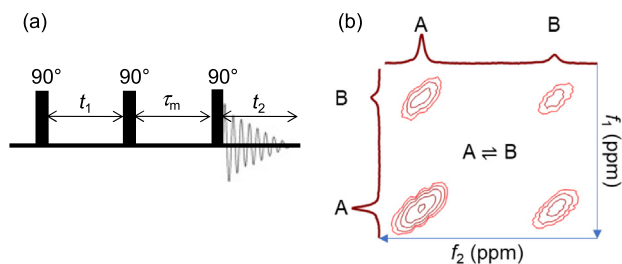


Fig. 27. (a) Pulse sequence of a 2D EXSY experiment. (b) A ^{31}P 2D EXSY spectrum of two non-coupled spins, A and B. Cross peaks (*) indicate considerable chemical exchange between the spins within the mixing time (τ_m). The spectrum is symmetrical about the diagonal axis. For an application of EXSY see Case Study 10.

$$\tau_{m,optimal} = \frac{1}{\frac{1}{T_1} + k} \quad (16)$$

$$\ln \frac{r+1}{r-1} = k\tau_m \quad (17)$$

For the previously discussed simple system with two exchanging spins (Scheme 2b), the rate constant, k , can be calculated using Eq. (17), where $r = 4x_Ax_B(I_{AA} + I_{BB})/(I_{AB} + I_{BA}) - (x_A - x_B)^2$ in which I is the integrated volume under the appropriate signal, and x_A and x_B are the mole fractions of spins of the two species A and B, respectively. Unless instrument time is limited, it is advised to conduct a detailed analysis of the integrated volumes (I_x) as a function of τ_m and determine k using Eq. (17). An alternative approach that minimises the experiment length is to run a series of one-dimensional versions of EXSY. The approach is based on carefully choosing a small number of t_1 values (N^2 t_1 values are required if N sites are in exchange), then Fourier transforming the spectra in f_2 only. The resulting set of 1D spectra can be analysed to obtain the kinetic information for the system of interest [263].

As shown above, choosing the mixing time and extracting kinetic data from an EXSY experiment is straightforward in two-spin systems (e.g. A and B in Scheme 3). For multi-spin systems, (A, B, C; or A, A', B etc.) the mathematics becomes more complicated and matrix analysis of results is required for extracting kinetic data [255].

Lastly, it is noteworthy that certain nuclei are more suited for magnetisation transfer and/or EXSY experiments than others. Most importantly, scalar coupling, relaxation times, and the range of chemical shifts involved, play interrelated and significant roles in whether or not any particular nucleus is well suited for these techniques. Nuclei that generally relax more slowly offer the advantage of monitoring the approach to magnetic equilibrium in magnetisation transfer over a longer time period. A review by Orrell presents examples of successful application of 2D EXSY for different nuclei [264].

4.4.2. Line shape analysis

The second common approach to monitoring a dynamic equilibrium system involves line shape analysis. In principle this is a straightforward method for determining rate constants of exchange; however, in practice it can be difficult to separate the effects of exchange from those of relaxation and field inhomogeneity. The applicable timescale is isotope dependent, but for ^1H is typically in the 10–100 ms range. It is based on the appearance of signals in an NMR spectrum depending on nuclear properties of the spin, such as T_2 relaxation time, and on the rates of exchange. In the slow exchange regime, two distinct signals are observed. As exchange becomes faster these broaden, reaching a coalescence point at which they merge into one (the minimum between the signals is no longer observed). As the exchange becomes faster still, the signal becomes averaged and the natural line width is restored, in the fast exchange limit (Fig. 28). The simplest mathematical description of these effects for systems without scalar coupling is provided by the Bloch-McConnell equations [265].

In practice, line shape analysis is performed over a range of conditions that change the rates of exchange. The variables involved include, for example, temperature, concentration of ligand, and pH. Variable temperature line shape analysis also provides activation parameters via the Arrhenius (Eq. (18)) and Eyring (Eq. (19)) equations.

$$k(T) = Ae^{-\frac{E_a}{RT}} \quad (18)$$

$$k(T) = \frac{k_B T}{h} e^{\frac{AS^\ddagger}{R}} e^{-\frac{AH^\ddagger}{RT}} \quad (19)$$

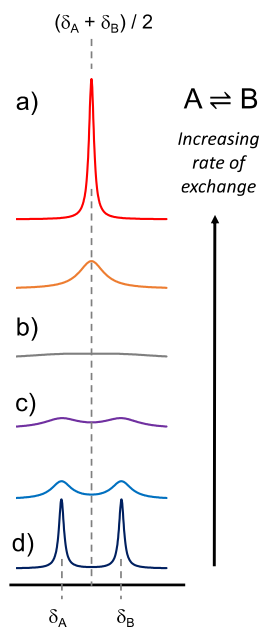


Fig. 28. Signals arising from two non-coupled but exchanging spins, A and B. (a) signal averaging in the fast exchange regime, (b) coalescence point, (c) signal broadening in the slow exchange regime, (d) slow or no exchange. For examples of the application of line-shape analysis see Case Studies 3 and 8.

Although the analysis of line shape, e.g. the coalescence point, can be approximated visually, software has been developed to allow for quantitative analysis by computational simulation of the spectra and fitting of experimental data. This is essential when the exchange process is mechanistically more complex than the simple two-site (A, B) system exemplified above; see Case Study 3 for an example.

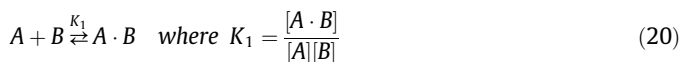
4.5. Titrations

The versatility of NMR as a tool for equilibrium *kinetic* measurements has already been discussed, and its utility in determining thermodynamic parameters is also very important [266]. NMR titrations can be of great importance in the study of the kinetics of a complex reaction, as the determination of association/isomerisation events *in isolation* can be used to greatly reduce the number of parameters that require to be fitted in a global kinetic model. While titrations are commonly used in the laboratory as tools for quantitative analysis of the concentration of an analyte, their implementation in NMR studies is often somewhat different. Rather than being utilised to determine the concentration of an analyte using a well-defined equilibrium (or set of equilibria), they are instead used to determine the nature and magnitude of the equilibrium constants themselves. In this section, we discuss the study of reversible molecular associations, using three examples: a single reversible association, a competitive association, and a cooperative association. A common experimental design for an NMR titration is one in which the concentration of a single component is varied systematically and the system response is plotted as a function of this variation. Depending on the rates of the equilibria, the response might be a change in the chemical shift of a key resonance, or a change in the integral of that resonance.

4.5.1. Single equilibrium

The simplest titration experiments relate to an equilibrium that describes a single reversible association between two species, that we refer to herein as generic species A and B. The nomenclature

can, and should, be changed to more chemically-relevant terms for the specific system of interest, for example M (metal complex) and L (ligand), or Cat (catalyst) and Sub (substrate).



To determine K_1 , the speciation of the system is measured at different concentrations of one of the components, while all of the others are kept constant. This speciation can be measured in two ways, depending on the rate of equilibration. In the case where the rate is slow at the NMR timescale (see Section 4.4.2), the concentrations are determined directly from the spectrum: they are proportional to the integrals of the separate signals due to each species I_x , Eq. (21).

$$K_1 = \frac{I_{A \cdot B}}{I_A I_B} \quad (21)$$

If the rate is faster than the NMR timescale, then species A will give rise to a signal (or number of signals) with the chemical shift (δ) tending towards that of A·B as species B is added. In this scenario, the absolute concentration of [A·B] can be calculated starting from Eq. (22), which states that the observed shift is a weighted average of the limiting shifts of pure A and pure A·B [267].

$$\delta = x_A \delta_A + x_{A \cdot B} \delta_{A \cdot B} \quad \text{where } x_A + x_{A \cdot B} = 1 \quad (22)$$

Since the concentration of A·B cannot exceed the initial concentration of A (i.e. $[A]_0$, which is kept constant during the titration), Eq. (23) can be used to calculate the concentration of A·B, provided that $[A]_0$ is known.

$$x_{A \cdot B} = \frac{[A \cdot B]}{[A]_0} = \frac{\delta - \delta_A}{\delta_{A \cdot B} - \delta_A} \quad (23)$$

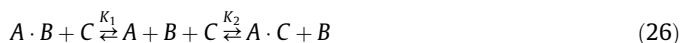
To extract K_1 , Eq. (24) is employed, using the known total concentrations $[A]_0$ and $[B]_0$ to give [A·B] as the only variable. Rearrangement for solution as a quadratic equation, and combination with Eq. (23) then allows fitting of Eq. (25), to a full dataset by minimising the sum-square error.

$$K_1 = \frac{[A \cdot B]}{[A][B]} = \frac{[A \cdot B]}{([A]_0 - [A \cdot B])([B]_0 - [A \cdot B])} \quad (24)$$

$$\frac{\delta - \delta_A}{\delta_{A \cdot B} - \delta_A} = \frac{K_1 [A]_0 + K_1 [B]_0 + 1 - \sqrt{(-K_1 [A]_0 - K_1 [B]_0 - 1)^2 - 4K_1^2 [A]_0 [B]_0}}{2K_1} \quad (25)$$

4.5.2. Competitive equilibria

The situation is more complex for a system of several coupled equilibria, Eq. (26), where B and C compete for A. This situation might be encountered for example when a catalyst (A) can bind both the substrate (B) and the product (C), with the latter leading to inhibition of catalysis.



Here the two constants, K_1 and K_2 , can be determined by non-linear regression of Eq. (27) and Eq. (28) [268]

$$[A] = -\frac{a}{3} + \frac{2}{3} \sqrt{(a^2 - 3b) \cos\left(\frac{\theta}{3}\right)}, \quad (27)$$

$$[A \cdot B] = \frac{[B]_0 \left\{ 2\sqrt{(a^2 - 3b) \cos\left(\frac{\theta}{3}\right)} - a \right\}}{3K_1 + \left\{ 2\sqrt{(a^2 - 3b) \cos\left(\frac{\theta}{3}\right)} - a \right\}} \quad (28)$$

$$[A \cdot C] = \frac{[C]_0 \left\{ 2\sqrt{(a^2 - 3b) \cos\left(\frac{\theta}{3}\right)} - a \right\}}{3K_2 + \left\{ 2\sqrt{(a^2 - 3b) \cos\left(\frac{\theta}{3}\right)} - a \right\}}$$

$$\text{where } \theta = \frac{-2a^2 + 9ab - 27c}{2\sqrt{(a^2 - 3b)^3}}$$

$$a = K_1 + K_2 + [B]_0 + [C]_0 - [A]_0;$$

$$b = K_1([C]_0 - [A]_0) + K_2([B]_0 - [A]_0) + K_1K_2$$

$$c = -K_1K_2[A]_0$$

In the case of competitive titration experiments it is common to start with a known concentration of two components and then systematically change the concentration of the competitor while measuring the system response by NMR. This results in a plot and fitting of data that look very similar to those for a single reversible association. Competitive equilibria are particularly useful for the *indirect* determination of molecular association in cases where the study of the complex of interest is not spectroscopically feasible. In such cases, a competitor whose binding *can* be quantified spectroscopically can be titrated in the presence of different concentrations of the molecule of interest, allowing the thermodynamics of the interactions of interest to be determined.

4.5.3. Cooperative equilibria

For systems of equilibria where multiple components can associate in a sequential manner, the degree to which each association event affects subsequent associations can be quantified as the cooperativity of the system, α . Equilibria that are completely uncooperative (association at each site is independent of association at other sites) have $\alpha = 1$. Systems where association makes subsequent associations more favourable, have positive cooperativity, $\alpha > 1$, and analogously for negative cooperativity where subsequent associations are less favourable, $\alpha < 1$ [269]. An illustrative example of a cooperative system is one in which *A* can bind with two molecules of *B* sequentially, Eq. (29). This situation might be encountered for example when *B* is a ligand at a metal site (*A*) and only the monoligated form (*A*·*B*) is catalytically active; under these conditions larger K_1 and lower α values lead to more efficient catalysis.



$$K_1 = \frac{[A \cdot B]}{[A][B]} \quad \text{and} \quad K_2 = \alpha K_1 = \frac{[B \cdot A \cdot B]}{[A \cdot B][B]} \quad (30)$$

Statistical factors (2 and 1/2) are used in weighting the equilibria because of the equivalence of the two association sites (in *A* and in *B*·*A*·*B*) [270]. For a fast exchange system, the degree to which *A* is saturated with *B* is a measurable ‘occupancy parameter’, θ_A , defined in this example by Eq. (31) and determined experimentally in a manner analogous to Eq. (23).

$$\theta_A = \frac{\frac{1}{2}[A \cdot B] + [B \cdot A \cdot B]}{[A]_0} \quad (31)$$

When the concentration of *B* is much greater than the total concentration of *A*, i.e. $[A]_0$, then the concentration of non-associated (‘free’) *B* can be approximated as $[B]_0$. Using the equilibria in Eq. (29), θ_A can be expressed as a function of $[B]_0$, depending on K_1 and α ; Eq. (32).

$$\theta_A = \frac{K_1[B]_0 + \alpha K_1^2[B]_0^2}{1 + 2K_1[B]_0 + \alpha K_1^2[B]_0^2} \quad (32)$$

4.5.4. Preparing the sample for analysis

The following is a typical procedure. Two stock solutions (I and II) are prepared. Solution I contains only component, e.g. *A*, and is prepared first, at an accurate and precise concentration. A large excess of *B* is then dissolved in a sample of solution I to give solution II, in which *A* is essentially only present in the form *A*·*B*. The large excess of *B* in solution II ensures that small volumes of it can be added to solution I in the NMR titration, to give data that spans a large range of speciation, with a manageable total sample volume in the NMR tube. As large numbers of solution transfers are typically conducted in an NMR titration, great care must be taken to ensure volumetric accuracy in any dilutions, and minimisation of solvent evaporation. All stock solutions should be prepared freshly (where practical), stored in sealed vessels, and transferred using microsyringes to prevent evaporation.

Although there is no time dependence in mathematical models, the stability of substrates and the rate of adjustment of a system to a new equilibrium must always be considered when designing a titration experiment. If the system is still equilibrating at the time of measurement, then the integral data extracted will not reflect the equilibrium populations and will therefore introduce large errors in the data. For this reason, it is useful to repeat measurements for systems in slow exchange and compare integrals to verify that the system has reached equilibrium before proceeding with the next aliquot of solution II. Removing part of the solution already in the NMR tube leads to errors due to solvent evaporation/transfer loss and should be avoided if possible. We advise use of specialised titration NMR tubes (Fig. 2d). These have a screw cap lid designed to facilitate sequential addition of aliquots, allowing resealing, and thorough mixing of the sample in the upper chamber by repeated inversion of the tube.

4.5.5. Model selection

The first point to consider when fitting data to a model is the functionality and symmetry of the compounds being studied, and thus the likely stoichiometry of association. If the stoichiometry of association is 1:1 then a simple bimolecular association, which gives a quadratic response curve (Fig. 29a) will usually give a good fit for the data. If a number of identical association sites are avail-

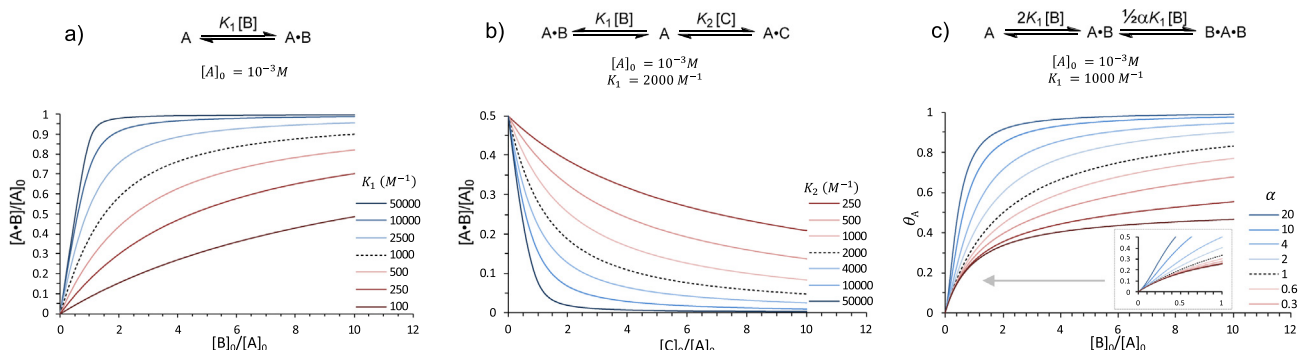


Fig. 29. Comparison of titration curves for (a) simple, (b) competitive, and (c) sequential association with positive cooperativity, $\alpha > 1$, and sequential association with negative cooperativity, $\alpha < 1$, systems. See Case Studies 1 and 10 for examples.

able, then models with stoichiometry 2:1 or higher must be considered. The first model to examine in such a case is a non-cooperative 2:1 termolecular association (single equilibrium) which has a steeper initial response (Fig. 29b) than the quadratic curve of 1:1 association (Fig. 29a). If the non-cooperative 2:1 model does not fit, then the simple single equilibrium association should be split into multiple binding events, whose equilibrium constants are linked by a cooperativity constant (α ; Eq. (29)). Fitting of the cooperativity constant (Fig. 29c) should allow the model to incorporate systematic deviations if cooperative binding is the cause. In the case of a positively cooperative system, the data will have sigmoidal character, with an initial lag in uptake compared to the non-cooperative fit, followed by a large increase as more guest is added. A negatively cooperative association will have a faster uptake but also an earlier plateau when compared to a non-cooperative model of the same stoichiometry.

4.6. Analysis of intermediates using DOSY

Pulsed field gradient (PFG) NMR experiments can be used to determine the translational self-diffusion coefficients, D_T , of molecules in solution. Because D_T depends on molecular size, shape, conformational flexibility, and density, its measurement can be very valuable for probing interactions and intermediates in mechanistic studies. Such experiments invariably employ a diffusion-ordered spectroscopy (DOSY) display method [271]. DOSY allows one to probe the structure, interactions, and reactions of small to medium sized molecules [272–274], in a way that is complementary to other approaches; see for example Case Studies 2, 12 and 15. DOSY can be applied to mechanistic work in a qualitative, or quantitative manner. However, due to the absence of a general relationship between D_T and molecular weight, especially for small molecules, quantitative interpretations must be made with caution [275–277].

4.6.1. The DOSY experiment

In a typical DOSY experiment, a one-dimensional PFG is applied along the z-axis, after the standard 90° excitation, resulting in the phases of the nuclear spins being dependent on their position in the sample. In the absence of any diffusion, the effect of the first PFG can be negated by reversing the direction of all the spins in the horizontal plane (xy-plane) (e.g. with a spin or stimulated echo sequence) and then applying a second, identical, PFG. Molecules will of course diffuse randomly in the time between the two PFGs, and the root mean square displacement z_{rms} of a molecule along one dimension from some initial position after a time t is given by Eq. (33). This diffusion leads to vertical mixing, and therefore incomplete refocussing by the second PFG. The greater the extent of vertical mixing, the greater the attenuation of the observed signal intensity, I , relative to I_0 , the signal in the absence of the paired PFGs.

By measurement of a series of 1D spectra (Fig. 30a) in which the PFG strength, g_z is varied, the diffusion coefficient D_T can be determined by regression of Eq. (34), in what is referred to as a Stejskal-Tanner plot (Fig. 30b) [278,279]. However, fitting to a linearised form distorts the statistical weight of the experimental data points, and non-linear regression of the Stejskal-Tanner equation, Eq. (35), is recommended. Both equations require the effective diffusion time, Δ_{ef} , (closely related to the delay (Δ) between the PFGs) [278], and the duration, δ , of the PFG. The latter two are usually fixed, and only g_z varied; this avoids complications arising from T_1 and T_2 relaxation. It is common to transform the resulting series of 1D spectra into a 2D representation, with one dimension the chemical shift and the other the fitted diffusion coefficient D_T , Fig. 30c

$$z_{rms} = \sqrt{2D_T t} \quad (33)$$

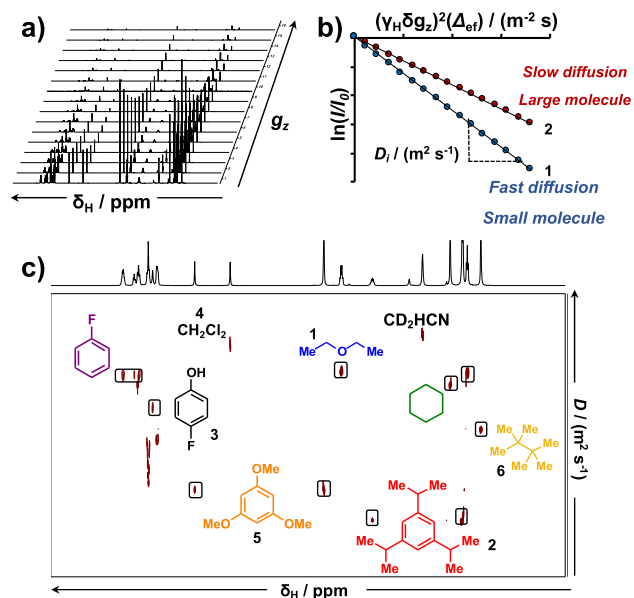


Fig. 30. An example ^1H DOSY analysis of a mixture of small organic molecules in CD_3CN (400 MHz, $\Delta = 75$ ms, $\delta = 1.1$ ms, 20°C). (a) Stacked 1D ^1H NMR spectra obtained at different gradient strengths (g_z), with quadratic ramping from $0.05 G_{\text{max}}$ to $0.95 G_{\text{max}}$ (16 increments; $G_{\text{max}} = 53.5 \text{ G cm}^{-1}$). (b) Linearised Stejskal-Tanner plots for two example molecules (Et_2O (1), 1,3,5-triisopropylbenzene (2)); the diffusion coefficient of each species is represented by the gradient. (c) 2D ^1H DOSY NMR spectrum. Spectral overlap in the aromatic region ($\delta_{\text{H}} = 7\text{--}8$ ppm) between resonances from p-F-PhOH (3) and 1,3,5-triisopropylbenzene (2) leads to compromised apparent diffusion coefficients; other species, for example 4, 5 and 6, are better resolved.

$$\ln\left(\frac{I}{I_0}\right) = -(\gamma g_z \delta)^2 \Delta_{ef} D_T \quad (34)$$

$$\frac{I}{I_0} = e^{-(\gamma g_z \delta)^2 \Delta_{ef} D_T} \quad (35)$$

4.6.1.1. Nucleus, solvent, co-solutes, and temperature control. Although ^1H is ubiquitous, the narrow chemical shift range and prevalence of homonuclear coupling can lead to spectral overlap, precluding accurate determination of D_T values. Pure shift methods (Section 3.5) can be used to achieve significant improvements in DOSY resolution [280–282]. Enhancements can also be achieved by combining DOSY with other 2D NMR techniques – including COSY, HSQC, NOESY and TOCSY – to create 3D DOSY experiments [283–285]. $^{13}\text{C}\{^1\text{H}\}$ DOSY has greater spectral resolution than ^1H , but requires polarisation transfer (^{13}C INEPT, DEPT) [286]. Spectral congestion can sometimes be avoided by using ^{19}F or ^{31}P DOSY, if the chemistry permits it [287,288]. ^6Li DOSY in combination with ^1H -DOSY and $^6\text{Li}\{^1\text{H}\}$ -HOESY, has been usefully applied for study of aggregation in organolithium compounds [289].

The self-diffusion coefficient, D_T , varies with solution viscosity, which in turn depends on the identity of the solvent, the concentration of the sample, and the identity and concentration of any co-solutes. In general, greater D_T values will be observed for more dilute samples, and in samples prepared with low viscosity solvents. For mixtures of multiple compounds – and particularly during the selection of appropriate internal diffusion standards (Section 4.6.2.3) – it is crucial to consider the possibility of intermolecular complexation and self-association, and D_T values that change significantly with concentration are diagnostic of such interactions. In addition to viscosity, the choice of solvent also determines susceptibility to convection. In general, a more viscous

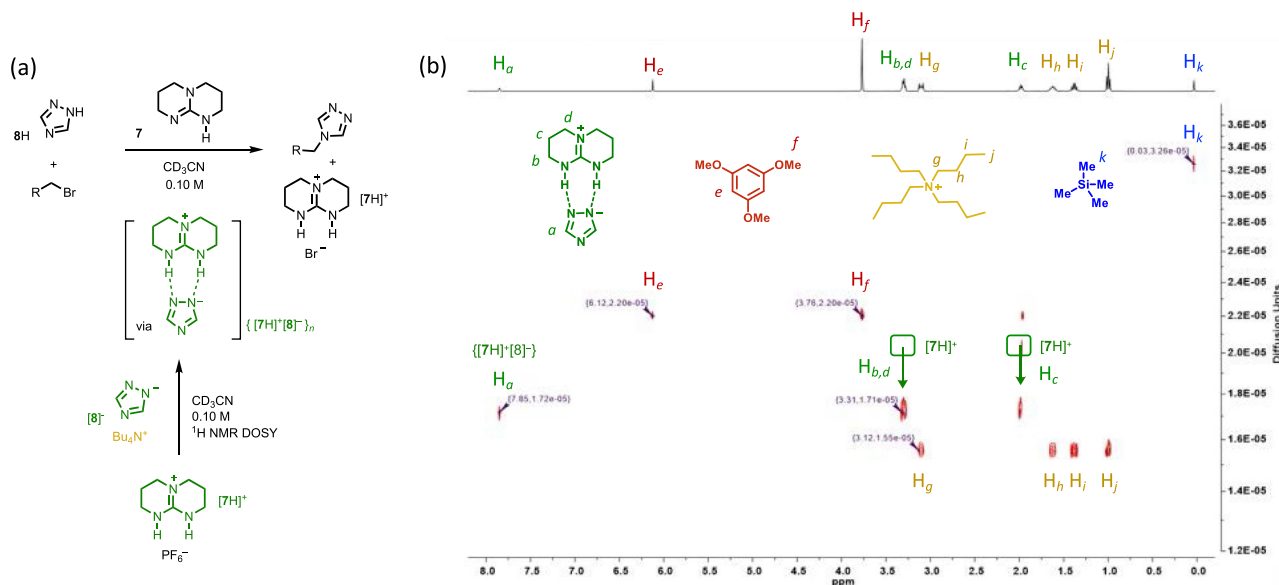


Fig. 31. (a) alkylation of triazole at the 4-position, mediated by strong neutral organic base 7. (b) ^1H DOSY NMR analysis employed during mechanistic analysis to establish that a doubly-H bonded ion pair $\{[7\text{H}]^+[8]^{-}\}$ is generated, in which the nitrogens at the 1- and the 2-positions are protected from alkylation, thus accounting for the unusual selectivity (the alkylation of 1,2,4-triazole usually occurs at the 1-position) [27].

solvent with high density and low thermal expansion coefficients should be selected to suppress convective flow. However, for mechanistic studies it is essential that DOSY experiments are conducted in the same solvent, or one of the range of solvents, as the reaction under investigation.

Convective flow during DOSY can lead to highly misleading results [290], and must be eliminated or otherwise suppressed in experiments where quantitative accuracy in D_T values is required. Ideally, cryoprobes should be avoided, and the experiments run under ambient conditions. Elevated VT gas flow rates can be applied to minimise temperature gradients, but must not be so high as to affect the physical stability of the sample in the probe. Variable temperature experiments must be accompanied by careful temperature calibration, ensuring also that the sample has reached thermal equilibrium. Greatly reduced convective flow can be achieved by using NMR tubes with thicker walls/narrower bores.

4.6.1.2. Pulse sequence and gradient parameters. There are many pulse sequences for DOSY NMR. A ‘stimulated echo’ pulse sequence with bipolar and spoiler gradients [291] is a good starting point for 2D DOSY experiments on organic samples. The *Oneshot* sequence permits the acquisition of good quality DOSY spectra without phase cycling and can significantly reduce experiment times [292]. If spectral resolution is an issue, 3D pulse sequences, including COSY-iDOSY [285], DQF-COSY-iDOSY [284], and HSQC-iDOSY [283] can be employed. PSYCHE-iDOSY can be used for pure shift ^1H -detected DOSY experiments [280]. ^1H DOSY experiments in non-deuteriated solvents should make use of a sequence that suppresses the residual solvent signal(s). Two commonly employed PFG shapes [293] are the sine bell and the smoothed trapezoid [278], and ideally the gradient pulse strength is incremented in a way that produces evenly distributed data points in the Stejskal-Tanner plot. The total number of increments n dictates the dynamic range of the DOSY experiment, and for small and medium sized molecules ($M_w = 50 - 1000 \text{ g mol}^{-1}$) n should be between 10 and 20.

4.6.2. Interpreting DOSY in mechanistic studies

There are two general approaches for the interpretation of diffusion coefficients for small and medium-sized molecules [275].

One uses variations on the Stokes-Einstein equation; the other uses empirical power laws to extract molecular weight information based on calibration curves generated from internal or external reference compounds.

For example, a dual H-bonding association between the cation $[\text{TBDH}]^+$ ($[7\text{H}]^+$) and the 1,2-nitrogens of the 1,2,4-triazolate anion $[8]^-$ has been proposed as the mechanism by which TBD (7) catalyses the alkylation of 1,2,4-triazole (8H), with high selectivity for addition at the 4-position, Fig. 31 [27]. Although X-ray crystallography identified $\{[7\text{H}]^+[8]^{-}\}$ in the solid state, simple ^1H NMR chemical shift analysis in solution was ambiguous. However, NMR diffusion studies provided important information about this interaction under the conditions of catalysis. ^1H NMR-DOSY spectra of $[7\text{H}]^+\text{PF}_6^-$ (0.10 M) and an equimolar mixture of $[7\text{H}]^+\text{PF}_6^-$ (0.10 M) and $[\text{Bu}_4\text{N}]^+[8]^-$ (0.10 M), were measured in CD_3CN at 20°C using Me_4Si and 1,3,5-trimethoxybenzene as internal reference compounds. In a qualitative sense, the decrease in the diffusion constant for $[7\text{H}]^+$ (from $D_T = 2.1 \times 10^{-5} \text{ cm}^2 \text{ s}^{-1}$ [see open green boxes in Fig. 31] to $1.7 \times 10^{-5} \text{ cm}^2 \text{ s}^{-1}$) upon the addition of $[8]^-$, and the observation that $[7\text{H}]^+$ and $[8]^-$ then share the same diffusion constant was strongly suggestive of solution-phase association, $\{[7\text{H}]^+[8]^{-}\}_n$. Using the diffusion of Me_4Si ($D_T = 3.2 \times 10^{-5} \text{ cm}^2 \text{ s}^{-1}$) to standardise between the samples allowed a Stokes-Einstein based estimation of the volumetric ratio of $\{[7\text{H}]^+[8]^{-}\}$ versus $[7\text{H}]^+$ as 1.23. This was compared with a computed (KS-DFT; PBE0 + GD3BJ/6-311 + G(d,p)) volumetric ratio of 1.24, supporting the conclusion that the association is predominantly monomeric, i.e. $n = 1$.

4.6.2.1. Stokes-Einstein. The Stokes-Einstein equation (Eq. (36)) is based on diffusion of a perfectly spherical particle (volume V ; mass M ; density ρ ; radius R) under ideal conditions. It cannot be usefully applied in a direct manner to the molecules of interest in most mechanistic investigations. Instead, a number of modifications are made to allow application. One common modification, Eq. (37), includes correction factors that account for solute size, f_s , and non-spherical geometry, f_g .

$$D_T = \frac{k_B T}{6\pi\eta R} = \frac{k_B T}{6\pi\eta} \left(\frac{4\pi}{3V}\right)^{\frac{1}{3}} = \frac{k_B T}{6\pi\eta} \left(\frac{4\pi\rho}{3M}\right)^{\frac{1}{3}} \quad (36)$$

$$D_T = \frac{k_B T}{6f_s f_s \pi \eta R} \quad (37)$$

Gierer and Wirtz derived Eq. (38), that expresses f_s in terms of the radius ratio $\alpha = R_{\text{soliv}}/R$ [294]; although the equation tends to systematically overestimate D_T when $M_w < 1000 \text{ g mol}^{-1}$. The SEGWE method, Eq. (39), developed by the group of Morris, introduces an effective molecular density $\rho_{\text{eff}} = \rho/f_g^3$ to predict the diffusion coefficients of small and medium-sized organic molecules [276,277]. The radius ratio α is approximated from the relative molecular masses of the solute (M_w) and solvent (M_w^{sol}). Using an extensive benchmarking set ($M_w < 1,500 \text{ g mol}^{-1}$) a universal value of effective density $\rho_{\text{eff}} = 0.627 \text{ g cm}^{-3}$, Eq. (40), was found to give the best overall agreement with experimental diffusion coefficients. This expression is generally applicable to many small organic molecules. However, for concentrated solutions, especially those comprising electrostatically charged solutes (as generated for example in organic acid-base reactions, or with cationic metal complexes often used as catalysts), the use of a series of standards is recommended.

$$f_s = \frac{2(1+\alpha)}{3\alpha(1+\alpha)+2}, \alpha = \frac{R_{\text{sol}}}{R} \quad (38)$$

$$D_T = \frac{k_B T}{6\pi\eta} \left(\frac{4\pi\rho_{\text{eff}}N_A}{3M_w} \right)^{\frac{1}{3}} \left(\frac{3\alpha(1+\alpha)+2}{2(1+\alpha)} \right), \alpha = \left(\frac{M_w^{\text{sol}}}{M_w} \right)^{\frac{1}{3}} \quad (39)$$

$$\rho_{\text{eff}} = \frac{\rho}{f_g^3} = 0.627 \text{ g mL}^{-1} \quad (40)$$

4.6.2.2. Empirical power laws. An alternative approach involves empirical power laws, and a common one is Eq. (41), in which K and β (typically $0.4 < \beta < 0.8$) depend upon the identity of the solvent, the temperature, viscosity, molecular density and molecular geometry [275].

$$D_T = KM_w^{-\beta}; \text{ and } \log D_T = -\beta \log M_w + \log K \quad (41)$$

A series of reference compounds of known M_w are used to generate a calibration curve, based on the logarithmic form of Eq. (41). The correct selection, and use of a substantial number, of reference compounds is crucial, and extrapolations outside the calibrated M_w range should be avoided.

4.6.2.3. Selection of reference compounds. Reference compounds for DOSY should have broadly comparable molecular densities (ρ_M) solvation characteristics, and geometries to the solute(s) of interest. Ideal reference compounds are direct homologues of the solute(s) of interest – although this is often impractical. The density of a molecule ρ_M can be estimated using Eq. (42) which approximates V_M by a summation of the van der Waals volumes $V_{A,i}$ of all the constituent atoms i , with each atom treated as a sphere of van der Waals radius r_i [299]. This approach works best when solute and reference compounds belong to the same geometry class, generally described as compact spheres, dissipated spheres/ellipsoids (DSEs) and extended discs [298]. Most small organic molecules diffuse as DSEs.

$$\rho_M = \frac{M_w}{V_M} = \frac{M_w}{\sum_i V_{A,i}} = \left(\frac{3}{4\pi} \right) \frac{M_w}{\sum_i r_i^3} \quad (42)$$

4.6.2.4. Internal versus external calibration. Reference compounds can be added to the sample of interest [286,287,295,296], or measured independently [297,298]. Although in principle, internal calibration eliminates the greatest number of systematic errors, for mechanistic investigations the difficulty of finding appropriate ref-

erence species that also have reaction compatibility can make the external technique simpler to apply. For internal calibration a single DOSY spectrum is acquired, with D_T of all components extracted from the same spectrum. The reference compounds must be inert and their signals well-resolved from each other, and from the reaction components. Ideally three or more internal standards should be used, however spectral congestion is often a major issue.

External calibration greatly reduces issues arising from spectral congestion, and from undesired influence of the reference on the mechanism or kinetics of the reaction being investigated. The calibration curves are generated using a series of reference compounds together with a universal internal standard, Eq. (43). Normalised diffusion coefficients for each reference compound, $D_{i,\text{norm}}$, are obtained from D_i and D_{IS} , the coefficient measured for the reference and alongside the internal standard IS, and $D_{\text{IS},\text{norm}}$, the coefficient of the internal standard in the same solvent, without any other solutes present. A double logarithmic plot of $\log_{10}[D_{i,\text{norm}}]$ vs $\log_{10}(M_w)$ gives the final calibration curve. Whilst separate external calibration curves must be generated for each solvent, once generated they are universally applicable. For example, calibration curves have been published for d_8 -THF, d_8 -toluene, CDCl_3 , CD_2Cl_2 , d_{12} -cyclohexane, d_6 -DMSO, and C_6D_6 , and can be applied directly [297,298].

$$\log_{10}[D_{i,\text{norm}}] = \log_{10}[D_{\text{IS},\text{norm}}] + \log_{10}[D_i] - \log_{10}[D_{\text{IS}}] \quad (43)$$

5. Use of isotopes

5.1. Introduction

Mechanistic studies in organic and organometallic chemistry frequently depend upon isotopic substitution experiments. Such experiments usually involve the incorporation of a stable, normally naturally low-abundant, isotope(s) into a reaction component – for example in a substrate, intermediate, catalyst, ligand, solvent etc. The fate, or influence, of the isotope is then determined so as to help elucidate mechanistic information. Chemical reactions of synthetic relevance are often complex, with many involving extended networks of coupled reactions – some slow, some fast, some reversible, some irreversible. In such networks it is often possible for multiple steps to be affected by a single isotopic substitution in the starting material. Nevertheless, when deployed judiciously, isotopic substitution experiments afford mechanistic insights of unsurpassed detail and subtlety, offering a direct, experimentally determinable outcome from key transition states in complex reactions, and providing robust quantitative benchmarks to support theoretical studies. NMR spectroscopy is uniquely suited to the monitoring of isotopically-enriched (or depleted) reactions in the solution phase, on account of its capacity to distinguish molecules that differ by virtue of isotopic constitution (isotopologues) and isotopic connectivity/configuration (isotopomers). Indeed, as reviewed below, when conducted in conjunction with NMR spectroscopy, isotopic substitution can be applied in a wide variety of ways.

For example, isotopic substitution can be used to perturb the rate of a chemical process, or the position of an equilibrium, and thus to extract mechanistic information (Section 5.3). Isotope ‘enrichment’ (the flux of an isotope through a reaction) can be used to probe the behaviour of intermediate species detected during stoichiometric and catalytic reactions. Strategic simplifications of NMR spectra, or the facilitation of multidimensional NMR techniques, can be achieved by selective installation of isotopes, allowing for example the structures of complex organometallics and ligand architectures to be deduced. The enrichment of a naturally low-abundance, NMR active isotope (e.g., ^{13}C , ^{15}N) in a substrate,

intermediate or catalyst can be used to enhance S/N during reaction monitoring, expedite spectral acquisition, aid in the detection of elusive reactive intermediates at low concentrations, and determine coupling constants that are typically unobservable at natural abundance (e.g. ^{13}C - ^{13}C , ^{13}C - ^{15}N).

Isotopic substitution studies in organic chemistry typically make use of nine key isotopes – encompassing both spin $\frac{1}{2}$ and quadrupolar nuclei – including seven that are directly-detectable by NMR spectroscopy (^2H , ^6Li , ^{10}B , ^{11}B , ^{13}C , ^{15}N , and ^{17}O) and two that are NMR silent (^{18}O , ^{34}S). It should be noted that NMR silence does not preclude the use of the corresponding nuclei in isotopic substitution experiments, as they can often be detected by secondary isotope shifts induced in proximate, NMR active nuclei.

Synthetic routes for the installation of isotopic labels range from the trivial to the very laborious. For exchangeable protons (e.g. **NH**, **OH**, **SH**), isotopic labelling can be done *in situ* using deuteriated isotopologues of protic solvents (e.g. MeOD, D_2O). Moreover, under appropriate conditions the precise ratio of protonated to deuteriated substrate can be controlled with the corresponding ratio of protonated/deuteriated solvent, allowing a technique referred to as ‘proton inventory’. ^2H labelling of non-labile positions is often possible with an appropriate choice of synthetic pathway, due to the diverse array of commercially available deuteriated precursors.

Isotopic substitution of heavy nuclei can be laborious and expensive, due to the relatively narrow range and cost of commercially-available precursors, but the benefits in terms of application in NMR-based mechanistic elucidation are frequently worth the effort. In contrast to the large range of complex isotopically labelled bio-organic precursors that are commercially available, those required for complex organic reactions are much more limited. This usually means that multistep synthesis from simple precursors is required. For ^{13}C -labelling, these include $^{13}\text{CH}_3\text{I}$, $^{13}\text{CH}_3\text{OH}$, $[1\text{-}^{13}\text{C}]$ -acetic acid, $[1,2\text{-}^{13}\text{C}_2]$ -acetic acid, $[1\text{-}^{13}\text{C}]$ -bromoacetic acid, $[1,2\text{-}^{13}\text{C}_2]$ -bromoacetic acid, $[1\text{-}^{13}\text{C}]$ -benzoic acid, $[1\text{-}^{13}\text{C}]$ -acetyl chloride, $[1,2,3\text{-}^{13}\text{C}_3]$ -acetone, $[^{13}\text{C}_6]$ -PhH and ^{13}CO . ^{15}N -labelling is often initiated from $^{15}\text{NH}_3$ or ammonium salts of the form $^{15}\text{NH}_4\text{X}$ (X = OH, Cl, NO_3 , OAc) or $(^{15}\text{NH}_4)_2\text{SO}_4$, whilst $^{10}\text{B}/^{11}\text{B}$ labelling typically begins with the corresponding $[^{10}\text{B}]$ - and $[^{11}\text{B}]$ - boric acids or esters. For heavier isotopes, commercial availability is more limited in scope. For example, for ^{18}O and ^{34}S labelling, the precursors are generally limited to $^{18}\text{O}_2$, $^{18}\text{OH}_2$ and $^{34}\text{S}_8$.

5.2. Atom accountancy and tracking

Sites of isotopic substitution are often employed as tracers (labels) during reaction monitoring [300]. In these cases, isotopic substitutions are made at selected sites within a substrate, and the connectivity of the label is tracked during the course of a reaction. In this way it is possible to trace the origin and destination of specific nuclei in a reaction, when this would otherwise remain unknown or ambiguous. This approach is particularly useful for distinguishing competing reaction pathways that lead to degenerate products (e.g. migrations), and therefore also for the investigation of stereochemistry. Isotopic substitution can also be used as a tool for spectroscopically resolving otherwise degenerate molecules during a reaction, by virtue of induced isotopic shifts or changes in scalar coupling. This is particularly useful for monitoring self-exchange and intermolecular competition reactions involving multiple isotopologues by NMR.

Isotopic substitutions are ideally suited to atom accountancy and tracking experiments, as the replacement of one isotope by another generally has a very small effect on the reactivity of a substrate (see Section 5.3), and therefore is unlikely to perturb the

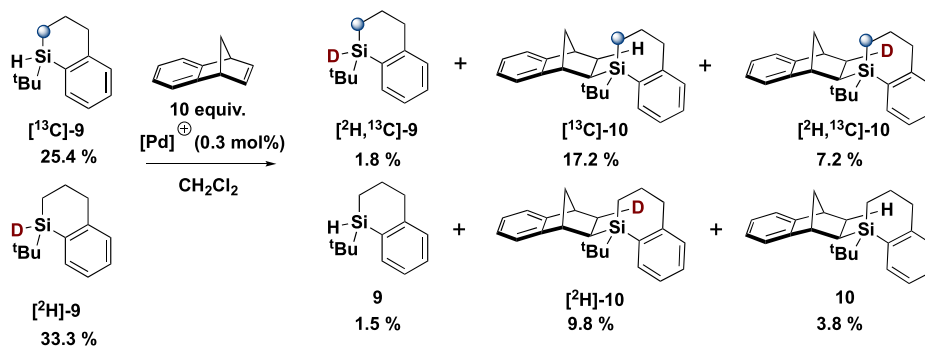
underlying reaction mechanism. Atom accounting experiments generally seek solely to track the position of an isotopic label in an intermediate or product, allowing qualitative, but often fundamental, deductions to be made about the reaction mechanism. However, when combined with quantitative NMR measurements and kinetic simulations, atom accounting experiments can be used to make quantitative assessments of rates and equilibria.

‘Crossover experiments’ with isotopically labelled substrates are a particularly powerful form of atom accounting [301–304]. In a crossover experiment, two different isotopologues of the same substrate are assembled together at the start of reaction, and the isotopic content of the products is then analysed after partial or complete reaction. If the substrate undergoes some form of fragmentation, or intermolecular exchange with another species during the reaction, there will be a degree of isotopic exchange (‘crossover’) evident in the distribution of the product isotopologues. The generation of crossover products can often be detected by NMR through changes in scalar coupling and isotope shifts. The outcome of such an experiment can help corroborate, or discount, a mechanistic proposal.

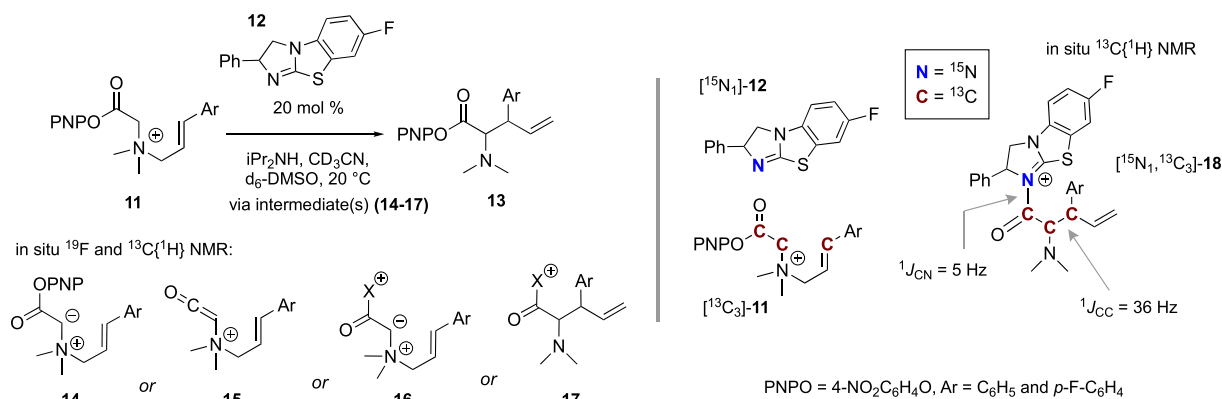
Caution must be exercised when using deuteriated substrates in crossover experiments, where peripheral pathways leading to statistical isotopic scrambling are competitive with the productive reaction. Facile exchange between protic solvents and a substrate, intermediate or product is a common cause of such scrambling. Indeed, the scrambling of isotopes in the product via other processes should always be tested, using reference materials.

The atom-accountancy approach has proved useful to us in a wide variety of mechanistic studies. The Pd-catalysed hydrosilylation of norbornenes is an example that demonstrates the value, and variety, of crossover experiments that can be conducted with isotopically labelled substrates, Scheme 4. By combining multiple $^2\text{H}/^{13}\text{C}$ crossover experiments with $^{29}\text{Si}\{^1\text{H}\}$ NMR spectroscopy [305], a range of conclusions were drawn about the mechanism of this fundamental process. Crossover experiments with rac- $[^{13}\text{C}]$ -**9** and rac- $[^2\text{H}]$ -**9** proceeded with only a trace of scrambling in the substrate (**9**) and gave all four possible product isotopologues – **10**, $[^{13}\text{C}]$ -**10**, $[^2\text{H}]$ -**10** and $[^{13}\text{C}, ^2\text{H}]$ -**10**. This was shown to be consistent with a process in which each molecule of product is generated from components of two separate molecules of the substrate, *via* two sequential turnovers of a ‘two silicon cycle’. Kinetic simulations were able to reproduce almost exactly the distribution of product isotopologues observed by $^{29}\text{Si}\{^1\text{H}\}$ NMR. It is important to note that the presence of both $^1J_{\text{Si-C}}$ coupling and $\gamma\text{-}^2\text{H}$ isotope shifts was pivotal for the NMR spectral resolution of the four products.

Changes in scalar coupling on use of different isotopologues can also be a very valuable mechanistic tool. For example, if an intermediate is detected in an *in situ* NMR investigation, and the structure of the intermediate is ambiguous, the presence or absence of specific scalar couplings over single or sequential bonds can provide definitive evidence of bond cleavage or bond generation, both inter- and intra-molecular. In a recent study of the [2,3]-rearrangement of **11**, catalysed by benzotetramisole **12**, a short-lived intermediate was detected by *in situ* ^{19}F NMR and by *in situ* $^{13}\text{C}\{^1\text{H}\}$ NMR using an ^{13}C -isotopically-enriched substrate. However the identity of the intermediate, amongst a number of possibilities including **14–17**, was unclear [32]. Synthesis of triply ^{13}C -labelled substrate $^{13}\text{C}_3$ -**11**, and ^{15}N -labelled catalyst ^{15}N -**12**, allowed *in situ* $^{13}\text{C}\{^1\text{H}\}$ NMR analysis of $^1J_{\text{CC}}$ and $^1J_{\text{CN}}$ couplings and chemical shifts, to provide definitive evidence that the bonds indicated in $[^{15}\text{N}_1, ^{13}\text{C}_3]$ -**18**, Scheme 5, were present, and thus support the conclusion that this is the intermediate. Confirmation that **18** is an intermediate en route to **13**, not a catalyst side product, was provided by isotope entrainment, see Section 5.4



Scheme 4. Mechanistic analysis of Pd-catalysed hydrosilylation by $^2\text{H}/^{13}\text{C}$ crossover. Example isotopologue distributions in reagents (**9**) and products (**10**) are reported as percentage abundance at 38% conversion. [Pd] = [(phen)PdMe(OEt)₂]



Scheme 5. Multiple NMR-active isotope labelling to allow detection of new C–N and C– bonds in transient intermediate **18**, via scalar couplings determined by *in situ* ^{13}C NMR spectroscopy [32]. For further examples see Case Studies 8 and 14.

5.2.1. Isotope shifts

Isotopic substitution typically leads to small but measurable perturbations in the chemical shifts of nearby nuclei [306]. These perturbations are termed *isotope shifts* and denoted by ${}^n\Delta\delta_X(I_H, I_L)$, where $\Delta\delta_X$ specifies the change in chemical shift of a reporter nucleus X that arises from isotopic substitution, I_H and I_L denote the two isotopes (heavy and light) being exchanged, and n denotes the number of intervening bonds between the reporter nucleus X and the site of isotopic substitution, Eq. (44). Primary isotope shifts arise when the reporter nucleus X and site of isotopic substitution are one and the same (i.e. $n = 0$), whereas secondary isotope shifts arise when $n > 0$. Primary isotope shifts are thus only possible for elements with at least two NMR active nuclei.

$${}^0\Delta\delta_X(I_H, I_L) = \delta_X(I_H) - \delta_X(I_L) \quad (44)$$

The equilibrium geometry of molecules (the global minimum on the potential energy surface) is generally regarded as being isotopically independent. Isotopic substitution does, however, change the vibrational frequencies of a molecule on the potential energy surface, and therefore the time-averaged molecular geometry [307,308]. It is these small, time-averaged structural changes that lead to perturbations in chemical shifts. Structural perturbations, and therefore isotope shifts, are largest when isotopic substitution is made at a site whose motion contributes to strongly coupled anharmonic modes.

Isotope shifts decrease in magnitude with increasing n , are approximately additive, and are largest when: (i) the reporter nucleus X has a broad chemical shift range (e.g. X = ^{13}C , ^{15}N , ^{19}F); and (ii) the fractional increase in mass upon isotopic substitution is largest (e.g., when $I_L = ^1\text{H}$; $I_H = ^2\text{H}$). Substitutions with heavier

isotopes generally, but not invariably, induce a decrease in chemical shift (${}^n\Delta\delta_X(I_H, I_L) < 0$). Typical primary isotope shifts for $^1\text{H}/^2\text{H}$ substitution ${}^0\Delta\delta(^2\text{H}, ^1\text{H}) < 100$ ppb, although values ${}^0\Delta\delta(^2\text{H}, ^1\text{H}) > 1$ ppm can be observed in strongly hydrogen-bonded systems; secondary isotope shifts induced in ^{13}C resonances by $^1\text{H}/^2\text{H}$ substitution are generally $0.1 \text{ ppm} < {}^1\Delta\delta_{13\text{C}}(^2\text{H}, ^1\text{H}) < 1.5$ ppm and $0.05 \text{ ppm} < {}^2\Delta\delta_{13\text{C}}(^2\text{H}, ^1\text{H}) < 0.1$ ppm. Larger secondary isotope shifts can be observed in systems with strong, intramolecular hydrogen bonding.

There are several ways in which isotope shifts can be leveraged during reaction monitoring by NMR. Exploiting isotope shifts is often the only way to detect the presence – and thereby quantify the incorporation – of isotopes that are either NMR silent (^{18}O , ^{34}S) or quadrupolar with very fast T_1 relaxation (^{33}S , ^{35}Cl); for this reason isotope shifts can be indispensable when measuring heavy-nuclei KIEs, see for example Case Study 3. Strategic isotopic substitutions in the vicinity of NMR active nuclei can also be deployed more generally to distinguish otherwise degenerate molecules, and to do so without perturbing their reactivity in any measurable way; such strategies are of great utility in the determination of KIEs by pairwise intermolecular competition experiments, and in the monitoring of self-exchange kinetics in degenerate reactions.

5.3. Kinetic isotope effects

5.3.1. Background

Isotopic substitution in a substrate can be used to perturb the rate of a chemical process or the position of an equilibrium. These perturbations are termed kinetic isotope effects (KIE) and equilibrium isotope effects (EIE), respectively [309,310]. The magnitude

and direction of change in rate or equilibrium constant brought about by isotopic substitution can be used to extract mechanistic information from complex reactions, offering insights that would otherwise elude all other forms of experimental investigation. These effects can be readily measured to a high degree of accuracy by NMR spectroscopy [311], particularly when combined with reaction monitoring methods (Section 2.2).

Isotope effects can be used, for example, to deduce the nature of rate-determining and product-determining steps in complex reaction pathways, and in certain cases serve as direct structural probes for key intermediates and transition states. Perturbations of reactivity and thermodynamic stability induced by isotopic substitution are often very small in magnitude, especially for heavy atom isotope effects. This presents the experimentalist with opportunities and challenges: whilst the isotope effect does not typically lead to fundamental changes in mechanism, analysis of the effect does necessitate precise measurements of rates and populations.

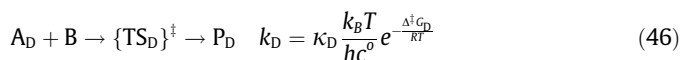
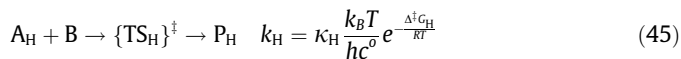
Kinetic isotope effects are generally reported as a ratio of rate coefficients (k), with the numerator being the rate coefficient for the lighter isotopologue, e.g. $k_{\text{H}}/k_{\text{D}}$, $k_{12\text{C}}/k_{13\text{C}}$, $k_{16\text{O}}/k_{18\text{O}}$, etc. Normal kinetic isotope effects (nKIEs) are observed when the lighter isotopologue reacts faster (e.g. $k_{\text{H}}/k_{\text{D}} > 1$); inverse kinetic isotope effects (iKIEs) are defined conversely (e.g. $k_{\text{H}}/k_{\text{D}} < 1$). Kinetic isotope effects are often further classified as primary or secondary. Primary effects (PKIEs) arise when a bond involving the isotopic label is cleaved in, or prior to, the rate-determining (absolute rates), substrate-committing (intermolecular competition), or product-determining (intramolecular competition) transition state (vide infra); secondary effects (SKIEs) arise when the isotopic label is in close proximity to, but not directly involved in, a bond that is cleaved during the reaction. Isotopic substitution in the solvent can also lead to changes in the rates of chemical processes and positions of equilibria; these changes are described as solvent isotope effects (SIEs). The largest SIEs typically arise in protic solvents, and can be induced by changes in the solvation of transition states, differences in gross solvent viscosity, changes in solvent auto-ionisation (and thus bulk pH and protonation states of substrate) and chemical exchange between a substrate, intermediate or transition state (OH, NH, SH) and the protic solvent. In the latter case, controlling the ratio of protic to deuterated solvent can be used to regulate the ratio of substrate isotopologues, in ‘proton inventory’ experiments.

For multi-step reactions, the successful detection of a KIE will depend critically upon the experimental methodology. Methods that depend upon the measurement of absolute rates will report any isotope effects that arise due to bonding changes in, or prior to, the rate-determining transition state; whilst isotopic perturbations to substrates or reagents engaged after this point will have effects on subsequent elementary steps, these perturbations will be irrelevant (i.e., experimentally undetectable) if they all happen after the rate-determining transition state for the overall reaction. The situation is different, however, for competition reactions, which report on isotope effects that arise due to bonding changes in, or prior to, the isotope-committing transition state. The isotope-committing and rate-determining transition states are often one and the same in multi-step reactions, but need not be so; this nuance is explored in subsequent sections [310,311].

5.3.2. Theory

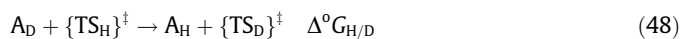
All of the concepts described below are general, i.e. applicable to the measurement of KIEs for any element, but for simplicity all are described in terms of $^1\text{H}/^2\text{H}$ KIEs ($k_{\text{H}}/k_{\text{D}}$). According to transition state theory, the kinetic isotope effect observed for an elementary, thermally-driven chemical process (e.g. $\text{A} + \text{B} \rightarrow \text{P}$) will depend upon the relative activation barriers of the two isotopologues, Eqs. (45) and (46). Specifically, in the case of a bimolecular process

with one isotopically substituted substrate (A_{H} , A_{D}) and one unlabelled substrate (B), leading irreversibly to the formation of the corresponding product isotopologues (P_{H} , P_{D}), the KIE ($k_{\text{H}}/k_{\text{D}}$) will depend upon the ratio of the transmission coefficients ($\kappa_{\text{H}}/\kappa_{\text{D}}$) and the difference in the free energies of activation ($\Delta^\ddagger G_{\text{D}} - \Delta^\ddagger G_{\text{H}}$), Eq. (47). The same definitions apply to KIEs for any element.



$$\frac{k_{\text{H}}}{k_{\text{D}}} = \frac{\kappa_{\text{H}}}{\kappa_{\text{D}}} \frac{e^{-\frac{\Delta^\ddagger G_{\text{H}}}{RT}}}{e^{-\frac{\Delta^\ddagger G_{\text{D}}}{RT}}} = \frac{\kappa_{\text{H}}}{\kappa_{\text{D}}} e^{\frac{\Delta^\ddagger G_{\text{D}} - \Delta^\ddagger G_{\text{H}}}{RT}} \quad (47)$$

The difference in the free energies of activation of the two isotopologues ($\Delta^\ddagger G_{\text{D}} - \Delta^\ddagger G_{\text{H}}$) is exactly equivalent to the free energy change ($\Delta^0 G_{\text{H/D}}$; Eq. (48)) that accompanies isodesmic proton-deuterium exchange (where the bonds broken are the same as the bonds formed) between the substrate and transition state, allowing an alternative formulation for the KIE, Eq. (49).



$$\frac{k_{\text{H}}}{k_{\text{D}}} = \frac{\kappa_{\text{H}}}{\kappa_{\text{D}}} e^{\frac{\Delta^0 G_{\text{H/D}}}{RT}} \quad (49)$$

If the proton of interest is distant from the reactive site, proton-deuterium exchange between substrate and transition state will have no effect on the ZPVE and thus no KIE will be observed at that position; if the nucleus of interest is close to the reactive site, proton-deuterium exchange between the substrate and transition state will lead to a change in ZPVE, and a KIE will likely be observed.

Regardless of the molecularity of the process (unimolecular, bimolecular), the nature of the transition state, and the identities of the nuclei (e.g., $^{12}\text{C}/^{13}\text{C}$, $^{10}\text{B}/^{11}\text{B}$, $^{14}\text{N}/^{15}\text{N}$), the framework of TST can very often be used to compute the KIE ($k_{\text{light}}/k_{\text{heavy}}$) for elementary processes. Such calculations typically depend upon the use of the Bigeleisen-Mayer equation, which expresses the KIE in terms of readily calculable molecular properties, and upon appropriate treatment of quantum-mechanical tunnelling [309,311–313].

The magnitudes of $^1\text{H}/^2\text{H}$ KIEs are governed largely by the change in zero-point vibrational energy (ZPVE), $\Delta^0 E_{0,\text{H/D}}$, accompanying isodesmic proton-deuterium exchange between the substrate and transition state (Eqs. (50) and (51)); heavy-atom KIEs are less dominated by changes in ZPVEs, with other contributions playing a significant role [309,311–313]. Isotopologous differences in the efficiency of quantum-mechanical tunnelling ($\kappa_{\text{H}}/\kappa_{\text{D}}$), Eq. (52), are important for both, but can be profound for primary $^1\text{H}/^2\text{H}$ KIEs.



$$\begin{aligned} \Delta^0 E_{0,\text{H/D}} &= \left(E_{\text{H},0}^{\text{A}} - E_{\text{D},0}^{\text{A}} \right) - \left(E_{\text{H},0}^{\ddagger} - E_{\text{D},0}^{\ddagger} \right) \\ &= \left(E_{\text{H},0}^{\text{A}} + E_{\text{D},0}^{\ddagger} \right) - \left(E_{\text{D},0}^{\text{A}} + E_{\text{H},0}^{\ddagger} \right) \end{aligned} \quad (51)$$

$$\frac{k_{\text{H}}}{k_{\text{D}}} \cong \left(\frac{\kappa_{\text{H}}}{\kappa_{\text{D}}} \right) e^{\frac{\Delta^0 E_{0,\text{H/D}}}{RT}} \quad (52)$$

5.3.3. Measuring KIEs: Isotopically enriched substrates

Kinetic isotope effects can be measured using various methods. For solution-phase reactions, NMR spectroscopy is perhaps the

most attractive technique for measuring KIEs, on account of its intrinsic ability to differentiate isotopologues. This distinction can be made by signal elimination, primary or secondary isotopic shifts, or differences in or absence of scalar coupling. Moreover, NMR provides wide accessibility and practical ease with which reactions can be monitored continuously *in situ*, under a broad range of conditions. Accurate quantification is the key to obtaining robust KIEs by NMR. This is especially important for heavy-atom KIEs, and major improvements in both hardware (stronger magnetic fields, cryoprobes) and techniques over the last few decades have removed many of the barriers that previously precluded its use for this technique. Indeed, KIEs for organic reactions can now be routinely determined using a raft of different methods (conventional 1D, DEPT, 2D HSQC, MQF) and reporter nuclei (^1H , ^{13}C , ^{19}F , ^{31}P), with isotopically enriched and non-enriched substrates.

Using isotopically labelled substrates, site-specific KIEs can be determined using three different approaches: (i) absolute rates, (ii) intermolecular competition, and (iii) intramolecular competition. Crucially, each method entails a different kinetic regime, and for complex reactions may report different KIEs. This is because the three approaches can report the effect that isotopic substitution has on different stages of the reaction pathway. Indeed, great insight can be obtained by comparing KIEs obtained under these three different regimes, and for this reason they should be considered to be highly complementary. For the same reason, all KIEs should be reported alongside a precise experimental methodology. All of the concepts described below are general, i.e. applicable to the measurement of KIEs for any element, but for simplicity all are described in terms of H/D KIEs ($k_{\text{H}}/k_{\text{D}}$).

5.3.3.1. Absolute rates. Determination of the rate of a chemical reaction is conceptually the simplest method for KIE analysis, i.e. $\text{rate}_{(\text{H})}/\text{rate}_{(\text{D})}$. Under this regime the reaction of interest is run independently with the unlabelled (AH) and labelled (AD) substrate; all initial conditions of the reaction, that is temperature, substrate concentrations, residual water content, impurity levels, reaction assembly, etc., must be strictly controlled or analysed to ensure direct comparability between the two reactions. This is most conveniently achieved by running the two reactions in parallel, using nominally identical reaction vessels and, other than differences due to isotopic labelling, identical stock solutions of all components.

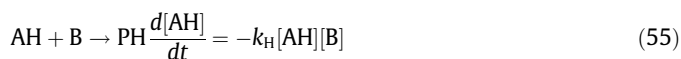
Knowledge of the empirical rate law is needed to ensure the ratio of the rate coefficients ($k_{\text{H}}/k_{\text{D}}$) is reflected in the relative rates; with this in hand, it is often possible to extract the KIE (i.e. the ratio of the rate coefficients) by using the method of initial rates, or by placing the reaction under pseudo first-order conditions, e.g. with excess B, Eqs. (53) and (54).



This method is appropriate if a large, and thus usually primary, KIE is expected. For smaller KIEs (e.g., SKIEs, heavy-atom KIEs) the results are often ambiguous, because experimental uncertainties are typically of a similar magnitude to, or substantially larger than, the value of the KIE. The detection of a KIE by absolute rates indicates that significant changes in bonding occur at the site of interest prior to, or in, the rate-determining transition state.

5.3.3.2. Intermolecular competition. In an intermolecular competition experiment, the two substrate isotopologues, e.g. AH and AD Eqs. (55) and (56), are co-reacted, i.e. converted to product(s) in the same reaction vessel. They therefore necessarily experience identical conditions, and if bimolecular processes are involved, compete for the same unlabelled substrate B (or more). Under this

regime the change in the relative concentrations of AH and AD as the reaction proceeds can be used to extract the KIE ($k_{\text{H}}/k_{\text{D}}$). For this method to work it must be possible to resolve the isotopologous substrates (AH, AD) or products (PH, PD). Using NMR spectroscopy this is often made possible by primary or secondary isotopic shifts, or scalar couplings. Intermolecular competition experiments are typically employed for processes that are first-order in the competing substrates.



For two competitive elementary processes, with an initial substrate ratio of $R_0 = [\text{AD}]_0/[\text{AH}]_0$, Eq. (57), the KIE ($k_{\text{H}}/k_{\text{D}}$) can be calculated using the Bigeleisen-Wolfsberg equation, Eq. (58), where F is the total fractional conversion of the substrate (AH + AD) to product, and R is the substrate ratio ($[\text{AD}]/[\text{AH}]$) at that specific fractional conversion.

$$\frac{d[\text{AH}]}{dt} = \left(\frac{k_{\text{H}}}{k_{\text{D}}}\right) \frac{1}{R}, \quad R = \frac{[\text{AD}]}{[\text{AH}]} \quad (57)$$

$$\frac{k_{\text{H}}}{k_{\text{D}}} = \frac{\ln\left((1-F)\left(\frac{1+R_0}{1+R}\right)\right)}{\ln\left((1-F)\left(\frac{R}{R_0}\right)\left(\frac{1+R_0}{1+R}\right)\right)}, \quad F = 1 - \frac{[\text{AH}] + [\text{AD}]}{[\text{AH}]_0 + [\text{AD}]_0} \quad (58)$$

There are various alternative formulations and approximations of the Bigeleisen-Wolfsberg equation. The form above is the complete expression, with R defined as the substrate ratio of the heavy isotopologue to the light isotopologue. For a normal KIE, the lighter isotopologue will react faster, the residual substrate will become increasingly enriched in the heavier isotopologue, and R will thus increase in magnitude as F rises from 0 to 1, when both substrates (AD, AH) have been completely consumed. For an inverse KIE, R will decrease in magnitude as F rises from 0 to 1.

There are a number of ways in which this equation can be used to determine the KIE, e.g. $k_{\text{H}}/k_{\text{D}}$. One of the least intensive approaches is to run the reaction to high, but not complete, conversion. The fractional conversion F and substrate ratio R are then determined in one quantitative measurement. This approach demands less NMR instrument time and will often give reasonable results for moderate to large KIEs, provided the reaction is run to a sufficiently high fractional conversion, usually $F > 0.75$. For more accurate results, particularly when low magnitude KIEs are to be determined, it can be useful to continuously monitor the reaction, so that a series of fractional conversions, F , and substrate ratios, R , can be obtained over the course of the reaction. The KIE can then be determined by non-linear regression of Eq. (59), a rearranged form of the Bigeleisen-Wolfsberg equation Eq. (58). When isotopically labelled substrates are synthetically accessible, this method is recommended for the determination of KIEs by intermolecular competition, and especially for SKIEs and heavy-atom KIEs.

$$F = 1 - \left(\frac{1+R}{1+R_0}\right) \left(\frac{R}{R_0}\right)^{\frac{k_{\text{H}}}{k_{\text{D}}}} \quad (59)$$

As is evident in Fig. 32, the substrate ratio R will be most sensitive to a KIE as F approaches 1, so in principle monitoring reactions to higher conversions should permit the determination of KIEs with progressively increasing precision by NMR. However, this only remains true in the limiting scenario that R and F can be determined with arbitrary accuracy. In practice, the decay in S/N with increasing conversion imposes a practical bound on the precision with which a KIE can be determined by intermolecular competi-

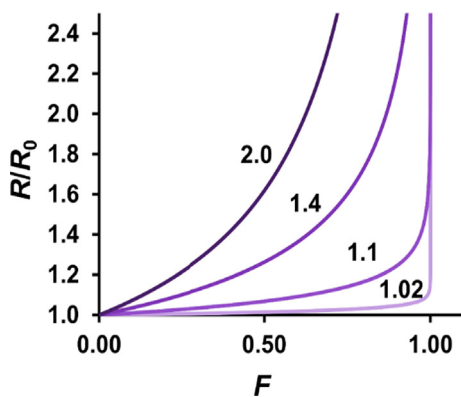


Fig. 32. Isotopologue ratio (R) versus fractional conversion (F) calculated using the Bigeleisen-Wolfsberg equation (Eq. (59)), for four different KIEs, indicating extent of conversion (F) required to attain significant change in isotopologue ratio (R). For examples of the application of KIE analysis see Case Studies 1, 3 and 8.

tion. Whilst the exact limit will depend upon the mode of detection, extent of spectral congestion, and initial concentration of the competing substrates, quantitative NMR monitoring of reactions beyond conversions of 95% becomes difficult.

For the accurate determination of moderate KIEs (e.g. $n\text{KIE} < 1.5$; $i\text{KIE} > 0.8$) conversions between 75 and 95% should be targeted. For small KIEs, higher conversions (85–95%) are desirable. Higher conversions can sometime be promoted by using an excess of a co-reagent or higher catalyst loadings. However, it is important to remember that the experimentally determined KIE is valid only under the conditions in which it was measured.

For small KIEs ($n\text{KIE} < 1.1$, $i\text{KIE} > 0.9$) and when $R_0 \approx 1$, it is reasonable to use a simplified form, Eq. (60), of the Bigeleisen-Wolfsberg equation, in which the ratio $(1 + R_0)/(1 + R) \approx 1$. This approximate form becomes more accurate with initial substrate ratios $R_0 < 1$, Fig. 33. With ($n\text{KIE} < 1.05$, $i\text{KIE} > 0.95$) and $R_0 < 0.05$, the error is negligible [311].

$$\frac{k_H}{k_D} \approx \frac{\ln(1-F)}{\ln\left((1-F)\left(\frac{R}{R_0}\right)\right)} \quad (60)$$

approximation only valid for small KIEs (< 1.1)

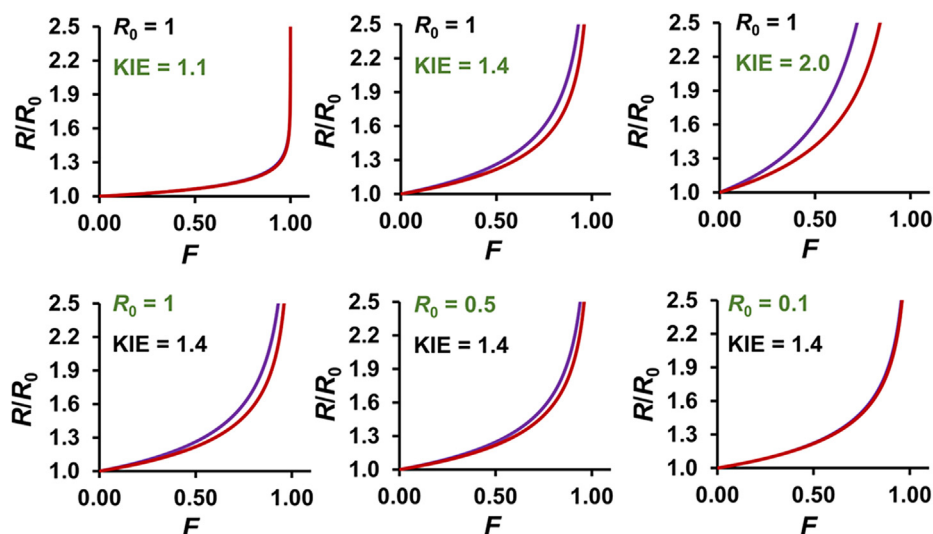


Fig. 33. Comparison of the full Bigeleisen-Wolfsberg equation (purple lines; Eq. (59)) and the approximate form (red lines; Eq. (61)) for three different KIEs and initial isotopologue ratios (R/R_0). For examples of the application KIE analysis see Case Studies 1, 3 and 8.

Under such conditions it is necessary only to measure the double ratio of substrate isotopologues, R/R_0 , allowing for elimination of some of the systematic errors in quantification, and use of Eqs. (61) and (62).

$$F \approx 1 - \left(\frac{R}{R_0}\right)^{\frac{k_H}{k_D}} \quad (61)$$

$$\frac{R}{R_0} \approx (1-F)^{\frac{1}{k_D}} \quad (62)$$

approximations only valid for small KIEs (< 1.1)

If the detection or accurate quantification of the two substrate isotopologues is difficult or impossible by NMR, an alternative method involves determination of the KIE by analysis of the product isotopologue ratio, R_p , Eq. (63). The simplified form (Eq. (64)) is valid for small KIEs (< 1.1). Because R_p will be most sensitive to the KIE at low fractional conversions, the method is only practicable for the analysis of sufficiently slow chemical reactions, or those that can be periodically activated, or restricted by stoichiometry.

$$\frac{k_H}{k_D} = \frac{\ln\left(1 - F\left(\frac{1+R_p}{1+R_p}\right)\right)}{\ln\left(1 - F\left(\frac{R_p}{R_p}\right)\left(\frac{1+R_p}{1+R_p}\right)\right)}, \quad F = \frac{[\text{PH}] + [\text{PD}]}{[\text{AH}]_0 + [\text{AD}]_0},$$

$$R_p = \frac{[\text{PD}]}{[\text{PH}]} \quad (63)$$

$$\frac{k_H}{k_D} \approx \frac{\ln(1-F)}{\ln\left(1 - F\left(\frac{R_p}{R_p}\right)\right)} \quad (64)$$

approximation only valid for small KIEs (< 1.1)

An even simpler variant of an intermolecular competition experiment uses a deficiency of a limiting reagent, B, i.e. a large excess of the two substrate isotopologues, such that $[\text{AH}] + [\text{AD}] \gg [\text{B}]$. Under these conditions the KIE can be estimated from the starting ratio of the substrate isotopologues, R_0 and the ratio $[\text{PH}]/[\text{PD}]$, Eq. (65). This is possible, Eq. (66), because the substrate ratio R remains approximately constant ($R \approx R_0$) as B is consumed. For accurate results, the reaction should be assembled in such a

way that $[AH] + [AD] > 20[B]$. This condition is ideally satisfied when AH and AD represent two isotopologues of a reactive solvent; although the possibility of a significant change in medium, e.g. viscosity or pH, compared to pure AH as solvent, should be borne in mind.

$$\left(\frac{k_H}{k_D}\right) \approx \frac{([AH] - [AH]_0)}{([AD] - [AD]_0)} R_0 = \frac{[PH]}{[PD]} R_0 = \frac{R_0}{R_p} \quad (65)$$

$$\frac{d[PH]}{dt} = \frac{d[AH]}{dt} = \left(\frac{k_H}{k_D}\right) \left(\frac{[AH]}{[AD]}\right) = \left(\frac{k_H}{k_D}\right) \frac{1}{R} \approx \left(\frac{k_H}{k_D}\right) \frac{1}{R_0} \quad (66)$$

approximations only valid for low conversion ($< 5\%$)

The KIE value obtained by intermolecular competition provides information about bonding changes that occur in, or prior to, the substrate-committing transition state. This is the first transition state at which the substrate is fully committed to the reaction, i.e., beyond which the substrate cannot be liberated back into the reactant pool.

For multi-step reactions, the transition state that commits a particular substrate may or may not be that which governs the overall rate of product evolution, and may or may not involve bonding changes at the isotopically differentiated site. If the isotope is not engaged, directly (bond cleavage/formation) or indirectly (e.g., rehybridisation), in or before the substrate-committing transition state, no KIE will be detected by intermolecular competition. Whether the isotope is engaged before or after the rate-determining transition state for the overall reaction is essentially irrelevant, contrary to experiments that probe the effect of isotopic substitution on the absolute rate of a multi-step reaction. The field of C–H activation contains numerous cases where the above issues have been overlooked when interpreting KIEs determined by intermolecular (or intramolecular, Section 5.3.3.3) competition of substrates of the type C–H/C–D.

5.3.3.3. Intramolecular competition. The final method for determining KIEs makes use of a single substrate comprising two (or more) homotopic reactive sites, e.g. A_D^H , that are different only by virtue of their isotopic constitution. Thus, a reagent (B) or other process, must select between two (or more) isotopically distinct but otherwise identical sites in a single substrate, Eqs. (67) and (68). In such a case the overall KIE can therefore be determined from the ratio or distribution of product isotopologues, and provided the product does not undergo further reaction, this can be measured at any point during the course of the reaction.



$$\left(\frac{k_H}{k_D}\right) = \frac{[P_D^{BH}]}{[P_{BD}^H]} \quad (69)$$

only valid for intramolecular competition

Again, the detection of a KIE by intramolecular competition does not necessarily report on the rate-determining transition state for the overall reaction. Thus, for example, if the step during which the isotopes are kinetically differentiated occurs after the rate-determining transition state, a large KIE may be still measured. Because the isotope selection always occurs within a single substrate, and not between two populations of isotopologues, intramolecular KIEs are also insensitive to processes that lead to the irreversible consumption of a substrate prior to bond forma-

tion/cleavage at the site of interest. An important consideration is that the presence of one isotope can affect the reaction of the other. In other words the net KIE can be a combination of, for example, a PKIE for the isotope lost in the bond-cleaving event, and a SKIE arising from the isotope(s) that remain. This effect is evident for example in the deprotonation (C–H versus C–D) of $ArCH_2D$ [314].

5.3.3.4. Chemical considerations. High quality data is required for the determination of KIEs, and this will only be obtained if the reaction of interest fulfils certain criteria, which vary between the various methods of KIE measurement. If the KIEs are determined by the consumption of the substrate, they will only be reliable in the absence of competing side reactions. Ideally, the substrate should be converted to the product or product mixture with perfect efficiency. Thus, it should not be consumed by other processes, including those that arise from the liberated product (s) or from intermediates. Subsequent decomposition of the product should not influence the measured KIE, provided that product generation is irreversible. Isotopic scrambling between, or within, isotopologues, or between the labelled substrate and other reagents, will impact on the measurement, and ideally should be eliminated completely. This is particularly important in the determination of $^1H/^2H$ KIEs, and should always be considered in cases where degenerate self-exchange between substrates and products might normally proceed unnoticed. For intermolecular competition reactions, the Bigeleisen-Wolfsberg equation can, in principle, only be employed if the reaction proceeds with a first-order dependence on the competing isotopologues in the step in which they are kinetically differentiated.

5.3.3.5. NMR considerations. Large primary $^1H/^2H$ KIEs can often be determined to a reasonable degree of accuracy by absolute rate measurements, or by appropriate end-point competition experiments (i.e. intramolecular competition, or intermolecular competition with an excess of labelled substrates), using standard NMR quantification methods.

For the determination of intermolecular KIEs by NMR, especially heavy-atom KIEs, continuous monitoring of the reaction is recommended. To obtain robust KIEs by this technique it must be possible to spectroscopically resolve the substrate (or product) isotopologues by NMR, and to obtain accurate integrals for both species. For the measurement of secondary $^1H/^2H$ KIEs and heavy-atom KIEs, where quantitative comparisons with theory are often required for interpretation, it is especially important to follow the key principles of accurate quantification, including: (i) the normalisation of all integrals against an inert internal standard; (ii) the use of long acquisition times and extended recycle times, i.e. for 90° pulses setting $t_R > 5 T_1$, where T_1 is the longitudinal relaxation time of the most slowly relaxing nucleus of interest; (iii) the consistent inclusion, or omission, of satellite signals (e.g., ^{13}C satellites in $^1H/^19F$ NMR) during signal integration; (iv) the optimisation of line shape, line width and S/N, especially in the cases of congested spectra, or nuclei with poorer sensitivity (e.g., ^{13}C NMR); (v) accurate calibration of pulse widths; and (vi) careful processing, including the consistent application of appropriate baseline and phase corrections, zero-filling and apodisation. Further details can be found in Section 3.

The optimum strategy for KIE determination by continuous monitoring will ultimately depend upon a compromise between multiple factors, including: (i) the availability of isotopically-enriched precursors, and the synthetic accessibility of labelled substrates, especially doubly-labelled substrates; (ii) the influence of KIEs elsewhere in the substrate; (iii) the feasibility of deconvoluting spectra with high precision and accuracy, often an issue for 1H NMR; (iv) the presence of additional NMR active nuclei in the sub-

strate under study (e.g., ^{19}F , ^{31}P); (v) the reaction velocity, with fast reactions requiring sufficiently NMR-sensitive nuclei, e.g. ^1H , ^{19}F ; and (vi) spectrometer hardware and instrument access, especially for low-sensitivity and slow-relaxing nuclei, e.g. ^{13}C , where stronger magnetic fields, the use of cryoprobes, and long acquisition times are all beneficial.

On the basis of sensitivity and T_1 , ^1H might appear the most attractive candidate as detection nucleus for KIE measurements. In practice, however, limited spectral dispersion and extensive homonuclear coupling in ^1H NMR often preclude its use for *in situ* monitoring. Fortunately, the favourable sensitivity, relaxation properties and spectral dispersion of ^{19}F NMR can often be leveraged for the measurement of competitive KIEs by the judicious use of isosteric $^1\text{H}/^{19}\text{F}$ substitutions and secondary $^3\Delta\text{F}$ ($^1\text{H}, ^2\text{H}$) isotope shifts. This approach is just one of many possible systems in which the 'reactive, reporter, resolving' approach [311] can be applied, Fig. 34.

In cases where spectral congestion precludes the use of ^1H NMR, and isosteric H/F substitutions cannot be made without profoundly affecting the reactivity of the substrate, $^{13}\text{C}\{^1\text{H}\}$ NMR monitoring, with inverse-gated ^1H decoupling to prevent differential signal enhancements by NOEs, can be employed. Provided adequate precautions are taken during spectral acquisition and processing, and of course provided also the ^{13}C -enriched substrates can be prepared, high quality KIEs can be obtained with *in situ* monitoring by $^{13}\text{C}\{^1\text{H}\}$ NMR, and analogously by $^{31}\text{P}\{^1\text{H}\}$, or $^{19}\text{F}\{^1\text{H}\}$ NMR.

This technique has been elegantly deployed by Bennet and co-workers in their pursuit of $^{12}\text{C}/^{13}\text{C}$ and $^{16}\text{O}/^{18}\text{O}$ KIEs for the enzyme-catalysed hydrolysis of sialyllactosides [315], Scheme 6. In this work, all of the KIEs were determined by intermolecular competitions between a singly ^{13}C -labelled α -sialyl-(2 \rightarrow 6)- β -1-t hiolactoside ([3- ^{13}C]-**24**, reaction A; or [2- ^{13}C]-**24**, Reactions B and C) and the appropriate doubly labelled isotopologue ([2,3- $^{13}\text{C}_2$]-**24**, [1- ^{18}O , 2- ^{13}C]-**24**, or [2- ^{13}C , 4- ^{18}O]-**24**), with ^{13}C

functioning as the reporter nucleus (by $^{13}\text{C}\{^1\text{H}\}$ NMR) in all cases. The two $^{16}\text{O}/^{18}\text{O}$ KIEs, one for the anomeric oxygen and the other for the leaving oxygen, were determined by using the ^{18}O -secondary isotope shift, and thus the ^{18}O labels functioned as both the resolving and the reactive nuclei. The $^{12}\text{C}/^{13}\text{C}$ KIE at the anomeric carbon (C-2) was determined using the $^1J_{\text{CC}}$ coupling in doubly-labelled [2,3- $^{13}\text{C}_2$]-**24** to resolve it from [3- ^{13}C]-**24**. In this case the ^{13}C label at C-3 is the reporter, and the ^{13}C label at C-2 is both the reactive and the resolving nucleus. This approach has also been employed to probe the hydrolysis of 4-nitrophenyl α -D-mannopyranoside [316], and an analogous methodology based on ^{19}F NMR has been deployed to investigate various substitution reactions of α -D-glucopyranosyl fluoride [317,318].

For reactions in which the spectral resolution of the two substrate, or product, isotopologues cannot be achieved with 1D NMR techniques, 2D NMR methods can be indispensable. ^1H -detected 2D [^{13}C , ^1H] heteronuclear single quantum coherence (HSQC) NMR provides significant enhancements in sensitivity (up to $\times 32$) relative to 1D $^{13}\text{C}\{^1\text{H}\}$ NMR, and also permits the use of shorter recycle delays (the longitudinal relaxation of ^1H nuclei is generally much faster than that of ^{13}C nuclei). Notwithstanding both of these factors, ^1H -detected [^{13}C , ^1H]-HSQC will generally demand longer experiment times than 1D $^{13}\text{C}\{^1\text{H}\}$ NMR to achieve good resolution in the ^{13}C dimension, and furthermore is constrained to substrates/products in which the reporter ^{13}C nucleus is directly bonded to a proton. More extensive optimisation of acquisition and processing parameters is also required to ensure accurate quantification in 2D NMR [319].

5.3.4. Measuring ^{13}C KIEs: Natural abundance substrates

In 1995, Singleton and co-workers reported a transformative new approach for the simultaneous determination of ^{13}C KIEs in a substrate at all but one carbon, and all at natural isotopic abundance, thus circumventing the synthetic challenge of individually

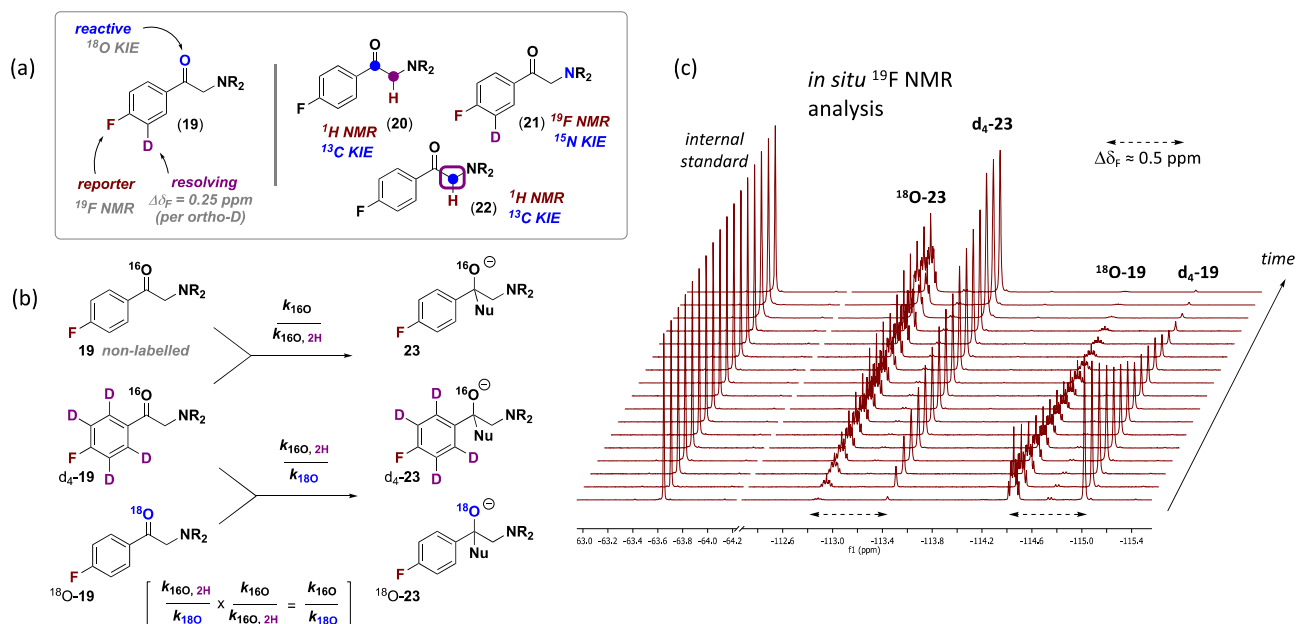
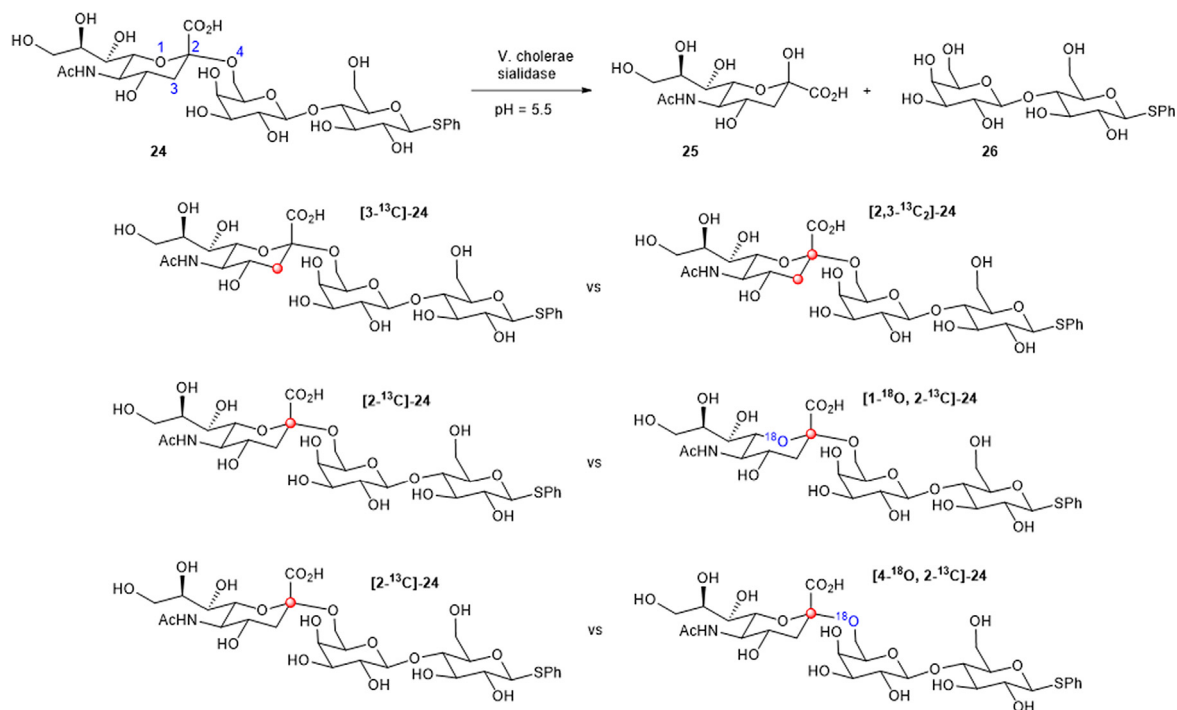


Fig. 34. (a) Generic examples (19–22) of substrates for determination of intermolecular competition heavy atom KIEs in a reaction involving addition to an aminoacetophenone, employing the 'reactive, reporter, resolving' strategy [311]. Note that in 22, the ^{13}C label acts as both the reactive and resolving nucleus. See Scheme 6, and Case Studies 1 and 3 further examples. (b) For substrate 19, two reactions are required: i. the unlabelled substrate (19) is competed with the deuterated substrate (d_4 -19) and ii. the deuterated substrate (d_4 -19) is competed with the ^{18}O -labelled substrate (^{18}O -19). (c) both reactions are analysed *in situ* by ^{19}F NMR (the reporter nucleus) – see stacked spectra for the competition of ^{18}O -19 with d_4 -19. The secondary $^3\Delta\text{F}$ ($^1\text{H}, ^2\text{H}$) isotope shift exerted by the two ortho deuterium atoms (the resolving nuclei; $\Delta\delta_{\text{F}} = 2 \times 0.25 = 0.5$ ppm) allows measurement of the initial (R_0) and evolving (R) ratios of substrates (e.g. ^{18}O -19/ d_4 -19) or products (e.g. ^{18}O -23/ d_4 -23) as a function of fractional conversion (F), determined by use of an inert ArCF_3 species as an internal standard. The R and F values can then be employed in Bigeleisen-Wolfsberg analysis (e.g. Eqs. (59) and (64)) and the pair of KIEs used to cancel out the effect of the ^2H resolving nuclei, leaving the desired $^{16}\text{O}/^{18}\text{O}$ KIE at the reactive nucleus – see lower section of (b).



Scheme 6. Bennet's design of intermolecular competition experiments for measuring $^{12}\text{C}/^{13}\text{C}$ and $^{16}\text{O}/^{18}\text{O}$ KIEs in the enzyme-catalysed hydrolysis of α -sialyl-(2 \rightarrow 6)- β -1-thiolactoside **24**, using *in situ* monitoring by ^{13}C NMR spectroscopy [314]. For measuring the $^{12}\text{C}/^{13}\text{C}$ KIE at the anomeric carbon ($[3-^{13}\text{C}]\text{-24}$ vs $[2,3-^{13}\text{C}_2]\text{-24}$), isotopologue differentiation is achieved using $^{13}\text{C}\text{-}^{13}\text{C}$ coupling; for both $^{16}\text{O}/^{18}\text{O}$ KIEs, isotopologue differentiation is facilitated by secondary isotope shifts. The use of doubly labelled substrates removes the need for KIE normalisation [315]. See Case Studies 1, 3 and 13 for other examples of double labelling.

preparing multiple, selectively ^{13}C -labelled substrates [320]. The technique involves running the reaction to high but not complete conversion, re-isolating the remaining substrate, and subjecting it to a single-point quantitative analysis by ^{13}C NMR, alongside an identical sample retained prior to reaction.

Conducting a reaction with a substrate at natural isotopic abundance is essentially equivalent to running a large number of parallel intermolecular competition experiments simultaneously, with the unlabelled substrate A composed exclusively of ^{12}C , and present in vast excess, competing with a small population of a series of singly ^{13}C -labelled isotopomers $[i-^{13}\text{C}]\text{-A}$. For each of the isotopomers the ratio $R_i = [[i-^{13}\text{C}]\text{-A}]/[\text{A}] \ll 1$, thus allowing simplified Bigeleisen-Wolfsburg equations, Eqs. (70) and (71), to be employed.

$$F \approx 1 - \left(\frac{R_i}{R_{i,0}} \right)^{1 - \left(\frac{k_{12\text{C}}}{k_{13\text{C}}} \right)_i} \quad (70)$$

$$\left(\frac{k_{12\text{C}}}{k_{13\text{C}}} \right)_i \approx \frac{\ln(1-F)}{\ln \left[(1-F) \left(\frac{R_i}{R_{i,0}} \right) \right]} \quad (71)$$

approximations only valid for small KIEs (< 1.1)

At the heart of the Singleton technique is a protocol, see *i-v* below, for obtaining the ratios $R_i/R_{i,0}$ for each position in the carbon skeleton with high precision. It should be noted that a similar approach has been employed to determine intramolecular $^{12}\text{C}/^{13}\text{C}$ KIEs at natural abundance [321].

- (i) Run reaction. For substrate analysis, the reaction under study should be run to high conversion ($F > 0.85$), rapidly quenched if necessary, and F determined accurately (e.g., *via* GC, qNMR). A sub-stoichiometric quantity of a

co-reactant or reagent can also be used to control the conversion of the key substrate by exhaustion, although this may lead to a change in kinetic regime, especially if the co-reactant/substrate is typically present in large excess. The unreacted substrate is then isolated from the reaction mixture.

- (ii) Select internal reference. An internal reference carbon in the substrate should be selected. The reference carbon should be chosen on the basis that it is expected to afford a negligible KIE (ideally $0.999 < \text{KIE}_{\text{ref}} < 1.001$). Electronic structure computations can be used here to direct or validate the selection of the appropriate carbon.
- (iii) NMR spectrum 1. A quantitative $^{13}\text{C}\{^1\text{H}\}$ NMR spectrum is acquired, with inverse-gated ^1H -decoupling, for the re-isolated substrate, observing all the key principles of accurate quantification by NMR (Section 3). Note that the longitudinal relaxation times of all carbon nuclei in the substrate should be determined, and that for 90° pulses the recycle delay t_R should be set longer than $5T_1$, where T_1 is the longitudinal relaxation time of the slowest relaxing carbon. It is possible that recycle delays of several minutes could be required to satisfy this criterion. Each peak i , corresponding to a different isotopomer population, should be integrated, I_i , and each integral should be divided by that of the reference carbon, I_{REF} this gives the ratio R_i , Eq. (72).

$$\frac{I_i}{I_{\text{REF}}} = R_i, \frac{I_{i,0}}{I_{\text{REF},0}} = R_{i,0} \quad (72)$$

- (iv) NMR spectrum 2. A second quantitative $^{13}\text{C}\{^1\text{H}\}$ NMR spectrum is acquired, for the identical sample of the substrate, reserved before reaction, using all of the same NMR acquisition and processing parameters, to obtain $R_{i,0}$, Eq. (72).

- (v) Calculate KIE. The $^{12}\text{C}/^{13}\text{C}$ KIE at each position, $k_{12\text{C}}/k_{13\text{C}}$, is calculated using Eqs. (70) and (71), where F is the fractional conversion and $R_i/R_{i,0}$ is the double ratio of substrate concentrations for species $[i-^{13}\text{C}]$ -A.

Whilst errors in the measurement of $R_i/R_{i,0}$ will propagate through to the calculated KIE, this effect is mitigated at higher F , and for this reason the reaction under study should be run to high conversions (ideally $F > 0.85$). The two samples of substrate should be prepared identically, and the $^{13}\text{C}\{^1\text{H}\}$ NMR spectra acquired back-to-back without intervening samples, and the whole sequence should be repeated several times (ideally > 6 times) to assess the uncertainty in the KIE.

To permit the re-isolation of sufficient quantity of unreacted substrate for quantitative $^{13}\text{C}\{^1\text{H}\}$ NMR analysis with reduced sensitivity from inverse-gated decoupling, the reaction should be run on a comparatively large scale. When financial or practical constraints demand smaller scale reaction, it is possible to employ other NMR techniques than the routine single-pulse $^{13}\text{C}\{^1\text{H}\}$ NMR. Indeed, Jacobsen and co-workers have demonstrated two effective alternatives for enhancing sensitivity in single-point measurements: (i) use of DEPT in the determination of $^{12}\text{C}/^{13}\text{C}$ KIEs of protonated carbons; [322] and (ii) multiple quantum filtered (MQF) $^{19}\text{F}\{^1\text{H}\}$ NMR for measuring $^{12}\text{C}/^{13}\text{C}$ KIEs of carbons directly bonded to fluorine [323], see Section 5.6.

The Singleton technique can also be employed to determine KIEs for reactions run only to low conversions (ideally $F < 0.1$) followed by analysis of the product. Such an approach is especially efficient for associative reactions, because the KIEs can then be determined for all carbons in both substrates in one series of experiments, rather than two. The procedure for calculating $R_{i,p}/R_{i,p,\infty}$ is analogous to $R_i/R_{i,0}$, except that $R_{i,p,\infty}$ is calculated using product isolated from a reaction run to full conversion, Eq. (73). For accurate analysis, it is essential that the reaction be run to complete ($F = 1.000$) conversion.

$$\left(\frac{k_{12\text{C}}}{k_{13\text{C}}}\right)_i \approx \frac{\ln(1-F)}{\ln\left(1-F\left(\frac{R_{i,p}}{R_{i,p,\infty}}\right)\right)} \quad (73)$$

approximation only valid for small KIEs (< 1.1)

5.4. Isotopic entrainment

Isotopic entrainment involves the analysis of the flux (entrainment) of a small quantity of isotopically labelled species into, or through, a reaction sequence involving unlabelled or differently labelled reactants. It can be used to interrogate the kinetic behaviour of intermediate species detected during stoichiometric and catalytic reactions, and with careful design, establish the reversibility of formation of all species in the process: substrates, intermediates, products and side products. The archetypal kinetic profile of an intermediate, from initial accumulation to steady-state evolution and eventual depletion, is not necessarily indicative of its role in a productive reaction or catalytic cycle. For example, species that are peripheral to the primary process can often exhibit qualitatively similar kinetic behaviour to species that are directly involved. In an isotopic entrainment experiment, the isotopically labelled substrate or intermediate is spiked into the active reaction, and the flux of the newly introduced isotope amongst all key species is then monitored continuously. The isotopic incorporation profiles, in conjunction with kinetic simulation, can be used to decipher whether an intermediate is intrinsic to a process, or is peripheral to it, i.e. generated via an unproductive side reaction or “off-cycle” event in a catalytic cycle [28,32,324,325].

Pre-requisite information, gained through kinetic analysis of the reaction of interest, includes the NMR spectroscopic identification of species produced during the reaction at a pseudo steady-state concentration, and an indication or hypothesis of the substrate(s) contributing to its generation, and the product(s) of its decay.

The isotopic entrainment experiment involves a rapid isotopic perturbation of the reaction, usually by manual addition of the isotopically labelled component. Subsequent direct or indirect NMR analysis of the resultant isotope ratios (%), as a function of reaction progress, with the aid of kinetic modelling, establishes the component chronology and enables evaluation of mechanistic hypotheses. To illustrate the concept, we consider a simple catalytic process involving conversion of substrate into a product, with a species ‘I’, suspected to be an intermediate, being detected during the reaction. The reaction is initiated and, after being allowed to run to low conversion, usually about 15% conversion of the substrate (Sub), an identical amount of a labelled form of the substrate (Sub*) is added, and the % isotope incorporation in Sub/Sub*; I/I*; and Prod/Prod* repeatedly analysed *in situ* by NMR spectroscopy until conversion is complete. A number of limiting regimes can be envisaged; here we just consider regimes A, B, and C, Fig. 35. At the point of introduction of Sub* (see dashed vertical line in Fig. 35) the isotope ratio in the total substrate pool is raised from 0% to an amount reflecting the Sub* added in relation to the Sub remaining.

In regime A, species ‘I’ is in equilibrium with Sub but is not ‘on pathway’ to Prod. Note that detection of species I, which is transient under this regime, can lead to it being erroneously assigned as an intermediate. However, the equilibrium (K_{eq}) causes the isotope fraction in Sub to be reduced, and the isotope fraction in I to be raised, as the system evolves.

The isotope fraction in Prod rises rapidly, eventually reaching 50%, reflecting the total Sub/Sub* added. In regime B, the irreversible reaction of Sub with Cat means that the isotope ratio in Sub remains constant, and the isotope ratio in ‘I’, a genuine intermediate in the reaction, rises to meet the same level of isotope incorporation as Sub. The rate of rise of isotope incorporation in the product is now dependent on ‘I’ and is thus attenuated compared to regime A, but still eventually reaches 50%. In regime C, where Sub directly converts to Prod, the isotope incorporation rises rapidly, in a manner analogous to regime A. However, the rate of rise of isotope incorporation in ‘I’ is now dependent on Prod, and there is a lag-period before it rises, eventually reaching 50%, with a characteristic sigmoidal profile.

The synthesis of pure samples of appropriately labelled substrates or intermediates, or precursors to such species, is required in advance of performing the isotopic entrainment experiment. For reactions intended to be monitored by ^{19}F NMR spectroscopy, preparation of a deuterium-labelled substrate which induces a significant isotopic shift would be suitable. Numerous other labelling strategies can be devised for monitoring by other nuclei. For example, in the catalytic enantioselective [2,3]-rearrangement of allylic ammonium ylides, Scheme 5, $^{13}\text{C}\{^1\text{H}\}$ NMR spectroscopy was employed to assess the productivity of the intermediate *N*-acylated isothiourea species (**18**), by isotopic entrainment [32]. Doubly-labelled substrate, 1,2- $^{13}\text{C}_2$]-**11** was introduced into a reaction with ^{13}C -labelled substrate, 1- $^{13}\text{C}_1$]-**11** at pseudo-steady state and the extent of label-incorporation ($n = 1, 2$), in substrate ($^{13}\text{C}_n$ -**11**), intermediate ($^{13}\text{C}_n$ -**18**), and product ($^{13}\text{C}_n$ -**13**), as a function of conversion were shown to be consistent only with a process in which there is irreversible conversion of **11** to **18**, and of **18** to **13**; i.e. scenario B, in Fig. 35.

5.5. Signal elimination and spectral simplification

There are instances where comprehensive analysis of the ^1H spectrum for a molecule can prove problematic, for example due

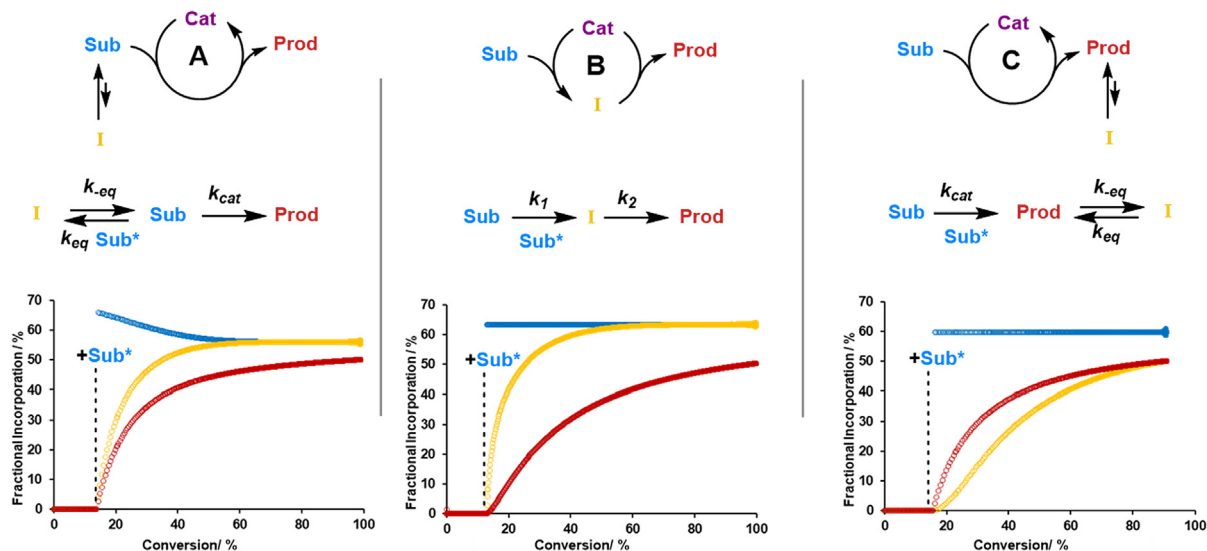


Fig. 35. Three simple generic regimes (A, B, C) for isotopic entrainment (of Sub*) in a catalytic reaction. Species 'I' is a genuine intermediate in regime B, but not one in regime A, despite its concentration, [I], rising then falling as the reaction proceeds. For examples of isotope entrainment see Case Studies 10, 13, and 14.

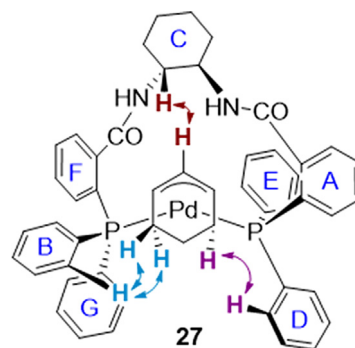
to significant signal overlap. Employing NOESY (Nuclear Overhauser Effect Spectroscopy) for structural assignment can assist in the elucidation of complex structures. NOESY, a through-space correlation technique, enables identification of signals arising from protons existing close to each other in space which may not necessarily be linked by bonds [4,326].

Application of NOESY to structural deconvolution of a complex can be assisted by applying signal elimination for selected NOEs, thereby achieving spectral simplification. This strategy first requires identification of the key NOE signals in the spectrum of the compound of interest that potentially provide important structural information through proximity to specific nuclei in the molecule. Subsequently, analogues of the compound may be prepared, introducing selective deuterations which result in the 'deletion' of specific NOE signals. Careful consideration of the absence of characteristic NOE signals for a compound can aid in the clarification of the stereochemical configuration of a molecule, as well as conformation and orientation of various groups within the molecule or ligand [327–329]. For example, the NMR-elucidation of the solution-phase structure of the monomeric form of the η^3 -cyclohexenyl complex **27** (Fig. 36) was key to kinetic and computational interrogation of a prominent mechanism in asymmetric catalysis [330].

The process was significantly assisted by the examination of specific NOE signals, with assignments supported by a series of ^2H -complexes. Key to the analysis was the deletion of specific NOE signals when the following sets of perdeuterations were made: (i) rings E, D, G, B; (ii) rings B, E; (iii) rings D, G; and (iv) ring C. All of the combinations required synthesis, some quite extensive, but the information gained was pivotal to the overall mechanistic investigation [330].

5.6. Using natural abundance satellites

Careful examination of satellite peaks in NMR spectra can be immensely useful for the assignment of the geometry of molecules [331]. For example, it is not possible to confirm *cis*- or *trans*- double bond geometry in symmetrical stilbenes and analogous alkenes from the main signals in their ^1H NMR spectra alone. However, approximately 2% of the molecule will be present as the isotopologue in which one of the two alkene carbons is ^{13}C . This enables assignment of the double bond configuration simply by inspection



also prepared as:
 d_9 -**27**, d_{10} -**27**, d_{20} -**27**, and d_{47} -**27**

Fig. 36. Key NOE contacts established in an η^3 -cyclohexenyl complex $[(\eta^3\text{-C}_6\text{H}_9)\text{Pd}(\text{TSL})]^+$, with their distinction enabled by synthesis and NOE analysis of a series of strategically ^2H labelled complexes (d_n -**27**; $n = 9, 10$ [three isotopomers], **20**, **47**) that eliminate specific NOE contacts [330].

of the ^1H - ^1H coupling evident in the satellites of the ^{13}C isotopically-desymmetrised molecule. For a simple stilbene, a 1,2-disubstituted alkene, 3J coupling applies, whereas longer range 5J coupling will be observed for stilbenes which are tetrasubstituted [4,332,333]. Given that the *cis* and *trans* coupling constants only differ slightly, it is prudent to study both isomers of the compound, if available.

Analysis of satellite peaks is widely used in organometallic and inorganic chemistry for supporting the determination of geometry in complexes, or their interaction with various ligands [334]. A Pt-SnCl₃ bond in a complex was evidenced by the presence of satellite signals in a ^{195}Pt NMR spectrum, indicative of coupling of ^{195}Pt with ^{119}Sn and ^{117}Sn , both NMR active nuclei with a spin = $\frac{1}{2}$ and natural abundances of 8.6% and 7.6% respectively [335].

In terms of reaction monitoring by NMR spectroscopy, analysis of satellite signals can be especially fruitful for the identification of species giving rise to unassigned peaks in the spectrum. If a reaction is being monitored by ^1H NMR spectroscopy, for example, satellite signals for an unknown peak which may be attributed to ^1H - ^{29}Si coupling can help identify a silicon-containing intermedi-

ate or by-product. When integrating very small peaks in an NMR spectrum, for example those corresponding to an intermediate observed during a reaction, referencing to a satellite peak of the substrate, product, or internal standard can be an effective way to achieve better accuracy, due to the similarity in peak intensity.

In $^{19}\text{F}\{^1\text{H}\}$ NMR spectra of organofluorine compounds, the main ^{12}C - ^{19}F signals which appear are accompanied by a smaller doublet for the ^{13}C - ^{19}F satellites. The sensitivity increase, due to improved signal-to-noise ratio for the satellites in comparison to the analogous peak in a ^{13}C spectrum, allows the $^{12}\text{C}/^{13}\text{C}$ isotope ratio to be determined by integrating the satellite peaks. In circumstances where representative integrals for the satellites are unobtainable, for example due to interference from the parent peak, a technique used to generate NMR spectra in which the ^{12}C signals are suppressed may be applied. Multiple-quantum filtered (MQF) $^{19}\text{F}\{^1\text{H}\}$ NMR spectra enable accurate satellite integrals to be obtained, Fig. 37. This strategy has been very effectively developed and applied by Kwan and Jacobsen in a detailed study of concerted nucleophilic aromatic substitution reactions [323]. For example, in Fig. 37, the right hand ^{13}C - ^{19}F satellite at the benzylic position ($\text{Ar}^{13}\text{CH}_2\text{F}$, not shown) can be integrated against the right hand ^{13}C - ^{19}F satellite of the CF_3 group (shown), using the latter as an internal reference during conversion of ArCH_2Br into ArCH_2F . The change in the integrated ratio (R/R_0) as a function of fractional conversion, F , (Section 5.3.3.2) then allows the ^{13}C KIE to be determined for the benzyl bromide substitution process. Although, in principle, the quantitation may be affected by transverse relaxation during the pulse sequence, the technique was validated by comparison of the ^{13}C KIE determined using the MQF $^{19}\text{F}\{^1\text{H}\}$ NMR technique with the Singleton method (Section 5.3.4), which was found to be 1.059 by both methods [323].

There are situations in which the suppression of satellite signals is desirable. An abundance of satellite signals and hence likely signal overlap can mask minor impurities in complex spectra. NMR experiments such as DISPEL can be implemented to remove satellites where necessary [180]. Conversely, experiments such as INADEQUATE can be used to selectively study satellites [336]. Natural abundance distributions can be determined by NMR spectroscopy, using the natural abundance of one compound to

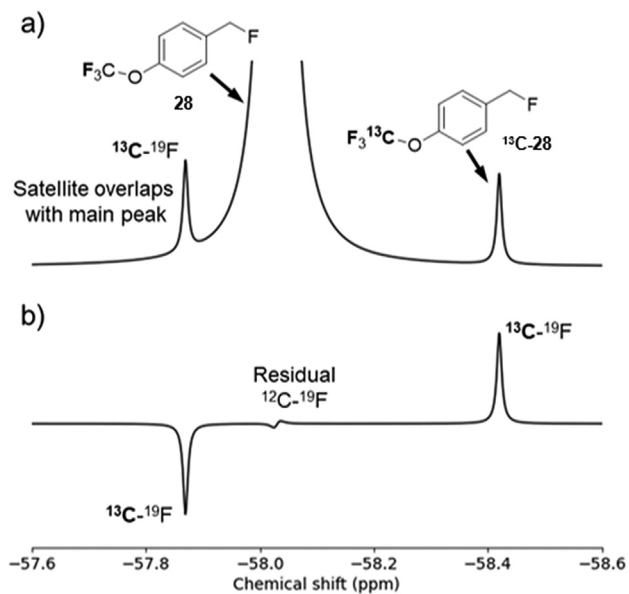


Fig. 37. Schematic illustration of (a) satellite signals in a $^{19}\text{F}\{^1\text{H}\}$ NMR spectrum, and (b) the use of multiple-quantum filtered (MQF) $^{19}\text{F}\{^1\text{H}\}$ NMR techniques to enable their accurate integration.

provide a reference for another. The technique is particularly useful for quantifying the enrichment of a sample which has been isotopically labelled. This strategy was applied to evaluate the ^{10}B incorporation in vinylboronic acid pinacol ester, using natural abundance (80.2/19.8; $^{10}\text{B}/^{11}\text{B}$) potassium 4-fluorophenyltrifluoroborate as a reference, and superimposing the ^{11}B and ^{10}B NMR spectra [28], see Case Study 13.

5.7. Enhanced sensitivity, S/N

Low signal-to-noise ratio is an inherent problem for low-abundance NMR-active nuclei; ^{13}C for example has a natural abundance of 1.1%, and ^{29}Si is <5% abundant. Enrichment of samples by means of isotopic labelling can be a simple way to address this. For example, poor S/N in a $^{13}\text{C}\{^1\text{H}\}$ NMR spectroscopic study of the dimerisation reaction of carbene **30** to **31** made kinetic analysis challenging. Installing a ^{13}C label (99%) on the carbene carbon increased the effective concentration of the process being analysed by a factor of >86, and revealed much useful information about the mechanism and side products (**32**) of this reaction, Fig. 38[314].

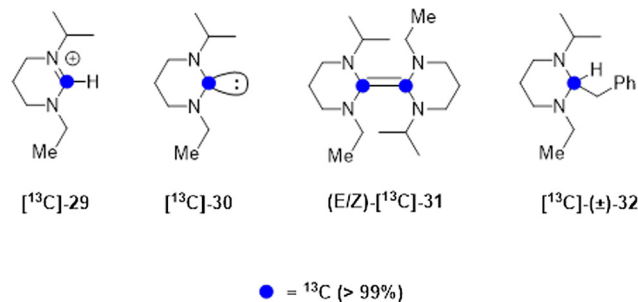


Fig. 38. An example of the use of ^{13}C -labelling to enhance S/N in a mechanistic investigation of NHC reactivity [314].

6. Case studies

The 15 Case Studies below have been selected to provide illustrations of the different aspects of the various approaches for the application of NMR in mechanistic investigation that have been covered in Sections 1–5. They are based on recent publications from the authors' group and from others. None of them are comprehensive descriptions of the work, nor do they focus on the overall mechanistic conclusions, or the full background that stimulated the investigation; the reader is encouraged to go to the primary cited publication for further details if they are intrigued. Instead, each case study outlines one or more of the main mechanistic or technical questions, and how NMR spectroscopy allowed these to be answered. The focus of the discussion in each case is on the practical details of how these key experiments were conducted, most often using information drawn from the Supporting Information to the primary publication. The aim of this approach is to give the reader a sense of how the problems were actually tackled, rather than simply summarising the conclusions from each study. Table 3 provides a list of all of the major topics discussed in Sections 1–5 and indicates in which of the case studies these techniques have been applied. Thus if one is interested in a specific technique, the key case studies to read, and the reference to the primary publication, can easily be located. The Case Studies highlight the extremely versatile nature of the NMR technique, allowing exquisite details to be elucidated from relatively small volumes of reactions, under the 'normal' reaction conditions relevant to their application.

Table 3
NMR and mechanistic techniques described in Sections 2–5, and the 15 Case Studies in which they feature.

Technique	Case Study	1	2	3	4	5	6	7	8	9	10	11	12	13	14	15
<i>Ex situ</i> sampling		•									•					
<i>In situ</i> , continuous		•	•	•			•	•	•	•	•	•		•		•
<i>In situ</i> , interrupted		•														
<i>In situ</i> , periodic activation															•	•
Interleaving; <i>pseudo</i> time				•												
Interleaving techniques					•	•										
Flow NMR					•	•										
Variable Temperature NMR			•	•												
Rapid Injection NMR			•				•									
Stopped Flow NMR				•					•							
Rapid Quenched Flow		•														
<i>In situ</i> Illumination NMR																•
Hyperpolarisation												•				
¹⁹ F NMR		•		•					•	•	•		•	•	•	•
¹ H NMR		•	•		•	•	•	•	•	•	•	•	•	•	•	•
³¹ P NMR								•	•							
^{10,11} B NMR		•							•					•		
¹³ C NMR		•			•			•				•			•	•
²⁹ Si NMR															•	•
Relaxation (<i>T</i> ₁ , <i>T</i> ₂)						•			•			•				
Spatially-selective NMR							•									
Pure Shift and SHARPER									•							
Equilibrium Kinetics									•		•	•				
Kinetics/Steady-state				•	•							•			•	
Kinetics/RPKA								•								•
Kinetics/VTNA										•						
Kinetics/Catalyst Speciation					•			•						•	•	•
Kinetics/Simulation				•							•			•		
Line shape analysis				•					•							
EXSY											•					
Titration		•									•					
DOSY			•										•			•
Isotopes/Tracking											•			•	•	•
Isotopes/Scalar Coupling									•						•	
Isotope Shifts		•		•							•			•	•	•
Isotopes/KIEs and EIEs		•		•						•						
Isotopes/Entrainment											•			•	•	•
Isotopes/ <i>S/N</i>												•			•	•
Isotopes Natural Abundance		•												•		•

6.1. Case study 1: Base-catalyzed Aryl-B(OH)₂ protodeboronation revisited: From concerted proton-transfer to liberation of a transient Arylanion [24]

Techniques: *Ex situ* sampling; *In situ*, continuous; *In situ*, interrupted; Rapid Quenched Flow; ¹⁹F NMR; ¹H NMR; ^{10,11}B NMR; ¹³C NMR; Titration; Isotope Shifts; Isotopes/KIEs and EIEs

In a recent mechanistic study the Lloyd-Jones group employed a range of *in situ* and *ex situ* NMR monitoring techniques to analyse the base-catalysed protodeboronation of arylboronic acids **33** to **62**. In the first part of study they focused on obtaining the rate constant (*k*_{PDB}) for the protodeboronation of each arylboronic acid at 70 °C, and at high pH, where the arylboronic acid is exclusively in the boronate form: [ArB(OH)₃][−]. The half-lives (*t*_{0.5} = ln2/*k*_{PDB}) (Table 4) spanned nearly 10 orders of magnitude and demanded a range of methods (Section 2) to study the series.

The slowest reactions, with *t*_{0.5} in the range of days to months (**33–43**) were monitored using an interrupted *in situ* NMR method. The arylboronic acid was dissolved in dioxane/water (1/1) containing an internal standard (propionic acid for ¹H NMR; and TFA for ¹⁹F NMR) and transferred to a J Young valve NMR tube and the final component, KOH, charged. A series of NMR spectra were obtained, every 6 h to every 4 days, at 27 °C (the probe temperature) but keeping the NMR tube in an oil bath at 70 °C between measurements.

For reactions with an intermediate rate, *t*_{0.5} in the range of minutes to hours (**44–54**), an *ex situ* NMR protocol was used. The aryl-

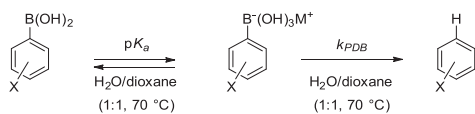
boronic acid was dissolved in dioxane/water (1/1) together with a TFA internal standard and further dioxane. The mixture was heated to 70 °C and a *t*₀ spectrum obtained by transferring an aliquot to an NMR tube and analysing it by ¹⁹F NMR. Once this spectrum was obtained, aqueous KOH was added to the reaction vessel and the mixture was vigorously stirred. Aliquots were transferred to individual NMR tubes and these kept at 70 °C for a range of time periods, before being quenched (HCl) and analysed by ¹⁹F NMR.

For the faster reactions, with a *t*_{0.5} in the range of milliseconds to seconds (**55–62**) the rapid quench-flow method (Section 2.4.1) was employed. The arylboronic acid and TFA (internal standard and stabiliser) were dissolved in dioxane/water (1/1) and an aliquot analysed by ¹⁹F NMR spectrum to give a *t*₀ spectrum. The remaining solution was then loaded into the reagent syringe of the rapid quench-flow apparatus and the thermostat set to 70 °C. The second reagent syringe was primed with a solution of KOH in dioxane/water (1/1), and the quench syringe primed with aqueous HCl (large excess over the KOH). Once the system had thermally equilibrated to 70 °C, the reagents were driven through the mixer and the control software set to allow reaction ageing time periods ranging from 2 ms to 30 s, depending on the boronic acid, before ‘instant’ automated quench by the HCl. A quench-sample was collected for each time point and analysed by ¹⁹F NMR to build the kinetic profile in pseudo time format.

The temporal concentration data (for formation of the product, consumption of the starting material, or both) for all 30 boronic acids were analysed using a simple first-order rate equation to

Table 4

Half-lives for protodeboronation (k_{PDB}) of arylboronates **33–62** at 70 °C in 1:1 H₂O/Dioxane at pH > 12.

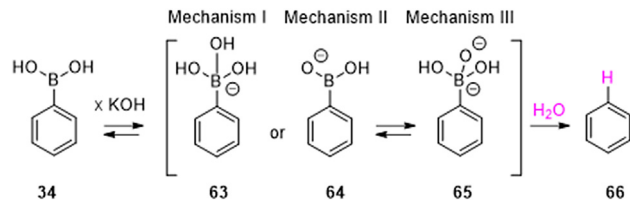


Substrate; X	$t_{0.5}$	Method
33 3-F	7 months	Interrupted, <i>in situ</i>
34 H	6 months	Interrupted, <i>in situ</i>
35 4-F	4 months	Interrupted, <i>in situ</i>
36 3,4-F ₂	3 months	Interrupted, <i>in situ</i>
37 3,5-F ₂	3 months	Interrupted, <i>in situ</i>
38 3-Cl	8 weeks	Interrupted, <i>in situ</i>
39 3,5-(CF ₃) ₂	7 weeks	Interrupted, <i>in situ</i>
40 4-Me	7 weeks	Interrupted, <i>in situ</i>
41 3,4,5-F ₃	7 weeks	Interrupted, <i>in situ</i>
42 4-MeO	5 weeks	Interrupted, <i>in situ</i>
43 3,5-(NO ₂) ₂	16 h	Interrupted, <i>in situ</i>
44 2-F-4-MeO	34 h	<i>ex situ</i>
45 2-F	19 h	<i>ex situ</i>
46 2,4-F ₂	8 h	<i>ex situ</i>
47 2,5-F ₂	3 h	<i>ex situ</i>
48 2-F-4-CF ₃	2 h	<i>ex situ</i>
49 2,3-F ₂	2 h	<i>ex situ</i>
50 2,4,5-F ₃	1 h	<i>ex situ</i>
51 2,3,4-F ₃	39 min	<i>ex situ</i>
52 2-F-5-NO ₂	15 min	<i>ex situ</i>
53 2,3,5-F ₃	10 min	<i>ex situ</i>
54 2,3,4,5-F ₄	3 min	<i>ex situ</i>
55 2,6-F ₂ -4-MeO	7 s	rapid quench-flow
56 2,6-F ₂	5 s	rapid quench-flow
57 2,4,6-F ₃	1 s	rapid quench-flow
58 2,3,6-F ₃	235 ms	rapid quench-flow
59 2,3,4,6-F ₄	66 ms	rapid quench-flow
60 2,3,5,6-F ₄	11 ms	rapid quench-flow
61 2,3,5,6-F ₄ -4-MeO	9 ms	rapid quench-flow
62 2,3,4,5,6-F ₅	2.6 ms	rapid quench-flow

obtain k_{PDB} . With the rate data in hand attention was turned to probing a range of previously proposed mechanisms (I – III; Scheme 7).

A pH-rate profile was constructed for one of the more rapidly reacting arylboronic acids, **56**, using the *ex situ* NMR protocol, *vide supra*, but with an additional buffer added to control the pH. Using a selection of buffer systems, k_{obs} was determined at various pH values, and $\log k_{\text{obs}}$ versus pH plotted. By fitting an appropriate model to this data, we were able to determine that the reaction proceeds *via* a monoanionic mechanism, thus ruling out Mechanism III (Scheme 7). This conclusion was reinforced by testing for saturation kinetics, again using the *ex situ* NMR protocol, but in this case adding KOH at various concentrations. The rate was pH independent above a pH threshold where all of the ArB(OH)₂ had been converted to [ArB(OH)₃][−].

Twenty of the thirty arylboronic acids (**33–52**) proved stable enough for rapidly conducted ¹¹B{¹H} NMR pH titrations. In each case, the arylboronic acid was dissolved in dioxane/water (1/1) to give a 0.05 M solution, which was stirred and heated to 70 °C. While monitoring using a pH meter, KOH was added in small volumes to increase the pH by 0.5 pH units, between pH 7.11 and pH 13.01. At each stage an aliquot was transferred to an NMR tube and the sample analysed at 70 °C by ¹¹B NMR. The ¹¹B NMR chemical shift and line-width for ArB(OH)₂ species (26–28 ppm; broad) are very distinct from those of the boronate, [ArB(OH)₃][−] (3–5 ppm; relatively sharp). At pH 13, the chemical shift and sharper line-width indicated a tetrahedral (Mechanism I) not trigonal (Mechanism II) boron centre, with the speciation > 99% [ArB(OH)₃][−]. In between these limiting pH values, rapid exchange (10⁶ M s^{−1}) of

**Scheme 7.** Proposed mechanisms I–III for the base-catalysed protodeboronation of arylboronic acids.

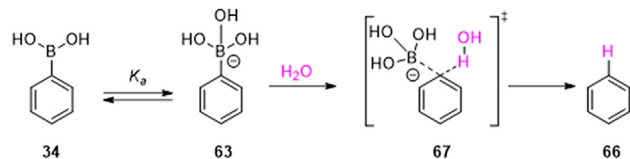
hydroxide between boron centres results in a single time-average peak (Section 4.5.1), allowing calculation of the speciation. The Henderson-Hasselbalch equation allowed the pK_a value for each boronic acid to be obtained from the NMR-derived ArB(OH)₂/[ArB(OH)₃][−] speciation. On comparison with the protodeboronation kinetics, it was evident there was not a simple correlation between the Lewis acidity of the boron centre (pK_a) and the rate of C–B cleavage (k_{PDB}).

A Hammett analysis was conducted by plotting $\log(k_{\text{PDB}}/k_{\text{H}})$ vs σ_{SL} , where k_{H} is the k_{PDB} value for **34** and σ_{SL} a modified Swain-Lupton parameter. The biphasic correlation indicated that two monoanionic pathways I_A and I_B were operative, with the division being clearly defined based on the electron-deficiency of the aromatic ring.

A KIE study (Section 5.3) was conducted on an electron-rich system, *p*-anisylboronate (**42**) following pathway I_A (Scheme 8). By following the interrupted *in situ* NMR method rate data was obtained in H₂O/dioxane (normal, k_{H}), in D₂O/dioxane (deuterated, k_{D}) and in L₂O/dioxane (L = H, D 1:1) This allowed for the absolute rate KIE, $k_{\text{H}}/k_{\text{D}}$, to be determined from the first two solvent systems, as 4.4. For the final system the KIE was determined by the ratio of products, giving a partitioning KIE of 4.4. Both KIE values agree, and the magnitude indicated a PKIE, consistent with a concerted form (I_A; Scheme 8) of the previously proposed general Mechanism I.

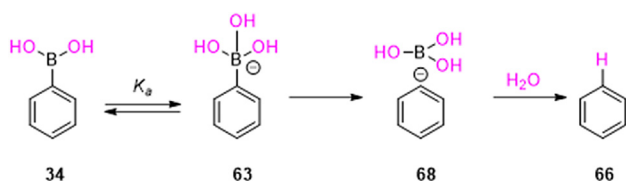
Of the remaining arylboronic acids, 2,6-fluorophenylboronate acid (**56**) was chosen as an electron-deficient system that primarily follows the faster pathway, I_B (Scheme 9). An analogous KIE study was conducted, but using the rapid quench flow NMR protocol, *vide supra*. The resulting absolute rate KIE, $k_{\text{H}}/k_{\text{D}}$, was 1.00, indicating that proton transfer is not involved in the rate-limiting step. The partitioning KIE was low, but not 1.00. Instead, the value of 1.26 is consistent with transfer of H/D from L₂O to a highly-reactive species, such as an aryl anion; pathway I_B, Scheme 9.

The mechanistic proposal (pathway I_B, Scheme 9) was explored by ^{10/11}B and ^{12/13}C heavy-atom KIE experiments. The former used two competition experiments (Scheme 10), both of which suggested that there was not the expected primary B-KIE. However, a possible explanation lay in an equal but opposite secondary isotope effect (SKIE) caused by rehybridization of the boron during the arylboronate to boric acid (B(OH)₃) conversion at stage one, the RLS, of pathway I_B. An analogous equilibrium isotope effect (EIE) would also be expected for arylboronate/arylboronic acid interconversion, and this was probed by competitive ¹⁹F NMR titra-

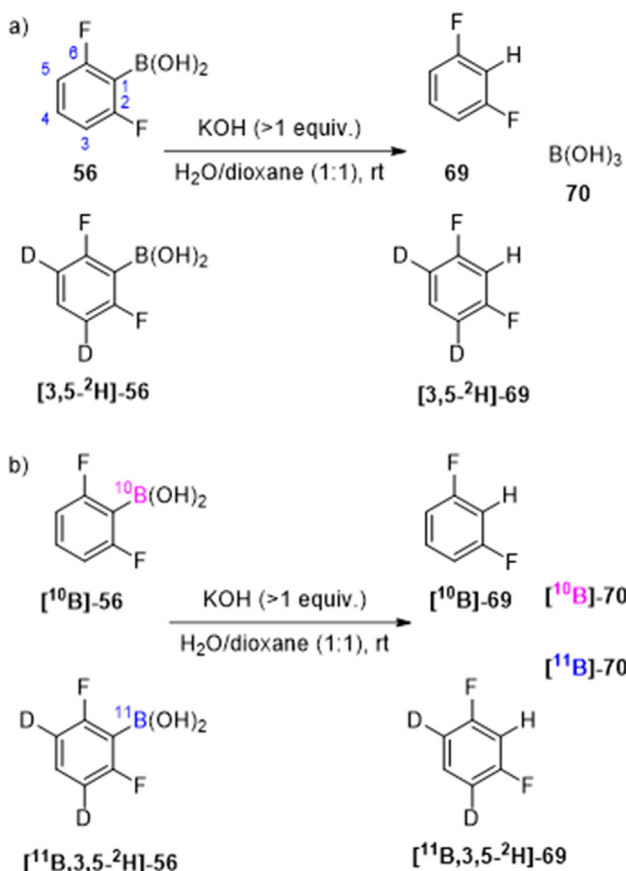
**Scheme 8.** Concerted mechanism (I_A) for the base-catalysed protodeboronation of arylboronic acids.

tions, **Scheme 11**, to gain supporting evidence. From these experiments a significant inverse secondary $^{10/11}\text{B}$ EIE was determined (1.02), a value which is sufficient to offset the expected normal boron PKIE in the RLS for pathway I_B .

A ^{13}C KIE is also expected to attend C–B cleavage in pathway I_B , and in this case was probed using the Singleton method (**Section 5.3.4**). Thus, a solution of 2,6-difluorophenylboronic acid in 1/1 dioxane/water containing TFA as an internal standard was warmed to 27 °C, and a solution of excess KOH added. After 77 min (~96% conversion) the reaction was quenched and the ^{13}C -enriched unreacted boronic acid (**56**) isolated. However, ^{13}C NMR analysis of the key carbon was strongly affected by the quadrupolar relaxation broadening caused by the adjacent boron. The boronic acid was therefore redissolved in dioxane/water, added to a J Young valve NMR tube, excess KOH added, and the tube shaken vigorously to effect complete protodeboronation. In a separate J Young valve NMR tube a sample of the unreacted (i.e. non- ^{13}C enriched) boronic acid was analogously protodeboronated. Both samples were analysed by ^{19}F NMR until protodeboronation was complete. This allowed indirect analysis of the



Scheme 9. Dissociative mechanism (I_B) for the base-catalysed protodeboronation of arylboronic acids.



Scheme 10. Competition experiments performed to determine B-KIE, (a) D-KIE background and (b) B-KIE experiment.

boronic acid **56**, by ^{13}C DEPT-55 analysis of the cleanly *in situ* generated 1,3-difluorobenzene products **69**. The $^{12}\text{C}/^{13}\text{C}$ PKIE value for the ipso carbon (C1 in **56**) was determined to be 1.029, consistent with the primary KIE calculated computationally (DFT) for pathway I_B .

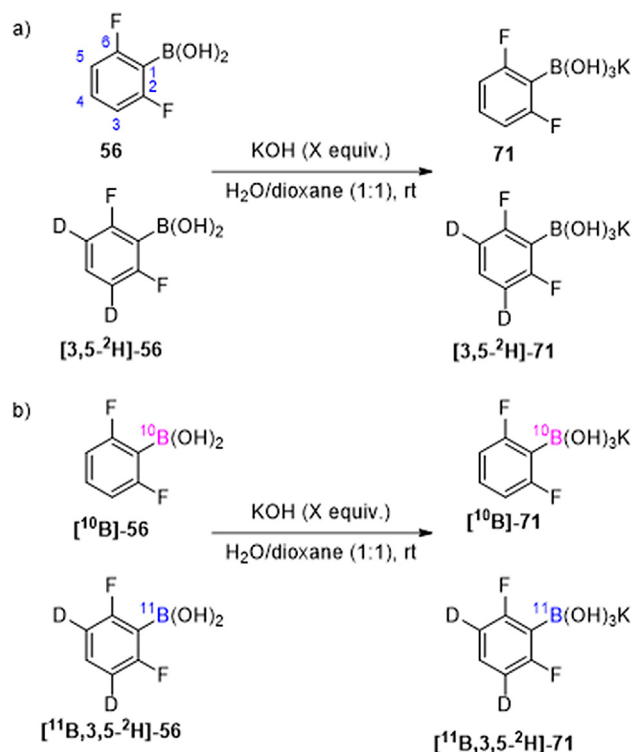
This mechanistic study is an example of the power of the application of different *in situ* and *ex situ* NMR monitoring techniques to ensure capture of relevant kinetic data. It also shows how helpful ^{19}F NMR can be when dealing with a system that has overlapping or complex ^1H NMR spectra, allowing informative titration, KIE and EIE NMR experiments. All of the individual techniques outlined above are readily accessible to the mechanistic chemist, and through a well-considered combination, complex systems can be readily tackled.

6.2. Case study 2: A dinuclear mechanism implicated in controlled carbene polymerization [337]

Techniques: *In situ*; continuous; ^1H NMR; Rapid-Injection NMR, DOSY

In a recent study into the development and mechanistic understanding of (π -allyl)palladium carboxylate dimers (**75**, **76**) as a new class of initiators for the polymerisation of ethyl diazoacetate (EDA: **72** **Scheme 12**) Toste and collaborators utilised variable temperature (VT) and rapid injection (RI) NMR techniques to great effect.

In preliminary ^1H NMR studies it had been found that there was good separation of the peaks, allowing for all of the major species to be clearly followed. The team used the following protocol for their analysis. Firstly, they calibrated their NMR spectrometer probe temperature using the methanol thermometer technique. This involved determining the ^1H NMR chemical shift of a 4% sample of MeOH in CD_3OD , for which reference calibration curves of chemical shift difference between Me and OH, versus temperature,

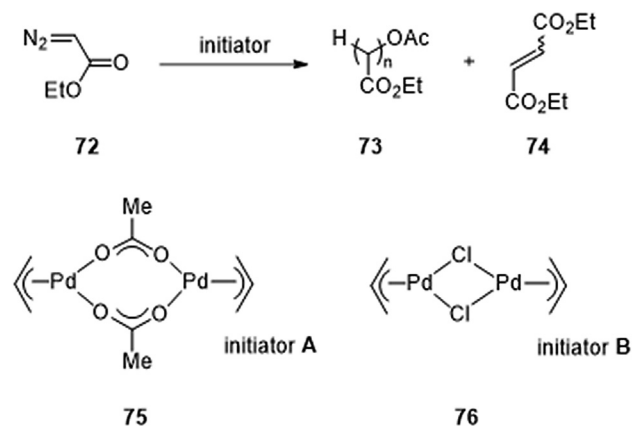


Scheme 11. NMR titration equilibrium experiments to determine the EIE, (a) D-EIE background and (b) B-EIE experiment.

have been published [50]. After calibration, they charged a solution of the EDA (0.47 M) and their chosen internal standard of 1,1,2,2-tetrachloroethane (1 μL) to a J Young valve NMR tube. This was submitted to the spectrometer and tuning, locking, shimming, 90° pulse calibration and T_1 measurement were carried out at -40°C . The sample was then ejected from the NMR spectrometer and put into a dry-ice acetone bath at -78°C . Next, the Pd initiator (**75**, 9.5 mM) was injected into the NMR tube, to give a total volume of 736 μL , and the NMR tube submitted back to the NMR spectrometer. The data collection was started (t_0) once the lock signal stabilised, and the dead time between resubmission and reaching the desired -40°C was recorded. A series of NMR spectra were recorded over 1 h and the resulting data modelled in plots of [conc] vs t , for both the EDA and palladium dimer. The modelled data revealed that the dimer decayed with first order kinetics, and that the EDA had a more complex first/second order relationship – findings consistent with their proposed dinuclear mechanism.

An interesting finding from their *in situ* kinetics study was the migration of the methyl group from one of the acetate groups in the palladium dimer. Utilising DOSY (Section 4.6) they were able to identify that the new peak in the NMR arises from the acetate becoming attached to the chain end of the polymer, further supporting the mechanistic hypotheses regarding initiation events.

To conclude their studies Toste and collaborators looked to elucidate comparative rates of initiation for the acetate complex **75**, Scheme 12, versus the chloride bridged complex used in previous work, complex **76**. The dead time in the VT NMR studies outlined above meant key data was missing for the first 200 s, during which the initiator was mostly consumed. This aspect was addressed using the rapid injection method (Section 2.4.4.1). Firstly, 400 μL from a stock solution of the initiator (3.69 μM in toluene- d_8) was charged into an NMR tube. Separately a solution of the EDA was prepared (0.92 mM) with 1,4-bis(trifluoromethyl)benzene as internal standard and transferred to the injection reservoir in the RI-NMR equipment. The NMR tube was then inserted into the NMR spectrometer with the cap removed and under a flow of N_2 , and the tube cooled to -20°C . The injection system was lowered into the NMR spectrometer and allowed to cool over a period of 10 s, after which 200 μL of the EDA solution was injected at a rate of 150 $\mu\text{L/s}$. The reaction was monitored *in situ* from the point of injection via ^1H NMR, with a spectrum recorded every 19 s over twelve minutes. From the data obtained, Toste and collaborators were able to determine that initiator **75** was much more effective than **76**. They were also able to derive information about the relative propensity for the two initiators to dimerise rather than polymerise the EDA from the RI-NMR experiments. These observations,



Scheme 12. General conditions for the polymerisation of ethyl diazoacetate (**72**) with (π -allyl)palladium dimers (**75**, **76**) as initiator.

along with the support of DFT calculations, allowed the proposal of a dinuclear mechanism, in which both Pd centres play a role.

This study highlights the substantial increase in insight available by application of specialist techniques. The use of VT-NMR allowed elucidation of the kinetic orders, and gave important general mechanistic information. By employing the RI-NMR technique, processes occurring at the very beginning of the reaction were analysed, under carefully controlled temperature conditions, revealing information that would be missed by standard *in situ* monitoring. Overall, the *in situ* NMR study yielded important information about the relative activity of the two catalysts **75** and **76**, and provided additional understanding regarding which more readily undergoes the undesired dimerization.

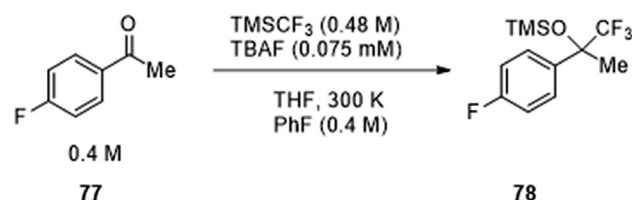
6.3. Case study 3: Anion-initiated trifluoromethylation by TMSCF_3 : Deconvolution of the siliconate-carbanion dichotomy by stopped-flow NMR/IR [25]; and difluorocarbene generation from TMSCF_3 : Kinetics and mechanism of NaI-mediated, and Si-induced, anionic chain reactions [26]

Techniques: *In situ* continuous; Interleaving pseudo-time; Variable Temperature NMR; Stopped Flow NMR; ^{19}F NMR; Kinetics at Steady-state and Simulation; Line shape analysis; Isotope Shifts; Isotopes/KIEs and EIEs

Over the last decade, there has been much interest in use of the reagent trimethyl(trifluoromethyl)silane (TMSCF_3) for CF_3 and CF_2 transfer, including applications at industrial scale. The Lloyd-Jones group recently published two mechanistic studies on the reagent, exploring CF_3 transfer to ketones and aldehydes and CF_2 transfer to alkenes. Both studies utilised a wide range of techniques, especially ^{19}F NMR, to elucidate detailed information.

The study began by using *in situ* ^{19}F NMR to characterise the reaction of 4-fluoroacetophenone (**77**) with TMSCF_3 , initiated by Bu_4NF (TBAF, Scheme 13).

200 μL of a stock solution containing **77** and the internal standard (fluorobenzene) in THF was added to an NMR tube, followed by a further 200 μL of a stock solution of TMSCF_3 in THF. A rubber septum was used to seal the NMR tube, allowing for later addition of the TBAF initiator without the system being exposed to air. The NMR tube was loaded into the NMR spectrometer at 300 K and the sample was shimmed, tuned and the first spectrum obtained ($t = 0$). The sample was then ejected and 50 μL from a stock solution of TBAF in THF was rapidly injected, using a microsyringe with the needle inserted through the rubber septum of the NMR tube. The NMR tube was vigorously shaken (vertically) during the addition, and again once the needle was removed, to ensure full mixing. The NMR tube was resubmitted to the spectrometer, shimmed, tuned, and a spectrum obtained. The time between the TBAF being added and the first spectrum being obtained was recorded by a stopwatch, to include as an adjustment when later analysing concentration vs time as recorded by the spectrometer. Spectra were taken at regular intervals, over time periods that depended on the specific reaction conditions. Three side-products were evident in the ^{19}F NMR spectra, and identified as fluoroform (CF_3H , **81**), a



Scheme 13. Reaction conditions for the *in situ* ^{19}F NMR spectroscopic analysis of the reaction between TMSCF_3 and 4-fluoroacetophenone (**77**).

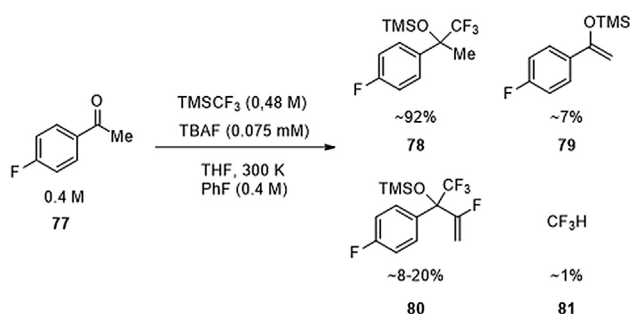
silylenol ether (**79**), and a homologated product (**80**; Scheme 14) generated from **79**.

Having identified the product, and side-products, spectra were stacked and each peak integrated, using the fluorobenzene internal standard to determine absolute concentrations of each species. The results were found to vary between batches of TBAF, and so this was replaced with $[\text{Ph}_3\text{SiF}_2][\text{Bu}_4\text{N}]$ ('TBAT'), an anhydrous initiator that gave consistent results and much faster reactions. Using the *in situ* ^{19}F NMR method, the effects of potential contaminants in the TMSCF_3 were tested by addition of a series of possible "inhibitors", about 200 s after initiation, and then resubmitting the NMR tube to the spectrometer to analyse the change in rate reaction. The *in situ* method was also employed to determine how the identity of the CF_3 source (comparing Me_3SiCF_3 with Et_3SiCF_3 and $(i\text{Pr})_3\text{SiCF}_3$) affected the rate of reaction and generation of enol ether **79** and analogues.

Whilst the initial *in situ* studies gave useful information regarding the effects of different initiators, reagents and inhibitors, detailed kinetic analysis remained elusive due to the fast rate at which the reaction initiated and proceeded to completion. Thus, stopped-flow (SF-NMR) (Section 2.4.4.2) was employed, allowing detailed analysis of the first 5–100 s of the reaction, allowing efficient control of mixing and temperature. For the reaction of interest, Scheme 14, classic SF-NMR (Fig. 12a) with a fixed-ratio two reservoir system would require a very large quantity of each component (R_3SiCF_3 , ketone, and initiator) and a lengthy procedure for flushing out the previous samples in the reservoirs and flow lines between runs, to fully evaluate the kinetics. Instead, a triple reservoir, variable ratio SF-NMR system (Fig. 39) was employed. For the three-component reaction (Scheme 14) this required just four stock solutions to be prepared.

The following protocol was followed for the SF-NMR experiments. A stock solution of TMSCF_3 and ketone in THF was prepared and transferred into a Schott reagent bottle, which was capped with a three-valve cap with threaded ports. A TBAT stock solution was also prepared in the same manner. A further Schott bottle containing a 'wash solution' of TMSCF_3 and TBAT was prepared, and this then was used to dehydrate the flow lines in the SF-NMR system prior to use in this very water-sensitive reaction. Next, the SF-NMR flow-cell assembly was lowered into the NMR spectrometer and shimming and tuning performed. The three syringe drives were each loaded with the appropriate reagent and flushed through the system, followed by anhydrous THF. The syringes were loaded again and kinetic studies were run using a 600 μL shot volume, a 1 mL s^{-1} flow rate, and a spectrum acquisition time of 0.5 s with 1 s relaxation delay. Typically, there was one scan per spectrum.

Using this system, the initial rate of reaction, as a function of the concentrations of all three components (TMSCF_3 , ketone, and TBAT), was rapidly and efficiently analysed. For TBAT and ketone,



Scheme 14. Trifluoromethylation of **77** by TMSCF_3 , analysed *in situ* by ^{19}F NMR spectroscopy.

plots of initial rate vs initial concentration gave positive straight-line correlations, indicative of first-order dependence on both components. However, for TMSCF_3 initial rate vs reciprocal initial concentration gave a positive straight-line correlation, indicative of inverse first-order with respect to TMSCF_3 ; i.e. the reagent is an inhibitor of the overall process.

SF-NMR analysis using 10 mol% TBAT allowed identification of a silicate intermediate, $[(\text{CF}_3)_2\text{SiMe}_3]^-$, and by interleaving a combination of datasets obtained with varying delays between the reaction being triggered and the first spectrum, temporal concentration data was obtained for the full reaction evolution, acquiring 30 data points at 0.29 s intervals over a pseudo time period of 8.7 s. The short-lived silicate intermediate, $[(\text{CF}_3)_2\text{SiMe}_3]^-$, was shown to be generated in direct proportion to the TBAT, and to be in a very rapid dynamic equilibrium with TMSCF_3 and an undetected low concentration of a highly reactive CF_3 anionoid. The latter process gave rise to dynamic-line broadening of the silicate species, which was constant throughout the reaction. However, for the TMSCF_3 the dynamic line-broadening was found to develop as the reaction proceeded, and the TMSCF_3 concentration was depleted. This dynamic line-broadening was successfully simulated using a three-spin exchange process in which TMSCF_3 and the silicate are in rapid dissociative equilibrium with a k_{ex} rate ranging from approximately 180 s^{-1} to 2325 s^{-1} between 2 and 22 °C, Fig. 40. The data for k_{ex} at the various temperatures was used in an Eyring analysis, plotting $\ln(k_{\text{ex}}/T)$ vs $1/T$, to give ΔG^\ddagger and $T\Delta S^\ddagger$ for the dissociation (**82** \rightarrow **84** + CF_3) at 27 °C, the temperature at which the kinetics of the CF_3 transfer reaction were studied. This data could not be obtained directly due to the silicate signal being indistinguishable from the baseline at this temperature.

To further probe the mechanism, isotopically labelled substrates were synthesised to determine ^{13}C and ^2H KIEs. To obtain the ^2H KIE for enol ether (**79**) generation, the standard *in situ* ^{19}F NMR procedure was conducted, using the CD_3 isotopologue of the ketone (d_3 -**77**, Scheme 15) in two different experiments.

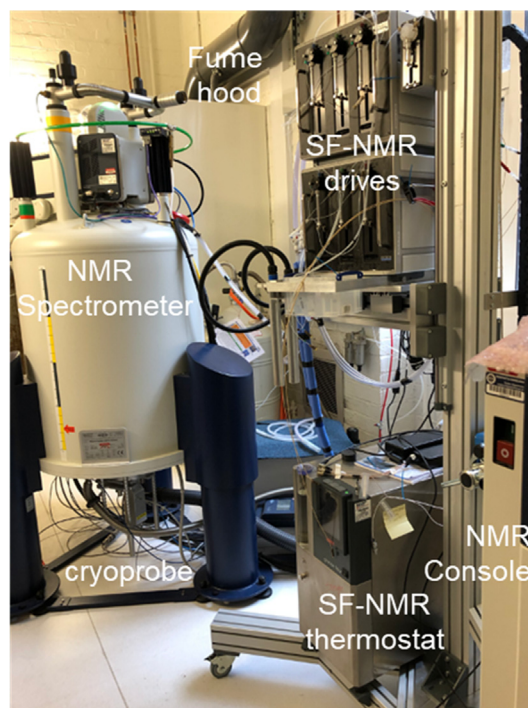


Fig. 39. The variable ratio input stopped-flow NMR system (see schematic configuration in Fig. 12b) employed for the study; in this case with two flow probes – one dedicated to anhydrous work [15].

Comparison of the relative selectivity for product (d_3 -**78**) over enol silane (d_2 -**79**) afforded $k_H/k_D = 6.4$, i.e. a large a primary ^2H KIE. Co-reaction of d_3 -**77**, with **77**, and analysis of the relative rates of generation of $\text{CF}_3\text{D}/\text{CF}_3\text{H}$ afforded $k_H/k_D = 6.1$. To obtain the ^{13}C KIE data for addition of CF_3 to the carbonyl carbon (C-2), intermolecular competitions were again analysed by ^{19}F NMR, through the following pair of experiments: (i) **77** versus d_4 -**77**, affording $k_{[d_0,12\text{C}]} / k_{[d_4,12\text{C}]}$; and (ii) ^{13}C -**77** vs d_4 -**77**, affording $k_{[d_4,12\text{C}]} / k_{[d_0,13\text{C}]}$. The deuteration of the aromatic ring in d_4 -**77** leads to a secondary isotopic shift of 0.54 ppm in the *para*-fluorine signal, allowing [aryl- d_4] to be distinguished from [aryl- h_4] in all of the substrates, intermediates, and products.

The requisite $^{12}\text{C}/^{13}\text{C}$ KIE was isolated algebraically from the two experimentally-determined KIEs by normalisation, and determined to be small ($^{12}\text{C}/^{13}\text{C}$ KIE = 1.008), consistent with a pre-complexation type nucleophilic addition rather than a direct attack at the carbonyl carbon.

$$\frac{k_{[\text{aryl}-d_0,2-^{12}\text{C}]}}{k_{[\text{aryl}-d_0,2-^{13}\text{C}]}} = \left(\frac{k_{[\text{aryl}-d_0,2-^{12}\text{C}]}}{k_{[\text{aryl}-d_4,2-^{12}\text{C}]}} \right) \left(\frac{k_{[\text{aryl}-d_4,2-^{12}\text{C}]}}{k_{[\text{aryl}-d_0,2-^{13}\text{C}]}} \right) \quad (74)$$

The kinetic, thermodynamic, and KIE data were then used to identify the correct DFT methods for computational studies, and in turn to deduce a general mechanism for CF_3 transfer from $\text{R}_3\text{-SiCF}_3$ species to electrophiles, in which the free CF_3 anionoid is the reactive intermediate.

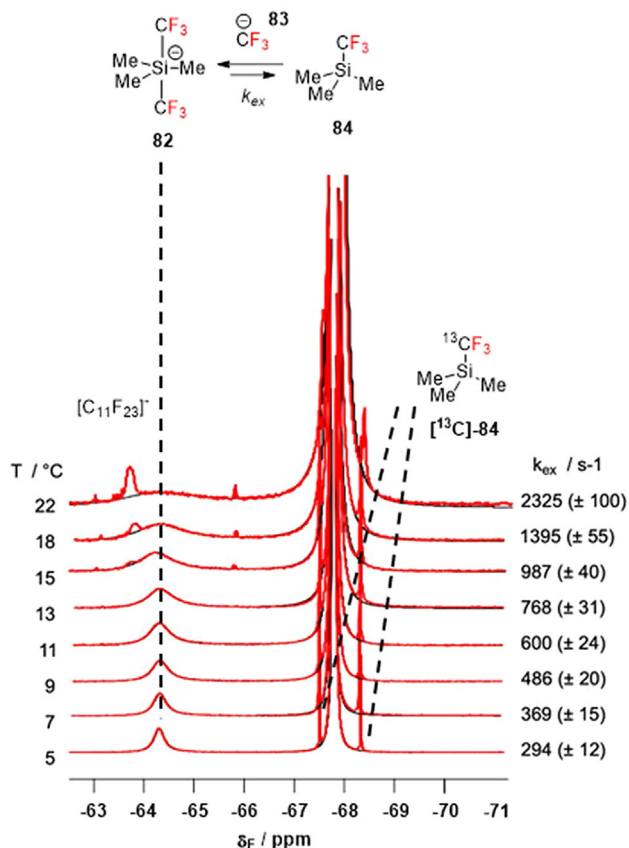
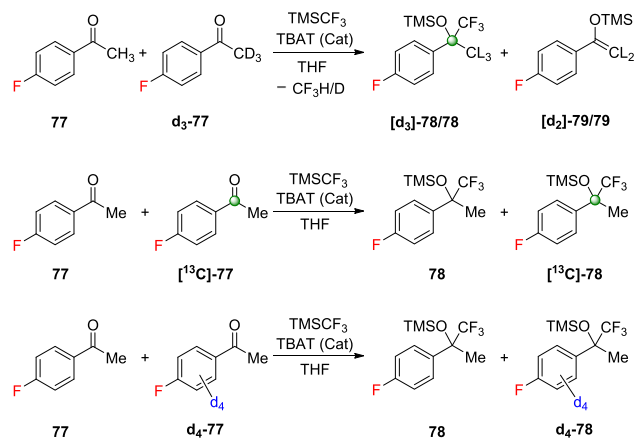


Fig. 40. ^{19}F NMR variable temperature lineshape analysis of silicate-carbanion equilibrium. Experimental data, obtained by SF-NMR Fig. 39, is coloured red, the fitted data is coloured black. The CF_3 anionoid is not detected. Under these conditions (large excess of TMSCF_3 , as evident from ^{13}C -satellites, which are not included in the fitting), the lineshape of the silicate is only dependent on the dissociation rate (k_{ex}). As the temperature is raised, decomposition leads to a mixture of perfluoroalkenes and perfluorocarbanions, dominated by $[\text{C}_{11}\text{F}_{23}]^-$.



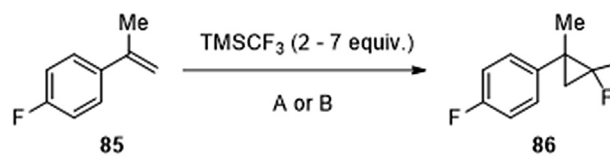
Scheme 15. Intermolecular competition experiments for determination of $^1\text{H}/^2\text{H}$ and $^{12}\text{C}/^{13}\text{C}$ KIEs by ^{19}F NMR spectroscopy (L = H/D). Aryl deuteration in the substrate leads to a significant secondary isotope shift in δ_{F} , facilitating accurate relative quantification of the isotopologues by ^{19}F NMR.

In the second study, a general mechanism for the generation of CF_2 from TMSCF_3 was elucidated, mostly by use of an alkene as a trapping agent for the CF_2 . Reactions were again initiated by TBAT, and these processes compared with initiation by NaI , the latter being the preferred option in synthesis when the desired outcome is the *gem*-difluorocyclopropanation product, **Scheme 16**.

The study began by determining KIEs to probe the nature and geometry of the transition state for transfer of CF_2 to the alkene, and employed the abovementioned double-labelling technique (allowing distinction of $\text{Ar}-d_0$ from $\text{Ar}-d_4$ by a net secondary isotopic shift of 0.54 ppm) to facilitate *in situ* ^{19}F NMR analysis of intermolecular competitions of strategically labelled 4-fluoro- α -methyl styrenes (**Scheme 17**).

By plotting $[\text{Ar}-d_0]/[\text{Ar}-d_4]$ against fractional conversion (F) and fitting the data according to the full Bigeleisen-Wolfsberg equation (see **Section 5.3.3.2**), for first order competition, the KIEs were readily estimated. The ^{19}F NMR spectra were found to be better resolved in chlorobenzene than THF, and on repeating the reactions in this solvent, the KIEs more precisely determined, but of the same magnitude. The three KIEs were all fully consistent with those calculated for addition of a free CF_2 singlet carbene to the alkene.

LFERs were then determined, again by competition, this time between 4-fluoro- α -methyl styrene and different *para*-substituted α -methyl styrenes, with a large deficiency of the TMSCF_3 . Reactions were run until completion and then analysed by ^{19}F NMR. The log of the ratio of the two difluorocyclopropanation products (determined by integrating the diastereoisotopic CF_2 signals) was found to correlate with σ^+ , affording a small negative ρ^+ value. This again was consistent with a concerted asynchronous singlet CF_2 addition process, conclusively showing that



A: 5 mol% TBAT, THF, rt
B: 5-200 mol% NaI, THF, 65 °C

Scheme 16. Difluorocyclopropanation of 4-fluoro- α -methylstyrene (**85**) by TMSCF_3 , using TBAT or NaI as initiator.

the TMSCF_3 is an indirect source of CF_2 . However, the mechanism for the liberation of the CF_2 required further mechanistic study of both the NaI and TBAT initiated systems by *in situ* ^{19}F NMR (Scheme 18).

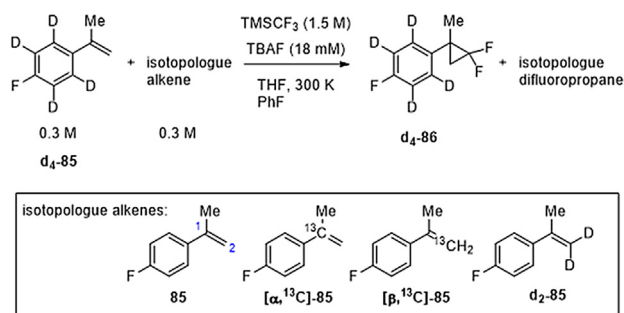
A wide range of experiments were conducted. These included (i) testing the stability of the system in the absence of one of each of the components; (ii) understanding the inhibitory effects of various additives by charging in these compounds during the *in situ* analysis; (iii) evaluating the effect of different solvents and determining what effect changing the cation and anion of the initiator had on the system; and (iv) analysis of the evolution of the difluorocyclopropanation product versus the TMSF reaction co-product, in the form of a ‘concentration-concentration plot’. Indeed using this single *in situ* ^{19}F NMR analysis technique, large amounts of data were extracted, and supported by detailed computational studies, of a wide range of mechanistic hypotheses, that eliminated various possibilities, including radical and cationic chain reactions, and the liberation of CF_2 directly from TMSCF_3 . It was eventually concluded that CF_2 generation from TMSCF_3 proceeds by an anionic chain reaction in which a CF_3 anionoid (Fig. 40) is again a key intermediate. However, in this case the carbanion transfers fluoride anion to TMSCF_3 , thus generating CF_2 and a fluorosiliconate analogous to **82**.

The two related Case Studies above are examples of how a complex reaction mechanism can be broken down into a series of smaller parts, and each part analysed through simple to apply *in situ* ^{19}F NMR protocols, readily accessible to any mechanistic chemist with access to an NMR spectrometer.

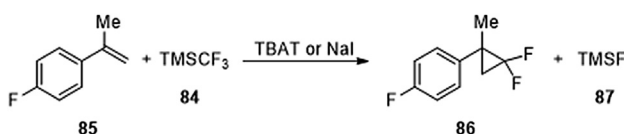
6.4. Case study 4: Insight into catalyst speciation and hydrogen co-evolution during enantioselective formic acid-driven transfer hydrogenation with bifunctional ruthenium complexes from multi-technique operando reaction monitoring [158]

Techniques: Interleaving; Flow-NMR; ^1H NMR; ^{13}C NMR; Kinetics at Steady-state; Catalyst Speciation

Tracking the concentrations of catalytic intermediates during the course of a reaction can provide valuable mechanistic information about the dominant catalytic species and reaction pathways. An example of how interleaving techniques can be used to provide additional insights into catalytic reactions was recently reported



Scheme 17. Reaction conditions for the KIE study between d_4 -**85** and isotopologues of **85**.

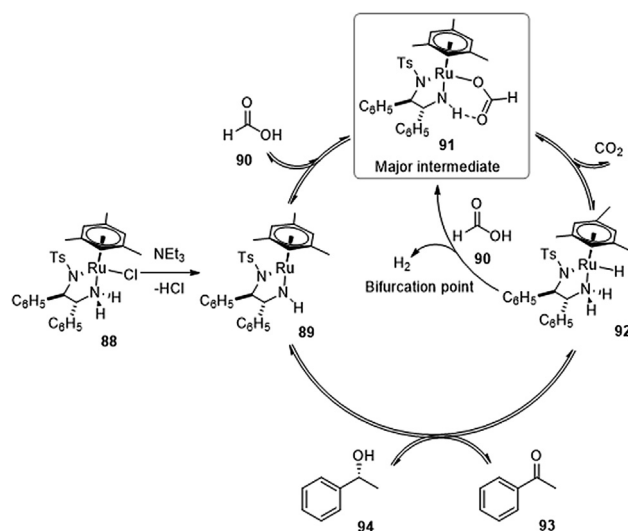


Scheme 18. General reaction conditions for the *in situ* ^{19}F NMR spectroscopy monitoring of the difluorocyclopropanation of **85** by TMSCF_3 .

by Hintermair and collaborators. In this work, the asymmetric transfer hydrogenation of acetophenone (**93**) to 1-phenylethanol (**94**) with the Ikariya–Noyori catalyst [(mesitylene) $\text{RuCl}(\text{R,R})$ -(TsDPEN)] (**88**) was monitored in a formic acid/triethylamine mixture (Scheme 19).

A combination of online flow NMR, UV–Vis spectroscopy, inline liquid chromatography and head-space mass spectrometry were used to provide complementary information about the reaction. Whilst in principle data for each of these techniques could be acquired independently, measuring the data simultaneously using NMR, UV–Vis flow cells, HPLC and headspace-MS sampling in a single reaction vessel, allowed direct comparison between data from the different techniques. A peristaltic pump was used to circulate the reaction mixture from the reaction vessel to the NMR and UV–Vis flow cells via narrow diameter polyether-etherketone (PEEK) tubing (total volume approximately 4 mL, flow rate 4 mL/min). A sampling valve on this flow loop allowed the periodic collection and automated dilution of 50 μL aliquots of the reaction mixture for analysis by chiral HPLC. The reaction vessel and transfer tubing were jacketed, with two heat exchangers and thermocouples located at various positions in the flow loop used to maintain a constant reaction temperature of 40 $^\circ\text{C}$. Headspace-MS samples were taken directly from the headspace of the reaction vessel. As several of the catalytic intermediates are air-sensitive, the reaction was performed under an argon atmosphere, with the flow loop pressure maintained by use of a back-pressure regulator to prevent outgassing of CO_2 or H_2 in the flow cells. Automated tuning and shimming routines were performed on the NMR flow cell prior to the addition of catalyst and substrate. Acquisition was started and catalyst added. After a 15 min delay to allow the initial speciation of the catalyst to be determined, substrate (**93**) was added to start the reaction.

Three different NMR experiments were performed, with selective and non-selective NMR spectra acquired in an alternating pattern, and ^{13}C spectra interleaved at intervals. Non-selective ^1H NMR experiments with 8 scans were used to measure reaction progress and substrate/product concentrations. However the catalyst signals were of too low intensity to be quantified, and thus selective ^1H experiments with an excitation bandwidth of 3 ppm, centred on a hydride peak at -5 ppm, were performed, with 8 scans and at higher receiver gain, to monitor the ruthenium-hydride intermediate. As the reaction volume was continuously moving



Scheme 19. Proposed catalytic cycle for the asymmetric transfer hydrogenation of acetophenone (**93**) to 1-phenylethanol (**94**) using formic acid/triethylamine as the hydrogen source, catalysed by [(mesitylene) $\text{RuCl}(\text{R,R})$ -(TsDPEN)] (**88**).

through the NMR flow cell, only a very short relaxation delay (1 s) was required, because the sample within the detection volume was continually replaced with freshly magnetised sample. To compensate for the decrease in signal intensity resulting from incomplete magnetisation of the sample flowing into the NMR cell, a correction factor was applied to each peak for both selective and non-selective spectra, using integral values recorded under static conditions (see Case Study 5). For integrals recorded using the selective experiment, an additional correction factor was calculated using the 1,3,5-trimethoxybenzene internal standard to compensate for the increased receiver gain used for these experiments. Offline sampling confirmed the same reaction kinetics, but with much less detailed information than the online flow analysis, highlighting the power of the latter technique.

An induction period of 2 h was observed at the start of the reaction, during which time formic acid was consumed but there was no significant product formation. Hydrogen formation was detected by ^1H NMR during the induction period, accompanied by a shift in the position and linewidth of the formic acid peak. ^{13}C NMR showed the formation of CO_2 during this time, however the signal intensity was too low to quantify. Combining the NMR results with data recorded by headspace MS confirmed that hydrogen and carbon dioxide were formed in a 1:1 ratio during the induction period. Once the ratio of formic acid to triethyl amine dropped from the initial 2.5:1 to 1.5:1, turnover converting **93** to **94** was observed, with a corresponding decrease in the rate of hydrogen formation.

Activation of the chloride pre-catalyst **88** was rapid, reaching completion before the first spectrum was acquired. Although formate complex **91** was observed as the major catalyst species in both ^1H and ^{13}C NMR spectra, overlap with formic acid peaks meant that hydride **92** was the only catalyst species that could be quantified from NMR data. 16-electron species **89** had no distinguishable peaks in the NMR spectrum, however the strong purple colour allowed the concentration of **89** to be tracked by UV–Vis spectroscopy, so that two of the three catalytic intermediates could be monitored during the reaction. The concentration of hydride **92** showed the same time-dependent distribution as product, with concentration increasing after the initial induction period. No change in product enantioselectivity was observed during the reaction, suggesting that the low concentration of **89** prevented product from re-entering the reaction cycle. Based on these observations a parasitic reaction of hydride **92** with formic acid was proposed as being the cause of the initial induction period, with turnover commencing once the concentration of formic acid dropped below a critical level. When the reaction was repeated with an initial ratio 1.5:1 formic acid to triethylamine, no induction period was observed.

This Case Study highlights the substantial benefits of monitoring catalytic intermediates and reaction products simultaneously. Hintermair and collaborators used interleaved data from three different NMR experiments, combined with online UV and inline HPLC and headspace MS, to monitor all reagents, products and by-products of the reaction, along with two out of three on-cycle catalytic intermediates, to deduce the existence of a parasitic side-reaction. This detailed insight allowed mechanism-informed modification of the reaction conditions to both eliminate the induction period and inhibit the unwanted reaction.

6.5. Case study 5: Practical aspects of real-time reaction monitoring using multi-nuclear high-resolution flow NMR spectroscopy [39]

Techniques: Flow NMR; ^1H NMR; Relaxation (T_1 , T_2)

Hintermair and collaborators have pioneered the use of flow NMR techniques to study intermediates in reactions with lifetimes

greater than a few minutes. In a recent publication they reported in detail on the design of apparatus, flow effects (Fig. 41) and data treatment, for their closed-loop continuous-flow system (Fig. 10), which can be coupled to standard high-resolution NMR spectrometers without requiring probe modifications [39]. The stirred reaction vessel ensures efficient mixing of analytes before they are circulated throughout the system by a HPLC pump. Temperature control is achieved by thermally jacketed tubing, which is connected to an NMR flow tube located inside the thermostated probe. A by-pass loop is added for safety reasons. Similar to all flow experiments, the hydrodynamics of the system are of particular importance in the sense of affecting the measurements, therefore the impact from the flow must be analysed for a given experimental set-up. In practice, laminar flow at a relatively low Reynolds number leads to back-mixing in the transfer line. Because the dead time between the reaction being initiated in the reaction vessel and it being measured by NMR in the flow tube is dependent on the flow rate, the latter needs careful optimisation. In addition, the hydrodynamics also determine the intrinsic in-flow and out-flow effects of the system, which must be taken into consideration in order to obtain quantitative results. These in- and out-flow effects remain two universal considerations for on-line flow NMR measurements.

The in-flow effect arises from incomplete pre-magnetisation before the reaction mixture arrives at the NMR flow tube for detection. A period of approximately $5 \times T_1$ is required for spins to reach thermal equilibrium. Thus attenuated signal intensities and distorted quantification will arise in flow NMR experiments if the T_1 values of nuclei are longer than the residence time of the flowing analytes inside the magnet. The study evaluated the impact of the in-flow effect on signal intensities and confirmed its pure dependence on the intrinsic T_1 values of spins at a given flow rate. More rapidly relaxing species are less affected as they build up magnetization more rapidly, so this in-flow effect exerts a more substantial influence on slowly-relaxing spins. Previous approaches included the introduction of pre-magnetization coils [133] and reduced flow rates [338], both at the cost of elongated dead time. In this work Hintermair proposed the use of a correction factor $CF = I_{\text{static}}/I_{\text{flow}}$, derived from recording spectra under flow and stationary conditions. Applying this correction factor to the measured signal integrals during reaction under flow conditions yielded corrected signal integrals, following mathematical relationship $I_{\text{corrected}} = CF \times I_{\text{measured}}$. For reactions involving spins of substantially different T_1 values, the required corrections can be significant. This correction factor method can also be applied to spectra rendered non-quantitative due to an insufficient relaxation delay, where I_{static} is a reference spectrum acquired under fully quantitative conditions and I_{flow} is a spectrum acquired with an insufficient relaxation delay.

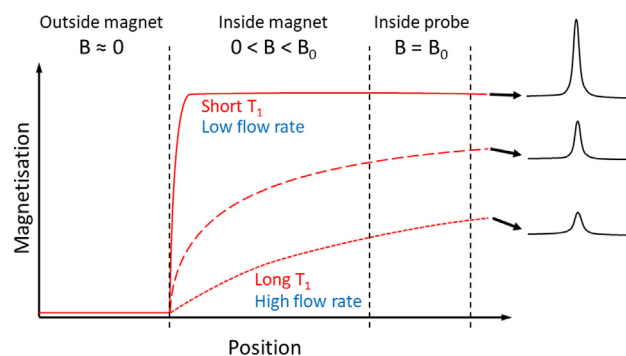


Fig. 41. In-flow effects on signal intensity for flowing samples with different T_1 relaxation times or flow rates [39].

The out-flow effect, on the other hand, is due to the continuous loss of the excited nuclei from the detection volume. This effect leads to flow-dependent enhancements in the rates of both FID decay and z-magnetization restoration. Decreased effective T_1 and T_2 values (T_1^* and T_2^*) under flowing conditions were determined [339], as compared to the intrinsic T_1 and T_2 values under static conditions, using the relationships below, where t_B denotes the residence time of spins within the magnetic field.

$$\frac{1}{T_1^*} = \frac{1}{T_1} + \frac{1}{t_B} \quad (75)$$

$$\frac{1}{T_2^*} = \frac{1}{T_2} + \frac{1}{t_B} \quad (76)$$

The reduced T_1^* from out-flow effects was found to permit shorter repetition times between scans, allowing either a higher temporal resolution, or more signal averaging (and higher S/N) within a given timeframe. It is important to note that at high flow rates, the in-flow effect dominates and constitutes a major consideration for quantitative measurements. The study also elucidated an initial enhancement of signal intensities in the presence of flow when repetition times are set too short. This phenomenon can be sidestepped either by adjusting the experimental parameters or by applying the correction factor stated above. The reduced T_2^* can lead to broadened peaks at higher flow rates, nevertheless, in practice the effect of out-flow on measured linewidths is usually small compared to that of B_0 field inhomogeneity.

After evaluating the significance of flow effects for quantitatively assessing chemical reactions, data treatments in flow NMR experiments were explored. Flow experiments in general require large quantities of materials, therefore expensive deuterated solvents are not recommended. Using protiated solvents poses two challenges: solvent signal suppression, and field locking of the spectrometer. The former is circumvented by a solvent suppression scheme called WET [63] that is particularly useful for flow experiments. The issue of field locking is dealt with through use of modern instruments capable of maintaining field stability in the absence of deuterated internal standards. Advancements in recent software offer solutions for baseline and phase correction, peak deconvolution, signal drift etc., in order to obtain qualitative and quantitative results. Moreover, the exclusion of deuterated solvents obviates any undesired kinetic solvent isotopic effects (Section 5.3) which can interfere with mechanistic studies.

This Case Study shows that on-line NMR analysis equipment provides a very useful approach to monitor chemical reactions in real time, enriching the family of flow NMR experiments. The technique addresses the mixing limitations in conventional static experiments, and can be time- and labour-efficient owing to the automated circulatory feature. The dead time of the system makes it ideal for application to reactions with half-lives of a few minutes or greater. Detailed analysis allowed elucidation of the significant roles of flow effects on achieving quantitative results, and solvent suppression and software solutions can assist with data acquisition and processing. The study highlights the value of a firm knowledge of the relationship between nuclear properties of analytes and the experimental parameters before one sets out to make measurements.

6.6. Case study 6: Still shimming or already measuring? – Quantitative reaction monitoring for small molecules on the sub-minute timescale by NMR [340]

Techniques: *In situ* continuous; Rapid Injection NMR, ^1H NMR; Spatially-Selective NMR

The use of NMR spectroscopy for monitoring fast reactions with sub-minute kinetics is frequently constrained by the need for a relaxation delay between FID measurements. The maximum data density is limited to around 3 to 15 spectra per minute, depending on the pulse flip angle and relaxation time constants of the reaction species. Recently, Kind and Thiele showed that spatially-selective NMR techniques (Section 2.3), combined with a simple rapid injection device, can be used to monitor a reaction at up to 60 spectra per minute (Scheme 20).

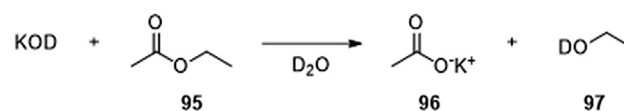
Kind and Thiele chose the base-catalysed hydrolysis of ethyl acetate (95) as the process for study. To allow fast mixing of the two reagents, they constructed a simple rapid injection device consisting of a standard 5 mm NMR tube equipped with two fluorinated co-polymer tubes. The NMR tube was pre-loaded with ethyl acetate in D_2O , and a solution of potassium deuteroxide (KOD) was injected via a syringe through one of the FEP tubes to start the reaction, with the other FEP tube providing a vent for displaced air. Mixing was induced by the impact of the rapidly injected KOD solution, and was complete after approximately 1.5 s. The NMR tube was weighed before and after the reaction to confirm that the correct quantity of base had been added.

Using non-selective *pseudo*-2D pulse-acquire experiments the kinetic time courses for the reaction were measured with 90° and 15° pulse angles and 1 s acquisition time. Relaxation delays of 15 s and 5 s were required for the 90° and 15° pulses respectively to ensure that the magnetisation was fully recovered between scans, giving temporal resolutions of 3 and 12 spectra/minute. In both non-selective experiments significant line broadening was observed, along with significant distortions to the peak shape. These changes were attributed to variations in the local magnetic field homogeneity caused by the increase in volume after the injection of the KOD solution.

To improve temporal resolution, a spatially selective NMR experiment was tested (Fig. 42). A magnetic field gradient of 12.6 G/cm was applied along the axis of the tube, causing the Larmor frequency of the protons to vary as a function of position. Band-selective pulses of 300 Hz bandwidth were used to excite 0.06 mm slices of the NMR tube, with 32 slices acquired from a 0.5 cm region. The small sample region was chosen intentionally, as the magnetic field is more homogenous over small volumes, allowing sharper peaks to be recorded. Small shifts in peak position were observed between slices due to magnetic field inhomogeneity along the z-axis, however these were easily corrected during processing. Using a small sample region also meant that any regions of poor mixing towards the top and bottom of the NMR tube were excluded, however this came at a cost of 95 times lower signal-to-noise than the non-selective experiment.

As each slice could be excited independently from the rest of the sample, no relaxation delay was required, and spectra were recorded for each slice in turn with an acquisition time of 1 s. After a complete cycle through all slices the process was repeated. Since the time between successive measurements on any given slice was $>5 \times T_1$, the magnetisation in each slice had time to recover before the next pulse without the need for a relaxation delay. Using this spatially selective experiment the temporal resolution was increased to a remarkable 60 spectra/min.

The same ester hydrolysis was measured using the spatially-selective pulse sequence, with the increased temporal resolution



Scheme 20. Alkali ester hydrolysis of ethyl acetate with potassium deuteroxide.

allowing additional points to be measured at the start of the reaction. Loss of signal and large distortions in peak shape were observed immediately after addition of the KOD solution, caused by the movement of the sample during mixing producing similar effects to convection. These distortions were short lived, and after 8 s sharp peaks were observed for all resonances. The frequency-shifted pulses used for the spatially-selective NMR experiments imparted a phase shift between different slices, requiring each spectrum to be individually phased before integration. Whilst the largest source of error in the non-selective experiments was that due to the wide integration regions needed to encompass the broad peaks, integration errors in the spatially-selective experiments primarily resulted from the low signal-to-noise ratio.

As all product and reagent peaks were well resolved in the selective experiments, rate constants were calculated for each peak and then averaged to give a single value. Measured rate constants for both selective and non-selective reactions were comparable with reported literature values measured using conductivity or titration. The uncertainty in the rate constant was higher for the 90° non-selective experiment than for the 15° or selective experiments due to the smaller number of points available for fitting.

This Case Study reports an impressive application of spatially-selective NMR techniques in the monitoring of reactions with rate constants that are of a similar order of magnitude to relaxation processes. The selective experiment allows a valuable increase in temporal resolution, crucial for fast reactions, as well as mitigating the effects of magnetic inhomogeneity due to the addition of reagents, albeit at the cost of reduced signal-to-noise ratio compared to non-selective experiments.

6.7. Case study 7: Mono-oxidation of bidentate bis-phosphines in catalyst activation: Kinetic and mechanistic studies of a Pd/Xantphos-catalyzed C–H functionalization [341]

Techniques: *In situ* continuous and interrupted; Rapid quenched flow; ^1H NMR; ^{31}P NMR; ^{13}C NMR; Kinetics RPKA; and Catalyst Speciation

Blackmond and collaborators recently reported a detailed mechanistic investigation of a palladium-catalysed direct C–H functionalisation of imidazole **99**, Scheme 21. These types of transformations were previously proposed to involve a concerted metalation-deprotonation mechanism, wherein the base acts as a ligand coordinated to the metal centre and mediates the deproto-

nation. The finding that the chelating ligand xantphos proved superior to monodentate ligands in the reaction was contradictory to the proposed mechanism, as it would require a penta-coordinate palladium transition state or de-chelation of the xantphos from the palladium centre (as compared to dissociation of a monodentate phosphine, with significantly lower activation energy), thus prompting an *in situ* NMR study.

The reaction was followed by ^1H NMR spectroscopy and Reaction Progress Kinetic Analysis (RPKA, Section 4.3.7.1) performed to obtain information about the mechanism. ‘Different excess’ experiments revealed no dependence of reaction rate on the concentration of **98**, and a positive order with respect to **99**. At high concentrations of **99**, the plots of concentration of **100** against time started to coincide, indicating saturation kinetics. Performing the experiments at different pre-catalyst loadings revealed first-order kinetics with respect to the Pd. Moreover, the reaction is zeroth-order with respect to both bases (KOPiv and DIPEA), but the rate depends on the identity of the carboxylate, and to a lesser extent on the counterion. However, ‘same excess’ experiments showed a lack of agreement between time-adjusted plots. Product inhibition was disproved by further experiments, indicating that the lack of agreement is due to processes involving degradation of the catalyst.

$^{31}\text{P}\{^1\text{H}\}$ NMR spectroscopy (in DMAC- d_9) was then used to probe the palladium speciation. The PdCl_2 -Xantphos pre-catalyst was mixed with various combinations of reaction components and changes in the ^{31}P NMR signals analysed. It was found that the pre-catalyst interacts with pyrrole **98** in the presence of KOPiv to form a new species, **101**, which was isolated, characterised via X-ray diffraction (Fig. 43), and determined to be the oxidative addition complex of pyrrole **98** to the corresponding catalyst (with mono-oxide of Xantphos as a ligand). Moreover, upon cooling the catalytic system to ambient temperature, intermediate **101** was detected in solution (the corresponding bis-phosphine and bis-oxide complexes were also detected). Intermediate **101** was shown to be competent in coupling of **98** with **99** under catalytic conditions, and to stoichiometrically react with KOPiv + **99** to give **100**. Under catalytic conditions, no induction period was observed. Moreover, Xantphos bis-phosphine inhibits the reaction with **101** as catalyst, suggesting stronger binding of the latter to Pd(II). The non-coinciding time-normalised plots in the RPKA experiments were attributed to catalyst decomposition, as an increase of the bis-oxide concentration, with simultaneous decrease of those of the mono-oxide and bis-phosphine, was observed as the reaction progressed.

The role of the bases in the reaction was also studied via $^{31}\text{P}\{^1\text{H}\}$ and $^{13}\text{C}\{^1\text{H}\}$ experiments and found to be two-fold, promoting both formation of the catalyst via reduction of Pd(II), and direct C–H functionalisation via anion metathesis of Br. The Pd(II)-pivalate species is the resting state under the reaction conditions, hence explaining the saturation kinetics in **99** and the zeroth order with respect to base. These results, along with KIE analysis and computational modelling, led to elucidation of the full mechanism of the reaction.

This Case Study demonstrates the power of a multinuclear NMR analysis for *in situ* interrogation of the structure of intermediates in

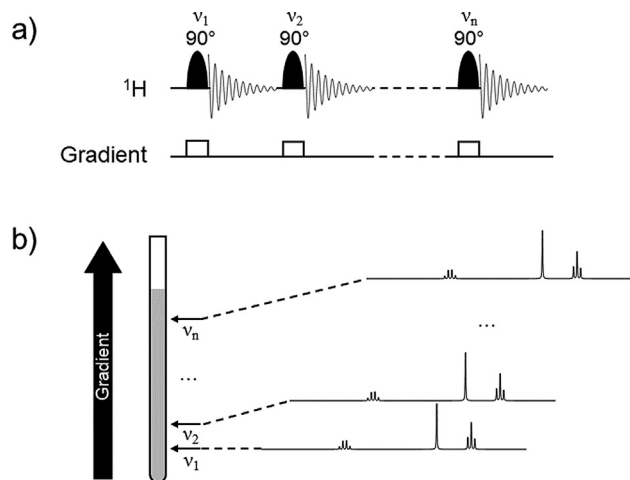
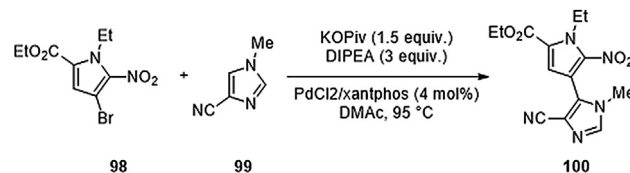


Fig. 42. (a) Pseudo-2D spatially-selective pulse sequence. The frequency of the 90° pulses is shifted between each increment. (b) Schematic of spatially-selective experiment used to extract spectra from different regions of the NMR sample.



Scheme 21. Palladium-catalysed C–H functionalisation of imidazole **99**.

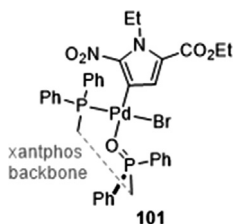


Fig. 43. The structure of intermediate **101**, characterised via X-ray diffraction.

catalytic reactions. When this is conducted in combination with visual kinetic analysis (Section 4.3.7), very detailed information can be revealed regarding the roles of the species at the various stages of the overall full catalytic cycle.

6.8. Case study 8: SHARPER reaction monitoring: Generation of a narrow linewidth NMR singlet, without X pulses, in an inhomogeneous magnetic field [190]

Techniques: *In situ* continuous; Stopped-Flow NMR; ^{19}F NMR; ^1H NMR; $^{10,11}\text{B}$ NMR; ^{31}P NMR; Relaxation (T_1 , T_2); Pure shift and SHARPER; Equilibrium Kinetics; Line shape analysis; Isotopes and Scalar Couplings

Pure shift NMR is a technique that is of growing interest due to its ability to remove the effects of coupling, resulting in singlet peaks and thus spectral simplification. The Uhrin group recently developed SHARPER (Sensitive, Homogeneous And Resolved Peaks in Real time) and selective SHARPER (*sel*-SHARPER) pure shift pulse sequences, which are of particular relevance for reaction monitoring. An introduction to SHARPER and other pure shift techniques was provided in Section 3.5. The SHARPER technique removes heteronuclear coupling using a chunked acquisition with gradients and 180° pulses used to refocus an on-resonance peak whilst removing all heteronuclear coupling in the manner of a CPMG pulse sequence. A key feature of the SHARPER sequence is that all pulses are applied to the observe nucleus channel, meaning that it can be used to decouple nuclei that share the same channel, as is often the case for ^1H and ^{19}F .

To demonstrate the utility of the SHARPER technique, spectra of fluorobenzene were recorded using a standard ^{19}F pulse-acquire sequence and the SHARPER sequence with 256 acquisition chunks, each lasting 34 ms, giving a total acquisition time of 17.9 s. The SHARPER sequence successfully removed all heteronuclear coupling, producing a single peak with half-height linewidth of 0.14 Hz and eight times increase in signal-to-noise ratio compared to a pulse-acquire spectrum with the same acquisition time. Small sidebands were observed as a side-effect of the chunked acquisition, however reducing the chunk duration to 5 ms effectively eliminated these artefacts. Whilst reducing the chunk duration improved the quality of the spectrum, a small decrease in signal-to-noise ratio and increase in linewidth were observed due to relaxation during the spin-echo pulses.

Modifying the SHARPER experiment to include selective 180° pulses, with an additional spin-echo element prior to the first chunk, produced a selective version of the experiment (*sel*-SHARPER) which additionally removed homonuclear couplings. This was demonstrated on a sample containing 2- ^{2}H -1,3,4-trifluorobenzene, with a *sel*-SHARPER experiment using 128 acquisition chunks of 13.6 ms duration successfully removing ^{19}F - ^{19}F , ^1H - ^{19}F and ^2H - ^{19}F couplings to produce a single, sharp peak.

The refocusing effects of the SHARPER sequence are also capable of removing line broadening resulting from poor magnetic homogeneity. To demonstrate this, an inhomogeneous field was generated by deliberately offsetting the x , y , z , z^2 , z^3 , xy , xz , and

yz shims by 500 units, resulting in broad peaks with linewidths of around 40 Hz. Using a *sel*-SHARPER experiment with 128 chunks and 13.6 ms chunk time, the linewidth was reduced to 0.34 Hz with the integrated signal intensity 60% of the well-shimmed sample. As with the non-selective SHARPER experiment, small sidebands were observed which decreased in intensity with decreasing chunk duration. Similar results were observed for dynamic inhomogeneities caused by sparging small bubbles of nitrogen gas through the solution in the NMR tube, using a SHARPER experiment with 64, 128, 256 or 512 chunks of durations 8.5, 4.25, 2.13 or 1.06 ms respectively. Again, using a smaller chunk duration improved the quality of the spectrum, with line width roughly halving when moving from 64 to 256 chunks. Whilst better homogeneity and correspondingly narrower linewidths were measured when the rate of bubbling was slow, increasing the rate of bubbling resulted in greater stability between measurements due to the more constant number of bubbles in each spectrum.

The application of SHARPER for reaction monitoring was demonstrated using two reactions. The protodeboronation of 2,3,6-trifluorophenyl boronic acid (**58**; see Case Study 1) was monitored using a stopped flow NMR system (Section 2.4.4.2) to rapidly mix water/dioxane solutions of the boronic acid and potassium hydroxide. ^{19}F *sel*-SHARPER measurements (128 acquisition chunks) were made at reaction times between 13 and 208 s. Sharp peaks (0.5 Hz) were observed for the product, however the reagent peaks were broadened due to reversible chemical exchange between the boronic acid and the corresponding boronate (**102**), Fig. 44. A linewidth correlation factor, Eq. (77), was determined for the SHARPER experiment. In Eq. (77), the $\delta_{(\text{PFG+pulses})}$ term accounts for the additional relaxation that occurs during the pulsed field gradients and 180° pulses that are applied between the acquisition chunks. After correction for this effect, the natural linewidth was then used to calculate the rate constant for chemical exchange in 2,4-difluorophenyl boronic acid (**46**) based on the decrease in linewidth observed when the concentration of hydroxide was increased.

$$\Delta_{1/2} \approx \text{natural linewidth} \times \frac{t_{\text{chunk}} + \delta_{(\text{PFG+pulses})}}{t_{\text{chunk}}} \quad (77)$$

The oxidation of diphenylphosphine was monitored under aerobic conditions using ^{31}P *sel*-SHARPER. Air was bubbled at a rate of 180 mL/h through a sample of diphenylphosphine in toluene- d_8 , with the reaction monitored by standard ^{31}P NMR and *sel*-SHARPER for a total of 228 spectra (2400 s). To minimise the effect of bubbling gas, and the large ^{31}P - ^1H coupling, the chunk size was reduced to 0.8 ms, with a total of 400 chunks acquired for each SHARPER spectrum. Whilst signal intensity was lower for the SHARPER experiments than for the standard pulse-acquire sequence, signal-to-noise ratio was improved by eight times and line widths reduced from 30 Hz to 2.8 Hz, resulting in less scatter between reaction time points.

This Case Study shows how the SHARPER and *sel*-SHARPER experiments are powerful additions to the reaction monitoring toolkit, removing hetero- and homonuclear coupling along with the effects of poor magnetic homogeneity, producing sharp singlet peaks with increased signal-to-noise. Using these pulse sequences, kinetic information can be obtained for challenging reactions where signal intensity is reduced by coupling or due to highly inhomogeneous biphasic conditions.

6.9. Case study 9: Base-free enantioselective C(1)-ammonium enolate catalysis exploiting aryloxides: A synthetic and mechanistic study [342]

Techniques: *In situ* continuous; *In situ*; ^{19}F NMR; Kinetics by VTNA; Isotopes/KIEs and EIEs

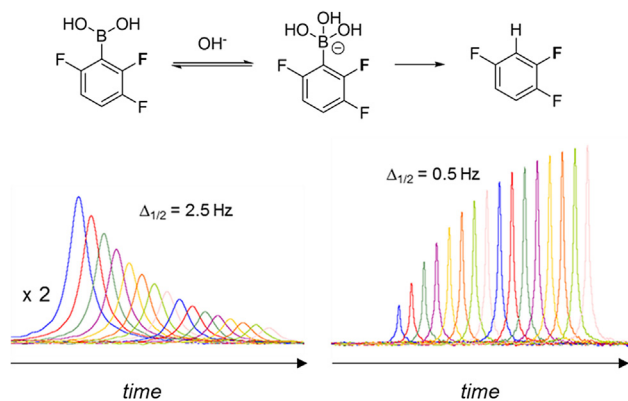
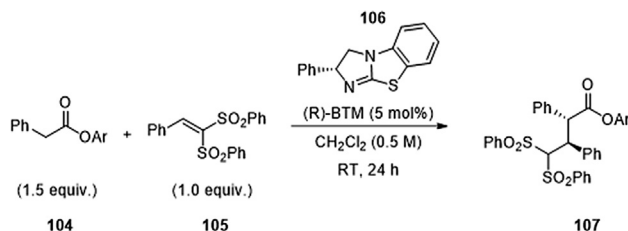


Fig. 44. sel-SHARPER spectra (2 scans per spectrum, 128 acquisition chunks, 8.5 ms chunk time) for the fluorine atom highlighted in bold for 1,3,4-trifluorophenyl boronic acid (**58**; left), the corresponding boronate anion (**102**; middle), and 1,3,4-trifluorobenzene (**103**; right) during the course of the protodeboronation reaction with KOH.

In a recent study, Smith and collaborators employed variable time normalised analysis (VTNA, Section 4.3.6.2), developed by Burés, to elucidate mechanistic information regarding the base-free enantioselective Michael addition of an ester (**104**) to vinyl bis-sulfones (**105**) via a C(1)-ammonium enolate (Scheme 22).

The VTNA analysis involved seven experiments, in which there was an increase or decrease in one reagent or product concentration, which allowed them to probe their mechanistic hypothesis, including product inhibition, without requiring any further experiments. The method of analysis was *in situ* $^{19}\text{F}\{^1\text{H}\}$ NMR, employing 1,3-difluorobenzene as an internal standard. Their original system (Scheme 22) was hard to analyse by ^1H NMR due to overlapping signals. Thus, the ^{19}F -labelled ester, vinyl bis-sulfone and organocatalyst were synthesised, Scheme 23, allowing easy quantification of all species via their distinct $^{19}\text{F}\{^1\text{H}\}$ signals. The catalyst loading was increased from 5 mol% to 20 mol% to reduce reaction time from 24 h to 3 h, reducing the time period required on the spectrometer.

Individual stock solutions of vinyl bis-sulfone (**108**), the fluorine tagged ester (**109**), organocatalyst (**110**) and 1,3-difluorobenzene, were prepared, allowing accurate assembly of the reaction *in situ* at the required concentrations without the need to measure small quantities of reagents. Next, they charged the required volumes of solution of **108**, **109**, 1,3-difluorobenzene and CD_2Cl_2 into an NMR tube, submitted it to the NMR spectrometer, locked the sample to CD_2Cl_2 , shimmed, and acquired their initial $^{19}\text{F}\{^1\text{H}\}$ spectrum. The sample was then ejected, and the reaction initiated by charging organocatalyst **110** to the tube, followed by vigorous shaking to dissolve the solid and mix the resulting solution thoroughly. After resubmitting, locking, and shimming, spectra were recorded, taking note of the dead time between initiation and recording of the first spectrum, which was then taken into account in the VTNA



Scheme 22. Conditions for the base-free enantioselective Michael addition of an ester to vinyl bis-sulfone.

for which time, t , is included in the x-axis formula. Then by plotting a normalised time axis plot of $[\mathbf{111}]$ vs $\Sigma[\mathbf{109}]^a[\mathbf{108}]^b[\mathbf{110}]^c\Delta t$ and taking the first ten values they were able to obtain the order with respect to each species ($a, b, c = 1$) and k_{obs} from a linearized plot.

To conclude the study an inverse secondary isotope effect was determined, using two techniques, namely competition and parallel reactions, to analyse $[\text{}^2\text{H}_1]$ -**108**. For both techniques the same general procedure was followed as described for the *in situ* analysis. For the competition experiment a 50:50 mixture of $[\text{}^2\text{H}_1]$ -**108** and **108** was co-reacted. As these two species have clearly defined isotopically shifted signals in the $^{19}\text{F}\{^1\text{H}\}$ spectrum, this allowed for the relative consumption of each starting material to be followed during the reaction. This data could then be used to determine $k_{\text{H}}/k_{\text{D}} = 0.88$, an inverse SKIE, supporting a mechanism in which the Michael addition (and resulting change in hybridisation at the labelled carbon) is the turnover-limiting step. The parallel reaction technique required two separate reactions to be carried out in two NMR tubes, one with the deuterated vinyl bis-sulfone and one with the non-deuterated. The same *in situ* VTNA analysis was performed and the resulting $k_{\text{H}}/k_{\text{D}}$ value of 0.89 agreed well with the previous result.

This study highlights how much information can be obtained through VTNA. Smith and collaborators were able to obtain the reaction order and information about catalyst inhibition, and elucidate information regarding the turnover-limiting step, all from a few well-considered *in situ* ^{19}F NMR experiments. By utilising ^{19}F NMR they could study a system which had a complex ^1H spectrum, but a simpler and readily integrated ^{19}F spectrum, thus highlighting one of the main reasons researchers turn to ^{19}F NMR. Whilst VTNA cannot be used alone to determine the full kinetics, it does powerfully complement other tools for investigating mechanism.

6.10. Case study 10: Aryl trifluoroborates in Suzuki–Miyaura coupling: The roles of endogenous aryl boronic acid and fluoride [25]

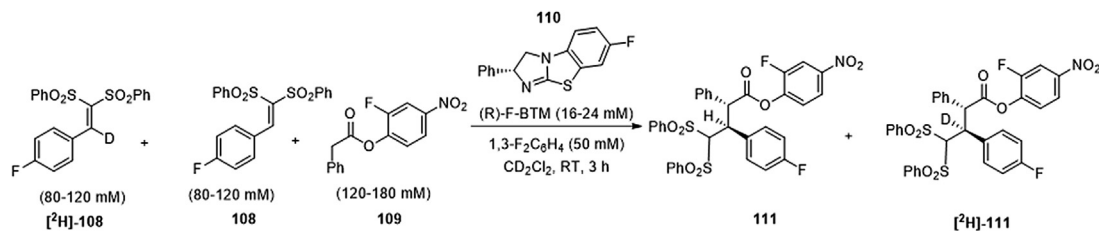
Techniques: *Ex situ* sampling; *In situ* continuous; ^{19}F NMR; $^{10,11}\text{B}$ NMR; Equilibrium kinetics; Kinetic Simulation; EXSY; Titration; Isotope tracking, Shifts, Entrainment.

Some while ago, the Lloyd-Jones group set out to elucidate why aryl trifluoroborates can be more efficient than aryl boronic acids when employed in the Suzuki–Miyaura cross-coupling reaction. To study the system they chose the reaction between 4-fluorophenyltrifluoroborate (**112**) and 1,3-bis(trifluoromethyl)-5-bromobenzene (**113**; Scheme 24).

Following optimisation of the solvent, base, and reaction conditions, the mechanistic investigation began with a series of ^{19}F and ^{11}B NMR base titrations. Thus trifluoroborate **112**, or the corresponding boronic acid **35**, was dissolved in THF/ D_2O , and then base added as a solid, in increments of 0.5 equivalents up to a total of 4. Approximately 5 min after each addition of base, an aliquot of the solution was taken and analysed by ^{19}F and ^{11}B NMR. The resulting spectra showed that the trifluoroborate **112** was hydrolysed to the boronic acid **35** as more base was added, and that **35** was in equilibrium with aryl boronate **115** which then underwent protodeboronation (see Case Study 1) to give fluorobenzene (**1**) (Scheme 25).

The rapid equilibrium between the boronic acid and the boronate (**35** and **115**) resulted in a time-averaged ^{19}F NMR chemical shift and by plotting the change in chemical shift ($\Delta\delta_{\text{F}}$) relative to pure **35** versus the concentration of base added, it was possible to determine the speciation (**35** versus **115**).

An interesting result from this study was the observation that when the solvent was 10/1 (v/v) THF/ D_2O the protodeboronation to generate **1** was suppressed. This was further studied by analysing the change in chemical shift of the boronic acid **35** relative to the fluorobenzene (**1**) by ^{19}F NMR. Aliquots of a stock solution of



Scheme 23. Fluorine tagged system developed by Smith and co-workers to allow for the study of the reaction in Scheme 22 by ¹⁹F NMR.

the aryl boronate **115**, generated *in situ* from trifluoroborate **112** and potassium carbonate in D₂O were diluted with THF:D₂O in various ratios, then analysed by ¹⁹F NMR after 15 min. In solutions in 10/1 (v/v) THF/D₂O no protodeboronation product was detected, even after 12 days, but for 5/1 (v/v) THF/D₂O protodeboronation was detected. The results indicated that the trifluoroborate **112** participates in a hydrolytic equilibrium with the boronic acid **35**, and that the extent of equilibration can be reduced by lowering the concentration of the water, ultimately resulting in suppression of the protodeboronation.

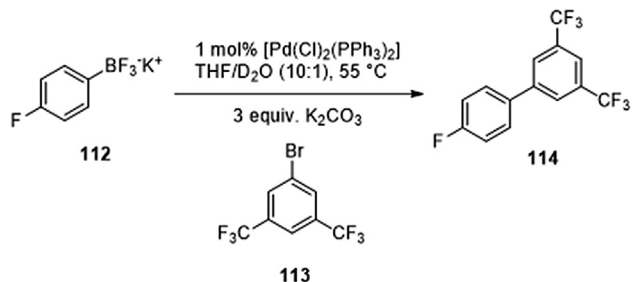
At higher water concentrations, an intermediate, tentatively assigned as the mixed species [ArBF₂(OD)]⁻K⁺ (**117**), was detected by ¹⁹F NMR. To understand the processes generating and consuming this species, trifluoroborate **112** and potassium carbonate were dissolved in 1/10 (v/v) THF/water and transferred to an NMR tube, and 2D ¹⁹F EXSY experiments (Section 4.4.1.2) were performed. The resulting 2D spectrum showed exchange between the [ArBF₂(-OD)]⁻K⁺ (**117**), the aryl boronate **116**, and KF (Fig. 45), i.e. in rapid equilibrium.

Further experimental and computational work indicated that the more fluorine atoms coordinated to the boron in the [ArBF_{3-n}(OH)_n]⁻ species, the higher the barrier to transmetalation of the Ar group to Pd in the Suzuki-Miyaura coupling. It was therefore concluded that ArB(OH)₂ (**35**) or [ArB(OH)₃]⁻ (**115**) are the most active species for the transmetalation, even though present in very low concentrations. To test this experimentally an isotope entrainment study (section 5.4) was conducted, using an *in situ* ¹⁹F NMR protocol. Thus, samples of d₀-**112** and d₄-**35** were dissolved in 10/1 (v/v) THF/D₂O in varying ratios, followed by Cs₂CO₃, bromoarene (**113**) and benzotrifluoride (internal standard). After addition of the palladium catalyst, at 0 °C, an aliquot was taken and delivered to a 5 mm O.D. J Young valve NMR tube. To initiate the reaction the

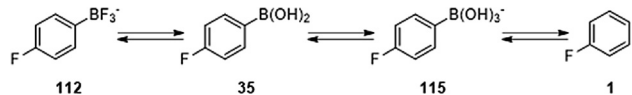
NMR tube was agitated in a water bath at 55 °C, after which it was loaded into the preheated (at 55 °C) probe in the NMR spectrometer and spectra recorded every 100 s for the first 1000 s, every 200 s for the next 1000 s, and every 600 s for the remainder of the reaction. The spectra were analysed, and each peak integrated to generate temporal concentration data, as well as isotope distributions. Plots of isotope distribution in the biaryl product (d₄/d₀-**114**) as a function of conversion of aryl showed that the Suzuki-Miyaura cross-coupling proceeded in parallel with the establishment of the equilibrium between aryltrifluoroborate **112** and aryl boronic acid **35**, with the cross-coupling product being predominantly d₄-**114**. The data conclusively showed that the most reactive transmetalating species was derived from the aryl boronic acid d₄-**35**, not the aryltrifluoroborate d₀-**112**.

The same *in situ* ¹⁹F NMR protocol was used to compare reactions using solely the aryltrifluoroborate **112** versus the aryl boronic acid **35**, and confirmed that the latter results in faster Suzuki-Miyaura coupling than the trifluoroborate, but generates more unwanted side reactions. Maintaining a low concentration of the aryl boronic acid/boronate (**35/115**) via slow hydrolytic release from the aryltrifluoroborate **112** is one of the major reasons why the overall Suzuki-Miyaura coupling is more efficient using **112**.

This Case Study shows how use of a variety of NMR techniques including ¹⁹F EXSY, *in situ* ¹⁹F monitoring and titration experiments, allowed key mechanistic information regarding the reactions of aryl trifluoroborates to be elicited. The study highlights



Scheme 24. Suzuki-Miyaura cross-coupling reaction between aryl potassium trifluoroborate (**112**) and an aryl bromide (**113**).



Scheme 25. Aryltrifluoroborate hydrolysis to aryl boronic acid, aryl boronate, and finally fluorobenzene via protodeboronation.

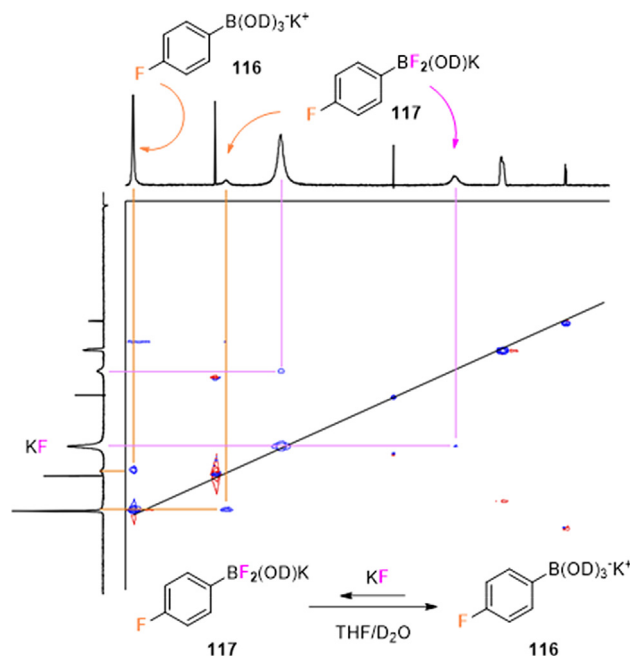


Fig. 45. Exchange between aryl difluoroborate, **117** and aryl boronate **116** + KF, detected by ¹⁹F EXSY (τ = 40 ms).

once again the advantages of ^{19}F NMR, bringing both high sensitivity and wide chemical shift dispersion, and allowing ready analysis and quantification of *in situ* NMR spectra.

6.11. Case study 11: Sub-minute kinetics of human red cell fumarate: ^1H spin-echo NMR spectroscopy and ^{13}C rapid-dissolution dynamic nuclear polarization [343]

Techniques: *In situ* continuous; Hyperpolarisation; ^1H NMR; ^{13}C NMR; Relaxation (T_1 , T_2); Equilibrium Kinetics; Steady state Kinetics; Isotope S/N enhancement.

Enzymatic reactions are ubiquitous in nature, yet they are very challenging to study by NMR spectroscopy due to the micromolar concentrations of reaction species in *in vivo* samples, combined with the high reaction rate of many enzymatic reactions. ^1H NMR spectroscopy would require an unreasonably large number of scans to acquire sufficient signal-to-noise ratio, which is not practical for reactions that are completed in under a minute. For reactions performed *in vitro* with whole cells or cell extracts, other species in the sample result in complex spectra, often with very broad lines due to the presence of paramagnetic species. As a result, many enzymatic reactions are studied in isolation or under pseudo-equilibrium conditions with high concentrations of substrate.

A recent study by Shishmarev and collaborators aimed to study the reversible hydration of fumarate to *L*-malate, catalysed by the fumarase (fumarate hydratase) enzyme in red blood cell hemolysate, prior to the establishment of equilibrium kinetics (Scheme 26). In addition to monitoring the reaction with ^1H spin-echo experiments, the use of rapid dissolution Dynamic Nuclear Polarisation (DNP) to increase the signal-to-noise ratio was investigated.

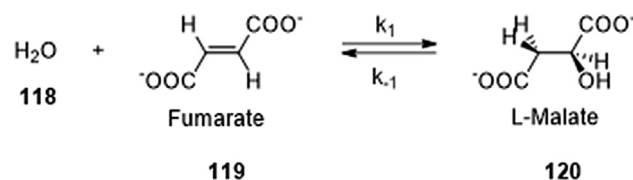
Initial studies were carried out using hemolysate extracted from human red blood cells, which was bubbled with carbon monoxide prior to measurement to ensure that all haemoglobin was stabilised in the diamagnetic Fe(II) form. Following thermal pre-equilibration of the hemolysate at 37 °C in the NMR spectrometer, a solution of sodium fumarate in phosphate-buffered saline (PBS) was injected through a thermostatically controlled mixer. The reaction was monitored by single scan ^1H spin-echo spectra for two different concentrations of fumarate, with spectra acquired every 5 s for 20 min. The spin-echo pulse sequence was chosen to minimise line broadening caused by inhomogeneous magnetic fields in the hemolysate.

Due to the value chosen for the spin-echo delay, modulations caused by spin-spin coupling meant that both malate CH_2 peaks had negative intensities and required inversion before kinetic analysis. The concentrations of fumarate and malate were calculated from the two equivalent CHs in fumarate and the two CH_2 protons in malate. As no internal standard was employed, the concentrations at each time point were calculated with reference to the initial concentration of fumarate so that total mass balance was maintained over the course of the reaction, and in this way, was not impacted by the signal loss from decaying net DNP in enhanced experiments.

The resulting time-course data was fitted using the Michaelis-Menten model for enzyme kinetics with product inhibition, where $V_{\text{max}}^{\text{Fum}}$ and $V_{\text{max}}^{\text{Mal}}$ are the forward and reverse velocities and K_m^{Fum} and K_m^{Mal} are the Michaelis constants for fumarate and malate respectively:

$$\frac{d[\text{Fum}]}{dt} = -k_1[\text{Fum}] + k_{-1}[\text{Mal}]$$

$$\frac{d[\text{Mal}]}{dt} = k_1[\text{Fum}] - k_{-1}[\text{Mal}]$$



Scheme 26. Reversible hydration of fumarate to *L*-malate, catalysed by the fumarase (fumarate hydratase) enzyme.

$$k_1 = \frac{V_{\text{max}}^{\text{Fum}}}{K_m^{\text{Fum}} \left(1 + \frac{[\text{Mal}]}{K_m^{\text{Mal}}} \right) + [\text{Fum}]}$$

$$k_{-1} = \frac{V_{\text{max}}^{\text{Mal}}}{K_m^{\text{Mal}} \left(1 + \frac{[\text{Fum}]}{K_m^{\text{Fum}}} \right) + [\text{Mal}]}$$

Both Michaelis constants, K_m^{Fum} and K_m^{Mal} , were found to have values in the micromolar range, below the sensitivity level of the NMR experiment, preventing the values from being accurately determined. Values for both forward and reverse reactions were calculated using literature values for K_m . Repeating the experiment with whole red blood cells showed no reaction until a surfactant was added to break down the cell wall, after which the reaction proceeded as before.

Having established that the time scale of the reaction was suitable for study by DNP, the same experiment was repeated using hyperpolarised $[1,4-^{13}\text{C}]$ -fumarate. Hyperpolarised fumarate was generated by dissolving $[1,4-^{13}\text{C}]$ -fumaric acid in $\text{DMSO}-d_6$ along with a trityl radical and a gadolinium chelate. Irradiating this sample with microwaves at 1.2 K for 1.5 h produced a sample of hyperpolarised fumarate which was rapidly dissolved in PBS buffer and immediately used in the experiment. Kinetic time-courses were recorded using single scan ^{13}C pulse-acquire spectra with a pulse flip angle of 4°. Using a very low pulse flip angle allowed small amounts of the hyperpolarised signal to be sampled every 1 s for a total of 256 spectra, with no need for a relaxation delay between spectra. The signal-to-noise ratio was significantly improved, with much less scatter in the data than for the thermally polarised ^1H spin-echo experiments.

As the hyperpolarised signal is non-renewable, the total signal decayed over the course of the reaction due to sampling and relaxation processes, becoming indistinguishable from noise after 120 s, Fig. 46. The maximum signal for malate was observed at $t_{\text{max}} = 20$ s. The kinetic equations were therefore more complicated than for the ^1H spectra, since in addition to the reversible chemical kinetics an irreversible T_1 relaxation term was required. It is important to note that whilst signal was only observed from the hyperpolarised species (indicated with an asterisk), non-hyperpolarised species were also present in the reaction and contributed to the kinetic equilibrium. The data was fitted using these equations with a partially constrained Markov chain Monte Carlo method, combined with parameter sensitivity analysis to estimate errors. Each measurement of the spectrum reduces the available polarization by a factor equal to the cosine of the pulse flip angle, therefore an additional term for the pulse angle was included when fitting the model. Because the reaction was carried out with a large excess of substrate, the enzyme was assumed to be fully saturated for the duration of the reaction so the estimated Michaelis constants from the ^1H experiments were used. This yielded Michaelis-Menten parameters that were similar to those found using the ^1H spin-echo method, along with T_1 relaxation time constants for both species

$$\frac{d[\text{Fum}^*]}{dt} = -\frac{1}{T_1^{\text{Fum}}}[\text{Fum}^*] - k_1[\text{Fum}^*] + k_{-1}[\text{Mal}^*]$$

$$\frac{d[\text{Fum}]}{dt} = \frac{1}{T_1^{\text{Fum}}} [\text{Fum}^*] - k_1 [\text{Fum}] + k_{-1} [\text{Mal}]$$

$$\frac{d[\text{Mal}^*]}{dt} = -\frac{1}{T_1^{\text{Mal}}} [\text{Mal}^*] + k_1 [\text{Fum}^*] - k_{-1} [\text{Mal}^*]$$

$$\frac{d[\text{Mal}]}{dt} = \frac{1}{T_1^{\text{Mal}}} [\text{Mal}^*] + k_1 [\text{Fum}] - k_{-1} [\text{Mal}]$$

$$k_1 = \frac{V_{\text{max}}^{\text{Fum}}}{K_m^{\text{Fum}} \left(1 + \frac{[\text{Mal}] + [\text{Mal}^*]}{K_m^{\text{Mal}}} \right) + [\text{Fum}] + [\text{Fum}^*]}$$

$$k_{-1} = \frac{V_{\text{max}}^{\text{Mal}}}{K_m^{\text{Mal}} \left(1 + \frac{[\text{Fum}] + [\text{Fum}^*]}{K_m^{\text{Fum}}} \right) + [\text{Mal}] + [\text{Mal}^*]}$$

This Case Study demonstrates how hyperpolarisation techniques such as rapid dissolution DNP can be used to provide kinetic information for fast reactions, with improved signal-to-noise compared to ^1H spectra acquired with a similar data density. The data can be readily processed using Michaelis-Menten kinetics, modified to account for relaxation, however preparation of hyperpolarised samples requires specialist knowledge and equipment.

6.12. Case study 12: Glycosylation intermediates studied using low temperature ^1H - and ^{19}F -DOSY NMR: New insight into the activation of trichloroacetimidates [344]

Techniques: ^{19}F NMR; ^1H NMR; DOSY

A recent study by Pedersen and collaborators elucidated the intermediates in glycosylation, a key reaction in carbohydrate chemistry, using low temperature ^1H - and ^{19}F -DOSY NMR experiments. The system studied was the activation of trichloroacetimi-

date (TCA) donors by three different catalysts: BF_3OEt_2 , TMSOTf and TMSNTf₂ (Scheme 27). Despite recent advances in the use of NMR to probe the mechanism of glycosylation, deconvolution of the complex spectra obtained to identify intermediates remained a challenge. DOSY-NMR measurement (Section 4.6) of molecular diffusion, which is dependent on the shape, size and interaction with other species, was used to resolve the various species in the reaction mixture. Furthermore, as most catalysts used in the glycosylation are fluorinated, both ^{19}F - and ^1H -DOSY were used to determine which structures were catalyst bound (^{19}F -active) or unbound (^{19}F -silent).

TCA donor **121** was dissolved in CD_2Cl_2 (0.4 M), along with an internal reference compound 1,3,5-tris-(trifluoromethyl)-benzene, which was utilised for both the ^1H - and ^{19}F -DOSY experiments. To this was added the catalyst to be studied. DOSY analysis of the catalyst in the absence of **121** was also conducted, to ensure that no aggregation occurred at low temperatures which would affect the measurements.

From initial observations with BF_3OEt_2 and TMSOTf, it was identified that the mechanism of activation was dependent on the catalyst and the counter-ion. Despite the near-equal sizes of the donor and the product, and thus poorly-resolved DOSY signals, comparison of the ^1H - and ^{19}F -DOSY spectra allowed for identification of the intermediates with fluorine-containing catalyst attached. These were identified as glucosyl fluorides and triflates for the BF_3OEt_2 and TMSOTf catalysts respectively. In contrast, the third catalyst, TMSNTf₂, was found by ^{19}F -DOSY to transfer the TMS group to **121**. Whilst DOSY does not provide structural detail, once the activated complex had been identified, detailed analysis, by ^1H NMR, ^{19}F NMR, COSY, edHSQC, ^1H -DOSY, ^{19}F -DOSY, NOESY and N-H-HSQC, confirmed the structure of the activated complex as **128**, Scheme 28.

In the final part of the study the M_w s of the intermediates were explored, utilising the external calibration curve protocol [298], in which only one internal standard is required. For the ^1H -DOSY analysis, six compounds ranging in M_w from 74 to 1226 (Fig. 47) were selected, all of which were carbohydrate-based structures, ensuring that the influence of shape and size on the diffusion was relevant to the system under study. The diffusion for each compound was measured individually against the 1,3,5-tris(trifluoromethyl)benzene internal standard. Once each data point had been obtained, a calibration curve of $\log D$ vs $\log M_w$ was generated, with all compounds normalised to $\log D_{\text{ref}} = -9.137$, where D_{ref} is the diffusion coefficient for the internal standard. This procedure was repeated for ^{19}F -DOSY, albeit with only one fluorinated

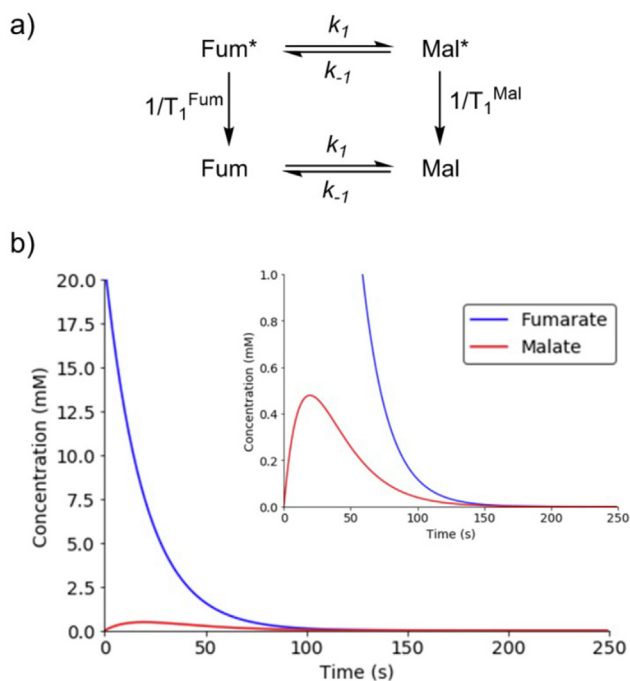
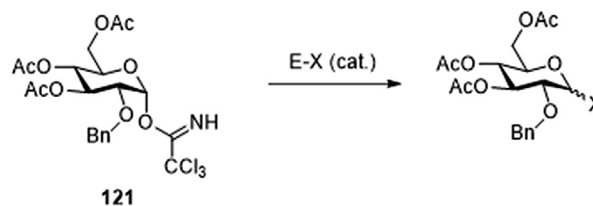
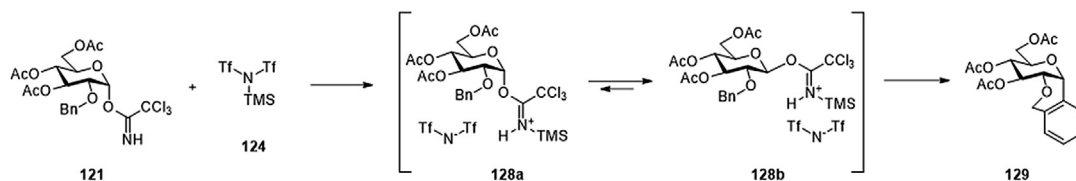
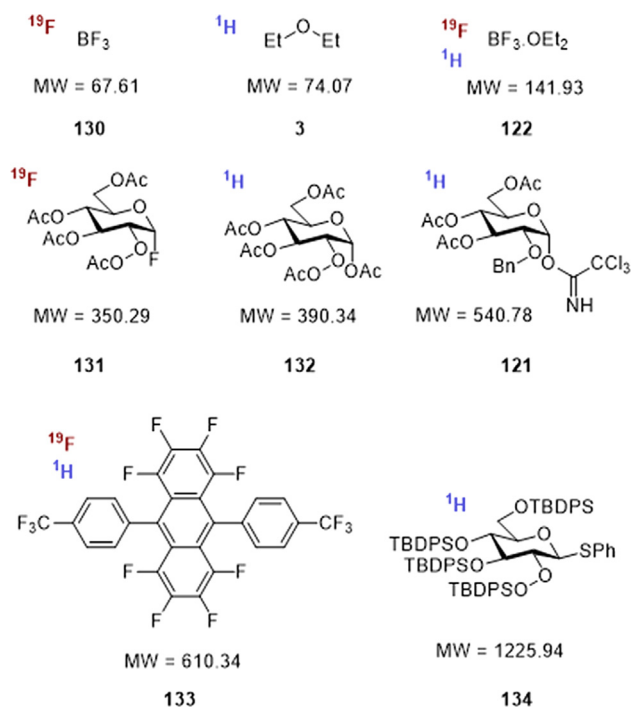


Fig. 46. (a) Graphical representation of kinetic and relaxation processes occurring in the hydration reaction of hyperpolarised fumarate to malate (asterisk indicates hyperpolarised species) (b) Simulated time courses for fumarate and maleate based on the equations below with the kinetic and relaxation parameters determined by Shishmarev et al. [343].



cat. =	BF_3OEt_2	TMSOTf	TMSNTf ₂
	122	123	124
X =	OEt ₂	OTf	NTf ₂
	125	126	127

Scheme 27. Activation of trichloroacetimidate donor **121** by three different catalysts: BF_3OEt_2 , TMSOTf and TMSNTf₂.

Scheme 28. Formation of the activated TCA complex with Tf₂NTMS.Fig. 47. Substrates used to construct the ¹⁹F- and ¹H- DOSY calibration curves.

carbohydrate in the calibration curve due to the limited range available, Fig. 47.

With the calibration curves in hand, the *M_w* for the glycosylation intermediate **128** was compared with the *M_w* values predicted by the ¹H-DOSY and ¹⁹F-DOSY calibration curve. The former was found to be more reliable. This is a good demonstration of the importance of selection reference species with the correct molecular shape when interpreting diffusion coefficients: the ¹⁹F-DOSY calibration curve was mostly generated using non-carbohydrate structures, resulting in less accurate reference species.

This case study highlights the power of DOSY NMR when analysing complex systems: standard NMR methods resulted in numerous overlapping peaks, making identification of intermediates very hard. By clever use of both ¹⁹F- and ¹H-DOSY, the species that were bound to the catalysts could be identified, as well as the *M_w*s of the intermediates. This study also highlights that DOSY had to be used in conjunction with other NMR methods for full elucidation of the structure.

6.13. Case study 13: Kinetics and mechanism of the Arase-Hoshi R₂BH-catalyzed alkyne hydroboration: Alkenylboronate generation via B-H/C-B metathesis [28]

Techniques: *In situ* continuous; ¹⁹F NMR; ¹H NMR; ^{10,11}B NMR; Kinetics Catalyst Speciation and Simulation; Isotope Shifts, Tracking, Entrainment, and Natural Abundance.

The Lloyd-Jones group recently investigated the mechanism of Arase-Hoshi hydroboration, Fig. 48a, using *in situ* ¹⁹F and ¹H

NMR spectroscopic monitoring of the reaction evolution. The process involves dialkylborane-catalysed addition of dialkoxyboranes (e.g. **136**) to alkynes (e.g. **135**). Having identified three species (*E*-**138**, **139**, **140**) by ¹H NMR that contained the catalyst-derived Cy₂B moiety, the two key questions to answer were i) which of *E*-**138**, **139** and **140**, if any, are genuine intermediates in the reaction, and ii) if they are, how do they convert into the final product (*E*-**137**), to regenerate the Cy₂BH catalyst for the next cycle.

Isotope entrainment analysis (Section 4.4) provided rich detail on the provenance and fate of *E*-**138**, **139** and **140**. The aryl-d₄ isotopologue of **133** was readily synthesised and afforded the expected upfield isotope-shift (Δδ = 0.5 ppm) in the ¹⁹F NMR spectrum of d₄-**135**, relative to **135**. The same upfield shift of 0.5 ppm was reliably propagated into all intermediates, products and side-products derived from d₄-**135**, as compared to those from **135**. In the key experiment, Cy₂BH was synthesised *in situ* in a J Young valve NMR tube by adding cyclohexene (10 μL) to 600 μL of 1,4-dioxane/CHCl₃ (100/1, v/v) followed by Me₂S·BH₃ (4.3 μL, 10 mol %) under an N₂ atmosphere. After closing the tube and vigorously shaking the contents, the solution was left to age for 1 h. The spectrometer was prepared with the probe temperature set to 296 K, and then shimmed (¹H) and tuned (¹⁹F) without a deuterium lock by using a dummy sample containing a solution of *E*-**137** and 1-fluoronaphthalene (internal standard) in the same volume of 1,4-dioxane/CHCl₃ (100/1, v/v) employed for the entrainment sample. After ejection of the dummy sample, the reaction was then initiated in the J Young valve NMR tube by adding reagent (**136**, 75 μL, 0.52 mmol), then 1-fluoronaphthalene (25 μL), and finally **135** (26 μL, 0.23 mmol), before sealing the tube, vigorously shaking it to mix, and loading into the spectrometer.

A series of ¹⁹F NMR spectra were acquired over a period of 1800 s until enough **135** had been consumed to generate detectable quantities of the species of interest (*E*-**137**, *E*-**138**, **139**, **140**). The NMR tube was then ejected from the spectrometer and d₄-**135** (27 μL, 0.23 mmol) added to the tube under an N₂ atmosphere. After sealing the tube and vigorously shaking it to mix, the sample was returned to the spectrometer and a series of ¹⁹F NMR spectra acquired (see dashed vertical line in Fig. 48b) until the reaction was complete.

Monitoring the reaction as it evolved allowed the following five conclusions to be drawn, simply by analysing the ratio d₄/d₀ in all detected species as a function of conversion (Fig. 48b). (i) **135** undergoes *irreversible* reactions. (ii) The isotope ratio in *E*-**138** shows that it is generated from **135**, and that it too only undergoes irreversible reactions. (iii) The isotope ratio in **139** only reaches 52% d₄. It is irreversibly generated from **135** and undergoes no further reactions. (iv) The isotope ratio in the final hydroboration product **137** begins to rise after a short but perceptible induction period. The induction period shows that **137** is *indirectly* connected to **135**, via an intermediate (*E*-**138**). (v) Diboryl intermediate **140** only accumulates d₄-isotope in the final stage of reaction, showing that **140** is generated from **137**, and not vice versa.

With the productive reaction sequence established as **135** → **138** → **137** → **140**, the step that liberates the product **137** from intermediate **138** by reaction with **136** was investigated using isotopically labelled reagents ¹⁰B-**136** and Cy₂B²H. This

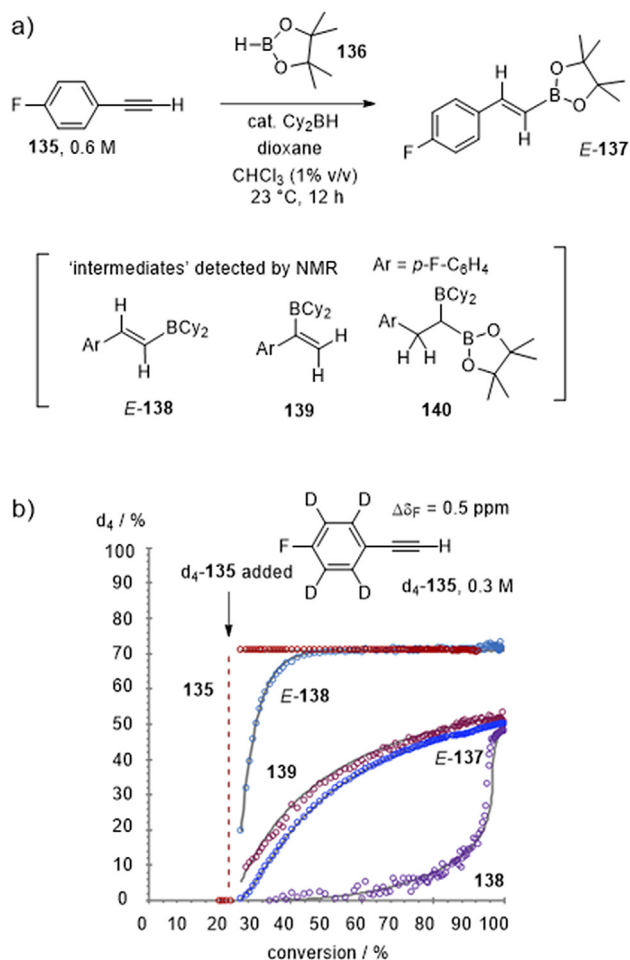


Fig. 48. (a) Arase-Hoshi hydroboration analysed by ^{19}F NMR with possible intermediates and side products (**138–140**); (b) Isotope entrainment of d_2 -**135** into the catalytic cycle.

apparently simple pair of experiments required careful design: the reaction of **136** with **138** liberates Cy_2BH , which must be trapped (a) to avoid $^2\text{H}/^1\text{H}$ exchange with **136**, and (b) to avoid consumption of **137** to generate **140**. Again, *in situ* NMR analysis, this time by ^{10}B , ^{11}B , and ^1H , proved highly effective in allowing analysis of single 'turnover' of the catalyst in the presence of 1-pentyne as a scavenger for Cy_2BH . The very high ^{10}B incorporation (>98%) in **137** was confirmed, Fig. 49, by $^{10}\text{B}/^{11}\text{B}$ NMR analysis using the $^{10}\text{B}/^{11}\text{B}$ natural abundance in 4-F- $\text{C}_6\text{H}_4\text{BF}_3\text{K}$ as an internal reference for integration (Section 5.6).

The final piece in the jigsaw was a detailed kinetic simulation, using numerical analysis methods (Section 4.3.5), of the kinetics of the catalytic process, using the data obtained by *in situ* ^{19}F NMR spectroscopic monitoring. The activation barrier to the turnover rate-limiting step, $\text{138} + \text{136} \rightarrow \text{137} + \text{Cy}_2\text{BH}$, was determined from the simulation to be $20.3 \text{ kcal mol}^{-1}$, a value in good agreement with the computationally (M06L/6-311++G**) estimated barrier for the metathesis process proceeding via a $\mu\text{-B-H-B}$ bridged, 2-electron-3-centre bonded B-C-B intermediate (**141**). The kinetic model was then tested, successfully, by prediction of the isotope entrainment data (Fig. 48b).

This Case Study highlights the interrogative power of the isotope entrainment technique. In combination with ^2H and ^{10}B labelling, kinetic analysis, and computational (DFT) studies of the proposed pathways, the method was able to eliminate three mechanistic proposals, and provide very strong supportive evidence for the remaining one, Fig. 49b.

6.14. Case study 14: Analysis of auto-induction, inhibition and auto-inhibition in a Rh-catalyzed C-C cleavage: Mechanism of decyanative aryl-silylation [49]

Techniques: *In situ* periodic activation; Variable Temperature NMR; ^{19}F NMR; ^1H NMR; ^{29}Si NMR; ^{13}C NMR; Kinetics Catalyst Speciation and Steady State; Isotope Entrainment, Scalar Coupling, Tracking.

The Lloyd-Jones group recently reported a detailed NMR study of the Chatani–Tobisu reaction of nitrile **143**, Fig. 50, a fascinating example of a Rh-catalysed carbon–carbon bond cleaving reaction process. However, finding a way to analyse the kinetics was initially challenging. The system requires heating to about $130 \text{ }^\circ\text{C}$ before catalysis begins. The reaction mixture is also extremely air-sensitive, making *ex situ* analysis via sampling very prone to complete inhibition of the bulk (remaining) reaction by trace aerobic contaminants.

Thus, the reactions were analysed in tightly-sealed J Young valve NMR tubes after careful assembly of the components at ambient temperature in the tube in a glove box. Preliminary analysis of the kinetics determined by ^{19}F NMR analysis in the spectrometer at $130 \text{ }^\circ\text{C}$ indicated that the generation of the silylation product (**145**), evolved in two distinct ways: phase I, involving catalyst acti-

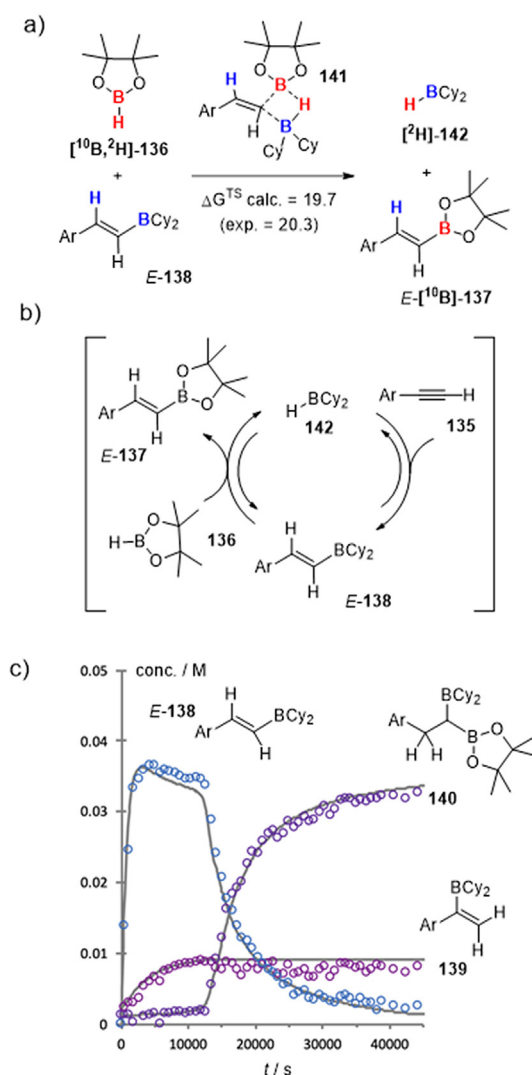


Fig. 49. (a) single turnover H/B isotopic labelling (red/blue = $^{10}/^{11}\text{B}$; $^1/2\text{H}$), (b) catalytic cycle; (c) kinetic simulation of catalyst speciation E-**138**, and irreversibly generated side-products **139** and **140**.

vation, then a short period of relatively fast catalytic turnover, and phase II, a long period of much slower turnover. The overall reaction profile was then compared with a sample in a sealed NMR tube that had undergone cycles of rapid heating to 130 °C in an oil-bath for a set period of time and then rapid cooling in a pentane bath, with intermittent analysis at the standard probe temperature (27 °C). The temporal concentration profile, with the time periods at 27 °C omitted, was near-identical to that recorded in the spectrometer at 130 °C, Fig. 50b. The method of *in situ* periodic activation allowed use of the cryoprobe NMR spectrometer (which in this case was limited in temperature range from 2 °C to 80 °C) and, by cycling between samples undergoing periodic activation, a series of reactions could be analysed in parallel, thus maximising the data generated in a given period of NMR spectrometer time.

The kinetics were then investigated in detail. In a glovebox, a series of separate J Young valve NMR tubes were charged with 400 μ L from a 2.0 mL stock solution containing $[\text{Rh}(\text{COD})\text{Cl}]_2$ (7.75 mg, 0.016 mmol), $\text{Me}_3\text{Si-SiMe}_3$ (**144**, 130 μ L, 0.64 mmol) and 1-fluoronaphthalene (internal standard, 40 μ L) in non-deuteriated mesitylene. To each of these NMR tubes was added a different volume (100–200 μ L) of a 1.0 mL stock solution containing 4-fluorobenzonitrile (**143**, 75.89 mg, 0.63 mmol) in mesitylene (1.0 mL total volume). The NMR tube contents were further diluted with additional mesitylene (0–100 μ L) and different volumes of $\text{Me}_3\text{Si-SiMe}_3$ (**144**, 0–26 μ L) such that each NMR tube contained a total volume of 600 μ L. The NMR tubes were sealed, removed from the glovebox, and then heated in parallel at 130 °C (oil bath). At designated time points, the samples were removed from the heat and rapidly cooled to room temperature in a pentane bath, before analysis by ^{19}F NMR spectroscopy, and then returned to the oil bath at 130 °C. Standard 5 mm O.D. borosilicate NMR tubes are remarkably resistant to the various forms of cylinder stress caused by repeated thermal shocks like this. However, great cau-

tion should be applied when using aqueous solutions due to the expansion in volume on freezing.

All of the components in the reaction, other than Ar-SiMe_3 (**145**), were found to influence the overall kinetics: the aryl nitrile (**143**) inhibits phase I, but accelerates phase II, the $\text{Me}_3\text{Si-SiMe}_3$ reagent **144**, accelerates phase I, and phase II at low concentrations, but becomes an inhibitor of phase II at high concentrations, and the Me_3SiCN co-product accelerates phase I, and inhibits phase II. Only the rhodium displayed a simple kinetic first-order dependence.

By normalising the temporal concentration profiles to the initial pre-catalyst-concentrations, it became evident that the reactions enter phase II after three molecules of Ar-SiMe_3 (**145**) had been

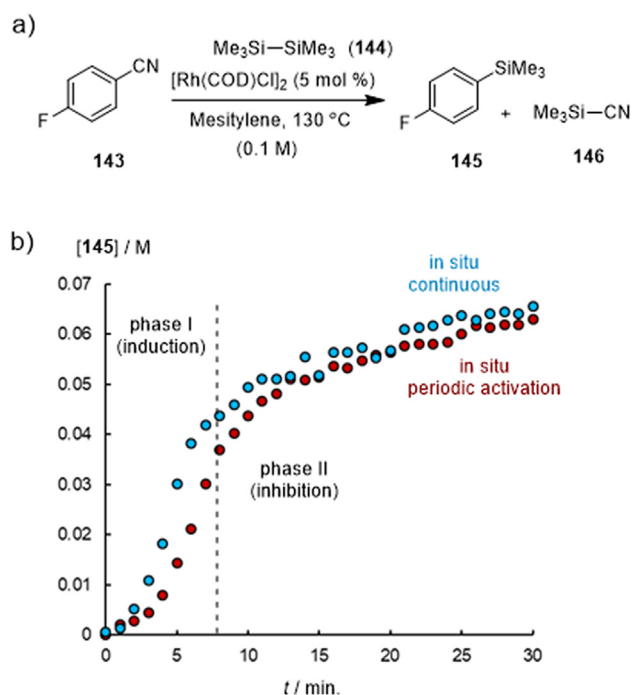


Fig. 50. (a) Chatani-Tobisu Rh-catalysed decyanative silylation of nitrile **143** using $\text{Me}_3\text{Si-SiMe}_3$; (b) Kinetics monitored *in situ* (Section 2.2.1) by ^{19}F NMR in a sealed J Young valve NMR tube. Comparison of data obtained by *in situ* periodic activation (130 °C for 60 s, then rapidly cooled to RT and analysed at 27 °C on a 400 MHz cryoprobe) versus *in situ* continuous monitoring (130 °C in the spectrometer, 400 MHz BBO + Probe). The slight deviation between the datasets is caused by the sensitivity of the reaction evolution to the length of the induction period.

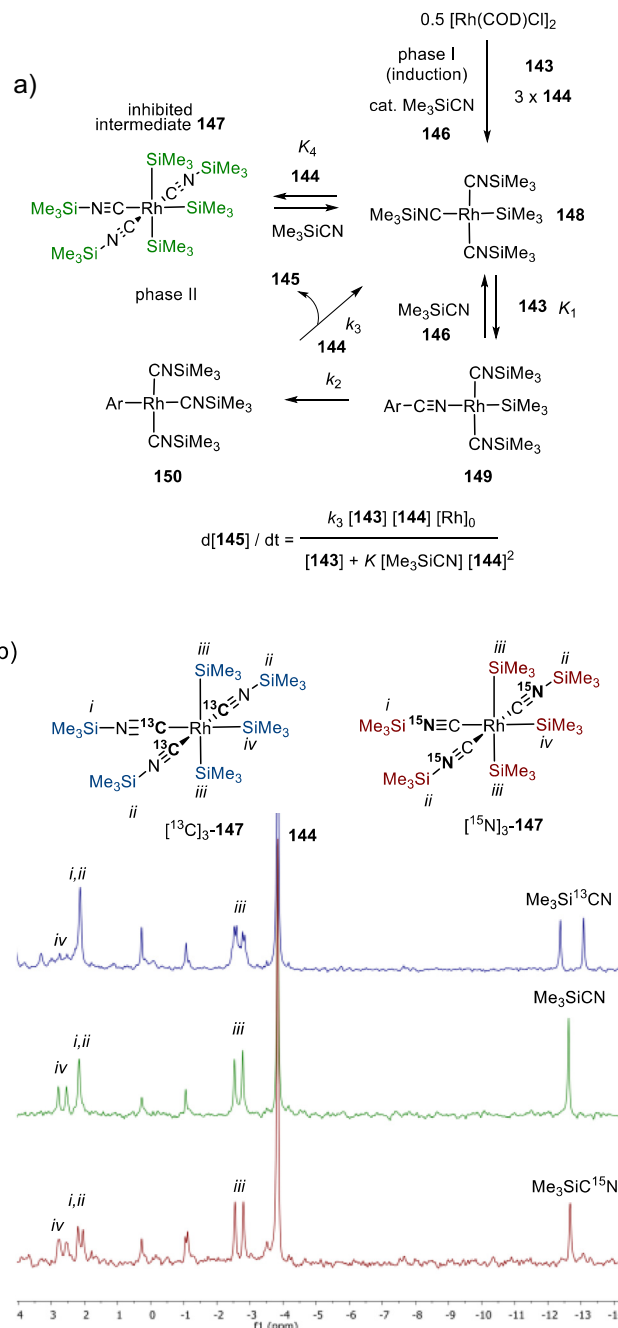


Fig. 51. (a) steady state rate analysis for kinetics in phase II in which the dominant speciation is the active catalyst species **148** an inhibited catalyst species **147**, both identified by ^1H , ^{13}C , ^{15}N , ^{19}F , and ^{29}Si NMR. (b) Partial ^{29}Si INEPT (79 MHz) NMR spectra of intermediate Rh species generated during phase II, initiated with $^{13}\text{C}_1$ -**143** (upper), **143**, (middle), and $^{15}\text{N}_1$ -**143**, (lower).

produced per rhodium atom. The absence of the Me_3SiCN co-product in the samples until the process transitions into phase II suggested that reversible coordination of three Me_3SiCN molecules to rhodium results in an inhibited form of the catalyst (**147**, Fig. 51). The rate of reaction in phase II was consistent with a King-Altman steady-state derivation of a minimal mechanism in which the resting state (the major speciation) of the rhodium is a composite of complexes **148** and **147**.

To explore the catalyst speciation and the structures of intermediates, solutions of $[\text{Rh}(\text{COD})\text{Cl}]_2$ (3.06 mg, 0.0062 mmol), $\text{Me}_3\text{Si-SiMe}_3$ (**144**, 52 μL , 0.26 mmol), and in separate experiments, **143**, $^{13}\text{C}_1$ -**143**, and $^{15}\text{N}_1$ -**143**, (15.2 mg, 0.125 mmol, in mesitylene, 0.5 mL) were mixed in a vial in the glove box, and the contents transferred to J Young valve NMR tubes. The NMR tubes were sealed, removed from the glove box, and heated to 130 °C for 60 min, then rapidly cooled to room temperature, before being analysed by ^{13}C , ^{15}N and ^{29}Si (Fig. 51b) NMR spectroscopy.

Careful analysis of the NMR spectra, noting that ^{103}Rh is 100% abundant and spin-half, allowed confirmation of the identity of the two resting state complexes (**147** and **148**), as well as $\text{Me}_3\text{Si}^{13}\text{C-N}/\text{Me}_3\text{Si}^{15}\text{N}$, and in further experiments, demonstration that their proportions are dependent on the concentrations of $[\text{Rh}]_{\text{TOT}}$, **143**, $\text{Me}_3\text{Si-SiMe}_3$, (**144**) and Me_3SiCN , all consistent with the steady-state rate analysis.

In this Case Study, despite technically challenging conditions (130 °C, extreme air-sensitivity) the use of multinuclear (^1H , ^{13}C , ^{15}N , ^{19}F , and ^{29}Si) NMR, together with isotopically labelled reactants and products under conditions of *in situ* periodic activation, afforded a wealth of mechanistic information on a chemical process that previously had been optimised on the basis of empirical screening.

6.15. Case study 15: Discovery of a photoinduced dark catalytic cycle using *in situ* illumination NMR spectroscopy [102]

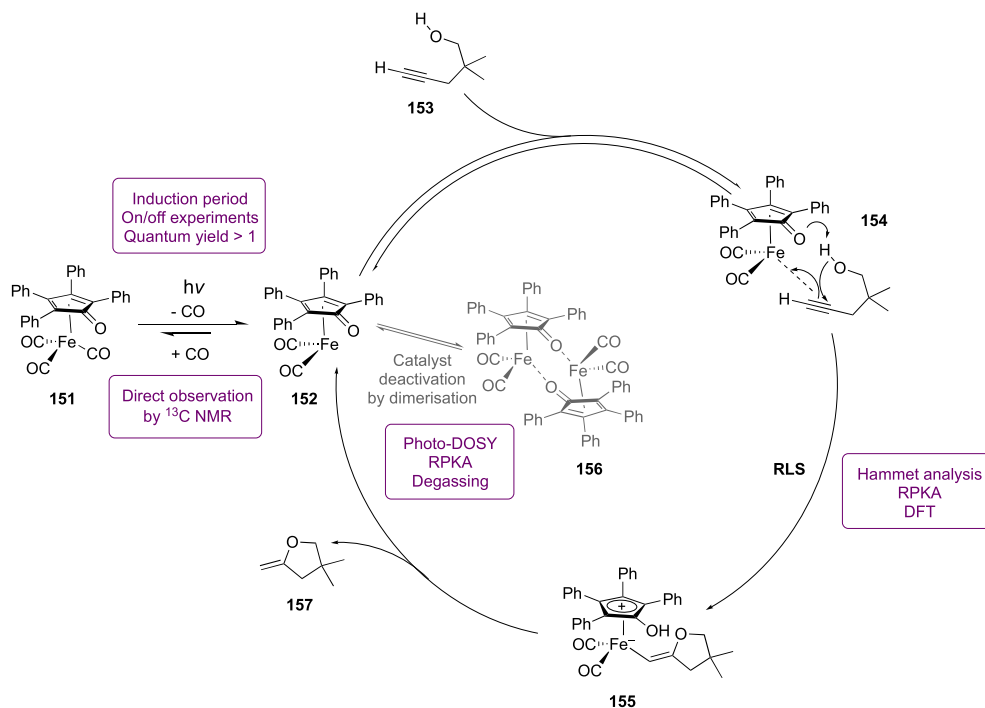
Techniques: *in situ* analysis continuous and periodic activation; light emitting diode light source; ^{13}C NMR; RPKA; Catalyst Speciation; DOSY; Isotopes for tracking; Isotopes for S/N.

A highly-selective photo-induced 5-exo cyclisation (Scheme 29) of alkynols to cyclic enol ethers using an iron-carbonyl based catalyst (**151**) was recently reported by the Merck process research group [102]. However, initial optimisation experiments revealed a significant reduction in product yield when the CO was allowed to vent from the reactor, prompting a detailed mechanistic study.

As a photochemical system this reaction posed unique challenges for mechanistic study. Traditional methods of *in situ* monitoring do not allow for irradiation of sample; on the other hand, the need for a closed system and the ability to monitor formation of CO, as well as the chromatographic instability of the product, precluded most traditional *ex situ* monitoring techniques. Simply monitoring the reaction by periodic activation would not allow for sufficient information to distinguish several mechanistic possibilities, e.g. whether photon absorption occurs on-cycle or off-cycle in an activation process. Thus, *in situ* illumination NMR spectroscopy (as discussed in Section 2.4.2.2) was employed to probe the reaction under constant and under variable illumination.

Initial NMR reaction monitoring under constant irradiation at 440 nm revealed the presence of an induction period in the reaction kinetics, implying a catalyst activation process. When the reaction was irradiated for 30 min and then kept in the dark whilst continuing to monitor the reaction by NMR, it was found that the reaction continued, but the rate decayed to almost zero over a period of hours. When irradiation was resumed, a second incubation period was observed and the reaction reacquired its original velocity. This direct NMR observation of ‘dark reactivity’ was made possible through the use of ‘on-off’ type switchable *in situ* illumination equipment, and provided very strong evidence that the role of the light in this reaction is to activate the catalyst, not to facilitate the catalytic cycle.

When a solution of the catalyst (**151**) was irradiated (in an external photoreactor at 450 nm) and UV-Vis spectra were recorded before and afterwards, a red-shift was observed which implied activation by photo-induced loss of a CO ligand to form a 16-electron complex (**152**). In order to observe this directly in the reaction, a ^{13}C labelled catalyst was prepared. This allowed for quantitative ^{13}C NMR monitoring of both free and Fe-bound



Scheme 29. Exo cyclisation of alkynols to cyclic enol ethers catalysed by a photoactivated iron-carbonyl catalyst.

^{13}C during the reaction, under constant and variable irradiation conditions. On constant irradiation of the reaction solution, free ^{13}C was detected in solution, and its concentration increased over a period of 30 min to reach a steady-state. Analogously, the signal from Fe-bound ^{13}C decreased to reach a steady state. When the irradiation was stopped, the concentration of free ^{13}C slowly decreased, and that of the Fe-bound ^{13}C pre-catalyst recovered, providing strong evidence for a reversible photo-induced catalyst activation process.

The *in situ* illumination-NMR device was also used to directly measure the quantum yield of the reaction using an NMR actinometry technique [345]. By using a reaction of known quantum yield (in this case the photo-oxidation of 2,4-dinitrobenzaldehyde) to calibrate the light intensity, and by measuring the rate of product formation at different concentrations of iron catalyst, the reaction quantum yield was determined as 3.06. This means that, on average, one photon is responsible for approximately three turnovers of the catalytic cycle, and provides further evidence for reversible photoinduced catalyst activation; photoinduced catalyst turnover would give a reaction quantum yield ≤ 1 .

More conventional kinetic analyses were also performed by NMR analysis under constant irradiation conditions, including linear free energy relationship analysis and RPKA. By way of a ^{13}C NMR material balance analysis, slow loss of ^{13}C from solution was detected. This loss of CO, presumably through an imperfect seal of the NMR tube, was linked to catalyst deactivation via Fe-complex dimerization, a process that was subsequently investigated by *in situ* illumination DOSY NMR spectroscopy.

This case study demonstrates the enormous potential of *in situ* illumination NMR spectroscopy as a mechanistic tool. Not only does it allow for many standard mechanistic analysis techniques to be conducted on photochemical reactions, but there are several additional techniques that are able to provide the researcher with unique information that is difficult to obtain by other routes, for example the ability to sequentially analyse 'light and dark' cycles and the measurement of the reaction quantum yield by NMR.

7. Summary and outlook

In Sections 1–6 above, we have explored a wide range of topics relating to mechanistic investigation of organic and organometallic reactions using NMR spectroscopy. We began in Section 1 by reflecting on the motivations for the study of reaction mechanisms, why NMR is so well suited to this, what spectrometers and facilities are generally available to the user, and the general experimental workflows employed. In Section 2 we moved on to practical aspects of the reaction itself: what NMR-active nuclei are inherently present, or can be integrated into the process to allow monitoring, what internal reference will be used, what solvent will the reaction be conducted in, what are the physical mixing requirements before and during the reaction, how sensitive is the reaction to air, moisture, light, etc., and what NMR tubes or other sample-presentation methods are appropriate. This led to considerations of the time-scale over which the reaction occurs, and the time available to the user for NMR analysis: will *in situ* or *ex situ* monitoring be more effective in terms of data density, operator availability, and required spectrometer time? Can the reaction be interrupted, or periodically activated, or are specialised techniques and equipment required, such as quenched-flow, flow, stopped-flow, rapid injection, electrochemistry, *in situ* illumination-NMR, high-pressure manipulations of liquids or gasses, or hyperpolarization of nuclei?

With the reaction parameters (nuclei, solvent, temperature, monitoring technique, environment, etc.) established, in Section 3 we considered the NMR data itself, both in terms of acquisition and of processing. A key factor to consider is temporal resolution: how

fast is the reaction, how many FIDs will be required for a satisfactory signal-to-noise ratio, how many data points are required, and over what time period for reliable kinetic analysis. The rate of relaxation of the probed nuclei is a key factor in this assessment, and it is wise to determine T_1 values for the various reactants, products, and intermediates if feasible, early on in the investigation. With these features in mind, we next considered how, for the reaction of interest, optimisation of the acquisition parameters on the spectrometer can lead to substantial benefit in terms of signal-to-noise, resolution, and quantitation. Specialist techniques such as pure shift NMR and SHARPER can allow great insight when spectra are congested, or the magnetic field is inhomogeneous, and spatially-selective acquisitions employing strong pulsed gradients are sometimes advantageous when reaction rates are faster than T_1 relaxation. We also touched upon the use of 2D methods and the tailoring of their application to reaction monitoring, in particular by non-uniform sampling, and minimising errors in extracting quantitative data from 2D spectra. The processing of the NMR data post-acquisition is another important aspect in getting the most out of an experiment, and we noted the benefits of carefully addressing processes such as phasing, base-line correction, zero-filling, and integration, as well as spectral deconstruction, principal component analysis, and spectral hard modelling.

Having reviewed the technical and practical aspects of the reaction assembly and NMR spectroscopy/spectrometer set-up, we transferred our attention in Sections 4 and 5 to the areas in mechanistic analysis where NMR can be a uniquely effective tool. Section 4 focused on the principles applied in the analysis of the kinetics of reactions, beginning by comparison of the fundamental differences between reactions at dynamic equilibrium, which can be analysed 'at leisure', and those that begin away from equilibrium, and for which, once started, there is a finite window of time during which the NMR data must be acquired. With the experimental data in hand, a variety of options for their analysis can be distinguished. For non-equilibrium kinetics, the classic techniques of initial rates versus full reaction evolution were evaluated, as well as the derivation of integrated rate laws, and the pre-equilibrium and steady-state approximations for linear and catalytic processes were discussed. Graphical and visual methods, such as RKPA and VTNA, were also compared, as well as the simulation of complex mechanistic models using numerical methods. For systems at dynamic equilibrium, two distinct approaches were distinguished. The first is where the chemically-unperturbed process is probed, either by NMR line shape analysis, or by selectively altering the spin polarisation equilibrium, allowing e.g. EXSY or magnetisation transfer. The second technique is where the chemical equilibrium is rapidly displaced using an external stimulus, e.g. light or heat, and then the relaxation kinetics are followed, either back to the original state, or to a new thermodynamic equilibrium. The equilibrium can also be displaced in a sequence of small chemical perturbations, and the changes in time-average chemical shifts (fast exchange) or speciation (slow exchange) monitored as an 'NMR titration'.

The use of isotopes formed the basis for Section 5. Isotopes lend themselves perfectly to NMR experiments. Isotopes allow selective labelling of atoms and molecules by virtue of their different NMR properties, and with minimal chemical perturbation, yet at the same time allow that perturbation to be measured to provide useful mechanistic information in the form of kinetic isotope effects. Thus a wide variety of experiments can be conducted, including atom accountancy, enhanced sensitivity when S/N is low at natural abundance, spectral simplification by eliminating signals, determining equilibrium and kinetic isotope effects, breaking symmetry, isotope entrainment to probe reaction flux and validity of proposed intermediates, application of isotope shifts to label by proxy, and use of natural abundance isotopes and satellites as internal standards.

Finally, in Section 6 we saw in a series of 'Case Studies' from the published literature how selected combinations of the features discussed in Sections 1–5 can be applied to elucidate kinetic and mechanistic details in a range of synthetic reactions and processes, with a clear focus in this section on the practical NMR aspects of the studies. We hope that these examples will inspire readers in the design of new mechanistic studies to explore and develop reactions of interest.

The chemical literature indicates that NMR has been the technique of choice in the majority of mechanistic studies in organic and organometallic chemistry that have been published over the last two to three decades. Looking forward, it is evident that continuing rapid advances in computation will continue to assist and refine the application of NMR, predicting chemical shifts and couplings and the energetic viability of proposed intermediates and transition states. Developments in non-cryogen high-field magnets will also bring major advances, allowing (physically) smaller spectrometers to be located in the chemical laboratory and interfaced more easily with other instrumentation and reaction vessels, and the means for more rapid and versatile chemical and physical manipulation of samples in the probe of the spectrometer. Whilst new techniques based on other physical and chemical properties continue to be developed, e.g. X-ray free-electron laser methods, we do not anticipate NMR being any less dominant in the coming decades, unless a fundamentally new technique emerges and becomes widely available.

Declaration of Competing Interest

The authors declare that they have no known competing financial interests or personal relationships that could have appeared to influence the work reported in this paper.

Acknowledgements

We thank the ERC (grant agreement numbers [340163] and [838616], GCL-J, RED, and AMRH), the SNSF (postdoctoral fellowship P2ZHP2181497, to AGD), Syngenta (CASE award to HJAD, studentship to NAF), AstraZeneca (CASE award to HH), the University of Edinburgh (Principal's Career Development Scholarship to PB; Edinburgh Global Researcher Scholarships to YB-T and YG), Criticat-EPSC-CDT (Scholarship to MMK), the China Scholarship Council (Scholarship to RW), and the University of Edinburgh School of Chemistry (KMG and GCL-J), for support.

References

- [1] About the Lloyd-Jones Research Group | Lloyd-Jones Website, (2020). <http://www.lloyd-jones.chem.ed.ac.uk/> (accessed August 31, 2020).
- [2] J.F. Bunnett, The Culture of Chemistry: A Graduate Course, *J. Chem. Educ.* 76 (8) (1999) 1058, <https://doi.org/10.1021/ed076p1058>.
- [3] S.A. Richards, J.C. Hollerton, *Essential Practical NMR for Organic Chemistry*, John Wiley & Sons, Chichester, UK, 2010, <https://doi.org/10.1002/9780470976401>.
- [4] J. Keeler, *Understanding NMR Spectroscopy, second ed.*, John Wiley and Sons, Chichester, U.K., 2010.
- [5] T.D.W. Claridge, *High-Resolution NMR Techniques in Organic Chemistry*, third ed., Elsevier, Amsterdam, London, 2016, <https://doi.org/10.1016/C2015-0-04654-8>.
- [6] T.N. Mitchell, *NMR – From Spectra to Structures an Experimental Approach, second ed.*, Springer, Berlin, New York, 2007.
- [7] J.B. Lambert, E.P. Mazzola, C.D. Ridge, *Nuclear Magnetic Resonance Spectroscopy: An Introduction to Principles, Applications, and Experimental Methods, second ed.*, John Wiley and Sons, Hoboken, New Jersey, 2019.
- [8] P. Giraudeau, F.-X. Felpin, Flow reactors integrated with in-line monitoring using benchtop NMR spectroscopy, *React. Chem. Eng.* 3 (4) (2018) 399–413, <https://doi.org/10.1039/C8RE00083B>.
- [9] T.A. Beek, Low-field benchtop NMR spectroscopy: status and prospects in natural product analysis, *Phytochem. Anal.* 32 (1) (2021) 24–37, <https://doi.org/10.1002/pca.2921>.

- [10] B. Blümich, *Mobile and Compact NMR*, in: G.A. Webb (Ed.), *Mod. Magn. Reson.*, Springer International Publishing, Cham, 2016, pp. 1–32, https://doi.org/10.1007/978-3-319-28275-6_75-1.
- [11] D.L. Olson, J.A. Norcross, M. O'Neil-Johnson, P.F. Molitor, D.J. Detlefsen, A.G. Wilson, T.L. Peck, *Microflow NMR: Concepts and capabilities*, *Anal. Chem.* 76 (2004) 2966–2974, <https://doi.org/10.1021/ac035426l>.
- [12] L.T. Kuhn, J. Bargon, *Transfer of Parahydrogen-Induced Hyperpolarization to Heteronuclei*, *Top. Curr. Chem.* 276 (2007) 25–68, <https://doi.org/10.1007/b135837>.
- [13] D. Guan, C. Godard, S.M. Polas, R.P. Tooze, A.C. Whitwood, S.B. Duckett, Using para hydrogen induced polarization to study steps in the hydroformylation reaction, *Dalt. Trans.* 48 (8) (2019) 2664–2675, <https://doi.org/10.1039/C8DT04723E>.
- [14] P.M. Richardson, A.J. Parrott, O. Semenova, A. Nordon, S.B. Duckett, M.E. Halse, SABRE hyperpolarization enables high-sensitivity ¹H and ¹³C benchtop NMR spectroscopy, *Analyst* 143 (14) (2018) 3442–3450, <https://doi.org/10.1039/C8AN00596F>.
- [15] R. Wei, A.M.R. Hall, R. Behrens, M.S. Pritchard, E.J. King, G.C. Lloyd-Jones, Stopped-Flow 19F NMR Spectroscopic Analysis of a Protodeboronation Proceeding at the Sub-Second Time-Scale, *Eur. J. Org. Chem.* 2021 (2021) 2331–2342, <https://doi.org/10.1002/ejoc.202100290>.
- [16] C.H. Cullen, G.J. Ray, C.M. Szabo, A comparison of quantitative nuclear magnetic resonance methods: Internal, external, and electronic referencing, *Magn. Reson. Chem.* 51 (2013) 705–713, <https://doi.org/10.1002/mrc.4004>.
- [17] G. Maniara, K. Rajamoorthi, S. Rajan, G.W. Stockton, Method performance and validation for quantitative analysis by ¹H and ³¹P NMR spectroscopy. Applications to analytical standards and agricultural chemicals, *Anal. Chem.* 70 (23) (1998) 4921–4928, <https://doi.org/10.1021/ac980573i>.
- [18] S. Akoka, L. Barantin, M. Trierweiler, Concentration measurement by proton NMR using the ERETIC method, *Anal. Chem.* 71 (13) (1999) 2554–2557, <https://doi.org/10.1021/ac981422i>.
- [19] S.K. Bharti, R. Roy, Quantitative ¹H NMR spectroscopy, *TrAC – Trends Anal. Chem.* 35 (2012) 5–26, <https://doi.org/10.1016/j.trac.2012.02.007>.
- [20] Wilmad, Wilmad-LabGlass Website, (2020). <https://www.wilmad-labglass.com/ProductList.aspx?t=109> (accessed April 16, 2020).
- [21] Norell, Norell Website, (2020). <https://nmrtubes.com/index.php> (accessed April 16, 2020).
- [22] W.S. Kahlson, Studies on the Etching of Glass, *J. Am. Ceram. Soc.* 14 (1931) 827–832, <https://doi.org/10.1111/j.1151-2916.1931.tb16576.x>.
- [23] Norell, Fluoropolymer NMR Tube Liners & Fluoropolymer Liner Tube Kits for ²⁹Si & ¹¹B Description & Instructions for Use, (2020). <https://nmrtubes.com/pdf/NORELLTubeLinerKitOperatingInstructions.pdf> (accessed September 2, 2020).
- [24] P.A. Cox, M. Reid, A.G. Leach, A.D. Campbell, E.J. King, G.C. Lloyd-Jones, Base-Catalyzed Aryl-B(OH)₂ Protodeboronation Revisited: From Concerted Proton Transfer to Liberation of a Transient Aryl Anion, *J. Am. Chem. Soc.* 139 (37) (2017) 13156–13165, <https://doi.org/10.1021/jacs.7b07444>.
- [25] M. Butters, J. Harvey, J. Jover, A.J. Lennox, G. Lloyd-Jones, P. Murray, Aryl trifluoroborates in Suzuki-Miyaura coupling: The roles of endogenous aryl boronic acid and fluoride, *Angew. Chemie – Int. Ed.* 49 (30) (2010) 5156–5160, <https://doi.org/10.1002/anie.201001522>.
- [26] M.P. Robinson, G.C. Lloyd-Jones, Au-Catalyzed Oxidative Arylation: Chelation-Induced Turnover of ortho-Substituted Arylsilanes, *ACS Catal.* 8 (8) (2018) 7484–7488, <https://doi.org/10.1021/acscatal.8b02302>.
- [27] H.J.A. Dale, G.R. Hodges, G.C. Lloyd-Jones, Taming Ambident Triazole Anions: Regioselective Ion Pairing Catalyzes Direct N-Alkylation with Atypical Regioselectivity, *J. Am. Chem. Soc.* 141 (17) (2019) 7181–7193, <https://doi.org/10.1021/jacs.9b02786>.
- [28] E. Nieto-Sepulveda, A.D. Bage, L.A. Evans, T.A. Hunt, A.G. Leach, S.P. Thomas, G.C. Lloyd-Jones, Kinetics and Mechanism of the Arase-Hoshi R2BH-Catalyzed Alkyne Hydroboration: Alkenylboronate Generation via B-H/C-B Metathesis, *J. Am. Chem. Soc.* 141 (46) (2019) 18600–18611, <https://doi.org/10.1021/jacs.9b10114>.
- [29] C.P. Johnston, T.H. West, R.E. Dooley, M. Reid, A.B. Jones, E.J. King, A.G. Leach, G.C. Lloyd-Jones, Anion-Initiated Trifluoromethylation by TMSCF₃: Deconvolution of the Silconate-Carbanion Dichotomy by Stopped-Flow NMR/IR, *J. Am. Chem. Soc.* 140 (35) (2018) 11112–11124, <https://doi.org/10.1021/jacs.8b06777>.
- [30] A. García-Domínguez, T.H. West, J.J. Primozić, K.M. Grant, C.P. Johnston, G.G. Cumming, A.G. Leach, G.C. Lloyd-Jones, Difluorocarbene Generation from TMSCF₃: Kinetics and Mechanism of NaI-Mediated and Si-Induced Anionic Chain Reactions, *J. Am. Chem. Soc.* 142 (2020) 14649–14663, <https://doi.org/10.1021/jacs.0c06751>.
- [31] J.R. Pankhurst, M. Curcio, S. Sproules, G.C. Lloyd-Jones, J.B. Love, Earth-Abundant Mixed-Metal Catalysts for Hydrocarbon Oxygenation, *Inorg. Chem.* 57 (10) (2018) 5915–5928, <https://doi.org/10.1021/acs.inorgchem.8b00420>.
- [32] T.H. West, D.M. Walden, J.E. Taylor, A.C. Brueckner, R.C. Johnston, P.-Y. Cheong, G.C. Lloyd-Jones, A.D. Smith, Catalytic Enantioselective [2,3]-Rearrangements of Allylic Ammonium Ylides: A Mechanistic and Computational Study, *J. Am. Chem. Soc.* 139 (12) (2017) 4366–4375, <https://doi.org/10.1021/jacs.6b11851>.
- [33] A.M.R. Hall, R. Broomfield-Tagg, M. Camilleri, D.R. Carbery, A. Codina, D.T.E. Whittaker, S. Coombes, J.P. Lowe, U. Hintermair, Online monitoring of a photocatalytic reaction by real-time high resolution FlowNMR spectroscopy, *Chem. Commun.* 54 (1) (2018) 30–33.

- [34] Victrex Technology International, PEEK Properties Guide, (2016). https://www.victrex.com/~media/literature/en/victrex_properties_guide_en_metric.pdf (accessed December 6, 2020).
- [35] J. Wolowska, G.R. Eastham, B.T. Heaton, J.A. Iggo, C. Jacob, R. Whyman, The effect of mechanistic pathway on activity in the Pd and Pt catalysed methoxycarbonylation of ethene, *Chem. Commun.* 23 (2002) 2784–2785, <https://doi.org/10.1039/b208450c>.
- [36] M.R. Aguilar, A. Gallardo, M. Del Mar Fernández, J.S. Román, In situ quantitative ¹H NMR monitoring of monomer consumption: A simple and fast way of estimating reactivity ratios, *Macromolecules* 35 (2002) 2036–2041, <https://doi.org/10.1021/ma0106907>.
- [37] M.R. Crimmin, A.G.M. Barrett, M.S. Hill, P.B. Hitchcock, P.A. Procopiou, Heavier group 2 element catalyzed hydrophosphination of carbodiimides, *Organometallics* 27 (4) (2008) 497–499, <https://doi.org/10.1021/om7011198>.
- [38] G.A. Grasa, A. Zanotti-Gerosa, S. Ghosh, C.A. Teleha, W.A. Kinney, B.E. Maryanoff, Efficient, enantioselective synthesis of a β, β-disubstituted carboxylic acid by Ru-XylPhanePhos-catalyzed asymmetric hydrogenation, *Tetrahedron Lett.* 49 (36) (2008) 5328–5331, <https://doi.org/10.1016/j.tetlet.2008.06.068>.
- [39] A.M.R. Hall, J.C. Chouler, A. Codina, P.T. Gierth, J.P. Lowe, U. Hintermair, Practical aspects of real-time reaction monitoring using multi-nuclear high resolution FlowNMR spectroscopy, *Catal. Sci. Technol.* 6 (24) (2016) 8406–8417, <https://doi.org/10.1039/C6CY01754A>.
- [40] D.A. Foley, A.L. Dunn, M.T. Zell, Reaction monitoring using online vs tube NMR spectroscopy: Seriously different results, *Magn. Reson. Chem.* 54 (6) (2016) 451–456, <https://doi.org/10.1002/mrc.4259>.
- [41] T. Bartik, B. Bartik, B.E. Hanson, T. Glass, W. Bebout, Comments on the Synthesis of Trisulfonated Triphenylphosphine: Reaction Monitoring by NMR Spectroscopy, *Inorg. Chem.* 31 (12) (1992) 2667–2670, <https://doi.org/10.1021/ic00038a069>.
- [42] A. Mix, P. Jutzi, B. Rummel, K. Hagedorn, A Simple double-chamber NMR tube for the monitoring of chemical reactions by NMR spectroscopy, *Organometallics* 29 (2) (2010) 442–447, <https://doi.org/10.1021/om900919f>.
- [43] D.F. Shriver, *The Manipulation of Air-sensitive Compounds*, McGraw-Hill, New York, 1969.
- [44] Sigma-Aldrich, Technical Bulletin AL-134: Handling Air-Sensitive Reagents, *Tech. Bull.* 2016 (2012). http://www.sigmaaldrich.com/content/dam/sigmaaldrich/docs/Aldrich/Bulletin/al_techbull_al134.pdf (accessed September 2, 2020).
- [45] B.S. Furniss, A.J. Hannaford, P.W.G. Smith, A.R. Tatchell, *Vogel's Textbook of Practical Organic Chemistry*, fifth ed., John Wiley & Sons Inc, 1989.
- [46] R.J. Errington, *Advanced Practical Inorganic and Metalorganic Chemistry*, CRC Press, 1997.
- [47] M.C. Pirrung, *The Synthetic Organic Chemist's Companion*, John Wiley & Sons Inc, Hoboken, 2007.
- [48] F. Susanne, D.S. Smith, A. Codina, Kinetic understanding using NMR reaction profiling, *Org. Process Res. Dev.* 16 (1) (2012) 61–64, <https://doi.org/10.1021/op200202k>.
- [49] E.C. Keske, T.H. West, G.C. Lloyd-Jones, Analysis of Autoinduction, Inhibition, and Autoinhibition in a Rh-Catalyzed C–C Cleavage: Mechanism of Decyanative Aryl Silylation, *ACS Catal.* 8 (9) (2018) 8932–8940, <https://doi.org/10.1021/acscatal.8b02809>.
- [50] M. Findeisen, T. Brand, S. Berger, A ¹H-NMR thermometer suitable for cryoprobes, *Magn. Reson. Chem.* 45 (2) (2007) 175–178, <https://doi.org/10.1002/mrc.1941>.
- [51] T.D.W. Claridge, Practical Aspects of High-Resolution NMR, in: *High-Resolution NMR Tech. Org. Chem.*, third ed., Elsevier, Amsterdam, London, 2016, pp. 61–132, <https://doi.org/10.1016/B978-0-08-099986-9/00003-8>.
- [52] D. Sheppard, R. Sprangers, V. Tugarinov, Experimental approaches for NMR studies of side-chain dynamics in high-molecular-weight proteins, *Prog. Nucl. Magn. Reson. Spectrosc.* 56 (1) (2010) 1–45, <https://doi.org/10.1016/j.pnmrs.2009.07.004>.
- [53] G.A. Barding, R. Salditos, C.K. Larive, Quantitative NMR for bioanalysis and metabolomics, *Anal. Bioanal. Chem.* 404 (4) (2012) 1165–1179, <https://doi.org/10.1007/s00216-012-6188-z>.
- [54] R. Wei, G.C. Lloyd-Jones, Unpublished Work, (2020).
- [55] W.R. Dolbier, *Guide to fluorine NMR for organic chemists, second ed.*, John Wiley & Sons Inc, Hoboken, New Jersey, 2016.
- [56] D.S. Glueck, Applications of ³¹P NMR spectroscopy in development of M (Duphos)-catalyzed asymmetric synthesis of P-stereogenic phosphines (M = Pt or Pd), *Coord. Chem. Rev.* 252 (21–22) (2008) 2171–2179, <https://doi.org/10.1016/j.ccr.2007.12.023>.
- [57] O. Kühn, *Phosphorus-31 NMR Spectroscopy: A Concise Introduction for the Synthetic Organic and Organometallic Chemist*, Springer-Verlag Berlin Heidelberg, 2008, 10.1007/978-3-540-79118-8.
- [58] K.E. Maudens, S.M.R. Wille, W.E. Lambert, Traces of phosgene in chloroform: Consequences for extraction of anthracyclines, *J. Chromatogr. B.* 848 (2) (2007) 384–390, <https://doi.org/10.1016/j.jchromb.2006.10.073>.
- [59] D.E. Clark, Peroxides and peroxide-forming compounds, *Chem. Health Saf.* 8 (5) (2001) 12–22.
- [60] N. Bloembergen, E.M. Purcell, R.V. Pound, Relaxation effects in nuclear magnetic resonance absorption, *Phys. Rev.* 73 (7) (1948) 679–712, <https://doi.org/10.1103/PhysRev.73.679>.
- [61] C. Reichardt, T. Welton, A.A. Properties, Purification, and Use of Organic Solvents, in: C. Reichardt, T. Welton (Eds.), *Solvents Solvent Eff. Org. Chem.*, fourth ed., Wiley-VCH, Weinheim, Germany, 2011, pp. 549–586, <https://doi.org/10.1002/9783527632220.app1>.
- [62] T.R. Hoye, B.M. Eklov, T.D. Ryba, M. Voloshin, L.J. Yao, No-D NMR (No-Deuterium Proton NMR) spectroscopy: A simple yet powerful method for analyzing reaction and reagent solutions, *Org. Lett.* 6 (2004) 953–956, <https://doi.org/10.1021/ol049979+>.
- [63] S.H. Smallcombe, S.L. Patt, P.A. Keifer, WET Solvent Suppression and Its Applications to LC NMR and High-Resolution NMR Spectroscopy, *J. Magn. Reson. Ser. A* 117 (2) (1995) 295–303, <https://doi.org/10.1006/jmra.1995.0759>.
- [64] G. Zheng, W.S. Price, Solvent signal suppression in NMR, *Prog. Nucl. Magn. Reson. Spectrosc.* 56 (3) (2010) 267–288, <https://doi.org/10.1016/j.pnmrs.2010.01.001>.
- [65] C. Vignali, A. Caligiani, G. Palla, Quantitative ²H NMR spectroscopy with 1H lock extender, *J. Magn. Reson.* 187 (1) (2007) 120–125, <https://doi.org/10.1016/j.jmr.2007.04.008>.
- [66] G.R. Fulmer, A.J.M.M. Miller, N.H. Sherden, H.E. Gottlieb, A. Nudelman, B.M. Stoltz, J.E. Bercaw, K.I. Goldberg, R. Gan, NMR Chemical Shifts of Trace Impurities: Common Laboratory Solvents, Organics, and Gases in Deuterated Solvents Relevant to the Organometallic Chemist, *Organometallics* 29 (2010) 2176–2179, <https://doi.org/10.1021/om100106e>.
- [67] P. Laszlo, Solvent effects and nuclear magnetic resonance, in: *Prog. Nucl. Magn. Reson. Spectrosc.*, Elsevier B.V., Amsterdam, 1967, pp. 231–402, [https://doi.org/10.1016/0079-6565\(67\)80016-5](https://doi.org/10.1016/0079-6565(67)80016-5).
- [68] P.W.A. Howe, Recent developments in the use of fluorine NMR in synthesis and characterisation, *Prog. Nucl. Magn. Reson. Spectrosc.* 118–119 (2020) 1–9, <https://doi.org/10.1016/j.pnmrs.2020.02.002>.
- [69] B.F. Chmelka, Materializing opportunities for NMR of solids, *J. Magn. Reson.* 306 (2019) 91–97, <https://doi.org/10.1016/j.jmr.2019.07.051>.
- [70] V. Rántzsch, M. Wilhelm, G. Guthausen, Hyphenated low-field NMR techniques: Combining NMR with NIR, GPC/SEC and rheometry, *Magn. Reson. Chem.* 54 (6) (2016) 494–501, <https://doi.org/10.1002/mrc.4219>.
- [71] R.J. Sullivan, S.G. Newman, Reaction Cycling for Kinetic Analysis in Flow, *J. Org. Chem.* 85 (8) (2020) 5464–5474, <https://doi.org/10.1021/acs.joc.0c00216>.
- [72] S.S. Zaleskiy, E. Danieli, B. Blümich, V.P. Ananikov, Miniaturization of NMR systems: Desktop spectrometers, microcoil spectroscopy, and “NMR on a Chip” for chemistry, biochemistry, and industry, *Chem. Rev.* 114 (11) (2014) 5641–5694, <https://doi.org/10.1021/cr400063g>.
- [73] A.J. Oosthoek-de Vries, P.J. Nieuwland, J. Bart, K. Koch, J.W.G. Janssen, P.J.M. van Buntum, F.P.J.T. Rutjes, H.J.G.E. Gardenius, A.P.M. Kentgens, Inline Reaction Monitoring of Amine-Catalyzed Acetylation of Benzyl Alcohol Using a Microfluidic Stripline Nuclear Magnetic Resonance Setup, *J. Am. Chem. Soc.* 141 (13) (2019) 5369–5380, <https://doi.org/10.1021/jacs.9b00039>.
- [74] J.F. Eccleston, S.R. Martin, M.J. Schilstra, Rapid Kinetic Techniques, *Methods Cell Biol.* 84 (2008) 445–477, [https://doi.org/10.1016/S0091-679X\(07\)84015-5](https://doi.org/10.1016/S0091-679X(07)84015-5).
- [75] T.E. Barman, S.R.W. Bellamy, H. Gutfreund, S.E. Halford, C. Lionne, The identification of chemical intermediates in enzyme catalysis by the rapid quench-flow technique, *Cell. Mol. Life Sci.* 63 (22) (2006) 2571–2583, <https://doi.org/10.1007/s00018-006-6243-z>.
- [76] F. Song, R.D. Cannon, M. Bochmann, Zirconocene-catalyzed propene polymerization: A quenched-flow kinetic study, *J. Am. Chem. Soc.* 125 (2003) 7641–7653, <https://doi.org/10.1021/ja029150v>.
- [77] E.S. Cueny, C.R. Landis, The Hafnium-Pyridyl Amido-Catalyzed Copolymerization of Ethene and 1-Octene: How Small Amounts of Ethene Impact Catalysis, *ACS Catal.* 9 (4) (2019) 3338–3348, <https://doi.org/10.1021/acscatal.9b00250>.
- [78] Y. Yu, R. Cipullo, C. Boisson, Alkynyl Ether Labeling: A Selective and Efficient Approach to Count Active Sites of Olefin Polymerization Catalysts, *ACS Catal.* 9 (4) (2019) 3098–3103, <https://doi.org/10.1021/acscatal.8b04624>.
- [79] C. Lionne, *Encyclopedia of Biophysics*, 2013. Doi: 10.1007/978-3-642-16712-6.
- [80] C.S.G. Seo, R.H. Morris, Catalytic Homogeneous Asymmetric Hydrogenation: Successes and Opportunities, *Organometallics* 38 (1) (2019) 47–65, <https://doi.org/10.1021/acs.organomet.8b00774>.
- [81] S. Kraft, K. Ryan, R.B. Kargbo, Recent Advances in Asymmetric Hydrogenation of Tetrasubstituted Olefins, *J. Am. Chem. Soc.* 139 (34) (2017) 11630–11641, <https://doi.org/10.1021/jacs.7b07188>.
- [82] O. Diebolt, P.W.N.M. van Leeuwen, P.C.J. Kamer, Operando spectroscopy in catalytic carbonylation reactions, *ACS Catal.* 2 (11) (2012) 2357–2370, <https://doi.org/10.1021/cs300471s>.
- [83] A.C. Brezny, C.R. Landis, Recent Developments in the Scope, Practicality, and Mechanistic Understanding of Enantioselective Hydroformylation, *Acc. Chem. Res.* 51 (9) (2018) 2344–2354, <https://doi.org/10.1021/acs.accounts.8b00335>.
- [84] H.-H. Carstensen, A.M. Dean, The Kinetics of Pressure-Dependent Reactions, in: R.W. Carr (Ed.), *Compr. Chem. Kinet.*, Elsevier B.V., Amsterdam, 2007, pp. 101–184, [https://doi.org/10.1016/S0069-8040\(07\)42004-0](https://doi.org/10.1016/S0069-8040(07)42004-0).
- [85] A. Bakac, *Physical Inorganic Chemistry: Principle, Methods, and Models*, John Wiley & Sons Inc, Hoboken, New Jersey, 2010.
- [86] T. Liu, R. Tyburski, S. Wang, R. Fernández-Terán, S. Ott, L. Hammarström, Elucidating Proton-Coupled Electron Transfer Mechanisms of Metal Hydrides with Free Energy- And Pressure-Dependent Kinetics, *J. Am. Chem. Soc.* 141 (43) (2019) 17245–17259, <https://doi.org/10.1021/jacs.9b08189>.
- [87] C.L. Dwyer, High Pressure NMR and IR Spectroscopy in Organometallic Chemistry, in: *Compr. Organomet. Chem. III*, Elsevier, 2007, pp. 483–507, <https://doi.org/10.1016/B0-08-045047-4/00020-0>.

- [88] W. Baumann, S. Mansel, D. Heller, S. Borns, Gas bubbles in the NMR tube: An easy way to investigate reactions with gases in the liquid phase, *Magn. Reson. Chem.* 35 (1997) 701–706, [https://doi.org/10.1002/\(SICI\)1097-458X\(199711\)35:10<701::AID-OMR160>3.0.CO;2-Q](https://doi.org/10.1002/(SICI)1097-458X(199711)35:10<701::AID-OMR160>3.0.CO;2-Q).
- [89] I.T. Horvath, J.M. Millar, NMR under high gas pressure, *Chem. Rev.* 91 (7) (1991) 1339–1351, <https://doi.org/10.1021/cr00007a003>.
- [90] Y. Atomi, High Pressure Bioscience, in: K. Akasaka, H. Matsuki (Eds.), High Press. Biosci. Basic Concepts, Appl. Front., Springer Netherlands, Dordrecht, 2015, pp. 627–659, <https://doi.org/10.1007/978-94-017-9918-8>.
- [91] N.J. Beach, S.M.M. Knapp, C.R. Landis, A reactor for high-throughput high-pressure nuclear magnetic resonance spectroscopy, *Rev. Sci. Instrum.* 86 (10) (2015) 104101, <https://doi.org/10.1063/1.4932676>.
- [92] A. Torres, N. Molina Perez, G. Overend, N. Hodge, B.T. Heaton, J.A. Iggo, J. Satherley, R. Whyman, G.R. Eastham, D. Gobby, High-pressure in situ NMR methods for the study of reaction kinetics in homogeneous catalysis, *ACS Catal.* 2 (11) (2012) 2281–2289, <https://doi.org/10.1021/cs300439n>.
- [93] J.N. Jaworski, C.V. Kozack, S.J. Tereniak, S.M.M. Knapp, C.R. Landis, J.T. Miller, S.S. Stahl, Operando Spectroscopic and Kinetic Characterization of Aerobic Allylic C-H Acetoxylation Catalyzed by Pd(OAc)₂/4,5-Diazafluoren-9-one, *J. Am. Chem. Soc.* 141 (26) (2019) 10462–10474, <https://doi.org/10.1021/jacs.9b04699>.
- [94] A.M. Wright, D.R. Pahls, J.B. Gary, T. Warner, J.Z. Williams, S.M.M. Knapp, K.E. Allen, C.R. Landis, T.R. Cundari, K.I. Goldberg, Experimental and Computational Investigation of the Aerobic Oxidation of a Late Transition Metal-Hydride, *J. Am. Chem. Soc.* 141 (27) (2019) 10830–10843, <https://doi.org/10.1021/jacs.9b04706>.
- [95] A.C. Brezny, C.R. Landis, Unexpected CO Dependencies, Catalyst Speciation, and Single Turnover Hydrogenolysis Studies of Hydroformylation via High Pressure NMR Spectroscopy, *J. Am. Chem. Soc.* 139 (7) (2017) 2778–2785, <https://doi.org/10.1021/jacs.6b12533>.
- [96] A.C. Brezny, C.R. Landis, Development of a Comprehensive Microkinetic Model for Rh(bis(diaza phospholane))-Catalyzed Hydroformylation, *ACS Catal.* 9 (3) (2019) 2501–2513, <https://doi.org/10.1021/acscatal.9b00173>.
- [97] P. Nitschke, N. Lokesh, R.M. Gschwind, Combination of illumination and high resolution NMR spectroscopy: Key features and practical aspects, photochemical applications, and new concepts, *Prog. Nucl. Magn. Reson. Spectrosc.* 114–115 (2019) 86–134, <https://doi.org/10.1016/j.pnmrs.2019.06.001>.
- [98] G.E. Ball, In situ photochemistry with NMR detection of organometallic complexes, in: J. Yarwood, R. Douthwaite, S. Duckett (Eds.), *Spectrosc. Prop. Inorg. Organomet. Compd. Tech. Mater. Appl.*, vol. 41, The Royal Society of Chemistry, Cambridge, UK, 2010, pp. 262–287, <https://doi.org/10.1039/9781849730853-00262>.
- [99] I. Kuprov, P.J. Hore, Uniform illumination of optically dense NMR samples, *J. Magn. Reson.* 171 (1) (2004) 171–175, <https://doi.org/10.1016/j.jmr.2004.08.017>.
- [100] C. Feldmeier, H. Bartling, E. Riedle, R.M. Gschwind, LED based NMR illumination device for mechanistic studies on photochemical reactions - Versatile and simple, yet surprisingly powerful, *J. Magn. Reson.* 232 (2013) 39–44, <https://doi.org/10.1016/j.jmr.2013.04.011>.
- [101] Y. Ji, D.A. DiRocco, J. Kind, C.M. Thiele, R.M. Gschwind, M. Reibarkh, LED-Illuminated NMR Spectroscopy: A Practical Tool for Mechanistic Studies of Photochemical Reactions, *ChemPhotoChem* 3 (10) (2019) 984–992, <https://doi.org/10.1002/cptc.201900109>.
- [102] D. Lehnher, Y. Ji, A.J. Neel, R.D. Cohen, A.P.J. Brunskill, J. Yang, M. Reibarkh, Discovery of a Photoinduced Dark Catalytic Cycle Using in Situ LED-NMR Spectroscopy, *J. Am. Chem. Soc.* 140 (42) (2018) 13843–13853, <https://doi.org/10.1021/jacs.8b08596>.
- [103] A. Seegerer, P. Nitschke, R.M. Gschwind, Combined In Situ Illumination-NMR-UV/Vis Spectroscopy: A New Mechanistic Tool in Photochemistry, *Angew. Chemie - Int. Ed.* 57 (2018) 7493–7497, <https://doi.org/10.1002/anie.201801250>.
- [104] C. Sandford, M.A. Edwards, K.J. Klunder, D.P. Hickey, M. Li, K. Barman, M.S. Sigman, H.S. White, S.D. Minter, A synthetic chemist's guide to electroanalytical tools for studying reaction mechanisms, *Chem. Sci.* 10 (26) (2019) 6404–6422.
- [105] Y.J. Tong, In situ electrochemical nuclear magnetic resonance spectroscopy for electrocatalysis: Challenges and prospects, *Curr. Opin. Electrochem.* 4 (1) (2017) 60–68, <https://doi.org/10.1016/j.coelec.2017.09.017>.
- [106] Z.-R. Ni, X.-H. Cui, S.-H. Cao, Z. Chen, A novel in situ electrochemical NMR cell with a palisade gold film electrode, *AIP Adv.* 7 (8) (2017) 085205, <https://doi.org/10.1063/1.4997887>.
- [107] S.-H. Cao, Z.-R. Ni, L. Huang, H.-J. Sun, B. Tang, L.-J. Lin, Y.-Q. Huang, Z.-Y. Zhou, S.-G. Sun, Z. Chen, In Situ Monitoring Potential-Dependent Electrochemical Process by Liquid NMR Spectroelectrochemical Determination: A Proof-of-Concept Study, *Anal. Chem.* 89 (7) (2017) 3810–3813, <https://doi.org/10.1021/acs.analchem.7b00249>.
- [108] P.F. da Silva, B.F. Gomes, C.M.S. Lobo, L.H.K. Queiroz Júnior, E. Danieli, M. Carmo, B. Blümich, L.A. Colnago, Electrochemical NMR spectroscopy: Electrode construction and magnetic sample stirring, *Microchem. J.* 146 (2019) 658–663, <https://doi.org/10.1016/j.microc.2019.01.010>.
- [109] B.F. Gomes, L.M.S. Nunes, C.M.S. Lobo, L.F. Cabeça, L.A. Colnago, In situ study of the magnetoelectrolysis phenomenon during copper electrodeposition using time domain NMR relaxometry, *Anal. Chem.* 86 (19) (2014) 9391–9393, <https://doi.org/10.1021/ac502361q>.
- [110] B. Gomes, C. Lobo, L. Colnago, Monitoring electrochemical reactions in situ with low field NMR: A mini-review, *Appl. Sci.* 9 (3) (2019) 498, <https://doi.org/10.3390/app9030498>.
- [111] S.-H. Cao, S. Liu, H.-J. Sun, L. Huang, Z.-R. Ni, W.-L. Jiang, M. Zhan, Z.-Y. Zhou, S.-G. Sun, Z. Chen, Versatile, Robust, and Facile Approach for in Situ Monitoring Electrocatalytic Processes through Liquid Electrochemical NMR Spectroscopy, *Anal. Chem.* 91 (3) (2019) 1686–1691, <https://doi.org/10.1021/acs.analchem.8b04006>.
- [112] U. Bussy, M. Boujtita, Review of advances in coupling electrochemistry and liquid state NMR, *Talanta* 136 (2015) 155–160, <https://doi.org/10.1016/j.talanta.2014.08.033>.
- [113] X.-P. Zhang, W.-L. Jiang, S.-H. Cao, H.-J. Sun, X.-Q. You, S.-H. Cai, J.-L. Wang, C.-S. Zhao, X. Wang, Z. Chen, S.-G. Sun, NMR spectroelectrochemistry in studies of hydroquinone oxidation by polyaniline thin films, *Electrochim. Acta* 273 (2018) 300–306, <https://doi.org/10.1016/j.electacta.2018.04.048>.
- [114] R. Boisseau, U. Bussy, P. Giraudeau, M. Boujtita, In situ ultrafast 2D NMR spectroelectrochemistry for real-time monitoring of redox reactions, *Anal. Chem.* 87 (1) (2015) 372–375, <https://doi.org/10.1021/ac5041956>.
- [115] B. Ferreira Gomes, F.J. Holzäuser, C.M. Silva Lobo, P. Ferreira da Silva, E. Danieli, M. Carmo, L.A. Colnago, S. Palkovits, R. Palkovits, B. Blümich, Sustainable Electrocoupling of the Biogenic Valeric Acid under in Situ Low-Field Nuclear Magnetic Resonance Conditions, *ACS Sustain. Chem. Eng.* 7 (22) (2019) 18288–18296, <https://doi.org/10.1021/acssuschemeng.9b02768>.
- [116] S.K. Küster, E. Danieli, B. Blümich, F. Casanova, High-resolution NMR spectroscopy under the fume hood, *Phys. Chem. Chem. Phys.* 13 (2011) 13172–13176, <https://doi.org/10.1039/c1cp21180c>.
- [117] R.L. Haner, P.A. Keifer, Flow Probes for NMR Spectroscopy, *Encycl. Magn. Reson.* (2009) 1–11, <https://doi.org/10.1002/9780470034590.emrstm1085>.
- [118] M.V. Gomez, A. De La Hoz, NMR reaction monitoring in flow synthesis, *Beilstein J. Org. Chem.* 13 (2017) 285–300, <https://doi.org/10.3762/bjoc.13.31>.
- [119] E. von Harbou, R. Behrens, J. Berje, A. Brächer, H. Hasse, Studying Fast Reaction Kinetics with Online NMR Spectroscopy, *Chemie-Ingenieur-Technik* 89 (2017) 369–378, <https://doi.org/10.1002/cite.201600068>.
- [120] M. Khajeh, M.A. Bernstein, G.A. Morris, A simple flowcell for reaction monitoring by NMR, *Magn. Reson. Chem.* 48 (7) (2010) 516–522, <https://doi.org/10.1002/mrc.2610>.
- [121] D.A. Foley, E. Bez, A. Codina, K.L. Colson, M. Fey, R. Krull, D. Piroli, M.T. Zell, B. L. Marquez, NMR flow tube for online NMR reaction monitoring, *Anal. Chem.* 86 (24) (2014) 12008–12013, <https://doi.org/10.1021/ac502300q>.
- [122] J. Bart, A.J. Kolkman, A.J. Oosthoek-de Vries, K. Koch, P.J. Nieuwland, H.J.W.G. Janssen, J.P.J.M. van Bentum, K.A.M. Ampt, F.P.J.T. Rutjes, S.S. Wijmenga, H.J.G. E. Gardeniers, A.P.M. Kentgens, A Microfluidic High-Resolution NMR Flow Probe, *J. Am. Chem. Soc.* 131 (14) (2009) 5014–5015, <https://doi.org/10.1021/ja900389x>.
- [123] G. Finch, A. Yilmaz, M. Utz, An optimised detector for in-situ high-resolution NMR in microfluidic devices, *J. Magn. Reson.* 262 (2016) 73–80, <https://doi.org/10.1016/j.jmr.2015.11.011>.
- [124] A.J. Oosthoek-de Vries, J. Bart, R.M. Tiggelaar, J.W.G. Janssen, P.J.M. van Bentum, H.J.G.E. Gardeniers, A.P.M. Kentgens, Continuous Flow 1 H and 13 C NMR Spectroscopy in Microfluidic Stripline NMR Chips, *Anal. Chem.* 89 (4) (2017) 2296–2303, <https://doi.org/10.1021/acs.analchem.6b03784>.
- [125] I. Swyer, S. von der Ecken, B. Wu, A. Jenne, R. Soong, F. Vincent, D. Schmidig, T. Frei, F. Busse, H.J. Stronks, A.J. Simpson, A.R. Wheeler, Digital microfluidics and nuclear magnetic resonance spectroscopy for in situ diffusion measurements and reaction monitoring, *Lab Chip* 19 (4) (2019) 641–653, <https://doi.org/10.1039/C8LC01214H>.
- [126] A. Chanda, A.M. Daly, D.A. Foley, M.A. LaPack, S. Mukherjee, J.D. Orr, G.L. Reid, D.R. Thompson, H.W. Ward, Industry perspectives on process analytical technology: Tools and applications in API development, *Org. Process Res. Dev.* 19 (1) (2015) 63–83, <https://doi.org/10.1021/op400358b>.
- [127] K.C.H. Tijssen, B.J.A. van Weerdenburg, H. Zhang, J.W.G. Janssen, M.C. Feiters, P.J.M. van Bentum, A.P.M. Kentgens, Monitoring Heterogeneously Catalyzed Hydrogenation Reactions at Elevated Pressures Using In-Line Flow NMR, *Anal. Chem.* 91 (20) (2019) 12636–12643, <https://doi.org/10.1021/acs.analchem.9b00895>.
- [128] M.T. Drexler, D.A. Foley, H.W. Ward, H.J. Clarke, IR and NMR Reaction Monitoring Techniques for Nucleophilic Addition Reactions. In Situ Monitoring of the Addition of Benzimidazole to a Pyridinium Salt, *Org. Process Res. Dev.* 19 (9) (2015) 1119–1127, <https://doi.org/10.1021/acs.oprd.5b00029>.
- [129] D.A. Foley, J. Wang, B. Maranzano, M.T. Zell, B.L. Marquez, Y. Xiang, G.L. Reid, Online NMR and HPLC as a reaction monitoring platform for pharmaceutical process development, *Anal. Chem.* 85 (19) (2013) 8928–8932, <https://doi.org/10.1021/ac402382d>.
- [130] D.A. Foley, C.W. Doecke, J.Y. Buser, J.M. Merritt, L. Murphy, M. Kissane, S.G. Collins, A.R. Maguire, A. Kaerner, ReactNMR and reactIR as reaction monitoring and mechanistic elucidation tools: The NCS mediated cascade reaction of α -thioamides to α -thio- β -chloroacrylamides, *J. Org. Chem.* 76 (23) (2011) 9630–9640, <https://doi.org/10.1021/jo201212p>.
- [131] I.D. Wilson, Hypernation and Concatenation, in: *NMR Spectrosc. Pharm. Anal.*, Elsevier, Amsterdam, 2008, pp. 449–469, <https://doi.org/10.1016/B978-0-444-53173-5.00019-6>.
- [132] M.V.S. Eilipe, Application of hypernated NMR in industry, *Nucl. Magn. Reson.* 45 (2016) 190–216, <https://doi.org/10.1039/9781782624103-00190>.

- [133] M. Maiwald, H.H. Fischer, Y.-K. Kim, K. Albert, H. Hasse, Quantitative high-resolution on-line NMR spectroscopy in reaction and process monitoring, *J. Magn. Reson.* 166 (2) (2004) 135–146, <https://doi.org/10.1016/j.jmr.2003.09.003>.
- [134] D.W. Jones, T.F. Child, NMR in Flowing Systems, in: *Adv. Magn. Opt. Reson.*, Academic Press Inc., New York, 1976, pp. 123–148, <https://doi.org/10.1016/B978-0-12-025508-5.50008-6>.
- [135] E. Bayer, K. Albert, Continuous-flow carbon-13 nuclear magnetic resonance spectroscopy, *J. Chromatogr. A* 312 (1984) 91–97, [https://doi.org/10.1016/S0021-9673\(01\)92766-9](https://doi.org/10.1016/S0021-9673(01)92766-9).
- [136] C.L. Perrin, I.A. Rivero, Apparatus for direct addition of reagents into a nuclear magnetic resonance (NMR) sample in the NMR probe, *Rev. Sci. Instrum.* 70 (4) (1999) 2173–2174, <https://doi.org/10.1063/1.1149737>.
- [137] S.E. Denmark, B.J. Williams, B.M. Eklov, S.M. Pham, G.L. Beutner, Design, validation, and implementation of a rapid-injection NMR system, *J. Org. Chem.* 75 (16) (2010) 5558–5572, <https://doi.org/10.1021/jo100837a>.
- [138] J.F. McGarrity, J. Prodoliet, T. Smyth, Rapid injection NMR: A simple technique for the observation of reactive intermediates, *Org. Magn. Reson.* 17 (1) (1981) 59–65, <https://doi.org/10.1002/mrc.1270170114>.
- [139] K.H. Mok, T. Nagashima, I.J. Day, J.A. Jones, C.J.V. Jones, C.M. Dobson, P.J. Hore, Rapid sample-mixing technique for transient NMR and photo-CIDNP spectroscopy: Applications to real-time protein folding, *J. Am. Chem. Soc.* 125 (2003) 12484–12492, <https://doi.org/10.1021/ja036357v>.
- [140] A.C. Jones, A.W. Sanders, M.J. Bevan, H.J. Reich, Reactivity of individual organolithium aggregates: A RINMR study of *n*-butyllithium and 2-methoxy-6-(methoxymethyl)phenyllithium, *J. Am. Chem. Soc.* 129 (2007) 3492–3493, <https://doi.org/10.1021/ja0689334>.
- [141] A. Gomez-Hens, D. Perez-Bendito, The stopped-flow technique in analytical chemistry, *Anal. Chim. Acta* 242 (1991) 147–177, [https://doi.org/10.1016/0003-2670\(91\)87060-K](https://doi.org/10.1016/0003-2670(91)87060-K).
- [142] R.O. Kühne, T. Schaffhauser, A. Wokaun, R.R. Ernst, Study of transient chemical reactions by NMR. Fast stopped-flow fourier transform experiments, *J. Magn. Reson.* 35 (1) (1979) 39–67, [https://doi.org/10.1016/0022-2364\(79\)90077-5](https://doi.org/10.1016/0022-2364(79)90077-5).
- [143] M.D. Christianson, E.H.P. Tan, C.R. Landis, Stopped-flow NMR: Determining the kinetics of [rac-(C₂H₄(-indeny)2)ZrMe][MeB(C₆F₅)₃]-catalyzed polymerization of 1-hexene by direct observation, *J. Am. Chem. Soc.* 132 (33) (2010) 11461–11463, <https://doi.org/10.1021/ja105107y>.
- [144] A.L. Dunn, C.R. Landis, Progress toward reaction monitoring at variable temperatures: a new stopped-flow NMR probe design, *Magn. Reson. Chem.* 55 (2017) 329–336, <https://doi.org/10.1002/mrc.4538>.
- [145] M.D. Christianson, C.R. Landis, Generalized treatment of NMR spectra for rapid chemical reactions, *Concepts Magn. Reson. Part A* 30A (4) (2007) 165–183, <https://doi.org/10.1002/cmr.a.20090>.
- [146] T.C. Eizenschmid, R.U. Kirss, P.P. Deutsch, S.I. Hommeltoft, R. Eisenberg, J. Bargon, R.G. Lawler, A.L. Balch, Para Hydrogen Induced Polarization in Hydrogenation Reactions, *J. Am. Chem. Soc.* 109 (26) (1987) 8089–8091, <https://doi.org/10.1021/ja00260a026>.
- [147] O. Semenova, P.M. Richardson, A.J. Parrott, A. Nordon, M.E. Halse, S.B. Duckett, Reaction Monitoring Using SABRE-Hyperpolarized Benchtop (1 T) NMR Spectroscopy, *Anal. Chem.* 91 (10) (2019) 6695–6701, <https://doi.org/10.1021/acs.analchem.9b00729>.
- [148] U.L. Günther, Dynamic Nuclear Hyperpolarization in Liquids, in: H. Heise, S. Matthews (Eds.), *Mod. NMR Methodol.*, Springer, Berlin, Heidelberg, 2011, pp. 23–69, https://doi.org/10.1007/128_2011_229.
- [149] G. Zhang, F. Schilling, S.J. Glaser, C. Hilty, Reaction monitoring using hyperpolarized NMR with scaling of heteronuclear couplings by optimal tracking, *J. Magn. Reson.* 272 (2016) 123–128, <https://doi.org/10.1016/j.jmr.2016.09.006>.
- [150] H. Zeng, Y. Lee, C. Hilty, Quantitative rate determination by dynamic nuclear polarization enhanced NMR of a diels-alder reaction, *Anal. Chem.* 82 (21) (2010) 8897–8902, <https://doi.org/10.1021/ac101670n>.
- [151] J.F. McGarrity, J. Prodoliet, High-Field Rapid Injection NMR: Observation of Unstable Primary Ozonide Intermediates, *J. Org. Chem.* 49 (23) (1984) 4465–4470, <https://doi.org/10.1021/jo00197a027>.
- [152] J. Grimaldi, J. Baldo, C. McMurray, B.D. Sykes, Stopped-Flow Nuclear Magnetic Resonance Spectroscopy, *J. Am. Chem. Soc.* 94 (22) (1972) 7641–7645, <https://doi.org/10.1021/ja00777a006>.
- [153] S. Funahashi, K. Ishihara, S.-I. Aizawa, T. Sugata, M. Ishii, Y. Inada, M. Tanaka, High-pressure stopped-flow nuclear magnetic resonance apparatus for the study of fast reactions in solution, *Rev. Sci. Instrum.* 64 (1) (1993) 130–134, <https://doi.org/10.1063/1.1144426>.
- [154] D.J. Cookson, B.E. Smith, Optimal conditions for obtaining quantitative ¹³C NMR, data, *J. Magn. Reson.* 57 (3) (1984) 355–368, [https://doi.org/10.1016/0022-2364\(84\)90253-1](https://doi.org/10.1016/0022-2364(84)90253-1).
- [155] G. Pintacuda, G. Otting, Identification of protein surfaces by NMR measurements with a paramagnetic Gd(III) chelate, *J. Am. Chem. Soc.* 124 (3) (2002) 372–373, <https://doi.org/10.1021/ja016985h>.
- [156] T. Madl, W. Bermel, K. Zangger, Use of relaxation enhancements in a paramagnetic environment for the structure determination of proteins using NMR spectroscopy, *Angew. Chemie – Int. Ed.* 48 (44) (2009) 8259–8262, <https://doi.org/10.1002/anie.200902561>.
- [157] L. Rouger, B. Charrier, M. Pathan, S. Akoka, P. Giraudeau, Processing strategies to obtain clean interleaved ultrafast 2D NMR spectra, *J. Magn. Reson.* 238 (2014) 87–93, <https://doi.org/10.1016/j.jmr.2013.11.008>.
- [158] D.B.G. Berry, A. Codina, I. Clegg, C.L. Lyall, J.P. Lowe, U. Hintermair, Insight into catalyst speciation and hydrogen co-evolution during enantioselective formic acid-driven transfer hydrogenation with bifunctional ruthenium complexes from multi-technique operando reaction monitoring, *Faraday Discuss.* 220 (2019) 45–57, <https://doi.org/10.1039/C9FD00060G>.
- [159] R.L. Vold, J.S. Waugh, M.P. Klein, D.E. Phelps, Measurement of Spin Relaxation in Complex Systems, *J. Chem. Phys.* 48 (8) (1968) 3831–3832, <https://doi.org/10.1063/1.1669699>.
- [160] R. Freeman, H.D.W. Hill, High-resolution studies of nuclear spin-lattice relaxation, *J. Chem. Phys.* 51 (7) (1969) 3140–3141, <https://doi.org/10.1063/1.1672474>.
- [161] R. Freeman, H.D.W. Hill, Fourier Transform Study of NMR Spin-Lattice Relaxation by “Progressive Saturation”, *J. Chem. Phys.* 54 (8) (1971) 3367–3377, <https://doi.org/10.1063/1.1675352>.
- [162] P.W. Percival, J.S. Hyde, Saturation-recovery measurements of the spin-lattice relaxation times of some nitroxides in solution, *J. Magn. Reson.* 23 (2) (1976) 249–257, [https://doi.org/10.1016/0022-2364\(76\)90206-7](https://doi.org/10.1016/0022-2364(76)90206-7).
- [163] R. Wei, C.L. Dickson, G.C. Lloyd-Jones, FLIPS – rapid estimation of T1 for quantitative NMR, *J. Org. Chem.* 86 (2021) 9023–9029, <https://doi.org/10.1021/acs.joc.1c01007>.
- [164] J.N. Dumez, Spatial encoding and spatial selection methods in high-resolution NMR spectroscopy, *Prog. Nucl. Magn. Reson. Spectrosc.* 109 (2018) 101–134, <https://doi.org/10.1016/j.pnmrs.2018.08.001>.
- [165] G.E. Wagner, P. Sakhaii, W. Bermel, K. Zangger, Monitoring fast reactions by spatially-selective and frequency-shifted continuous NMR spectroscopy: Application to rapid-injection protein unfolding, *Chem. Commun.* 49 (2013) 3155–3157, <https://doi.org/10.1039/c3cc39107h>.
- [166] F. Malz, H. Jancke, Validation of quantitative NMR, *J. Pharm. Biomed. Anal.* 38 (5) (2005) 813–823, <https://doi.org/10.1016/j.jpba.2005.01.043>.
- [167] D.J. Russell, C.E. Hadden, G.E. Martin, A.A. Gibson, A.P. Zens, J.L. Carolan, A comparison of inverse-detected heteronuclear NMR performance: Conventional vs cryogenic microprobe performance, *J. Nat. Prod.* 63 (2000) 1047–1049, <https://doi.org/10.1021/np0003140>.
- [168] R.R. Ernst, W.A. Anderson, Application of fourier transform spectroscopy to magnetic resonance, *Rev. Sci. Instrum.* 37 (1) (1966) 93–102, <https://doi.org/10.1063/1.1719961>.
- [169] G.N. Chmurny, D.I. Hoult, The Ancient and Honourable Art of Shimming, *Concepts Magn. Reson.* 2 (3) (1990) 131–149, <https://doi.org/10.1002/cmr.1820020303>.
- [170] A.M. Torres, W.S. Price, Common problems and artifacts encountered in solution-state NMR experiments, *Concepts Magn. Reson. Part A* 45A (2) (2016) e21387, <https://doi.org/10.1002/cmr.a.21387>.
- [171] H. Mo, J.S. Harwood, D. Raftery, Receiver gain function: The actual NMR receiver gain, *Magn. Reson. Chem.* 48 (3) (2010) 235–238, <https://doi.org/10.1002/mrc.2563>.
- [172] J.E. Power, M. Foroozandeh, R.W. Adams, M. Nilsson, S.R. Coombes, A.R. Phillips, G.A. Morris, Increasing the quantitative bandwidth of NMR measurements, *Chem. Commun.* 52 (14) (2016) 2916–2919, <https://doi.org/10.1039/C5CC10206E>.
- [173] M. Foroozandeh, M. Nilsson, G.A. Morris, Improved ultra-broadband chirp excitation, *J. Magn. Reson.* 302 (2019) 28–33, <https://doi.org/10.1016/j.jmr.2019.03.007>.
- [174] A.J. Shaka, P.B. Barker, R. Freeman, Computer-optimized decoupling scheme for wideband applications and low-level operation, *J. Magn. Reson.* 64 (3) (1985) 547–552, [https://doi.org/10.1016/0022-2364\(85\)90122-2](https://doi.org/10.1016/0022-2364(85)90122-2).
- [175] A.J. Shaka, J. Keeler, T. Frenkiel, R. Freeman, An improved sequence for broadband decoupling: WALTZ-16, *J. Magn. Reson.* 52 (2) (1983) 335–338, [https://doi.org/10.1016/0022-2364\(83\)90207-X](https://doi.org/10.1016/0022-2364(83)90207-X).
- [176] D. Marion, A. Bax, Baseline correction of 2D FT NMR spectra using a simple linear prediction extrapolation of the time-domain data, *J. Magn. Reson.* 83 (1) (1989) 205–211, [https://doi.org/10.1016/0022-2364\(89\)90307-7](https://doi.org/10.1016/0022-2364(89)90307-7).
- [177] G.A. Pearson, A general baseline-recognition and baseline-flattening algorithm, *J. Magn. Reson.* 27 (2) (1977) 265–272, [https://doi.org/10.1016/0022-2364\(77\)90076-2](https://doi.org/10.1016/0022-2364(77)90076-2).
- [178] D. Chang, C.D. Banack, S.L. Shah, Robust baseline correction algorithm for signal dense NMR spectra, *J. Magn. Reson.* 187 (2) (2007) 288–292, <https://doi.org/10.1016/j.jmr.2007.05.008>.
- [179] P. Güntert, K. Wüthrich, FLATT—A new procedure for high-quality baseline correction of multidimensional NMR spectra, *J. Magn. Reson.* 96 (2) (1992) 403–407, [https://doi.org/10.1016/0022-2364\(92\)90095-0](https://doi.org/10.1016/0022-2364(92)90095-0).
- [180] P. Moutzouri, P. Kiraly, A.R. Phillips, S.R. Coombes, M. Nilsson, G.A. Morris, 13C Satellite-Free 1H NMR Spectra, *Anal. Chem.* 89 (22) (2017) 11898–11901, <https://doi.org/10.1021/acs.analchem.7b03787>.
- [181] R. Stoyanova, T.R. Brown, NMR spectral quantitation by principal component analysis, *NMR Biomed.* 14 (4) (2001) 271–277, <https://doi.org/10.1002/nbm.700>.
- [182] E. Kristen, F. Alsmeyer, A. Bardow, W. Marquardt, Fully automated indirect hard modeling of mixture spectra, *Chemom. Intell. Lab. Syst.* 91 (2) (2008) 181–193, <https://doi.org/10.1016/j.chemolab.2007.11.004>.
- [183] N. Zientek, C. Laurain, K. Meyer, A. Paul, D. Engel, G. Guthausen, M. Kraume, M. Maiwald, Automated data evaluation and modelling of simultaneous 19F-1H medium-resolution NMR spectra for online reaction monitoring, *Magn. Reson. Chem.* 54 (6) (2016) 513–520, <https://doi.org/10.1002/mrc.4216>.
- [184] G.A. Morris, Reference Deconvolution, *eMagRes* 9 (2007) 125–131, <https://doi.org/10.1002/9780470034590.emrstm0449>.

- [185] K. Zangger, Pure shift NMR, *Prog. Nucl. Magn. Reson. Spectrosc.* 86–87 (2015) 1–20, <https://doi.org/10.1016/j.pnmrs.2015.02.002>.
- [186] L. Castañar, Pure shift 1H NMR: what is next?, *Magn. Reson. Chem.* 55 (1) (2017) 47–53, <https://doi.org/10.1002/mrc.4545>.
- [187] J.R. Garbow, D.P. Weitekamp, A. Pines, Bilinear rotation decoupling of homonuclear scalar interactions, *Chem. Phys. Lett.* 93 (5) (1982) 504–509, [https://doi.org/10.1016/0009-2614\(82\)83229-6](https://doi.org/10.1016/0009-2614(82)83229-6).
- [188] K. Zangger, H. Sterk, Homonuclear Broadband-Decoupled NMR Spectra, *J. Magn. Reson.* 124 (2) (1997) 486–489, <https://doi.org/10.1006/jmre.1996.1063>.
- [189] R.W. Adams, L. Byrne, P. Király, M. Foroozandeh, L. Paudel, M. Nilsson, J. Clayden, G.A. Morris, Diastereomeric ratio determination by high sensitivity band-selective pure shift NMR spectroscopy, *Chem. Commun.* 50 (19) (2014) 2512–2514, <https://doi.org/10.1039/c3cc49659g>.
- [190] A.B. Jones, G.C. Lloyd-Jones, D. Uhrin, SHARPER Reaction Monitoring: Generation of a Narrow Linewidth NMR Singlet, without X-Pulses, in an Inhomogeneous Magnetic Field, *Anal. Chem.* 89 (18) (2017) 10013–10021, <https://doi.org/10.1021/acs.analchem.7b02437>.
- [191] M. Foroozandeh, G.A. Morris, M. Nilsson, PSYCHE Pure Shift NMR Spectroscopy, *Chem. - A Eur. J.* 24 (53) (2018) 13988–14000, <https://doi.org/10.1002/chem.201800524>.
- [192] T.D.W. Claridge, *Introducing Two-Dimensional and Pulsed Field Gradient NMR*, in: *High-Resolution NMR Tech. Org. Chem.*, third ed., Elsevier, Amsterdam, London, 2016, pp. 171–202, <https://doi.org/10.1016/B978-0-08-099986-9.00005-1>.
- [193] S. Braun, H.-O. Kalinowski, S. Berger, *150 and More Basic NMR Experiments: A Practical Course, Second Exp.*, Wiley-VCH, Weinheim, Chichester, 1998.
- [194] P. Giraudeau, Quantitative 2D liquid-state NMR, *Magn. Reson. Chem.* 52 (6) (2014) 259–272, <https://doi.org/10.1002/mrc.4068>.
- [195] S.R. Davies, K. Jones, A. Goldys, M. Alamgir, B.K.H. Chan, C. Elgindy, P.S.R. Mitchell, G.J. Tarrant, M.R. Krishnaswami, Y. Luo, M. Moawad, D. Lawes, J.M. Hook, Purity assessment of organic chemical standards using a combination of quantitative NMR and mass balance, *Anal. Bioanal. Chem.* 407 (11) (2015) 3103–3113, <https://doi.org/10.1007/s00216-014-7893-6>.
- [196] R.K. Rai, P. Tripathi, N. Sinha, Quantification of Metabolites from Two-Dimensional Nuclear Magnetic Resonance Spectroscopy: Application to Human Urine Samples, *Anal. Chem.* 81 (24) (2009) 10232–10238, <https://doi.org/10.1021/ac902405z>.
- [197] S. Heikkinen, M.M. Toikka, P.T. Karhunen, I.A. Kilpeläinen, Quantitative 2D HSQC (Q-HSQC) via suppression of J-dependence of polarization transfer in NMR spectroscopy: Application to wood lignin, *J. Am. Chem. Soc.* 125 (2003) 4362–4367, <https://doi.org/10.1021/ja029035k>.
- [198] D.J. Peterson, N.M. Loening, QQ-HSQC: a quick, quantitative heteronuclear correlation experiment for NMR spectroscopy, *Magn. Reson. Chem.* 45 (11) (2007) 937–941, <https://doi.org/10.1002/mrc.2073>.
- [199] H. Koskela, I. Kilpeläinen, S. Heikkinen, Some aspects of quantitative 2D NMR, *J. Magn. Reson.* 174 (2) (2005) 237–244, <https://doi.org/10.1016/j.jmr.2005.02.002>.
- [200] H. Koskela, O. Heikkilä, I. Kilpeläinen, S. Heikkinen, Quantitative two-dimensional HSQC experiment for high magnetic field NMR spectrometers, *J. Magn. Reson.* 202 (1) (2010) 24–33, <https://doi.org/10.1016/j.jmr.2009.09.021>.
- [201] K. Hu, W.M. Westler, J.L. Markley, Simultaneous Quantification and Identification of Individual Chemicals in Metabolite Mixtures by Two-Dimensional Extrapolated Time-Zero 1H–13C HSQC (HSQC 0), *J. Am. Chem. Soc.* 133 (6) (2011) 1662–1665, <https://doi.org/10.1021/ja1095304>.
- [202] R.A. Chylla, K. Hu, J.J. Ellinger, J.L. Markley, Deconvolution of two-dimensional NMR spectra by fast maximum likelihood reconstruction: Application to quantitative metabolomics, *Anal. Chem.* 83 (12) (2011) 4871–4880, <https://doi.org/10.1021/ac200536b>.
- [203] F. Fardus-Reid, J. Warren, A. Le Gresley, Validating heteronuclear 2D quantitative NMR, *Anal. Methods* 8 (9) (2016) 2013–2019.
- [204] S.G. Hyberts, K. Takeuchi, G. Wagner, Poisson-gap sampling and forward maximum entropy reconstruction for enhancing the resolution and sensitivity of protein NMR data, *J. Am. Chem. Soc.* 132 (7) (2010) 2145–2147, <https://doi.org/10.1021/ja908004w>.
- [205] P.J. Sidebottom, A new approach to the optimisation of non-uniform sampling schedules for use in the rapid acquisition of 2D NMR spectra of small molecules, *Magn. Reson. Chem.* 54 (8) (2016) 689–694, <https://doi.org/10.1002/mrc.4444>.
- [206] I.E. Ndukwe, A. Shchukina, K. Kazimierczuk, C. Cobas, C.P. Butts, Extended Acquisition Time (EXACT) NMR-A Case for 'Burst' Non-Uniform Sampling, *ChemPhysChem.* 17 (18) (2016) 2799–2803, <https://doi.org/10.1002/cphc.201600541>.
- [207] D. Gołowicz, P. Kasprzak, V. Orekhov, K. Kazimierczuk, Fast time-resolved NMR with non-uniform sampling, *Prog. Nucl. Magn. Reson. Spectrosc.* 116 (2020) 40–55, <https://doi.org/10.1016/j.pnmrs.2019.09.003>.
- [208] R. Dass, W. Koźmiński, K. Kazimierczuk, Analysis of complex reacting mixtures by time-resolved 2d NMR, *Anal. Chem.* 87 (2) (2015) 1337–1343, <https://doi.org/10.1021/ac504114h>.
- [209] M. Mayzel, J. Rosenlöw, L. Isaksson, V.Y. Orekhov, Time-resolved multidimensional NMR with non-uniform sampling, *J. Biomol. NMR.* 58 (2) (2014) 129–139, <https://doi.org/10.1007/s10858-013-9811-1>.
- [210] P. Schanda, Fast-pulsing longitudinal relaxation optimized techniques: Enriching the toolbox of fast biomolecular NMR spectroscopy, *Prog. Nucl. Magn. Reson. Spectrosc.* 55 (3) (2009) 238–265.
- [211] T. Diercks, M. Daniels, R. Kaptein, Extended Flip-back Schemes for Sensitivity Enhancement in Multidimensional HSQC-type Out-and-back Experiments, *J. Biomol. NMR* 33 (4) (2005) 243–259, <https://doi.org/10.1007/s10858-005-3868-4>.
- [212] P. Schanda, B. Brutscher, Very Fast Two-Dimensional NMR Spectroscopy for Real-Time Investigation of Dynamic Events in Proteins on the Time Scale of Seconds, *J. Am. Chem. Soc.* 127 (22) (2005) 8014–8015, <https://doi.org/10.1021/ja051306e>.
- [213] E. Kupce, R. Freeman, Fast multidimensional NMR by polarization sharing, *Magn. Reson. Chem.* 45 (1) (2007) 2–4, <https://doi.org/10.1002/mrc.1931>.
- [214] D. Schulze-Sünninghausen, J. Becker, B. Luy, Rapid heteronuclear single quantum correlation NMR spectra at natural abundance, *J. Am. Chem. Soc.* 136 (4) (2014) 1242–1245, <https://doi.org/10.1021/ja411588d>.
- [215] J. Furrer, A robust, sensitive, and versatile HMBC experiment for rapid structure elucidation by NMR: IMPACT-HMBC, *Chem. Commun.* 46 (2010) 3396–3398, <https://doi.org/10.1039/c000964d>.
- [216] D. Schulze-Sünninghausen, J. Becker, M.R.M. Koos, B. Luy, Improvements, extensions, and practical aspects of rapid ASAP-HSQC and ALSOFASST-HSQC pulse sequences for studying small molecules at natural abundance, *J. Magn. Reson.* 281 (2017) 151–161, <https://doi.org/10.1016/j.jmr.2017.05.012>.
- [217] I.E. Ndukwe, A. Shchukina, K. Kazimierczuk, C.P. Butts, Rapid and safe ASAP acquisition with EXACT NMR, *Chem. Commun.* 52 (86) (2016) 12769–12772.
- [218] P. Giraudeau, L. Frydman, Ultrafast 2D NMR: An emerging tool in analytical spectroscopy, *Annu. Rev. Anal. Chem.* 7 (1) (2014) 129–161, <https://doi.org/10.1146/annurev-anchem-071213-020208>.
- [219] B. Gouilleux, B. Charrier, S. Akoka, F.X. Felpin, M. Rodriguez-Zubiri, P. Giraudeau, Ultrafast 2D NMR on a benchtop spectrometer: Applications and perspectives, *TrAC - Trends Anal. Chem.* 83 (2016) 65–75, <https://doi.org/10.1016/j.trac.2016.01.014>.
- [220] A. Tal, L. Frydman, Single-scan multidimensional magnetic resonance, *Prog. Nucl. Magn. Reson. Spectrosc.* 57 (3) (2010) 241–292, <https://doi.org/10.1016/j.pnmrs.2010.04.001>.
- [221] A. Herrera, E. Fernández-Valle, R. Martínez-Álvarez, D. Molero, Z. Pardo, E. Sáez, M. Gal, Real-Time Monitoring of Organic Reactions with Two-Dimensional Ultrafast TOCSY NMR Spectroscopy, *Angew. Chemie Int. Ed.* 48 (34) (2009) 6274–6277, <https://doi.org/10.1002/anie.200902387>.
- [222] A. Herrera, E. Fernández-Valle, R. Martínez-Álvarez, D. Molero-Vílchez, Z.D. Pardo-Botero, E. Sáez-Barajas, Monitoring organic reactions by UF-NMR spectroscopy, *Magn. Reson. Chem.* 53 (2015) 952–970, <https://doi.org/10.1002/mrc.4240>.
- [223] Z.D. Pardo, G.L. Olsen, M.E. Fernández-Valle, L. Frydman, R. Martínez-Álvarez, A. Herrera, Monitoring mechanistic details in the synthesis of pyrimidines via real-time, ultrafast multidimensional NMR spectroscopy, *J. Am. Chem. Soc.* 134 (5) (2012) 2706–2715, <https://doi.org/10.1021/ja210154g>.
- [224] L.H.K. Queiroz, P. Giraudeau, F.A.B. dos Santos, K.T. Oliveira, A.G. Ferreira, Real-time mechanistic monitoring of an acetal hydrolysis using ultrafast 2D NMR, *Magn. Reson. Chem.* 50 (7) (2012) 496–501, <https://doi.org/10.1002/mrc.3827>.
- [225] B. Gouilleux, B. Charrier, E. Danieli, J.-N. Dumez, S. Akoka, F.-X. Felpin, M. Rodriguez-Zubiri, P. Giraudeau, Real-time reaction monitoring by ultrafast 2D NMR on a benchtop spectrometer, *Analyst* 140 (23) (2015) 7854–7858, <https://doi.org/10.1039/C5AN01998B>.
- [226] M. Pathan, S. Akoka, I. Tea, B. Charrier, P. Giraudeau, "Multi-scan single shot" quantitative 2D NMR: A valuable alternative to fast conventional quantitative 2D NMR, *Analyst* 136 (2011) 3157–3163, <https://doi.org/10.1039/c1an15278e>.
- [227] É. Kupče, NMR with Multiple Receivers, in: H. Heise, S. Matthews (Eds.), *Mod. NMR Methodol.*, Springer, Berlin, Heidelberg, 2011, pp. 71–96, https://doi.org/10.1007/128_2011_226.
- [228] H. Kovacs, É. Kupče, Parallel NMR spectroscopy with simultaneous detection of 1H and 19F nuclei, *Magn. Reson. Chem.* 54 (7) (2016) 544–560, <https://doi.org/10.1002/mrc.4428>.
- [229] É. Kupče, R. Freeman, B.K. John, Parallel Acquisition of Two-Dimensional NMR Spectra of Several Nuclear Species, *J. Am. Chem. Soc.* 128 (30) (2006) 9606–9607, <https://doi.org/10.1021/ja063487e>.
- [230] P. Nolis, K. Motiram-Corral, M. Pérez-Trujillo, T. Parella, Interleaved Dual NMR Acquisition of Equivalent Transfer Pathways in TOCSY and HSQC Experiments, *ChemPhysChem* 20 (3) (2019) 356–360, <https://doi.org/10.1002/cphc.201801034>.
- [231] K. Motiram-Corral, M. Pérez-Trujillo, P. Nolis, T. Parella, Implementing one-shot multiple-FID acquisition into homonuclear and heteronuclear NMR experiments, *Chem. Commun.* 54 (96) (2018) 13507–13510, <https://doi.org/10.1039/C8CC08065H>.
- [232] T. Parella, P. Nolis, Time-shared NMR experiments, *Concepts Magn. Reson. Part A.* 36A (1) (2010) 1–23, <https://doi.org/10.1002/cmr.a.20150>.
- [233] É. Kupče, T.D.W. Claridge, NOAH: NMR Supersequences for Small Molecule Analysis and Structure Elucidation, *Angew. Chemie Int. Ed.* 56 (39) (2017) 11779–11783, <https://doi.org/10.1002/anie.201705506>.
- [234] É. Kupče, T.D.W. Claridge, Molecular structure from a single NMR supersequence, *Chem. Commun.* 54 (52) (2018) 7139–7142, <https://doi.org/10.1039/C8CC03296C>.
- [235] A.D. Blum, S.H. Smallcombe, R.L. Baldwin, Nuclear magnetic resonance evidence for a structural intermediate at an early stage in the refolding of ribonuclease A, *J. Mol. Biol.* 118 (3) (1978) 305–316, [https://doi.org/10.1016/0022-2836\(78\)90230-9](https://doi.org/10.1016/0022-2836(78)90230-9).
- [236] R. Callender, R.B. Dyer, Probing protein dynamics using temperature jump relaxation spectroscopy, *Curr. Opin. Struct. Biol.* 12 (5) (2002) 628–633, [https://doi.org/10.1016/S0959-440X\(02\)00370-6](https://doi.org/10.1016/S0959-440X(02)00370-6).

- [237] K. Yamasaki, Y. Obara, M. Hasegawa, H. Tanaka, T. Yamasaki, T. Wakuda, M. Okada, T. Kohzuma, Real-Time NMR monitoring of protein-folding kinetics by a recycle flow system for temperature jump, *Anal. Chem.* 85 (20) (2013) 9439–9443, <https://doi.org/10.1021/ac401579e>.
- [238] K. Akasaka, A. Naito, H. Nakatani, M. Imanari, Construction and performance of a temperature-jump NMR apparatus, *Rev. Sci. Instrum.* 61 (1) (1990) 66–68, <https://doi.org/10.1063/1.1141901>.
- [239] M. Frunzi, H. Xu, R.J. Cross, M. Saunders, NMR temperature-jump method for measuring reaction rates: Reaction of dimethylantracene with H₂O₂, *J. Phys. Chem. A* 113 (17) (2009) 4996–4999, <https://doi.org/10.1021/jp901230y>.
- [240] J. Rinnenthal, D. Wagner, T. Marquardsen, A. Krahn, F. Engelke, H. Schwalbe, A temperature-jump NMR probe setup using rf heating optimized for the analysis of temperature-induced biomacromolecular kinetic processes, *J. Magn. Reson.* 251 (2015) 84–93, <https://doi.org/10.1016/j.jmr.2014.11.012>.
- [241] C. Charlier, T.R. Alderson, J.M. Courtney, J. Ying, P. Anfinrud, A. Bax, Study of protein folding under native conditions by rapidly switching the hydrostatic pressure inside an NMR sample cell, *Proc. Natl. Acad. Sci. U. S. A.* 115 (18) (2018) E4169–E4178, <https://doi.org/10.1073/pnas.1803642115>.
- [242] H.F. Gilbert, The “rule of thumb” for deriving steady state rate equations, *J. Chem. Educ.* 54 (1977) 492–493, <https://doi.org/10.1021/ed054p492>.
- [243] E.L. King, C. Altman, A schematic method of deriving the rate laws for enzyme-catalyzed reactions, *J. Phys. Chem.* 60 (10) (1956) 1375–1378, <https://doi.org/10.1021/j150544a010>.
- [244] S. Cha, A simple method for derivation of rate equations for enzyme-catalyzed reactions under the rapid equilibrium assumption or combined assumptions of equilibrium and steady state, *J. Biol. Chem.* 243 (4) (1968) 820–825.
- [245] I.H. Segel, *Enzyme Kinetics*, John Wiley & Sons, Hoboken, New Jersey, 1975.
- [246] K.A. Johnson, R.S. Goody, Michaelis-Menten Paper, *Biochemistry* 50 (39) (2011) 8264–8269, <https://doi.org/10.1021/bi201284u>.
- [247] G.E. Briggs, J.B.S. Haldane, A Note on the Kinetics of Enzyme Action, *Biochem. J.* 19 (1925) 338–339, <https://doi.org/10.1042/bj0190338>.
- [248] S. Hearn, A. Bird, J. Hannon, Template Selected for Input Files J Input Files Scenarios, US 2005/0267723 A1, 2005.
- [249] K.A. Johnson, Z.B. Simpson, T. Blom, Global Kinetic Explorer: A new computer program for dynamic simulation and fitting of kinetic data, *Anal. Biochem.* 387 (1) (2009) 20–29, <https://doi.org/10.1016/j.ab.2008.12.024>.
- [250] T.E. Oliphant, Python for scientific computing, *Comput. Sci. Eng.* 9 (3) (2007) 10–20, <https://doi.org/10.1109/MCSE.2007.58>.
- [251] C.D.-T. Nielsen, J. Burés, Visual kinetic analysis, *Chem. Sci.* 10 (2) (2019) 348–353, <https://doi.org/10.1039/C8SC04698K>.
- [252] J. Burés, Variable Time Normalization Analysis: General Graphical Elucidation of Reaction Orders from Concentration Profiles, *Angew. Chemie – Int. Ed.* 55 (52) (2016) 16084–16087, <https://doi.org/10.1002/anie.201609757>.
- [253] D.G. Blackmond, Reaction progress kinetic analysis: A powerful methodology for mechanistic studies of complex catalytic reactions, *Angew. Chemie – Int. Ed.* 44 (28) (2005) 4302–4320, <https://doi.org/10.1002/anie.200462544>.
- [254] K.G. Orrell, V. Sik, D. Stephenson, Quantitative investigations of molecular stereodynamics by 1D and 2D NMR methods, *Prog. Nucl. Magn. Reson. Spectrosc.* 22 (2) (1990) 141–208, [https://doi.org/10.1016/0079-6565\(90\)80004-2](https://doi.org/10.1016/0079-6565(90)80004-2).
- [255] J. Jeener, B.H. Meier, P. Bachmann, R.R. Ernst, Investigation of exchange processes by two-dimensional NMR spectroscopy, *J. Chem. Phys.* 71 (11) (1979) 4546–4553, <https://doi.org/10.1063/1.438208>.
- [256] S. Forsén, R.A. Hoffman, Study of moderately rapid chemical exchange reactions by means of nuclear magnetic double resonance, *J. Chem. Phys.* 39 (11) (1963) 2892–2901, <https://doi.org/10.1063/1.1734121>.
- [257] S. Forsén, R.A. Hoffman, Exchange Rates by Nuclear Magnetic Multiple Resonance. III. Exchange Reactions in Systems with Several Nonequivalent Sites, *J. Chem. Phys.* 40 (5) (1964) 1189–1196, <https://doi.org/10.1063/1.1725295>.
- [258] P. Hodgson, G.C. Lloyd-Jones, M. Murray, T.M. Peakman, R.L. Woodward, Entropy-driven hydrogen bonding: Stereodynamics of a protonated, N, N-chiral “proton sponge”, *Chem. – A Eur. J.* 6 (2000) 4451–4460, [https://doi.org/10.1002/1521-3765\(20001215\)6:24<4451::AID-CHEM4451>3.0.CO;2-H](https://doi.org/10.1002/1521-3765(20001215)6:24<4451::AID-CHEM4451>3.0.CO;2-H).
- [259] A.D. Bain, D.A. Fletcher, Selective-inversion experiments applied to chemical exchange in coupled spin systems, *Mol. Phys.* 95 (6) (1998) 1091–1098, <https://doi.org/10.1080/00268979809483241>.
- [260] D. Shishmarev, P.W. Kuchel, NMR magnetization-transfer analysis of rapid membrane transport in human erythrocytes, *Biophys. Rev.* 8 (4) (2016) 369–384, <https://doi.org/10.1007/s12551-016-0221-y>.
- [261] M.M. Kucharski, A.J.B. Watson, G.C. Lloyd-Jones, Unpublished results, 2020.
- [262] C.L. Perrin, T.J. Dwyer, Application of Two-Dimensional NMR to Kinetics of Chemical Exchange, *Chem. Rev.* 90 (6) (1990) 935–967, <https://doi.org/10.1021/cr00104a002>.
- [263] C.L. Perrin, R.E. Engler, Accurate Rate Constants for Chemical Exchange from Improved Weighted Linear-Least-Squares Analysis of Multiple 1D-EXSY Data, *J. Magn. Reson. Ser. A* 123 (2) (1996) 188–195, <https://doi.org/10.1006/jmra.1996.0234>.
- [264] K.G. Orrell, Two-Dimensional Methods of Monitoring Exchange, *Encycl. Magn. Reson.* (2007) 1–8, <https://doi.org/10.1002/9780470034590.emrstm0580>.
- [265] H.M. McConnell, Reaction rates by nuclear magnetic resonance, *J. Chem. Phys.* 28 (3) (1958) 430–431, <https://doi.org/10.1063/1.1744152>.
- [266] P. Thordarson, Determining association constants from titration experiments in supramolecular chemistry, *Chem. Soc. Rev.* 40 (3) (2011) 1305–1323, <https://doi.org/10.1039/c0cs00062k>.
- [267] R.S. Macomber, An introduction to NMR titration for studying rapid reversible complexation, *J. Chem. Educ.* 69 (1992) 375–378, <https://doi.org/10.1021/ed069p375>.
- [268] Z.-X. Wang, An exact mathematical expression for describing competitive binding of two different ligands to a protein molecule, *FEBS Lett.* 360 (1995) 111–114, [https://doi.org/10.1016/0014-5793\(95\)00062-E](https://doi.org/10.1016/0014-5793(95)00062-E).
- [269] C. Hunter, H. Anderson, What is cooperativity?, *Angew. Chemie – Int. Ed.* 48 (41) (2009) 7488–7499, <https://doi.org/10.1002/anie.200902490>.
- [270] G. Ercolani, C. Pigué, M. Borkovec, J. Hamacek, Symmetry numbers and statistical factors in self-assembly and multivalency, *J. Phys. Chem. B* 111 (42) (2007) 12195–12203, <https://doi.org/10.1021/jp0740705>.
- [271] C.S. Johnson, Diffusion ordered nuclear magnetic resonance spectroscopy: principles and applications, *Prog. Nucl. Magn. Reson. Spectrosc.* 34 (3–4) (1999) 203–256, [https://doi.org/10.1016/S0079-6565\(99\)00003-5](https://doi.org/10.1016/S0079-6565(99)00003-5).
- [272] Y. Cohen, L. Avram, L. Frish, Diffusion NMR Spectroscopy in Supramolecular and Combinatorial Chemistry: An Old Parameter – New Insights, *Angew. Chemie Int. Ed.* 44 (4) (2005) 520–554, <https://doi.org/10.1002/anie.200300637>.
- [273] A. Macchioni, G. Ciancaleoni, C. Zuccaccia, D. Zuccaccia, Determining accurate molecular sizes in solution through NMR diffusion spectroscopy, *Chem. Soc. Rev.* 37 (3) (2008) 479–489, <https://doi.org/10.1039/B615067P>.
- [274] F. Zaccaria, C. Zuccaccia, R. Cipullo, A. Macchioni, Extraction of Reliable Molecular Information from Diffusion NMR Spectroscopy: Hydrodynamic Volume or Molecular Mass?, *Chem – A Eur. J.* 25 (42) (2019) 9930–9937, <https://doi.org/10.1002/chem.201900812>.
- [275] R. Evans, The interpretation of small molecule diffusion coefficients: Quantitative use of diffusion-ordered NMR spectroscopy, *Prog. Nucl. Magn. Reson. Spectrosc.* 117 (2020) 33–69, <https://doi.org/10.1016/j.pnmrs.2019.11.002>.
- [276] R. Evans, G. Dal Poggetto, M. Nilsson, G.A. Morris, Improving the Interpretation of Small Molecule Diffusion Coefficients, *Anal. Chem.* 90 (6) (2018) 3987–3994, <https://doi.org/10.1021/acs.analchem.7b05032>.
- [277] R. Evans, Z. Deng, A.K. Rogerson, A.S. McLachlan, J.J. Richards, M. Nilsson, G.A. Morris, Quantitative Interpretation of Diffusion-Ordered NMR Spectra: Can We Rationalize Small Molecule Diffusion Coefficients?, *Angew. Chemie Int. Ed.* 52 (11) (2013) 3199–3202, <https://doi.org/10.1002/anie.201207403>.
- [278] D. Sinnaeve, The Stejskal-Tanner equation generalized for any gradient shape—an overview of most pulse sequences measuring free diffusion, *Concepts Magn. Reson. Part A.* 40A (2) (2012) 39–65, <https://doi.org/10.1002/cmr.a.21223>.
- [279] E.O. Stejskal, J.E. Tanner, Spin Diffusion Measurements: Spin Echoes in the Presence of a Time-Dependent Field Gradient, *J. Chem. Phys.* 42 (1) (1965) 288–292, <https://doi.org/10.1063/1.1695690>.
- [280] M. Foroozandeh, L. Castañar, L.G. Martins, D. Sinnaeve, G.D. Poggetto, C.F. Tormena, R.W. Adams, G.A. Morris, M. Nilsson, Ultrahigh-Resolution Diffusion-Ordered Spectroscopy, *Angew. Chemie – Int. Ed.* 55 (50) (2016) 15579–15582, <https://doi.org/10.1002/anie.201609676>.
- [281] S. Glanzer, K. Zangger, Directly decoupled diffusion-ordered NMR spectroscopy for the analysis of compound mixtures, *Chem. – A Eur. J.* 20 (35) (2014) 11171–11175, <https://doi.org/10.1002/chem.201402920>.
- [282] M. Nilsson, G.A. Morris, Pure shift proton DOSY: diffusion-ordered 1H spectra without multiplet structure, *Chem. Commun.* (9) (2007) 933, <https://doi.org/10.1039/b617761a>.
- [283] G. Dal Poggetto, L. Castañar, M. Foroozandeh, P. Kiraly, R.W. Adams, G.A. Morris, M. Nilsson, Unexploited Dimension: New Software for Mixture Analysis by 3D Diffusion-Ordered NMR Spectroscopy, *Anal. Chem.* 90 (22) (2018) 13695–13701, <https://doi.org/10.1021/acs.analchem.8b04093>.
- [284] J.M. Newman, A. Jerschow, Improvements in Complex Mixture Analysis by NMR: DQF-COSY iDOSY, *Anal. Chem.* 79 (2007) 2957–2960, <https://doi.org/10.1021/ac061760g>.
- [285] M. Nilsson, A.M. Gil, I. Delgadillo, G.A. Morris, Improving pulse sequences for 3D DOSY: COSY-IDOSY, *Chem. Commun.* (13) (2005) 1737, <https://doi.org/10.1039/b415099f>.
- [286] D. Li, R. Hopson, W. Li, J. Liu, P.G. Williard, 13 C INEPT Diffusion-Ordered NMR Spectroscopy (DOSY) with Internal References, *Org. Lett.* 10 (5) (2008) 909–911, <https://doi.org/10.1021/ol703039v>.
- [287] G. Kagan, W. Li, R. Hopson, P.G. Williard, Internally Referenced Diffusion Coefficient–Formula Weight (D-FW) Analysis of 31 P Diffusion-Ordered NMR Spectroscopy (DOSY), *Org. Lett.* 11 (21) (2009) 4818–4821, <https://doi.org/10.1021/ol9019106>.
- [288] H. Subramanian, C.P. Jasperse, M.P. Sibi, Characterization of Brønsted Acid-Base Complexes by 19 F DOSY, *Org. Lett.* 17 (6) (2015) 1429–1432, <https://doi.org/10.1021/acs.orglett.5b00297>.
- [289] G. Kagan, W. Li, R. Hopson, P.G. Williard, 6 Li Diffusion-Ordered NMR Spectroscopy (DOSY) and Applications to Organometallic Complexes, *Org. Lett.* 12 (3) (2010) 520–523, <https://doi.org/10.1021/ol902713h>.
- [290] I. Swan, M. Reid, P.W. Howe, M. Connell, M. Nilsson, M. Moore, G. Morris, Sample convection in liquid-state NMR: Why it is always with us, and what we can do about it, *J. Magn. Reson.* 252 (2015) 120–129, <https://doi.org/10.1016/j.jmr.2014.12.006>.
- [291] D.H. Wu, A.D. Chen, C.S. Johnson, An Improved Diffusion-Ordered Spectroscopy Experiment Incorporating Bipolar-Gradient Pulses, *J. Magn. Reson. Ser. A* 115 (2) (1995) 260–264, <https://doi.org/10.1006/jmra.1995.1176>.

- [292] M.D. Pelta, G.A. Morris, M.J. Stchedroff, S.J. Hammond, A one-shot sequence for high-resolution diffusion-ordered spectroscopy, *Magn. Reson. Chem.* 40 (13) (2002) S147–S152, <https://doi.org/10.1002/mrc.1107>.
- [293] P. Groves, Diffusion ordered spectroscopy (DOSY) as applied to polymers, *Polym. Chem.* 8 (44) (2017) 6700–6708, <https://doi.org/10.1039/C7PY01577A>.
- [294] A. Gierer, K. Wirtz, Molekulare Theorie der Mikroeibung, *Zeitschrift Für Naturforsch A* 8 (1953) 532–538, <https://doi.org/10.1515/zna-1953-0903>.
- [295] D. Li, G. Kagan, R. Hopson, P.G. Williard, Formula Weight Prediction by Internal Reference Diffusion-Ordered NMR Spectroscopy (DOSY), *J. Am. Chem. Soc.* 131 (15) (2009) 5627–5634, <https://doi.org/10.1021/ja810154u>.
- [296] D. Li, I. Keresztes, R. Hopson, P.G. Williard, Characterization of Reactive Intermediates by Multinuclear Diffusion-Ordered NMR Spectroscopy (DOSY), *Acc. Chem. Res.* 42 (2) (2009) 270–280, <https://doi.org/10.1021/ar800127e>.
- [297] S. Bachmann, R. Neufeld, M. Dzemski, D. Stalke, New External Calibration Curves (ECCs) for the Estimation of Molecular Weights in Various Common NMR Solvents, *Chem. – A Eur. J.* 22 (25) (2016) 8462–8465, <https://doi.org/10.1002/chem.201601145>.
- [298] R. Neufeld, D. Stalke, Accurate molecular weight determination of small molecules via DOSY-NMR by using external calibration curves with normalized diffusion coefficients, *Chem. Sci.* 6 (6) (2015) 3354–3364, <https://doi.org/10.1039/C5SC00670H>.
- [299] A. Bondi, van der Waals Volumes and Radii, *J. Phys. Chem.* 68 (3) (1964) 441–451, <https://doi.org/10.1021/j100785a001>.
- [300] H. Maskhill, *The Investigation of Organic Reactions and their Mechanisms*, Blackwell Publishing, Oxford, UK, 2006.
- [301] R.G. Bergman, Use of Isotope Crossover Experiments in Investigating Carbon-Carbon Bond-Forming Reactions of Binuclear Diallylcobalt Complexes, *Acc. Chem. Res.* 13 (4) (1980) 113–120, <https://doi.org/10.1021/ar50148a003>.
- [302] E. Kühnel, D.P. Laffan, G. Lloyd-Jones, T. Martínez del Campo, I. Shepperson, J. Slaughter, Mechanism of methyl esterification of carboxylic acids by trimethylsilyldiazomethane, *Angew. Chemie – Int. Ed.* 46 (37) (2007) 7075–7078, <https://doi.org/10.1002/anie.200702131>.
- [303] F.A. Carroll, *Perspectives on Structure and Mechanism in Organic Chemistry*, second ed., John Wiley & Sons, Hoboken, New Jersey, 2010.
- [304] M. Gómez-Gallego, M.A. Sierra, Kinetic isotope effects in the study of organometallic reaction mechanisms, *Chem. Rev.* 111 (8) (2011) 4857–4963, <https://doi.org/10.1021/cr100436k>.
- [305] S. Rendler, M. Oestreich, C.P. Butts, G.C. Lloyd-Jones, Intermolecular chirality transfer from silicon to carbon: Interrogation of the two-silicon cycle for Pd-catalyzed hydrosilylation by stereoisotopochemical crossover, *J. Am. Chem. Soc.* 129 (2007) 502–503, <https://doi.org/10.1021/ja067780h>.
- [306] C.J. Jameson, The isotope shift in NMR, *J. Chem. Phys.* 66 (11) (1977) 4983–4988, <https://doi.org/10.1063/1.433800>.
- [307] D.R. Herschbach, V.W. Laurie, Influence of Vibrations on Molecular Structure Determinations. I. General Formulation of Vibration–Rotation Interactions, *J. Chem. Phys.* 37 (8) (1962) 1668–1686, <https://doi.org/10.1063/1.1733357>.
- [308] V.W. Laurie, D.R. Herschbach, Influence of Vibrations on Molecular Structure Determinations. II. Average Structures Derived from Spectroscopic Data, *J. Chem. Phys.* 37 (8) (1962) 1687–1693, <https://doi.org/10.1063/1.1733358>.
- [309] M. Saunders, K.E. Laidig, M. Wolfsberg, Theoretical Calculation of Equilibrium Isotope Effects Using ab Initio Force Constants: Application to NMR Isotopic Perturbation Studies, *J. Am. Chem. Soc.* 111 (1989) 8989–8994, <https://doi.org/10.1021/ja00207a001>.
- [310] E.M. Simmons, J.F. Hartwig, On the interpretation of deuterium kinetic isotope effects in C–H bond functionalizations by transition-metal complexes, *Angew. Chemie – Int. Ed.* 51 (13) (2012) 3066–3072, <https://doi.org/10.1002/anie.201107334>.
- [311] H.J.A. Dale, A.G. Leach, G.C. Lloyd-Jones, Heavy-Atom Kinetic Isotope Effects: Primary Interest or Zero Point?, *J. Am. Chem. Soc.* 143 (50) (2021) 21079–21099, <https://doi.org/10.1021/jacs.1c07351>.
- [312] J. Bigeleisen, M.G. Mayer, Calculation of equilibrium constants for isotopic exchange reactions, *J. Chem. Phys.* 15 (5) (1947) 261–267, <https://doi.org/10.1063/1.1746492>.
- [313] M. Wolfsberg, Theoretical evaluation of experimentally observed isotope effects, *Acc. Chem. Res.* 5 (7) (1972) 225–233, <https://doi.org/10.1021/ar50055a001>.
- [314] G.C. Lloyd-Jones, R.W. Alder, G.J.J. Owen-Smith, Intermolecular Insertion of an N, N-Heterocyclic Carbene into a Nonacidic C–H Bond: Kinetics, Mechanism and Catalysis by (K-HMDS)₂ (HMDS=Hexamethyldisilazide), *Chem. – A Eur. J.* 12 (20) (2006) 5361–5375, <https://doi.org/10.1002/chem.200600266>.
- [315] J. Chan, A.R. Lewis, M. Gilbert, M.-F. Karwaski, A.J. Bennet, A direct NMR method for the measurement of competitive kinetic isotope effects, *Nat. Chem. Biol.* 6 (6) (2010) 405–407, <https://doi.org/10.1038/nchembio.352>.
- [316] G. Speciale, M. Farren-Dai, F.S. Shidmoosavee, S.J. Williams, A.J. Bennet, C2-Oxyanion Neighboring Group Participation: Transition State Structure for the Hydroxide-Promoted Hydrolysis of 4-Nitrophenyl α -D-Mannopyranoside, *J. Am. Chem. Soc.* 138 (2016) 14012–14019, <https://doi.org/10.1021/jacs.6b07935>.
- [317] J. Chan, N. Sannikova, A. Tang, A.J. Bennet, Transition-state structure for the quintessential SN2 reaction of a carbohydrate: Reaction of α -glucopyranosyl fluoride with azide ion in Water, *J. Am. Chem. Soc.* 136 (35) (2014) 12225–12228, <https://doi.org/10.1021/ja506092h>.
- [318] J. Chan, A. Tang, A.J. Bennet, A stepwise solvent-promoted S_N2 reaction of α -d-glucopyranosyl fluoride: Mechanistic implications for retaining glycosyltransferases, *J. Am. Chem. Soc.* 134 (2012) 1212–1220, <https://doi.org/10.1021/ja209339j>.
- [319] N. Sannikova, A.R. Lewis, A.J. Bennet, Measurement of Kinetic Isotope Effects by Continuously Monitoring Isotopologue Ratios Using NMR Spectroscopy, first ed., Elsevier Inc., 2017, <https://doi.org/10.1016/bs.mie.2017.06.034>.
- [320] D.A. Singleton, A.A. Thomas, High-Precision Simultaneous Determination of Multiple Small Kinetic Isotope Effects at Natural Abundance, *J. Am. Chem. Soc.* 117 (36) (1995) 9357–9358, <https://doi.org/10.1021/ja00141a030>.
- [321] D.A. Singleton, M.J. Szymanski, Simultaneous Determination of Intermolecular and Intramolecular ¹³C and ²H Kinetic Isotope Effects at Natural Abundance, *J. Am. Chem. Soc.* 121 (40) (1999) 9455–9456, <https://doi.org/10.1021/ja992016z>.
- [322] E.E. Kwan, Y. Park, H.A. Besser, T.L. Anderson, E.N. Jacobsen, Sensitive and Accurate ¹³C Kinetic Isotope Effect Measurements Enabled by Polarization Transfer, *J. Am. Chem. Soc.* 139 (1) (2017) 43–46, <https://doi.org/10.1021/jacs.6b10621>.
- [323] E.E. Kwan, Y. Zeng, H.A. Besser, E.N. Jacobsen, Concerted nucleophilic aromatic substitutions, *Nat. Chem.* 10 (9) (2018) 917–923, <https://doi.org/10.1038/s41557-018-0079-7>.
- [324] H.M. Dintzis, Assembly of The Peptide Chains of Hemoglobin, *Proc. Natl. Acad. Sci. U. S. A.* 47 (3) (1961) 247–261, <https://doi.org/10.1073/pnas.47.3.247>.
- [325] J.M. Brown, J.E. MacIntyre, Allylic alkylation catalysed by platinum complexes; structure and reactivity of intermediates, and the overall stereoselectivity, *J. Chem. Soc. Perkin Trans. 2* (1985) 961–970, <https://doi.org/10.1039/p29850000961>.
- [326] M.H. Levitt, *Spin Dynamics: Basics of Nuclear Magnetic Resonance*, second ed., Wiley, Chichester, UK, 2008.
- [327] R.C. Breton, W.F. Reynolds, Using NMR to identify and characterize natural products, *Nat. Prod. Rep.* 30 (2013) 501–524, <https://doi.org/10.1039/c2np20104f>.
- [328] I. Pritišanac, J.M. Würz, T.R. Alderson, P. Güntert, Automatic structure-based NMR methyl resonance assignment in large proteins, *Nat. Commun.* 10 (2019) 1–12, <https://doi.org/10.1038/s41467-019-12837-8>.
- [329] K. Tripsianes, U. Schütz, L. Emmanouilidis, G. Gemmecker, M. Sattler, Selective isotope labeling for NMR structure determination of proteins in complex with unlabeled ligands, *J. Biomol. NMR* 73 (3–4) (2019) 183–189, <https://doi.org/10.1007/s10858-019-00241-9>.
- [330] C.P. Butts, E. Filali, G.C. Lloyd-Jones, P.O. Norrby, D.A. Sale, Y. Schramm, Structure-based rationale for selectivity in the asymmetric allylic alkylation of cycloalkenyl esters employing the Trost “Standard Ligand” (TSL): Isolation, analysis and alkylation of the monomeric form of the cationic η^3 -cyclohexenyl complex [(η^3 -c-C₆H₅), *J. Am. Chem. Soc.* 131 (2009) 9945–9957, <https://doi.org/10.1021/ja0099757>.
- [331] S.F. Fujiwara, Y.A. Arata, H.O. Ozawa, M.K. Kunugi, Nmr satellites as a probe for chemical investigations, *Pure Appl. Chem.* 32 (1972) 117–122, <https://doi.org/10.1351/pac197232010117>.
- [332] V.S. Fluxá, T.A. Jenny, C.G. Bochet, Geometry determination of tetrasubstituted stilbenes by proton NMR spectroscopy, *Tetrahedron Lett.* 46 (22) (2005) 3793–3795, <https://doi.org/10.1016/j.tetlet.2005.04.001>.
- [333] R. Rotta, Á. Cunha Neto, D.P. de Lima, A. Beatriz, G.V.J. da Silva, Configuration of stilbene derivatives by ¹H NMR and theoretical calculation of chemical shifts, *J. Mol. Struct.* 975 (1–3) (2010) 59–62, <https://doi.org/10.1016/j.molstruc.2010.03.079>.
- [334] B.M. Still, P.G.A. Kumar, J.R. Aldrich-Wright, W.S. Price, ¹⁹⁵Pt NMR - Theory and application, *Chem. Soc. Rev.* 36 (4) (2007) 665–686, <https://doi.org/10.1039/b606190g>.
- [335] I.R. Herbert, P.S. Pregosin, H. Ruegger, Carbonyl trichlorostannane complexes of platinum: chemistry and ¹¹⁹Sn, ¹⁹⁵Pt, and ¹³C NMR spectroscopy, *Inorg. Chim. Acta* 112 (1) (1986) 29–34, [https://doi.org/10.1016/S0020-1693\(00\)85656-X](https://doi.org/10.1016/S0020-1693(00)85656-X).
- [336] A. Bax, R. Freeman, S.P. Kempell, Natural abundance carbon-13-carbon-13 coupling observed via double-quantum coherence, *J. Am. Chem. Soc.* 102 (14) (1980) 4849–4851, <https://doi.org/10.1021/ja00534a056>.
- [337] A.V. Zhukhovitskiy, I.J. Kobylanskiy, A.A. Thomas, A.M. Evans, C.P. Delaney, N. C. Flanders, S.E. Denmark, W.R. Dichtel, F.D. Toste, A Dinuclear Mechanism Implicated in Controlled Carbene Polymerization, *J. Am. Chem. Soc.* 141 (16) (2019) 6473–6478, <https://doi.org/10.1021/jacs.9b01532>.
- [338] F. Dalitz, M. Cudaj, M. Maiwald, G. Guthausen, Process and reaction monitoring by low-field NMR spectroscopy, *Prog. Nucl. Magn. Reson. Spectrosc.* 60 (2012) 52–70, <https://doi.org/10.1016/j.pnmrs.2011.11.003>.
- [339] K. Albert, E. Bayer, High-performance liquid chromatography–nuclear magnetic resonance on-line coupling, *TrAC, Trends Anal. Chem.* 7 (8) (1988) 288–293, [https://doi.org/10.1016/0165-9936\(88\)80008-6](https://doi.org/10.1016/0165-9936(88)80008-6).
- [340] J. Kind, C.M. Thiele, Still shimming or already measuring? – Quantitative reaction monitoring for small molecules on the sub minute timescale by NMR, *J. Magn. Reson.* 260 (2015) 109–115, <https://doi.org/10.1016/j.jmr.2015.09.008>.
- [341] Y. Ji, R.E. Plata, C.S. Regens, M. Hay, M. Schmidt, T. Razler, Y. Qiu, P. Geng, Y. Hsiao, T. Rosner, M.D. Eastgate, D.G. Blackmond, Mono-Oxidation of Bidentate Bis-phosphines in Catalyst Activation: Kinetic and Mechanistic Studies of a Pd/Xantphos-Catalyzed C–H Functionalization, *J. Am. Chem. Soc.* 137 (41) (2015) 13272–13281, <https://doi.org/10.1021/jacs.5b01913>.
- [342] C. McLaughlin, A.M.Z. Slawin, A.D. Smith, Base-free Enantioselective C(1)-Ammonium Enolate Catalysis Exploiting Aryloxides: A Synthetic and

- Mechanistic Study, *Angew. Chemie Int. Ed.* 58 (42) (2019) 15111–15119, <https://doi.org/10.1002/anie.201908627>.
- [343] D. Shishmarev, A.J. Wright, T.B. Rodrigues, G. Pileio, G. Stevanato, K.M. Brindle, P.W. Kuchel, Sub-minute kinetics of human red cell fumarase: 1 H spin-echo NMR spectroscopy and 13 C rapid-dissolution dynamic nuclear polarization, *NMR Biomed.* 31 (3) (2018), <https://doi.org/10.1002/nbm.3870>.
- [344] Y. Qiao, W. Ge, L. Jia, X. Hou, Y. Wang, C.M. Pedersen, Glycosylation intermediates studied using low temperature 1H- and 19F-DOSY NMR: New insight into the activation of trichloroacetimidates, *Chem. Commun.* 52 (76) (2016) 11418–11421, <https://doi.org/10.1039/C6CC05272j>.
- [345] Y. Ji, D.A. DiRocco, C.M. Hong, M.K. Wismer, M. Reibarkh, Facile Quantum Yield Determination via NMR Actinometry, *Org. Lett.* 20 (8) (2018) 2156–2159, <https://doi.org/10.1021/acs.orglett.8b00391>.

Glossary

1,2-DCE: 1,2-dichloro ethane.

Absolute Rate Ratio: method used to determine the *KIE* of a reaction. In this experiment, two reactions, one containing a labelled substrate and the other an unlabelled one, are run in parallel. Comparison of the rates allows the determination of the *KIE*.

Acceleration by Sharing Adjacent Polarisation (ASAP): NMR technique which utilizes magnetisation transfer from donor protons to an acceptor proton. This allows the acceptor proton to return more rapidly to equilibrium magnetisation, shortening the relaxation delay necessary for an experiment.

Acquisition (AQ): recording of the *FID*. The time that is taken to record data is called the acquisition time. Sometimes the full data is not recorded in a single acquisition period, but rather in a series of acquisition chunks (pieces).

Actinometry Technique: method which determines the quantum yield of a photoreaction by using a reference chemical substance (the actinometer) which undergoes a well-characterised reaction when exposed to specific wavelengths of light.

Activation Energy: the minimum amount of energy needed to pass through the transition state and result in a chemical reaction.

Ageing Loop: part of tubing in a flow chemistry reactor. It takes the reactants a defined amount of time to pass through this tubing during which the reaction is evolving.

Aliquot: sample of a reaction mixture.

Analogue to Digital Converter: device which transforms a measured signal, like voltage (NMR signal), to a binary number.

Apodisation: multiplication of the *FID* with a mathematical weighting function. Used to increase the *signal-to-noise ratio* or resolution, and avoid *sinc wiggles*.

Arrhenius Equation: mathematical correlation between the temperature and the rate constant. It is closely related to the *Eyring equation*.

Autocatalysis: when a reaction is catalysed by the product of the same reaction.

Autooxidation: oxidation of a molecule catalysed by its oxidised form. A type of autocatalysis.

Backwards Linear Prediction: mathematical method used to reconstruct the first data points of an *FID* by extrapolation.

Bandwidth (Pulse): range of frequencies which is excited by a pulse.

Baseline Correction: process of flattening a spectral baseline by applying mathematical operations.

BBO Probe: double resonance broad band NMR probe, optimised for *X nucleus* detection.

Benchtop NMR: compact low field NMR spectrometer. It contains magnets which do not require cryogenic cooling. Usually has a lower *signal-to-noise ratio* than cryogenic magnets.

Bigeleisen-Wolfsberg equation: mathematical equation which expresses the correlation between the substrate (or product) isotope ratio, the reaction progress (*Fractional Conversion, F*) and the *KIE*.

Bilinear Rotational Decoupling (BIRD): pulse sequence element used to discriminate ¹³C-bound protons from those bound to ¹²C, for example in *pure shift* NMR.

Briggs-Haldane Rate Expression: mathematical model for steady state kinetics using the *microscopic rate constants*, without assumption of rapid pre-equilibria.

Calibration Factor: multiplication constant used to normalise data to a known reference sample.

Charge Transfer (Electrochemistry): transfer of electrical charge within a solution.

Chemical Environment: surrounding atoms, interactions, charges, and electron density around a nucleus.

Chemical Shift: difference in the resonance frequency relative to a reference nuclear environment at a given magnetic field. The chemical shift depends strongly on the *chemical environment* of the observed nucleus.

Chemically-Different: having different interactions with the surrounding atoms, different types of neighbouring atoms or different electron density on the surrounding nuclei or even the observed nucleus.

Chirp Pulse: a smoothed rectangular pulse during which the excitation frequency is changed in a linear manner (swept).

Chirped, Ordered Pulses for Ultra-broadband Spectroscopy (CHORUS): NMR experiment, which utilizes *chirp pulses* to excite nuclei over a larger *bandwidth* than

normal 90° pulses do. This approach allows reliable NMR quantification of signals over a wide frequency range.

Coalescence: merging of two NMR peaks caused by rapid exchange processes (chemical, conformational, configurational etc.).

Coalescence Lifetime: exchange time constant at which two peaks stop becoming distinguishable from each other.

Coalescence Point: conditions under which the dip between two overlapping peaks just disappears.

Coaxial Insert: NMR tube insert which includes a coaxial capillary. This device allows measurement of an *external standard* separated from the sample solution.

Compact Spheres (DOSY): approximation in molecular geometry where molecules are described as spheres.

Competitive Equilibrium: coupled system of two equilibrium reactions, for example binding of a catalyst with two competing substrates.

Continuous Flow: NMR *flow system* in which a fraction of the reaction mixture is pumped into the NMR spectrometer, measured, and pumped back in the reaction vessel.

Convective Flow: movement of molecules or particles in solution driven by temperature gradients. Horizontal gradients give rise to *Hadley convection* while vertical gradients give rise to *Rayleigh-Bénard convection*.

Cooperative Equilibrium: system of sequential equilibria in which disturbances in one equilibrium affect the positions of others.

Correlated Spectroscopy (COSY): 2D NMR experiment used to observe short-range (2–5 bond) through-bond coupling between nuclei of the same type (usually ¹H–¹H).

Coupling Constant: magnitude in Hz of the *J-coupling* interaction with neighbouring spins. The larger the constant the stronger the interaction. *Coupling constants* may be measured from the distance between peaks in the coupling patterns for both coupled nuclei.

CPU: central processing unit.

Cross-Peak: signal in a 2D NMR spectra which correlates the two nuclei, for example through *scalar coupling* or exchange of magnetization.

Crossover Experiment: reaction set-up containing a doubly-labelled and an unlabelled form of the same substrate. The distribution and location of the labelled atoms in the product is then analysed to probe for intermolecular processes in which the substrate is fragmented between products.

Cryoprobe: NMR spectrometer hardware that transmits pulses and detects the resulting *FID* of the sample. In contrast to normal probes, *cryoprobe* coils are cooled by liquid helium or nitrogen resulting in higher *signal-to-noise ratio*.

d_n: prefix indicating the number of deuterium atoms in a molecule.

Dead Time: time period between the start of the reaction and the *acquisition* of the first NMR spectrum.

Decoupling: suppression of splittings due to *J-coupling* between nuclei.

Density Functional Theory (DFT): quantum mechanical method to calculate the electronic structure of a molecule.

DEPT-55: a modification of *Distortionless Enhancement by Polarization Transfer (DEPT)* using a proton pulse flip angle of 55° instead of the classical 45°, 90° or 135°. Useful for measurement of ¹³C *KIEs* by the *Singleton Method*.

Destruction of Interfering Satellites by Perfect Echo Low-Pass Filtration (DISPEL): NMR experiment which suppresses ¹³C satellites in ¹H spectra by use of a special pulse sequence. This method facilitates the identification of minor impurities that would otherwise overlap with major product satellite peaks.

Differentially-Relaxed Spins: state in which the spins have not had sufficient time to return to magnetic equilibrium between scans. This leads to errors in the integral as different spins will have relaxed by different amounts according to their individual *T₁* values.

Diffusion Coefficient (Self-Diffusion Coefficient): temperature-dependent constant which governs the random movement of particles or molecules in solution without a chemical potential gradient.

Diffusion-Ordered Spectroscopy (DOSY): 2D NMR experiment which plots ¹H NMR on one axis and the *translational self-diffusion coefficient (D_T)* in the other. Since diffusion is dependent on the sizes and charges of molecules or particles, this experiment can be used to estimate molecular weight, and to detect association, ion pairing etc. between species.

DIPEA: *N,N*-Diisopropylethylamine.

Dissipated Sphere/Ellipsoid (DSE): less tightly packed molecular geometry with an elongated main axis.

Distortionless Enhancement by Polarization Transfer (DEPT): NMR experiment which makes use of coherence transfer to enhance the signal of a low sensitivity nucleus such as ¹³C. Changing the pulse angle results in differentiation in sign between the signals of CH, CH₂ and CH₃ groups.

DMAC: dimethylacetamide.

Drift (Magnet): change of the magnetic field over time, that can result in signal broadening or artefacts in spectra. NMR spectroscopy generally uses deuterated solvents as a *lock reference* in combination with a field-frequency lock to maintain a stable magnetic field strength.

Dwell Time (DW): time between two *FID* data points.

Dynamic Equilibrium: conditions in which forward and backwards rates are the same and the concentrations of all species are constant.

Dynamic Nuclear Polarisation (DNP): NMR experiment which utilizes magnetisation transfer from unpaired electrons of a radical to nuclear spins resulting in signal enhancement.

Dynamic viscosity (η): measure of the resistance to flow of a fluid.

EDA: ethyl diazoacetate.

edHSQC (DEPT-edited HSQC): HSQC spectrum using DEPT editing where the sign of a peak depends on the number of protons attached to the relevant carbon (see DEPT and HSQC)

Effective Density (ρ_{eff}): empirical molecular density in the SEGWE model for the dependence of the diffusion coefficient on molecular weight.

End-Point Experiment: reaction using either a large excess of labelled substrates or intermolecular competition to determine the KIE. These experiments are alternatives to other kinetic experiments which do not run to full completion.

End-Point Ratio: ratio between two species at the completion of a reaction, for example of isotopologues.

Equilibrium Isotope Effect: difference in the equilibrium constants of reactions involving isotopologues or isotopomeric substrates.

Ernst Angle: optimised pulse angle that gives the highest signal to noise ratio for a given repetition rate in a simple one-pulse 1D NMR acquisition.

Ex Situ: latin phrase (lit. '[away] from the site'). In the context of NMR sampling methods it means that the reaction is set up outside the NMR spectrometer and only aliquots of the reaction are analysed.

Exchange Spectroscopy (EXSY): 2D NMR method using magnetisation transfer to detect chemical exchange.

Extended Disc: approximation in molecular geometry where molecules are described as discs.

External Calibration (DOSY): measurement of the diffusion reference compounds in one sample for use in interpreting diffusion coefficients in another.

External Lock: lock reference physically separated from the sample of interest (e.g. in a concentric capillary).

External Standard: reference substance which is physically separated from the sample (e.g. in a capillary), as opposed to an internal reference which is in the solution being analysed.

External Stimulus: excitation trigger which comes from outside of the reaction mixture (e.g. heat or light).

Eyring Equation: mathematical correlation between the temperature and the reaction rate constant. It is closely related to the Arrhenius equation, but applies to single elementary steps.

FEP: fluorinated ethylene propylene.

Flip Angle: see pulse flip angle.

Flow Cell: modified NMR tube which is used inside the probe of a spectrometer. It is connected to a reaction vessel by a flow system which pumps the solution into and out of the flow cell, in a continuous or stopped flow manner.

Flow NMR: experiments using a flow system to analyse a sample within the spectrometer.

Flow Rate: volume of a solution passed per unit of time.

Flow System: apparatus for transporting a reaction mixture through tubing.

Fourier Transformation (FT): mathematical operation which converts a function of time into a frequency spectrum or vice versa.

Fractional Conversion (F): ratio of the concentration of product at a certain time to that of the substrate concentration initially present at the beginning of the reaction.

Free Energy of Activation: see activation energy; difference in Gibbs energy between reactants and transition state in the model used for the Eyring equation.

Free Induction Decay (FID): signal detected by the spectrometer after an excitation pulse or pulse sequence.

Frequency-Domain Base Line Correction: subtraction of a function which fits the baseline of a spectrum.

Geminal (gem): two identical groups are located on the same atom.

Gierer-Wirtz Expression: mathematical correction to the Stokes-Einstein equation to allow for the relative sizes of solute and solvent molecules.

Globally-Optimised, Alternating-Phase, Rectangular Pulses (GARP): method for heteronuclear broadband decoupling.

Gyromagnetic Ratio (γ): physical property of a nucleus which describes the strength of the magnetic field produced by the spin of that nucleus.

Hadley Convection: flow resulting from horizontal temperature gradients in a fluid.

Hammitt Linear Free Energy Analysis: correlation of reaction rate with substituents in a series of analogous molecules.

Headspace: volume above the solution in a closed system.

Heavy Atom KIE: difference in rate observed after the substitution of a nucleus (not H) with a different isotope, e.g. ^{13}C for ^{12}C .

Henderson-Hasselbalch Equation: equation relating pH, $\text{p}K_{\text{aH}}$ and the fractional ionisation of an acid.

Heteronuclear Decoupling: method utilising a pulse sequence to suppress the effects of coupling between spins of different elements.

Heteronuclear Multiple Bond Correlation (HMBC): 2D NMR experiment which has a ^1H -spectrum on one axis and a heteronuclear spectrum on the other. The experiment is based on the J -coupling between the proton spins and the heteronuclear spins over multiple bonds.

Heteronuclear Overhauser Enhancement Spectroscopy (HOESY): 2D NMR experiment which has a ^1H -spectrum on one axis and a heteronuclear spectrum on the other. The experiment is based on through-space magnetisation transfer between a proton spin and a heteroatom spin via the nuclear Overhauser effect (NOE).

Heteronuclear Single Quantum Coherence (HSQC): 2D NMR experiment which has a ^1H -spectrum on one axis and a heteronuclear spectrum on the other. The experiment is based on the J -coupling between protons and heteronuclear spins connected by one bond.

Homotopic: description for two identical groups which, if one of them were to be substituted, would not produce a chiral compound. Groups that are homotopic have identical chemical shifts to one another.

Hyperpolarisation: technique which artificially greatly increases the population difference between spin states. Such alterations can be induced by microwave irradiation of free radicals, illumination of noble gases, or reaction with para-hydrogen.

Illumination NMR Spectroscopy: analysis of a reaction utilizing a setup which irradiates the sample with UV-vis light within the NMR probe.

In Operando: Latin phrase (lit. 'operationally'). In the context of NMR monitoring it means that the reaction is analysed while it is taking place.

In Situ: Latin phrase (lit. 'in the original place'). In the context of NMR sampling methods or monitoring it means that the reaction is run in an NMR tube, or in a flow cell inside the probe of the NMR spectrometer.

Incredible Natural Abundance Double Quantum Transfer Experiment (INADEQUATE): NMR experiment used to suppress signals from species lacking homonuclear coupling, for example to analyse one-bond couplings between rare nuclei (e.g. ^{13}C) at natural abundance.

Induction Period: initial phase of a reaction in which reaction is occurring, but little product is formed; usually indicative of a pre-activation or de-inhibition process.

In-Flow Effect: reduced signal intensities and distorted quantification arising from the incomplete pre-magnetisation in experiments using flow cells. The effect depends strongly on T_1 ; its counterpart is the out-flow effect.

Initial Rate: reaction rate in the very early stages of a reaction.

Insensitive Nuclei Enhanced by Polarisation Transfer (INEPT): method to transfer coherence between nuclei of different types via J -coupling, for example to enhance the signal intensity of a heteronucleus.

Interleaved (Sampling Method): pseudo real-time approach using repetitions of a given experiment in order to allow sampling at closer intervals.

Interleaving Process (In Situ Method): alternating between two or more different NMR experiments during a single reaction.

Internal Calibration: measurement of signals of a reference compound or compounds and species of interest in a single solution.

Internal Reference: stable compound that is in the same solution as the substrate of interest, and against which the chemical shift can be calibrated.

Internal Standard: stable compound of known concentration which is in the same solution as the species of interest. Comparison of signal integrals to that of the internal standard allows quantification.

Interrupted Flow: a quench-flow analysis technique in which flow is temporarily stopped to allow the reaction to 'age' (proceed for a certain amount of time) before flow is re-initiated for the quench.

Interscan Delay Time: time between the end of one acquisition and the beginning of the next.

Inverse-Gated Decoupling: method in which decoupling is only applied during the acquisition of the FID.

Inverse Kinetic Isotope Effect (iKIE): enhancement in rate when a nucleus is replaced by a heavier isotope.

Inversion Recovery: experiment utilizing a 180° pulse, followed by a variable delay and a 90° pulse. Used to measure the longitudinal relaxation time constant (T_1).

Inverted Signal: negative signal in the NMR spectrum.

Isodesmic Process: reaction in which all bonds broken are of the same type as those formed.

Isotope Enrichment: artificial enhancement of the isotopic ratio in a chemical compound.

Isotope Entrapment: experiment in which an isotopically-labelled species (e.g. product, substrate, intermediate) is added to a running reaction and the label redistribution in substrate, all intermediates (including catalysts) and products is monitored. The experiment reveals whether intermediates are on-pathway or off-pathway, and whether they are formed reversibly or irreversibly.

Isotopic Exchange: chemical reaction which substitutes an atom with its isotope.

Isotopic Scrambling: the deliberate, or unintended, exchange of isotopes within or between molecules or with the solvent.

Isotopic Shifts: changes in chemical shift due to the structural proximity of an isotope.

Isotopic Substitution Experiment: analysis of a reaction performed with labelled substrate. Such reactions can be used to reveal the behaviour of intermediates, determine the position of an equilibrium, or simply enhance the signal-to-noise ratio.

- Isotopologue:** identical compound but containing a different number of isotopes; e.g. 1- $^{13}\text{C}_1$ -acetic acid versus 1,2- $^{13}\text{C}_2$ -acetic acid.
- Isotopomer:** identical compound but with isotopes in different locations (position or stereochemistry) within the molecule; e.g. 1- $^{13}\text{C}_1$ -acetic acid versus 2- $^{13}\text{C}_1$ -acetic acid.
- J-coupling:** also called *scalar coupling*. Magnetic interaction between neighbouring nuclear spins, transmitted via intervening bonds and resulting in a splitting pattern in the NMR spectrum.
- J Young valve:** PTFE/glass screw-thread closure which reliably seals an NMR tube, protecting the contents from the atmosphere and vice versa.
- Kinetic Isotope Effect (KIE):** difference in rate observed after the substitution of a nucleus with its isotope. Provides valuable information about a mechanism and its turnover or rate-determining steps.
- Kinetic Modelling:** fitting experimental data with a mathematical function, or numerical methods, allowing further understanding of ongoing processes and dependencies (e.g. *reaction orders* or likely pathways).
- King-Altman Steady-State Derivation:** graphical method for derivation of steady-state rate equations for catalytic cycles.
- KOPiv:** potassium pivalate.
- Laminar Flow:** flow that comprises parallel streams of a liquid without lateral mixing or turbulence.
- Larmor Frequency:** frequency at which a nucleus precesses at a given magnetic field strength. It is determined by the *gyromagnetic ratio*.
- Line Shape Analysis:** mathematical analysis of peak shapes. This method can extract parameters such as T_2 relaxation times and exchange rates.
- Line Width:** the width, usually reported as that at half-height, of a peak in an NMR spectrum.
- Linear Free Energy Relationship (LFER):** correlation between reaction rate and a parameterised property in a series of substrates, e.g. Hammett sigma values.
- Linear Reaction System (Catalysis):** series of sequential reaction steps without branching or recycling.
- Lock Reference:** nucleus used by the lock system to provide a stable signal that is used to correct for drift in the magnetic field. ^2H is the most common lock reference nucleus.
- Locking:** The process of setting and stabilising the magnetic field during an NMR experiment.
- Longitudinal Relaxation (T_1):** also called *spin-lattice relaxation*; re-equilibration of the net nuclear magnetisation along the z axis. The time constant for this process, assuming exponential recovery, is T_1 .
- Lorentz Force:** force on a moving charged particle in a magnetic field. Its vector is perpendicular to the velocity and the magnetic field.
- Magnetic Field Gradient:** a smooth change, usually linear, in the magnetic field strength along a given axis.
- Magnetic Resonance Imaging (MRI):** technique which measures NMR signal as a function of position.
- Magnetisation Transfer:** transfer of spin polarisation to another nucleus or another chemical environment.
- Magnetisation Vector:** vector sum of all nuclear magnetic moments. At equilibrium, the net magnetisation vector is parallel to the applied magnetic field (z-axis).
- Markov Chain Monte Carlo Method:** class of algorithms using random samples from a probability distribution.
- Michaelis-Menten Rate Equation:** simplified rate equation for product formation from a fast equilibrium, classically used in the description of enzyme kinetics.
- Microscopic Rate Constant:** a constant reporting the dependency of the rate of an elementary step (unimolecular or bimolecular) on the concentration(s) of the species involved.
- Multiple Quantum Filter (MQF):** NMR method which can enable the selection of satellite peaks.
- Multiple Spin Systems:** molecules containing more than one nuclear spin.
- NMR Silent:** not detected by NMR spectrometry.
- Non-Cooperative Equilibrium:** sequence of equilibria in which disturbances in one equilibrium do not affect the others.
- Non-Coupled Spin System:** system without interactions between the nuclear spins.
- Non-Uniform Sampling (NUS):** NMR measurement method using partial sampling to construct a spectrum from a reduced number of time-domain points, reducing the total measurement time required.
- Normal Kinetic Isotope Effect (nKIE):** decrease in rate after the substitution of a nucleus with its heavier isotope.
- Nuclear Overhauser Effect (NOE):** magnetic interaction between nuclei that are close together in space, mediated by mutual dipolar coupling and resulting in transfer of signal intensity between them.
- Nuclear Overhauser Enhancement Spectroscopy (NOESY):** 2D NMR experiment which utilises the Nuclear Overhauser Effect to detect other nuclei in close proximity.
- Nuclear Spin:** quantum mechanical property of a nucleus.
- Nucleus Channel:** probe and spectrometer electronics and probe coil used to emit excitation pulses and receive signals for a particular nucleus. An NMR spectrometer usually has at least two channels, optimised for different nuclei.
- Number of scans:** number of measurements averaged for a given free induction decay (FID).
- Off-Cycle:** outside the catalytic cycle.
- Off-Pathway:** outside the main reaction sequence that leads to product.
- On-Cycle:** within the catalytic cycle.
- On-Pathway:** within the main reaction sequence that leads to product.
- On-Line NMR:** monitoring method in which the spectrometer is connected to the reaction mixture via a flow system.
- Oneshot Sequence:** a fast method of acquiring DOSY spectra without the need for extensive phase cycling.
- Out-Flow Effect:** artificial enhancement in the rate of decay of an FID caused by sample leaving the detection region. This effect results in a decrease in effective T_1 and T_2 under flowing conditions, increasing line broadening but permitting shorter repetition times between scans. At high flow rates the closely related in-flow effect dominates with its negative effects on quantification.
- Overfitting:** use of a model which includes more parameters than are required to fit the observed data. Although the model may appear to represent the data well, it might not reflect the correct mechanism.
- Para-Hydrogen Induced Polarisation (PHIP):** techniques which use para-hydrogen for hyperpolarisation to generate more intense NMR signals.
- Partial Order:** contribution of a particular species to the overall reaction order.
- PBS:** phosphate-buffered saline.
- PEEK:** polyether-etherketone.
- Peripheral Pathway:** side-reaction or reaction sequence which is not part of the main pathway but is attached to it.
- Phase Cycling:** changing the phases of radiofrequency pulses and receiver between scans in order to suppress unwanted signals.
- Phasing:** see phase correction.
- Photo Chemically Induced Dynamic Nuclear Polarisation (Photo-CIDNP):** hyperpolarisation technique using a radical generated by a photochemical reaction.
- Polarisation:** net magnetisation resulting from an unequal population of nuclear spin energy states.
- Polarisation Sharing:** see magnetisation transfer; transfer of nuclear spin magnetisation to another nuclear spin to enhance signals.
- Pre-Acquisition-Delay:** length of time between the pulse and the first point in the FID. This time must be sufficiently long to allow residual currents in the coil and electronics to dissipate before measurement begins.
- Pre-Magnetised:** allowed to approach equilibrium magnetization before measurement, e.g. in a flow cell.
- Primary Kinetic Isotope Effect (PKIE):** KIE arising when a bond between an isotopically labelled atom and a connected atom is cleaved during a reaction.
- Principal Component Analysis (PCA):** processing technique which identifies the most important variables influencing e.g. a series of NMR spectra.
- Probe:** a hardware component located in the spectrometer magnet that is used to apply RF pulses to the sample and to detect the resulting FID.
- Probe Head:** the upper section of the probe that contains the coils and receives the NMR tube containing the sample.
- Product Inhibition:** reduction in reaction rate caused by the product.
- Pseudo Real-Time Approach:** method of monitoring reactions by interleaving series of data obtained at different time points in separate experiments.
- Pulse-Acquire:** simplest NMR pulse sequence, which consists of one pulse followed by acquisition of the FID.
- Pulse Flip Angle:** angle through which a radiofrequency pulse rotates the net nuclear magnetic moment.
- Pulse Sequence:** program of pulses and delays used to excite an FID for acquisition.
- Pulsed Field Gradient (PFG):** spatially-dependent magnetic field which can be switched on and off (pulsed).
- Pure Shift:** class of NMR methods which achieve broadband homonuclear decoupling to make the spectrum less crowded. This method removes the effects of J-coupling between spins to transform all peaks into singlets.
- Pure Shift Yielded by Chirp Excitation (PSYCHE):** NMR experiment using chirp pulses to suppress the effects of homonuclear couplings.
- Purging:** exchange of the atmosphere in a closed system with inert gas.
- PTFE:** polytetrafluoroethylene, also known as Teflon.
- Quadratic Ramping:** increasing gradient strength in equal steps of gradient squared.
- Quadrupolar Nucleus:** atoms which have a nuclear spin quantum number above $\frac{1}{2}$.
- Quadrupolar Relaxation:** relaxation pathway available to nuclei with a nuclear spin quantum number above $\frac{1}{2}$. Also used of other nuclei that are relaxed via interaction with a quadrupolar nucleus.
- Quantitative Bandwidth (Spectrum):** frequency range over which equal numbers of spins give equal signal integrals.
- Quantum Yield:** the number of product molecules generated per absorbed photon in a photo-initiated or photo-mediated reaction.
- Quench-Flow:** flow system which has an additional inlet for a reagent or substrate which is added to stop the reaction after a fixed delay.
- Quenching:** rapid, and ideally complete, inhibition of a reaction by addition of a competing reagent or inhibitor, or cooling.
- Radiofrequency Filters:** devices which selectively transmit or attenuate signals within certain wavelength bands in order to diminish electrical interference.
- Radiofrequency Pulse (RF):** magnetic pulse in the radiofrequency range.

- Rapid Injection NMR (RI-NMR):** experiment in which a substrate is mechanically or manually injected quickly into a solution in an NMR tube already present in the probe head.
- Rate Constant:** a coefficient 'k' that is used in a *rate equation* to describe the velocity of a reaction, usually in conjunction with concentration term(s) and other rate constants.
- Rate Equation:** equation for reaction rate as a function of the concentrations of the reaction components (substrate, product, catalyst etc.). Expressions are referred to as closed-form if they do not involve integration and/or differentiation, open-form otherwise.
- Rate Law:** see *rate equation*.
- Rate Determining:** limiting the velocity of the reaction.
- Rate Determining Transition State (RDTS):** transition state whose formation controls the velocity of the reaction.
- Rate Limiting Step (RLS):** see *rate determining*; part of the reaction sequence which determines or limits the overall rate of the reaction.
- Rayleigh-Bénard Convection:** flow which arises from negative vertical temperature gradients.
- Reaction Order:** the exponent of the concentration of a reaction species in a simple rate law.
- Reaction Profile Kinetic Analysis (RPKA):** method for determination of the *rate law* under turnover conditions using a minimal set of experiments.
- Receiver Channel:** coil and electronics which detect the *FID*.
- Recovery Delay:** time between the end of one application of a pulse sequence and the beginning of the next, in which the *spins* are allowed to return to their equilibrium magnetisation.
- Reference Peak:** a signal used in the quantification of other species or in chemical shift calibration. It may come from an *internal standard*, an *external standard*, or *ERETIC*.
- Refocusing Pulse:** a pulse used in a *spin-echo* experiment to interchange transverse magnetisation components.
- Relative Rate:** velocity of one reaction (or *rate constant*) in comparison to another.
- Relaxation Agent:** substance which enhances the rate of nuclear *spin* relaxation. Mostly used to enhance *longitudinal relaxation* in order to speed up measurements.
- Relaxation Delay:** see *recovery delay*.
- Relaxation Rate:** velocity of the equilibration of the *nuclear spin* magnetisation.
- Relaxation Time:** time constant for the exponential recovery of z magnetization (T_1) or the exponential decay of transverse magnetization (T_2).
- Reporter Nucleus:** a nucleus at high abundance (natural or synthetic) that is studied in a substrate to gain information on another nucleus or set of nuclei.
- Resting State:** the most abundant species in a series of catalytic intermediates for a system at pseudo steady state. The *resting state* need not be *on-cycle*.
- Root Mean Square (RMS) Error:** quantification of the measure of agreement between two sets of data.
- Same Excess Experiment:** reaction set-up which tests for catalyst deactivation or product inhibition by changing the substrate concentration while keeping the excess of one substrate constant.
- Satellites:** small peaks near a main peak which result from the coupling of the observed *nuclear spin* to a nearby isotope of <100% abundance. The centre of the *satellite* pair is usually slightly offset from the main peak due to the effect of *isotopic shift*.
- Saturation:** equal population of nuclear *spin energy states*, with zero net nuclear magnetization.
- Saturation Recovery:** experiment utilizing a looped 90° pulse, a variable delay and final 90° to estimate the *longitudinal relaxation time* T_1 .
- Saturation Transfer:** experiment in which a reduction in the net magnetization of one site results in a reduction in that of another site with which it is undergoing *magnetization transfer*, for example by chemical exchange.
- Scalar Coupling:** see *J-coupling*.
- Secondary Kinetic Isotope Effect (SKIE):** difference in rates induced by proximity of an isotope to a reacting centre at which a bond to the isotope is not cleaved. The rate difference is usually smaller than that observed in a *primary isotope effect* (PKIE).
- Self:** selective.
- Self-Diffusion:** random movement of particles or molecules in solution without a chemical potential gradient.
- Sensitive, Homogeneous and Resolved Peaks in Real Time (SHARPER):** *pure shift* technique which produces single sharp peaks to compensate for broad peaks caused by magnetic inhomogeneities.
- Shape Factor (in NMR diffusion measurements):** correction factor for the shape of a field gradient pulse.
- Shigemi Tube:** one of a number of designs of NMR tube that minimise the amount of sample needed by including plugs of magnetic-susceptibility-matched glass above and below the active volume.
- Shim coils:** see *shims*.
- Shimming:** homogenisation of the magnetic field by the adjustment of electric currents passed through small coils to correct spatial variation of the static magnetic field B_0 .
- Shims:** coils used to correct the static magnetic field.
- Signal Amplification by Reversible Exchange (SABRE):** hyperpolarisation method using indirect magnetisation transfer from *para*-hydrogen.
- Signal Drift:** change in peak frequency over time. May be caused by changes in temperature or chemical composition.
- Signal-to-Noise Ratio (S/N):** ratio of peak intensity to baseline noise.
- Sinc Wiggles:** baseline distortions close to a peak, caused by truncation of the *FID*. Can be avoided by increasing the *acquisition* time or by applying a suitable window function.
- Singleton Method:** Experiment to determine *KIEs*, primarily ^{13}C but ^2H and ^{17}O also feasible, by running a reaction at natural isotopic abundance to high conversion, followed by recovery of the unreacted substrate. An alternative method runs the reaction to low conversion and analyses the product.
- Soft Pulse:** selective pulse which excites a limited region of a spectrum.
- Spatially Selective NMR:** experiments which use *magnetic field gradients* and *soft pulses* to selectively acquire the spectrum of a certain region (horizontal slice) of the NMR tube.
- Spectral Hard Modelling:** mathematical fitting of peaks in a spectrum; used to deconvolute and quantify overlapping peaks.
- Spectral Width (SW):** range of frequencies recorded in an NMR spectrum.
- Spike-In:** experiment set-up which adds a species to a reaction at a certain point and follows its outcome, or corroborates its identity or chemical shift.
- Spin:** see *nuclear spin*.
- Spin Echo:** a pulse sequence component comprising a 180° pulse positioned between two equal time delays. Used to refocus chemical shift evolution.
- Spin-Lattice Relaxation:** see *longitudinal relaxation* (T_1).
- Spin-Spin Relaxation:** see *transverse relaxation* (T_2).
- Staged-Initiation:** starting two or more identical experiments at different times but with the same observation window.
- Static Magnetic Field:** constant homogeneous magnetic field B_0 .
- Steady State Approximation:** Approximation that the kinetic analysis of a complex reaction involving unstable intermediates in low concentration can be simplified by setting the rate of change of each such intermediate equal to zero, so that the *rate equation* can be expressed as a function of the concentrations of chemical species present in macroscopic amounts.
- Stejskal-Tanner Equation:** relates the signal attenuation in a *DOSY* experiment to the effective diffusion time and diffusion coefficient.
- Stokes-Einstein Equation:** relates the *diffusion coefficient* of a species to its hydrodynamic radius. It assumes that the species is a hard sphere diffusing in a continuum solvent – poor approximations for small molecules in solution.
- Stokes-Einstein, Gierer-Wirtz Estimation (SEGWE):** modification of the *Stokes-Einstein equation* suitable for small molecules.
- Stopped-Flow NMR (SF-NMR):** system which rapidly mixes components to initiate reaction, then transports the nascent reaction mixture to the active volume in the *probe head* for analysis.
- Sum-Square Error:** see *Root Mean Square (RMS) error*.
- Swain-Lupton Equation:** modification of the Hammett equation to include separate weighted parameters for resonance and field effects.
- TCA:** trichloroacetimidate.
- TFA:** trifluoroacetic acid, $\text{CF}_3\text{CO}_2\text{H}$.
- Through-Space Correlation Techniques:** NMR experiments such as *NOESY* that measure interactions through space rather than through bonds.
- Time-Average Peak:** observed signal when two or more species are in rapid exchange. Because the reaction is fast, the peaks coalesce into one.
- Time Zero Peak Volume:** integral of a 2D peak where there has been no attenuation of the signal. This value is determined, for instance, by extrapolation in the HSQC_0 experiment.
- Total Correlation Spectroscopy (TOCSY):** 2D method for analysis of homonuclear coupling over multiple couplings. It is closely related to *COSY*.
- Transition State Theory (TST):** theory which relates reaction rate to the Gibbs energies of the starting materials and transition state(s).
- Translational Diffusion:** random movement of species in solution, driven by thermal forces.
- Translational Self-Diffusion Coefficient:** see *diffusion coefficient*.
- Transmission Coefficient (κ):** the fraction (0 to 1) of the transition state that leads to product rather than reverting to starting material(s).
- Transmitter Frequency Offset:** the transmitter offset (Bruker O1; Varian tof) determines the *Larmor frequency* that is at the centre of the spectrum recorded.
- Transverse Relaxation (T_2):** also called *spin-spin relaxation*; nuclear spin relaxation in the xy plane.
- TsDPEN:** (1R,2R)-(-)-N-(4-toluenesulfonyl)-1,2-diphenylethylenediamine.
- Tuning:** adjusting the *probe* capacitors to optimise transfer of radiofrequency power from transmitter to *probe* coil and from *probe* coil to preamplifier.
- Turnover:** one complete revolution of a catalytic cycle.
- Turn Over Rate Limiting Step:** see *rate determining* step; the section(s) of a catalytic cycle, or steps leading on to it, that limit the overall rate of a reaction.
- Two-Spin Exchange System:** two different *spins* which are in chemical exchange with each other.

Underfitting: usage of an incomplete model which cannot represent a set of data correctly.

Unlocked Mode: method in which a sample is run with the spectrometer not *locked* (not referenced to a deuterium nucleus).

Van der Waals Radius: effective radius of an atom.

Van der Waals Volume: effective volume occupied by an atom or molecule.

Variable Time Normalisation Analysis (VTNA): modification of *RPKA*. Used to determine a substrate order by graphical analysis of a series of temporal concentration data, plotted against a modified time axis, e.g. $\sum[A]^x \Delta t$. The value for x is manually varied until agreement between datasets is achieved.

Visual Kinetic Analysis (VKA): a graphical data analysis method in which data from several experiments are compared. The agreement or lack of agreement furthers mechanistic understanding.

VT-NMR: variable temperature NMR spectroscopy.

Water Suppression Enhanced through T_1 Effects (WET): NMR pulse sequence for suppressing solvent peaks using selective radiofrequency pulses and field gradient pulses.

Wideband, Alternating-Phase, Low-Power Technique for Residual Splitting Element (WALTZ): method for broadband heteronuclear *decoupling*.

X-Nuclei: heteroatom nucleus (not ^1H).

Zero-Filling: addition of zeros to the end of an *FID* before *Fourier transformation*.

Zero-Point Vibrational Energy (ZPVE): lowest possible energy state for a vibrating system in quantum mechanics.